Title
Development of New Imaging Agents for the Study of Cellular Copper Dynamics

Author
Ramos Torres, Karla Michelle

Publication Date
2016

Peer reviewed|Thesis/dissertation

Development of New Imaging Agents for the Study of Cellular Copper Dynamics

By

Karla Michelle Ramos Torres

A dissertation submitted in partial satisfaction of the

requirements for the degree of

Doctor of Philosophy

in

Chemistry

in the

Graduate Division

of the

University of California, Berkeley

Committee in charge:

Professor Christopher J. Chang, Chair
Professor Michelle C. Chang
Professor Seung-Wuk Lee

Summer 2016

Development of New Imaging Agents for the Study of Cellular Copper Dynamics

by Karla Michelle Ramos Torres

Abstract

Development of New Imaging Agents for the Study of Cellular Copper Dynamics

by

Karla Michelle Ramos Torres

Doctor of Philosophy in Chemistry

University of California, Berkeley

Professor Christopher J. Chang, Chair

Copper is an essential element in biological systems. Its participation as a catalytic and structural cofactor in enzymes that function in biological processes such as energy generation, oxygen transport, cellular metabolism and signal transduction renders it vital for the life of eukaryotic organisms. However, if misregulated, it can cause cellular oxidative damage through the production of highly reactive oxygen species. Consequently, it is not surprising that organisms have developed intricate cellular machineries to tightly regulate the trafficking of copper. The fascinating balance between the functional and pathological roles of copper has significantly motivated the study of the processes involved in the proper management of this metal in the cell by inspection of the total metal content in biological samples and its distribution into static and labile cellular pools. Traditional bulk techniques, in combination with biochemical and genetic methods, have been used to probe the static copper pool and provide a general understanding of how cells handle copper ions, allowing for the identification of major proteins and ligands involved in copper homeostasis. Alternatively, molecular imaging provides a complementary, versatile approach that can be used to monitor dynamic fluxes of the labile copper pools in real time with spatial and temporal resolution.

This dissertation describes the design, synthesis and characterization of new copper-responsive fluorescent sensors in order to expand the available toolbox for molecular imaging of copper dynamics. Application of a novel carbo-rhodol scaffold allowed for the development of the Copper CarboRhodol (CCR) and Copper CarboFluor (CCF) probes, that in combination with additional rhodol platforms extended the available color palette of copper-selective probes. Additionally, the design of unique metal binding motifs with altered ligand architectures, binding geometries and coordination units resulted in the synthesis of new copper-responsive fluorophores. Alteration of the coordination unit and inclusion of a tripodal ligand topology afforded a family of xanthene-based sensors with an assortment of fluorescent responses to copper and ability to sense fluctuations in endogenous, labile copper pools. Finally, development of a modified donor set that increases the number of available donors in the ligand framework was investigated as an alternative strategy to modulate the binding properties of the resulting copper sensors.

For my parents

... porque el amor de padre y madre no se cansa de entregar.

Table of Contents

Acknowledgments

Many people have played an important role in my professional development. This accomplishment is also theirs.

First and foremost, I am grateful to my advisor Professor Chris Chang for his guidance, patience and support throughout my graduate studies. His academic advice, ideas and encouragement to carry them out provided me with an excellent preparation in chemistry and chemical biology. His mentorship has challenged me and offered me priceless opportunities to grow in an intellectual and personal level. I am whole-heartedly thankful to the members of the Chang lab; without their scientific expertise, camaraderie and constant motivation this experience would have not been the same. I am especially grateful to Dr. Jeff Chan, whose mentorship when I joined the lab gave me a solid foundation to build upon in the years to come. I need to acknowledge the people who made each day a little easier, even when the chemistry gods were not in my favor: Cheri Ackerman, my share-the-struggle-with partner since day one, for her constant support, helpful discussions and for being my go-to resource to answer my biology questions without judgement; Allegra Aron for her friendship, countless coffee runs, valuable conversations and contagious drive, and Dr. Ryan Walvoord, who joined the Changstas towards the end of my stay in Berkeley and provided great synthetic chemistry insight, random facts about chemistry, sports and everything in between, and great tunes to accompany our late nights in lab. I am also thankful for helpful scientific discussions with Dr. Lakshmi Krishnamoorthy, Dr. Joey Cotruvo, Dr. Sheel Dodani and Dr. Brian Michel.

I would have never discovered my interest in scientific research if it were not for my undergraduate mentors. Professor Ingrid Montes, my undergraduate advisor Professor José Prieto and Dr. Gerardo Torres, thanks for instilling in me the passion for chemistry that drove me to pursue my doctorate degree.

I have been blessed to have an impressive support system throughout this experience and I could have not made it to the finish line without them.

Living 3,600 miles from the Puerto Rican warmth has not been easy, but I was fortunate to find a family away from home and outside the lab. Andrew Attar, Anna Parker, Tony Rizzuto, Frances Rodríguez, Cheri Ackerman, Dr. Pete Marsden, Alex Buyanin, Amanda Prasuhn, Andrew Neel, Richard Cooper – thanks for all the adventures that made my time in Berkeley one heck of a ride. Our weekend volleyball sessions, backpacking expeditions, skiing escapades and extravagant Thanksgiving dinners were much needed pick-me-ups throughout these past years. This journey would have not been possible without the constant support from the sisters I have gained in life. Janice Hernández, Mayra Hernández and Cynthia Agosto, although miles apart have been part of every achievement and defeat, a phone call away, with endless cheer and laughter.

My experience in Berkeley has blessed me with a partner-in-crime, Andrew, my better half. His pragmatic approach to life and science has given me new perspective and has helped me become a better person and scientist. Words can never express how grateful I am to have had his ceaseless love and encouragement throughout these past years.

My family, although far away has been cheering me along every step of the way. I am thankful for their continuous optimism, for all the phone calls and the care packages. I am especially grateful to my brother, Polito. His cheerful personality is contagious, and has helped me find joy in the

simpler things in life. Ironically, my time in Berkeley has brought me closer to him and I have grown more appreciative of his constant teasing and protection.

Finally, my parents to whom this thesis is dedicated to, warrant the most recognition for my achievements. I would not be where I am without their endless love and reassurance. The times when I was incredibly homesick, or when lab work was just too much, or when I had exciting news, the distance and the three time zones could not be more insignificant for them to make their presence felt. *Papi y mami, la vida no me pudo haber dado mejores ejemplos a seguir. De ustedes aprendí el valor del trabajo y la perseverancia. Gracias por su amor incondicional y su eterno apoyo.*

Chapter 1:

Thioether Coordination Chemistry for Molecular Imaging of Copper in Biological Systems

Portions of this work were published in the following scientific journal:
Ramos-Torres, K. M.; Kolemen, S.; Chang, C. J. "Thioether Coordination Chemistry for Molecular Imaging of Copper in Biological Systems", *Israel Journal of Chemistry* **2016** DOI: 10.1002/ijch.201600023

Abstract

Copper is an essential element in biological systems. Its potent redox activity renders it necessary for life, but at the same time misregulation of its cellular pools can lead to oxidative stress implicated in aging and various disease states. Copper is commonly thought of as a static cofactor buried in protein active sites; however, evidence of a more loosely bound, labile pool of copper has emerged. In order to help identify and understand new roles for dynamic copper pools in biology, we have developed selective molecular imaging agents for this metal, drawing inspiration from both biological binding motifs and synthetic model complexes that reveal thioether coordination as a general design strategy for selective and sensitive copper recognition. This Chapter summarizes some contributions, primarily from our own laboratory, on fluorescence- and magnetic resonance-based molecular imaging probes for studying copper in living systems using thioether coordination chemistry.

Introduction

Copper is an essential element for life.[1] Owing to its potent redox activity, the participation of this metal as a catalytic and structural cofactor in enzymes that function in biological processes spanning energy generation, oxygen transport, cellular metabolism and signal transduction renders it vital for the life of eukaryotic organisms.[2] However, this same redox promiscuity, when misregulated, can also lead to aberrant generation of reactive oxygen species (ROS) that has been linked to aging and different disease states including genetic disorders like Menkes[3-5] and Wilson's[6-8] diseases, neurodegenerative diseases like Alzheimer's,[9-12] Parkinson's[13] and Huntington's[14] diseases, and metabolic disorders such as diabetes and obesity.[15-17] For this reason, copper and other redox-active metals have been canonically thought of as buried cofactors within enzyme active sites and part of a tightly bound metal pool. However, a more loosely bound pool, termed the labile pool, in which copper and other metals can dynamically exchange with ligands on timescales commensurate with signaling, has been observed. This metal pool in which rapid ligand exchange and changes in metal concentration gradients can mediate signaling processes has been extensively studied in regard to redox-inactive alkali, alkaline earth and transition metals such as calcium, sodium, potassium and zinc. Nonetheless, recent work from our lab and others has revealed that despite its high reactivity, dynamic copper fluxes are observed in important physiological processes such as neuronal calcium signaling pathways,[18] spontaneous activity in neural circuits,[19] metabolic processes such as lipolysis,[20] and the activation of the mitogen-activated protein (MAP) kinase pathway relevant in normal physiology and in oncogenic serine/threonine-protein kinase B-Raf (BRAF) signaling and tumorogenesis.[21,22]

Against this backdrop, molecular imaging provides a versatile approach that can be used to monitor labile metal fluxes in real time with spatial and temporal resolution.[23-25] In combination with complementary biochemical and genetic methods, as well as direct readouts of total metal content, small-molecule probes with different readout signals, including fluorescence, colorimetric, and magnetic resonance (MR) relaxivity modalities, can be used effectively as pilot screening tools for quickly assessing metal status in different physiological states. As such, the development of metal-selective small molecule probes provides a potentially powerful toolbox that allows for the mapping of labile metal pools and the study of the roles of these dynamic fluxes.

In this chapter, we focus on the use of thioether coordination chemistry as a general design strategy for achieving copper-selective probes for molecular imaging – optical and magnetic resonance imaging, as an illustrative example of opportunities at the interface between inorganic chemistry and biology.

Bioinspired Strategies for Selective Copper Recognition

Owing to environmental heterogeneities in biological systems, the development of small molecule probes for biological use is inherently challenging. Because transition metals such as copper are far less abundant than their biologically relevant alkali/alkaline earth counterparts, selectivity poses one of the main challenges in probe design. Additionally for copper, redox specificity is required, as it can exist in two major oxidation states, Cu(I) and Cu(II). In the cellular setting, most of the copper that is undergoing dynamic exchange is in the Cu(I) state, owing to the reducing intracellular environment (average potential of – 0.25 V)[26] buffered in part by the thiol-containing low-molecular weight peptide glutathione (GSH). Preceding import across the plasma membrane, extracellular Cu(II) is reduced to the Cu(I) state by an insufficiently understood mechanism that presumably involves membrane reductases[27] after which intracellular accumulation of the metal ion is achieved primarily by the high-affinity Cu(I)-specific channel copper transporter 1 (CTR1). The prevalence of the intracellular Cu(I) state is further evidenced by the identification of Cu(I)-specific metallochaperones such as Atox-1,[28] which delivers Cu(I) to the p-type ATPases ATP7A/B, the copper chaperone for superoxide dismutase (CCS),[29,30] and the various Sco[31] and Cox[32] copper chaperones for mitochondrial copper pools to metalate enzymes such as cytochrome *c* oxidase (CcO). The specificity of this emerging class of proteins for copper binding is crucial for maintaining cellular homeostasis of this metal.

Metal and ligand considerations for copper coordination. Inspection of biological copper sites can give us insight into its preferred modes of binding. Coordination in protein copper-binding sites is typically dominated by histidine, cysteine and methionine residues. The makeup of each ligand set depends on the specific role, copper transport or enzymatic activity, of the binding site. However, the general use of these amino acid side chains can be viewed as also governed by the Hard and Soft Acids and Bases (HSAB) principle.[33,34] In line with this theory, soft acid Cu(I) and borderline Cu(II) will preferentially bind ligands with borderline to soft basicities, respectively, leading to a favored use of amino acid residues with nitrogen and sulfur donor atoms. Additionally, the number of donors as well as the coordination geometry can also impart a degree of selectivity between the possible metal oxidation states for these binding sites. Even though Cu(I) does not have a geometric preference based on a lack of ligand field stabilization energy (LFSE), it is often found in low-coordinate systems with 2, 3 or 4 ligands in linear, trigonal planar or tetrahedral geometries. Conversely, LFSE for Cu(II) results in higher coordinate (4, 5 or 6 ligands) systems with square planar and square pyramidal geometries.

Moreover, the chemical identity of the ligating groups can also lead to favored oxidation states for copper in the binding site. Coordination environments including histidine and cysteine residues are pH-dependent, as deprotonation of the imidazole ($pK_a \sim 6$ and 14) and thiol ($pK_a \sim 8.5$) side chains lead to anionic donors. While the chemical identity of the coordinating groups and their arrangement in a particular three-dimensional geometry confer a degree of specificity for metal binding, it is important to remember that proteins also control selectivity of their binding sites by

additional secondary sphere coordination effects that can further alter the local protein environment upon metal binding. For example, in the electron transfer enzyme Cu,Zn-superoxide dismutase (SOD1), the bridging histidine residue between the Cu and Zn sites has an altered pK_a, causing the imidazolate to form at physiological pH. (Type II center, Figure 1-1)

Furthermore, the ability of cysteines to form the thiolate renders them prone to oxidation, which can be correlated to a prevalence of cysteine-rich copper sites in reducing cellular compartments in comparison to more oxidizing intracellular locales. In contrast, the thioether side chain in methionine provides a neutral donor with pH-independent coordination as well as less susceptibility to oxidation. This inability to be ionized, in combination with a longer side chain, also gives methionine a slight hydrophobic nature.

Biological systems reveal methionine as an ideal ligand for Cu(I) binding. The use of sulfur-based ligands enhances the selectivity for the cuprous over the cupric state, as shown by higher Cu(II) affinity when including nitrogen donors in synthetic copper ligands.[35] However, the use of the sulfur donor cysteine over methionine (or vice versa) in cuproprotein binding sites can be associated to that specific protein's chemical role and surrounding biological environment. Cysteine copper binding is pH-dependent and susceptible to redox activity, but these same residues achieve tighter binding to the metal compared to methionine owing to their anionic charge. In contrast, methionine binds with weaker affinities when compared to the cysteine thiolate, but at the same time varying the number of methionine ligands can tune the affinity of the binding site. Additionally, methionine-rich sites provide a unique environment that stabilizes Cu(I) coordination as well as excellent selectivity over other biologically-relevant cations like Zn(II) and Fe(II).[36,37]

As a result, methionine has emerged as an important ligand for copper in biological systems. Copper centers involving methionine residues are prevalent in systems ranging from electron transfer proteins to copper trafficking proteins. Even though most S-donors in electron transfer protein copper sites are thiolate-based, there are a few examples of methionine copper interactions. Cupredoxins such as plastocyanin and azurin show the typical 2-histidine 1-cysteine copper coordination in a trigonal planar geometry. Additionally, these blue copper proteins possess a weakly bound methionine thioether sulfur in the axial position.[38,39] (Figure 1-1) Other electron transfer proteins with methionine binding within their active sites include Cytochrome *c* oxidase (CcO), which has a methionine ligand in its mixed valence Cu_A center.[40] As with electron transfer proteins, the copper trafficking counterparts also show prevalent cysteine thiolate coordination to copper instead of the thioether moiety. Bis-cysteinate Cu(I) coordination is a hallmark of cytosolic copper ligation, with many transport proteins exhibiting a *CXXC* binding motif. (Figure 1-1) Among the copper sensing and trafficking proteins that exhibit this motif are the eukaryotic copper chaperones CCS[41,30,29,42] and Atox1[43-47] as well as the Cu(I)-binding P-type ATPases ATP7A/B.[48-50] In comparison to cytosolic Cu(I) binding, which occurs in a very reducing environment, transport of extracellular copper into the cell is highly associated with methionine thioether binding. The homotrimeric copper transporter CTR1 contains a cell surface located N-terminal region with histidine and methionine-rich domains (Mets motif) that are implicated in copper transport across the membrane.[51-53] (Figure 1-1) Methionine motifs (MX_3M) in the transmembrane region are also important in shuttling copper down the pore of the protein.[54,51]

Perhaps the best-characterized methionine-copper coordination chemistry is that of protein networks involved in copper resistance, predominantly found in less redox-balanced spaces of prokaryotic organisms. In order to relieve the cytosol of excess copper, bacteria export the metal using the ATPase CopA, which binds copper in a similar fashion as ATP7A/B.[55] For gram-negative bacteria, this detoxifying process is not sufficient as there is still a need to manage the copper that accumulates in the periplasm. A canonical example of periplasmic, copper-handling machinery is the Cus pathway, an export system that is composed of three proteins, CusA, CusB and CusC.[56,57] The CusA and CusB proteins possess three-coordinate methionine-only binding sites[57,58] (Figure 1-1), whereas CusC does not appear to have metal binding features as observed by crystallographic experiments.[59] In contrast, CusF, a copper chaperone for CusB,[60] binds copper in a 2-methionine, 1-histidine binding site with a tryptophan residue that provides a cation-π interaction with the metal.[61,62] (Figure 1-1) In the relatively less studied Pco and Cop copper resistance pathways, where proteins are encoded by plasmid DNA in comparison to chromosomal DNA, methionine coordination is observed in the Cu(I) binding sites of PcoC and CopC, but not in their separate Cu(II) sites that mainly offer N and O donors as ligands.[63-67] Copper-handling systems like the Cus pathway, as well as the Pco/Cop copper resistance pathways, are characterized by higher-coordinate Cu(I) complexes (three or four ligands) when compared to the cysteine-dominated environments of the cytosolic copper proteins. This situation is in part due to the need to compensate for the weaker Cu(I)-binding affinity of thioethers in comparison to thiolates.

Synthetic compounds have exploited thioether donors for copper coordination. The ability of thioethers to coordinate to a variety of metals, and the effect of their moderate π-acidity[68] on the stabilization of low metal oxidation states have been historically important in motivating the study of thioether-metal complexes. The need for homoleptic thioether complexes in order to evaluate the effect of thioether ligation on the electronic structure of metal ions was satisfied by the development of crown thioethers. In seminal work, Cooper and coworkers studied the synthesis, conformational analysis and metal coordination of macrocycles including the 9S3, 12S3, 18S6, and 24S6 variations.[69] (Figure 1-2) Extensive efforts on the investigation of different metal complexes of crown thioethers (including nickel, cobalt, copper, ruthenium, rhodium and silver) indicate that thioethers present a marked preference for the lower, "softer" metal oxidation states. This behavior manifests itself in the redox properties of the complexes as well as in their magnetic and EPR features.[70]

Another important avenue for motivation of the study of thioether-metal complexation arose from the previous speculation (since confirmed[71,72]) of methionine copper coordination in blue copper proteins. In efforts to elucidate the origin of the unexpected redox, optical and EPR properties of these copper centers, Rorabacher and coworkers carried out an impressive set of studies on the copper complexes of macrocyclic tetra- and pentadentate thioethers in which they showed that coordination to thioethers shifts the Cu(II/I) potential to more positive values, enhances the rate of Cu(II/I) redox self-exchange kinetics, and generates unusually intense optical bands.[73,74] Furthermore, studies on mixed-donor macrocyclic ligands with N_xS_{4-x} and N_xS_{5-x} donor sets[35,75] (Figure 1-2) established important trends in copper coordination: (1) stability constants for Cu(II) complexes increase by 5-6 orders of magnitude for each replacement of a thioether sulfur donor by an amine nitrogen donor atom and (2) more positive Cu(II/I) redox potentials of macrocyclic donors with sulfur donors compared to aliphatic nitrogen atoms is credited to a

destabilization of the Cu(II) oxidation state rather than a stabilization of the Cu(I) state. Additional studies of tripodal ligands with mixed nitrogen and sulfur donors to investigate the effect of binding geometry on electron transfer kinetics of Cu(II/I) systems[76,77] provided further insight on copper-thioether coordination, demonstrating a narrow distribution of the stability constants of Cu(I) complexes in comparison to the Cu(II) counterparts and a noticeable effect of the geometry on the Cu(II) complexes. Interestingly, the compatibility of these ligands for copper sensing has been established with regard to their better stability towards oxidation in comparison to thiolate ligands, and in that the reported K_d values of these complexes fall within the window of 10^{-11} M (GSH) to 10^{-18} M (SOD1) for biological Cu(I) ligands.

Fluorescence-based Copper(I) Sensing Probes

Inspired by Nature's use of thioether ligation as well as the aforementioned work on copper coordination chemistry, we and others have extensively employed thioether receptor motifs to develop a series of recognition-based fluorescent probes for the detection of Cu(I).[78-80] Using this strategy, a fluorophore reporter is coupled to a chelator (receptor) that is specific for the metal of interest. Once bound to the analyte, a change in the optical properties of the sensor is observed, which can be reversed upon analyte dissociation. For a more in-depth discussion on the mechanisms and modes of small molecule fluorescence sensing of metal cations we refer to the following review articles.[81,82]

Selectivity of the receptor for the metal of interest can be achieved by careful design of the ligand using fundamental principles of coordination chemistry. Considering some of the basics of copper homeostasis (e.g., sulfur coordination, low coordination number), one can envision a few possible strategies for building receptors that can chelate Cu(I) with good selectivity and competitive binding constants. The common use of a photoinduced electron transfer (PeT) quenching mechanism as a turn-on/off switch for metal sensing sets up a particular stipulation for the receptor moiety; a substituted amine is customarily used as the PeT switch due to its lone pair interaction with the cationic analyte.[82-84] In PeT-based fluorescent sensors two important entities, the electron donor (the substituted amine) and the electron acceptor (the excited-state fluorophore), interact to produce an optical response upon analyte binding. In the unbound state, photoexcitation of the system leads to a charge-separated state in which the highest occupied molecular orbital (HOMO) of the donor lies in an energetically favorable state to transfer an electron to the excited-state fluorophore and hence quench the fluorescence relaxation pathway of this state. Upon analyte binding, the energy level of the HOMO of the electron-rich donor is lowered, causing electron transfer to be less thermodynamically favored, alleviating PeT and thus restoring fluorescence in this state.

Combining what has been learned from the studies of macrocyclic and aliphatic N_xS_{4-x} and N_xS_{5-x} copper complexes, as well as the characterization of numerous copper binding sites involved in copper homeostasis, we reason that thioether-rich ligands can satisfy the requirement for amine coordination needed for PeT modulation by metal binding while maintaining selectivity for Cu(I), and as a result can be used as the receptors of choice for synthetic copper sensors.

Use of a thioether-rich receptor (NS_4) for Cu^+ sensing: design of a first generation Cu^+ sensor. Use of a boron dipyrromethene (BODIPY) fluorophore coupled to an azatetrathia receptor (termed

NS4') gave rise to Coppersensor 1 (CS1),[85] the first Cu^+ responsive probe with visible excitation and emission profiles. (Figure 1-3) The NS4' receptor, an acyclic analog to the Cu(I)-binding tetrathiaza crown ether used in the important first small-molecule fluorescent sensor for Cu(I), CTAP-1,[86] binds the metal ion to produce a selective response. CS1 features a 10-fold increase in probe fluorescence upon metal binding with $K_d = 4 \times 10^{-12}$ M. (Figure 1-4) Additionally, the dye responds to exogenous $CuCl_2$ addition to HEK 293T cells in confocal imaging experiments, where the fluorescence enhancement can be reversed by addition of a membrane-permeable Cu(I) chelator. The ability of CS1 to reversibly detect labile copper in this system was validated by an independent study,[87] however its use to detect copper changes upon supplementation with $CuCl_2$ or Cu(gtsm) (Cu(II)-glyoxal-bis(N^4-methyl-3-thiosemicarbazonato)) in other mammalian cell lines, including CHO, M17, U87Mg and SH-SY5Y proved unsuccessful. These observations point to the fact that there is no one-size-fits all chemical probe for every biological model, and therefore characterization of the sensor in its intended biological or environmental system of use is necessary. Indeed, when used in combination with complementary techniques such as direct metal detection via inductively coupled plasma mass spectrometry (ICP-MS) and biochemical assays like DNA microarrays and protein profiling, CS1 has been applied to study copper dynamics in a wide range of bacterial,[88] plant[89] and yeast[90-92] models of copper accumulation and misregulation.

Design of more sensitive next-generation sensors for detection of endogenous levels of Cu^+ in living cells and tissue. Application of the NS4' receptor to different fluorophore platforms has yielded next-generation probes that allow the detection of endogenous copper levels in different biological models. For example, replacement of the fluorine atoms in the BODIPY core with the more electron-rich methoxy substituents afforded Coppersensor 3 (CS3).[18] (Figure 1-3) Increasing the electron density at the fluorophore (PeT acceptor component) resulted in a turn-on response enhancement (75-fold for CS3 vs 10-fold for CS1) as well as higher quantum yield ($\phi = 0.40$ for CS3 vs $\phi = 0.13$ for CS1). These improvements, in combination with a tighter binding affinity for Cu(I) ($K_d = 9 \times 10^{-14}$ M), allowed for the visualization of endogenous levels of labile copper in HEK 293T that could be depleted by treatment with the cell-impermeable chelator bathocuproine disulfonate (BCS). Additionally, CS3 was able to report on neuronal copper translocation upon depolarization with KCl. The biological interpretation suggested by these pilot experiments was confirmed by X-ray fluorescence microscopy (XFM) of analogous fixed samples, which directly showed that copper moves from somatic cell bodies to peripheral dendritic processes upon stimulation. (Figure 1-5a).

Additionally, work from others has exploited the use of CS3 as a complementary tool to study copper in other biological models. Among these studies are included the evaluation of CTR2 functions,[93,94] use of the probe to track the efficiency of copper depletion or supplementation treatments[95] and the implementation of the dye in screening assays to study the endogenous ATP7A-transport of copper into lysosomes as a response to elevation in copper levels.[96] More recently, a comprehensive suite of techniques, which were pursued after observations with the CS3 probe, revealed a new organelle termed the "cuprosome" that acts as storage for reversible sequestration of copper in response to zinc deficiency in the green algae *Chlamydomonas reinhardtii*.[97] The development and further use of Ctrl-CS3, a matched control dye to CS3 that is unable to bind copper due to the replacement of the thioether motifs with methylene units (Figure 1-3), allowed for the assessment of fluorescent hot spots that were observed with CS3 (but not with the control probe) in higher frequency in zinc-deficient cells than in control cells (Figure 1-

5b). In addition, CS3 (but not Ctrl-CS3) fluorescence was diminished upon copper chelation. Direct metal analysis techniques like Nano-SIMS and X-ray absorption spectroscopy, in combination with supplementary biochemical assays, were used to confirm the existence of these copper traps and suggest that the apparent reversible sequestration of copper in these compartments may play a role in minimizing protein mismetalation during zinc deficiency while maintaining copper stores for future use.

Despite the utility of the BODIPY-based probes in various biological models, the use of this fluorophore scaffold has been limited in other applications. Its relatively high hydrophobicity has led to restricted implementation of the probes to study more complex systems such as tissue and cell types with differential hydrophilicities due to uneven distribution and staining as well as limited photostability, particularly in the methoxy-substituted BODIPY forms, has hindered their use for prolonged imaging experiments. In efforts to improve the properties of these reagents, we recently developed a series of Cu(I)-responsive probes based on the rhodol scaffold. This hybrid fluorescein-rhodamine fluorophore shows high tunability in visible excitation/emission profiles and signal-to-noise responses, high optical brightness as well as improved hydrophilicity and photostability.[98] Indeed, the use of different amine substituents on the xanthone core gave rise to the Copper Rhodol (CR) family.[19] Of the five initial sensors, Copper Rhodol 3 (CR3) was the best performing with a 13-fold turn on response to Cu(I) *in vitro* (Figure 1-3). Further modification to the pendant aryl ring by substitution of the *ortho* methyl with a bulkier trifluoromethyl analog afforded Copper Fluor 3 (CF3, Figure 1-3). This CH_3 to CF_3 modification introduces two advantages: (1) non-radiative decay pathways by rotations about the aryl-aryl bond that decrease fluorescence quantum yield are diminished, and (2) reduced electron density in the aryl ring (PeT donor component) favors PeT quenching of the unbound probe. Consequently, CF3 exhibits an improved 40-fold fluorescence enhancement upon Cu(I) binding with a dissociation constant K_d = 3 x 10^{-13} M. The more hydrophilic nature of CR3 and CF3 compared to CS3 was confirmed by measurements of apparent octanol/water distribitution coefficients (logD values of 0.96, 1.15 and 3.46, respectively, where larger values indicate greater hydrophobicity).

The improved properties of the CF3 probe allowed its use for assessing labile Cu(I) dynamics in dissociated hippocampal neuronal cultures and retinal tissue by one- and two-photon microscopy. Molecular imaging of CF3 and the non-Cu(I)-responsive Ctrl-CF3 analog on dissociated hippocampal neurons and mouse retinal tissue that had been acutely treated with the copper chelator BCS showed decreased fluorescence for CF3 but unchanged signal for the control dye (Figure 1-6). After observing the presence of a labile copper pool in both systems, we sought to probe the effects of pharmacological (chelation with BCS) and genetic (CTR1 knockout) alteration of these copper pools on spontaneous activity, a fundamental property of developing neural circuits. In both cases, disruption of copper homeostasis resulted in increases in event frequency and the fraction of cells involved in spontaneous correlated activity, confirmed by calcium imaging. Taken together, the results identify a fundamental physiological role for copper in neural function. We have recently expanded this work to red-shifted versions that enable real-time monitoring of copper fluxes in other cell types, such as adipocytes, and these chemical probes have helped identify an essential role for copper in lipolysis, a major metabolic process in the body for burning fat.[20]

Finally, an added challenge for fluorescent probe design lies in the development of sensors with specific localization in order to assess exclusive pools of metal in subcellular compartments. In order to address this issue further modifications to the BODIPY core afforded Mito-CS1,[99] a mitochondrially-targetable probe that makes use of a triphenyl phosphonium targeting group for specific subcellular localization (Figure 1-3).[100] Mito-CS1 features a 10-fold turn-on response upon Cu(I) ligation with K_d = 7 x 10^{-12} M, localizes to the mitochondria in HEK 293T cells and patient fibroblasts, and responds well *in cellulo* in copper supplementation and chelation experiments. In combination with genetic models of copper misregulation and direct bulk metal measurements, the use of Mito-CS1 helped establish the concept of a prioritization of mitochondrial copper homeostasis over other cellular compartments, even in situations of systemic copper deficiency and mitochondrial metallochaperone malfunction. Specifically, molecular imaging experiments with patient-derived fibroblasts with mutations in the copper exporter ATP7A showed a relative increase in probe fluorescence that was confirmed by inductively coupled plasma optical emission spectroscopy (ICP-OES). Patient fibroblasts with mutations in mitochondrial copper metallochaperones SCO1 and SCO2 showed no appreciable difference compared to control fibroblasts in Mito-CS1 signal or ICP-OES measurements on isolated mitochondria, but showed decreased total copper levels vs wild type measured by ICP-OES (Figure 1-7). Combining these complementary techniques, Mito-CS1 imaging and ICP-OES results indicate that mitochondrial copper homeostasis is prioritized over other compartments even in the course of overall copper deficiency, presumably to preserve CcO and SOD activity.

Use of an NS3 receptor for sensing labile copper pools in living animals. Owing to the poor tissue-penetrating ability of visible light and the desire to apply Cu(I)-responsive probes to study thicker specimens like tissue and whole animals, efforts to develop sensors with longer-wavelength/near-infrared (NIR) excitation profiles have been applied. We combined an NS3 modified thioether receptor platform first reported by Fahrni[101] to the NIR fluorophore scaffold cyanine 7 to produce Coppersensor 790 (CS790).[102] (Figure 1-3) CS790 has a selective 15-fold turn-on response to Cu(I) with 760 nm excitation and 790 nm emission profile. Capping of the carboxylates with acetoxymethyl esters to aid in cell permeability and retention afforded CS790AM, which showed increases in fluorescence signal in HEK 293T cells that were pre-treated with $CuCl_2$ compared to control, as well as a reversal of this fluorescence enhancement when the copper chelator tris[2-(ethylthio)ethyl]amine (NS_3) was added. The probe was further capable of reporting changes in live hairless SKH-1 mice upon copper supplementation with $CuCl_2$ and chelation with ATN-224, the choline salt of tetrathiomolybdate currently in development as a treatment for Wilson's disease,[103] marking the first example of live-mouse copper imaging with a fluorescent sensor (Figure 1-8). Furthermore, CS790AM was used to monitor copper levels in $Atp7b^{-/-}$ mice, a murine model that is metabolically and phenotypically similar to Wilson's disease due to the inactivation of the ATP7B gene and subsequent anomalous accumulation of copper in several tissues.[6] Live-animal imaging showed increased fluorescence in livers of mutant mice relative to those from wild type mice, which could be reversed with copper chelator treatment. The collective results point to a path forward for the application of fluorescent copper probes to study physiology, disease diagnosis and monitor treatment of copper imbalance in whole animals.

Magnetic Resonance-based Copper Sensing Probes

Whereas metal-responsive fluorescent sensors provide a great tool to assess relative metal levels in living biological systems from the cell to tissue to organism level, the translational application to medicine can be limited by the intrinsic properties of the use of visible to near-infrared light as readout for metal activity. In this regard, magnetic resonance imaging (MRI) is a powerful, clinically-used molecular imaging technique that allows for the capture of three-dimensional images of organisms with up to cellular resolution.[104] Even though the most common contrast observed in MR images results from water molecules in different environments, the use of contrast agents with paramagnetic metals such as Mn^{2+}, Mn^{3+}, Fe^{3+}, Cu^{2+} and Gd^{3+} can be implemented to enhance image contrast. Of these paramagnetic metals, high spin Gd^{3+} is particularly well suited for this application and is indeed used in 40-50% of all clinical MRI applications.[105] The image enhancing abilities of coordination complexes of these metals relies on the ability to efficiently relax nearby nuclei and increase the relaxation rates of water protons.[106] Modulation of the relaxivity, the efficiency of a contrast agent to enhance the relaxation rate, by a specific analyte can therefore be applied to a sensing strategy.

The design of metal-responsive MR probes can implement the idea of relaxivity modulation to afford a toolbox that can be useful in studying complex contributions of metals to physiology and disease. There are a number of ways to affect the degree of relaxivity in a contrast agent sensor, including number of inner-sphere water molecules (q-modulation) as well as rotational tumbling time (τ_R-modulation). For a more in-depth discussion on the development and criteria for responsive MRI contrast agents as chemical sensors we refer the reader to the following review articles.[107-109]

Development of a MR-contrast agent for selective copper(II) sensing. Inspired by seminal work of Meade and coworkers in the development of EGad, a "smart" contrast agent that reports on β-galactosidase activity,[110,111] our laboratory reported the first copper-responsive MR-sensor Copper-Gad 1 (CG1).[112] (Figure 1-9) CG1 features a Gd^{3+} contrast agent platform coupled to an iminodiacetate ligand for Cu^{2+} binding, the prevalent oxidation state in extracellular fluids. In the absence of Cu^{2+}, the anionic carboxylate donors of the receptor hinder inner-sphere water access to the Gd^{3+} thereby minimizing relaxivity. Upon binding to Cu^{2+}, the Gd^{3+} is less sterically hindered leading to increased inner-sphere water access and proton relaxivity affording a turn-on response. CG1 presents a 41% increase in relaxivity upon selective binding of Cu^{2+} with $K_d = 167 \pm 48$ μM. We note that while binding was mostly selective to Cu^{2+}, the turn-on response was partially muted in the presence of 10-fold excess Zn^{2+}. Nevertheless, the response to Cu^{2+} was stronger, owing to its higher affinity on the Irving-Williams series, and provided a prototype candidate for prospective MR-based copper imaging in living systems.

Design of MR-contrast agents with thioether-rich receptors for copper (I) sensing. Following the initial results from the CG1 probe, we sought to improve upon the relatively modest sensitivity and change in relaxivity as well as selectivity versus Zn^{2+}. Additionally, we designed a new family of copper-responsive MR probes to be activated by Cu^{+} and/or Cu^{2+} in order to potentially track copper in its two biologically relevant oxidation states. To achieve this goal, we introduced various thioether-rich receptors to the Gd^{3+} contrast agent scaffold through a 2,6-dimethylpyridine linker to afford Copper-Gad probes 2-6 (CG2-CG6, Figure 1-9).[113] The pyridyl linker acts as a

coordination switch, where in the absence of analyte, the apo-receptor caps the Gd^{3+} center to minimize the interaction with inner-sphere water molecules and thus lowering the proton relaxivity. Upon analyte binding, the linker switches to a conformation that lowers the steric bulk around the Gd^{3+}, allowing for inner-sphere access of water and producing higher relaxivity. Introduction of thioether donors shifted the selectivity towards Cu^{+} binding in CG2-CG5, with relaxivity increases ranging from 92% to 360%, where higher turn-on responses correlate to higher S/N donor ratios. CG6 had a unique and equal response to Cu^{+} and Cu^{2+} due to a quick redox equilibration that favors the higher copper oxidation state, possibly due to the N/O/S donor set provided by the receptor. The composition and number of potential donors in the ligand set influences the binding affinities as well, where compounds with higher thioether coordination CG2 and CG3 presented higher Cu^{+} binding affinities, $K_d = 3.7 \times 10^{-14}$ M and 2.6×10^{-13} M, respectively. In comparison, sensors with only three potential donors (CG4 and CG5) showed lower affinities to Cu^{+} ($K_d = 1.4 \times 10^{-11}$ M and 3.2×10^{-11} M, respectively). The tetradentate N/S/O donor system in CG6 afforded a higher affinity for Cu^{2+} ($K_d = 9.9 \times 10^{-16}$ M) in comparison to the first-generation probe CG1. Additionally, to validate the potential use of these sensors for molecular imaging applications, we established that CG complexes are capable of visualizing changes in biologically relevant copper levels in T_1 phantom images at clinical field strengths.

We next evaluated the effects of anions on relaxivity changes for the CG probes. Relaxivity increases upon copper binding seen in the presence of phosphate anions are unaffected, however carboxylate-type anions including citrate, lactate and carbonate presumably bind to the Gd^{3+} contrast agent core and yield significantly lower increases in relaxivity upon analyte binding. To minimize anion sensitivity, we designed Copper-Gad 7 (CG7),[114] an analog to CG2 where the acetate groups on the Gd^{3+} contrast agent core are substituted by hexanedioate derivatives to shield the paramagnetic metal from biologically abundant anions by steric and electrostatic action (Figure 1-9). This modification led to a comparable relaxivity turn-on ratio to CG2 (340% for CG7 vs 360% for CG2) as well as an unperturbed selective binding of Cu^{+} over other biologically relevant cations in the N_2S_2 receptor. However, the Cu^{+} response for CG7 is not significantly affected by carboxylate or phosphate anions, revealing that the installation of peripheral carboxylate functionalities improves anion compatibility for MR-based copper sensing.

Design of a copper-responsive MR agent for biological imaging. As the CG series of MR-based probes features excellent *in vitro* properties, we were eager to explore their use in living systems, namely in *in cellulo* applications. However, due to the large size of contrast agent probes (like other typical Gd^{3+}-containing MR contrast agents such as Gd-DTPA and Gd-DOTA), we reasoned and confirmed that the Cu^{+}-responsive CG probes have poor cell membrane permeability and are largely confined to the extracellular space. In order to circumvent this issue, we introduced a polyarginine tag on the CG2 scaffold to improve cellular uptake of the probe. Synthesis of Arg_8CG2 resulted in a cell-permeable copper-responsive MR-based probe with comparable spectroscopic properties and response to Cu^{+} that allowed for the visualization of biological perturbations of copper levels in a murine Menkes disease model cell line.[115] Indeed, Arg_8CG2 showed greater cellular uptake compared to CG2 in HEK 293T cells as confirmed by ICP-MS studies of the lysed cells. Superior *in cellulo* relaxivity of Arg_8CG2 over CG2 was also established by copper supplementation and chelation experiments where HEK 293T cells treated with either $CuCl_2$ or the copper chelator BCS and later treated with probe (Arg_8CG2 or CG2) showed more pronounced differences in relaxivity (increases or decreases in the case of supplementation or

chelation respectively) for Arg_8CG2. Relaxivity measurements of the Menkes model fibroblast line WG1005, which bears a mutation in the *Atp7a* gene, compared to control fibroblasts MCH58, showed clear differences between the two cell lines as reported by Arg_8CG2. Furthermore, phantom imaging experiments of the two cell lines treated with copper or copper chelator resulted in clear contrast variations, pointing to the applicability of the MR-based probe for *in vivo* imaging (Figure 1-10) and representing a unique application for copper-responsive MRI.

Concluding Remarks

The use of thioether coordination chemistry for the selective ligation of copper has been exploited by biology and synthetic chemists alike. Structural and spectroscopic characterization of cuproprotein binding sites, in combination with the study of synthetic small-molecule model complexes, has revealed the privileged nature of the thioether moiety, via methionine coordination, as an important strategy for pH-independent and oxidation-resistant binding of the cuprous ion. Consequently, this type of binding has been extensively implemented in the development of copper-specific recognition moieties for molecular imaging applications. Indeed, the diverse array of small-molecule fluorescent copper sensors with varying properties (visible to NIR-excitation profiles, signal-to-noise contrast, hydrophilicity, etc.) has led to the identification of novel biological roles of copper as a signaling entity in addition to its canonical roles as a static cofactor within protein active sites. Furthermore, the use of thioether coordination of copper in different imaging modalities with more translatable potential, such as MRI, has pointed the way towards possible applications into disease diagnosis and treatment monitoring.

Despite the success of thioether coordination of copper as a strategy for selective metal sensing, the structural variety of the receptor moieties has been rather limited to the use of macrocyclic or aliphatic amines containing thioether donors. As such, apparent binding affinities of the resulting sensors, which can be narrowly altered by inclusion or modification of different reporter moieties (i.e. fluorophores), leave room for future innovation. Indeed, development of new ligands to explore effects of binding geometry and ligand topology/architecture on the affinity and selective binding of copper in biological systems is a worthwhile goal. The resulting expansion of the chemical toolbox of molecular probes will undoubtedly lead to new opportunities to discover and study new biology of copper and other metals.

Schemes and Figures

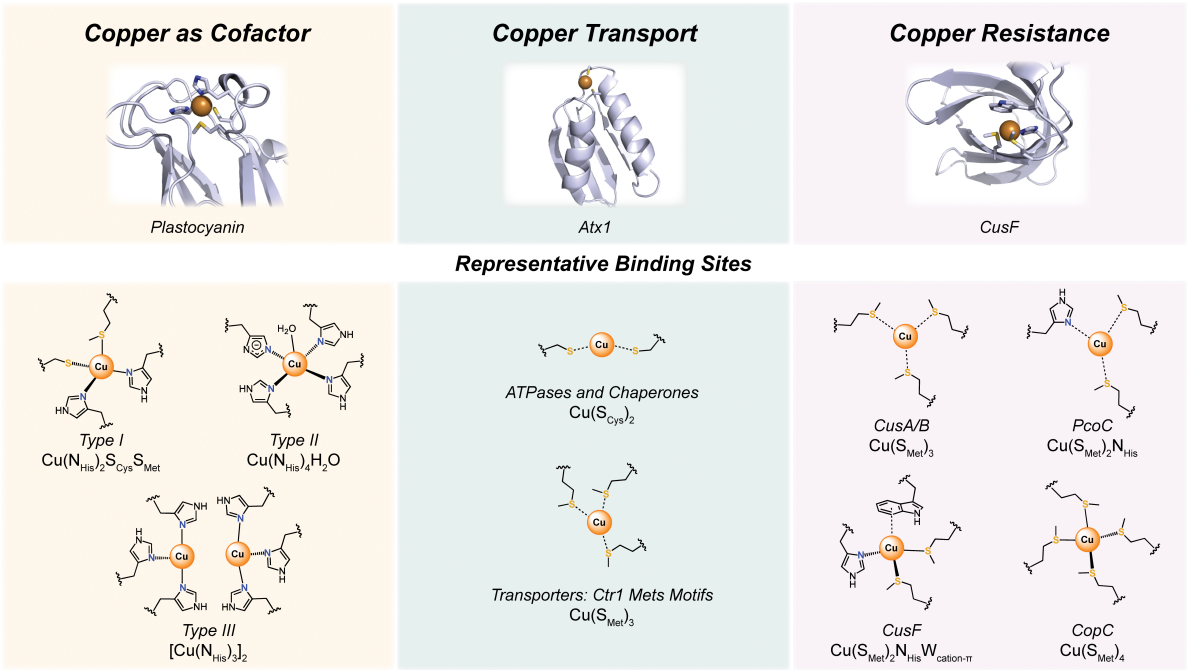

Figure 1-1. Examples of copper containing sites in Nature.

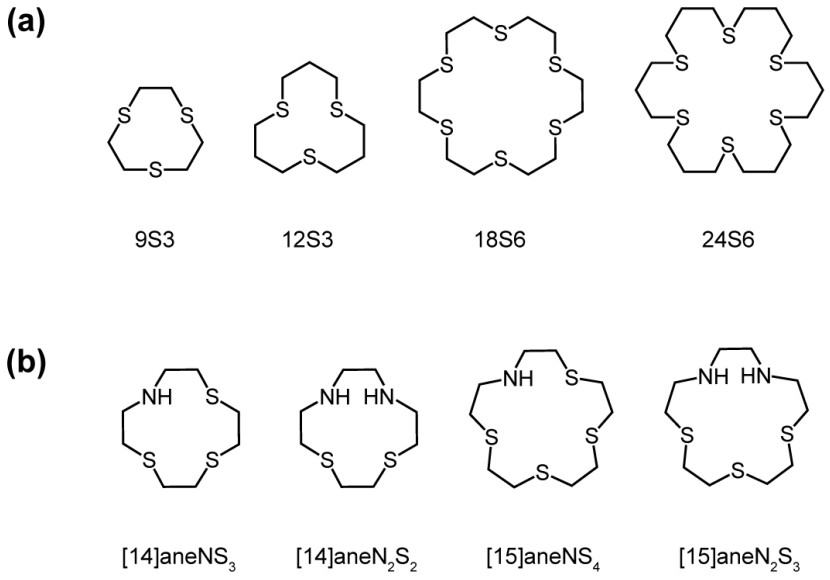

Figure 1-2. Metal binding (a) crown thioethers and (b) mixed-donor macrocyclic ligands with N_xS_{4-x} and N_xS_{5-x} donor sets

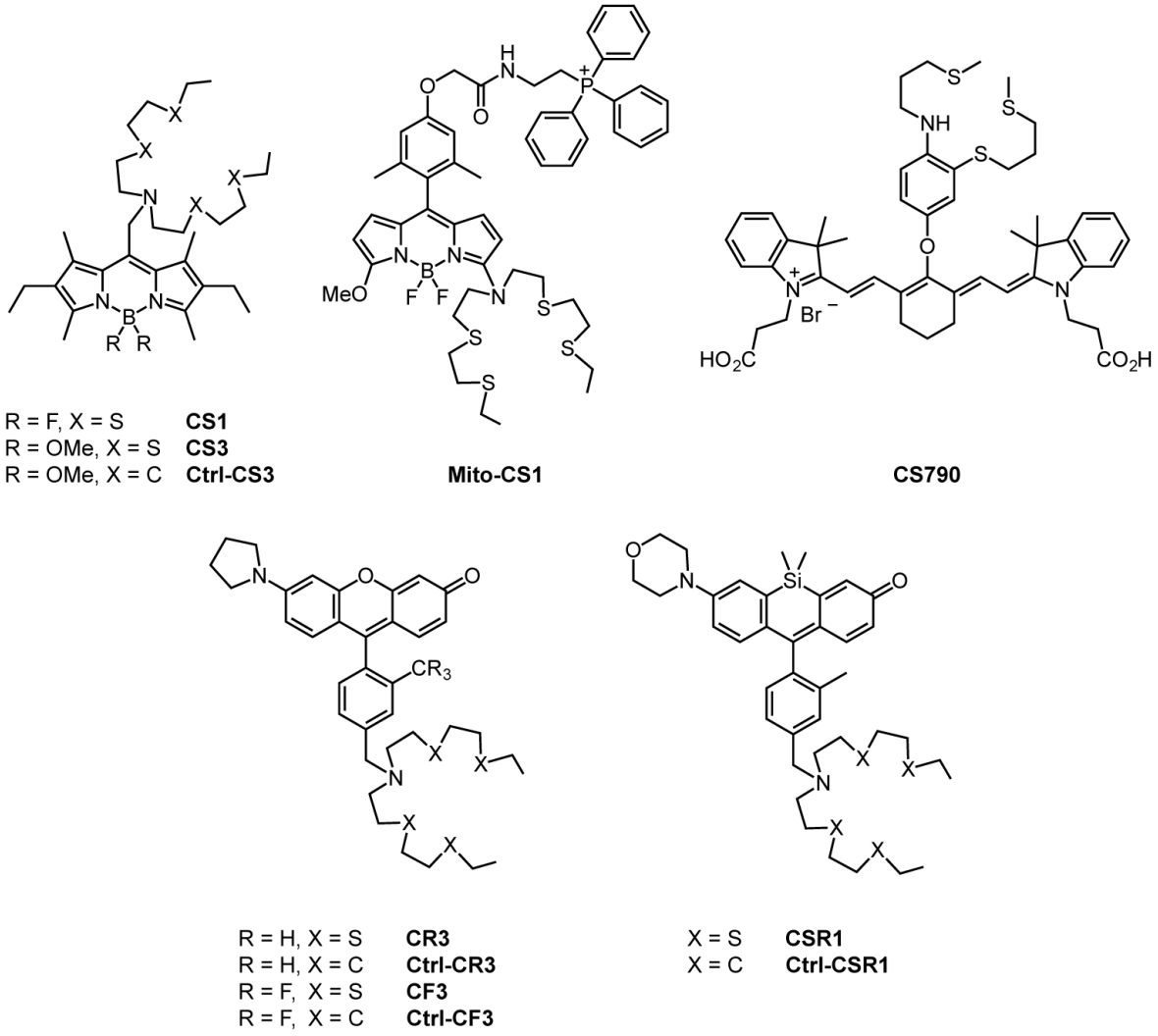

Figure 1-3. Cu^{+}-selective fluorescent probes bearing thioether receptors.

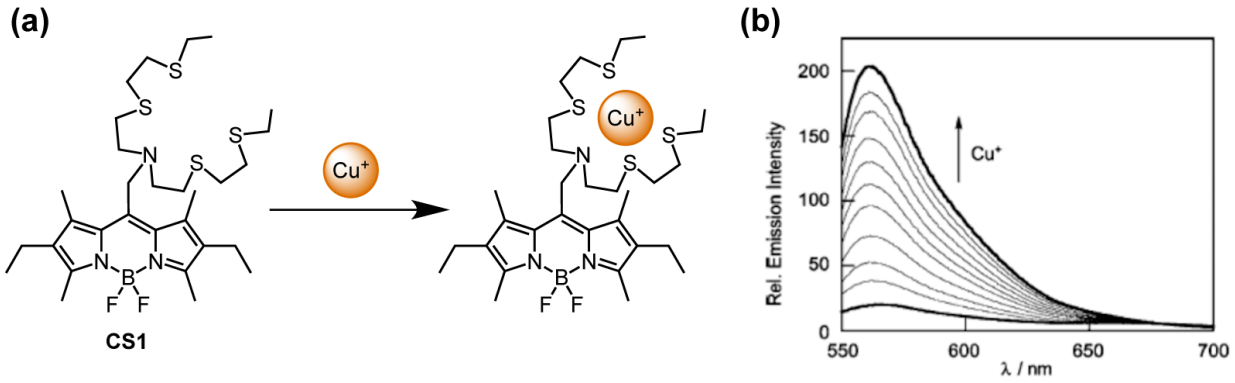

Figure 1-4. (a) Selective Cu^{+} recognition by CS1 and (b) fluorescence enhancement upon copper binding.

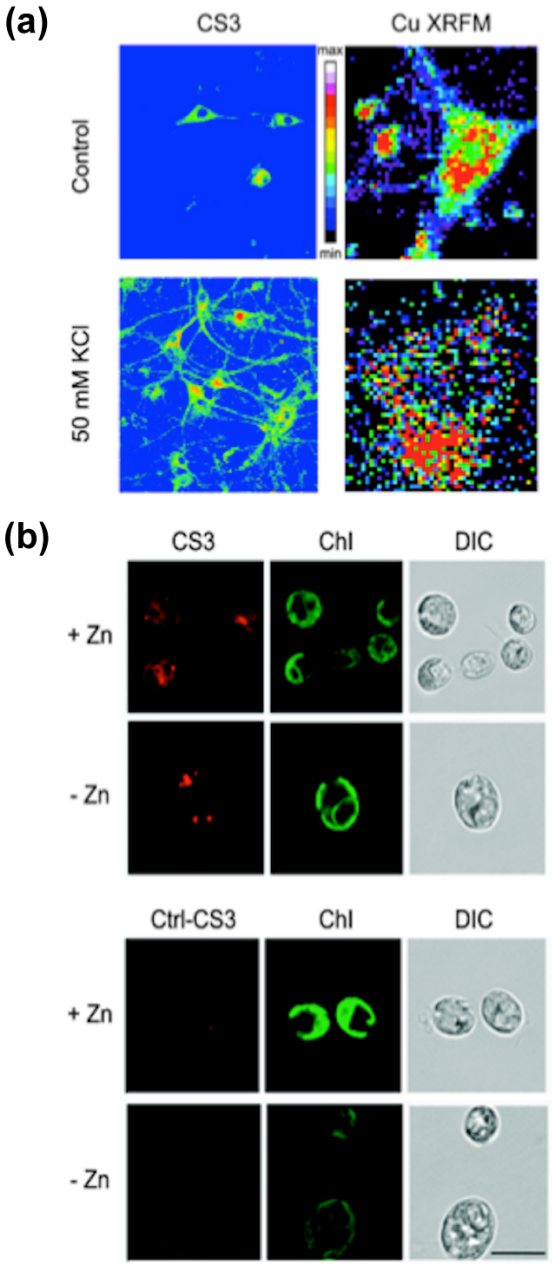

Figure 1-5. (a) Labile copper pool detection in rat hippocampal neuron cells with CS3 and XFM. (b) Monitoring copper accumulation in zinc-limited and zinc-replete wild-type *Chlamydomonas reinhardtii* (CC-4532) cells by using CS3 and Ctrl-CS3.

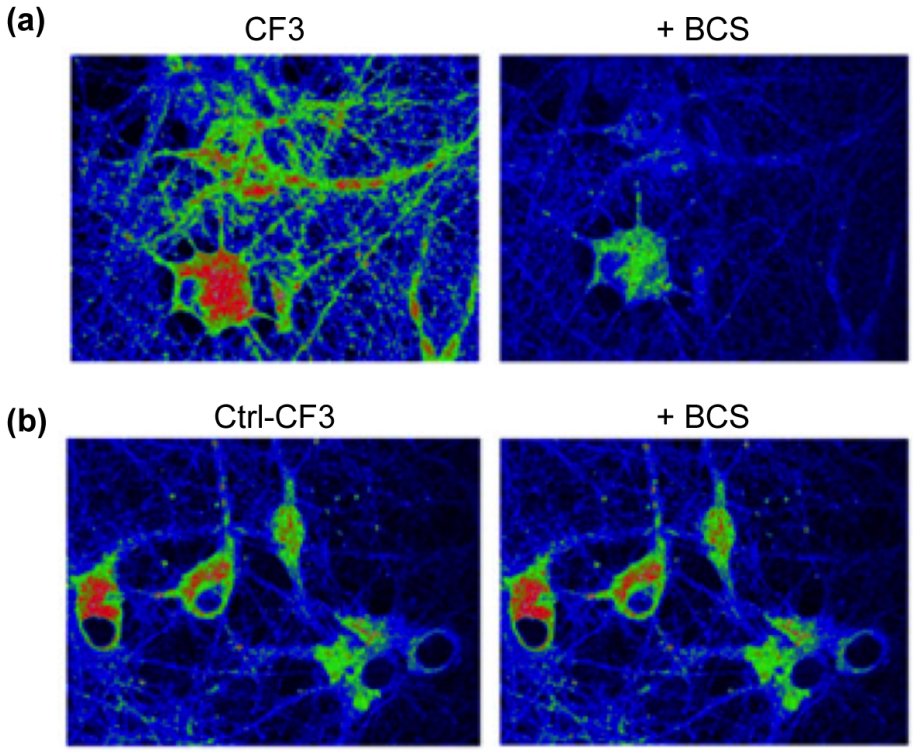

Figure 1-6. Two-photon imaging of (a) CF3 and (b) Ctrl-CF3 in hippocampal neurons in the absence and presence of copper chelator BCS.

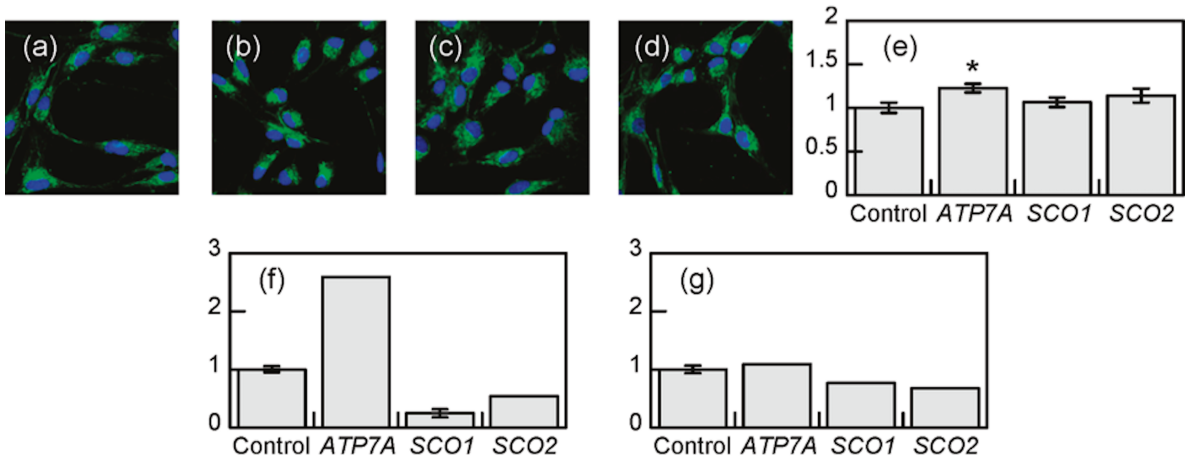

Figure 1-7. Live-cell molecular imaging of mitochondrial copper homeostasis in (a) control, (b) ATP7a, (c) SCO1 and (d) SCO2 patient fibroblasts with Mito-CS1. (e) Mean fluorescent intensities of (a)-(d). Measured total copper level in (f) patient fibroblasts and (g) mitochondria.

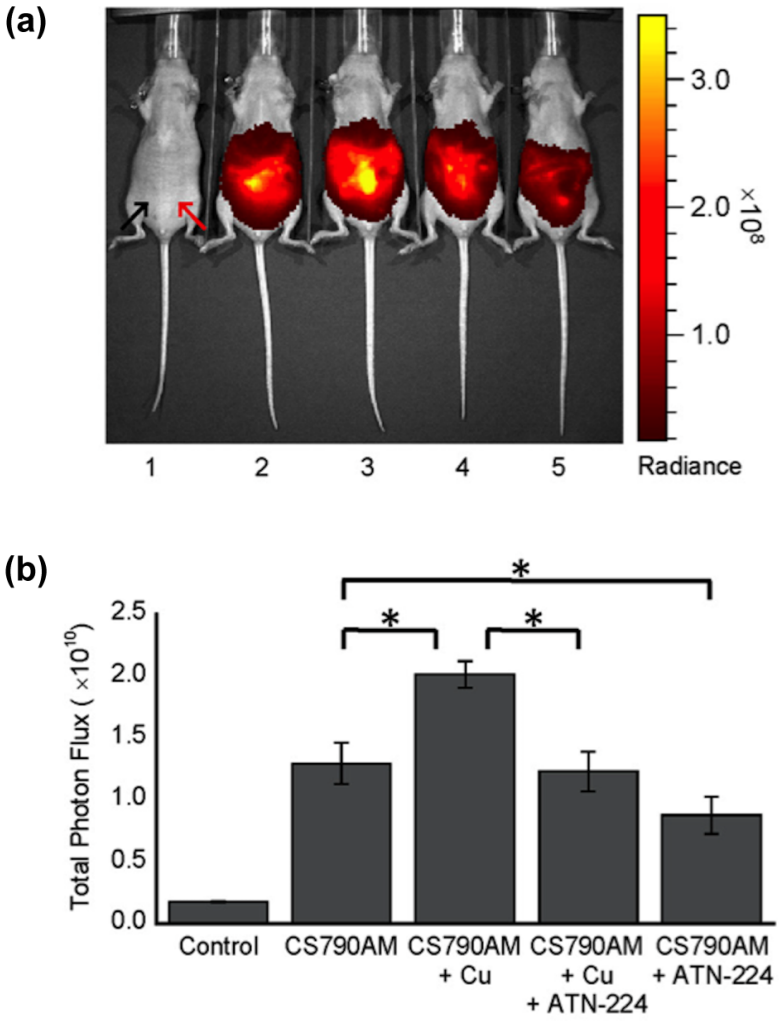

Figure 1-8. (a) Live SKH-1 mice imaging with fluorescent CS790AM probe. 1-vehicle only; 2-vehicle and CS790AM; 3-vehicle, $CuCl_2$ and CS790AM; 4-$CuCl_2$, ATN-224 and CS790AM; 5-vehicle, ATN-224 and CS790AM. (b) Calculated total photon flux from each mouse, 5 minutes after the injection of probe.

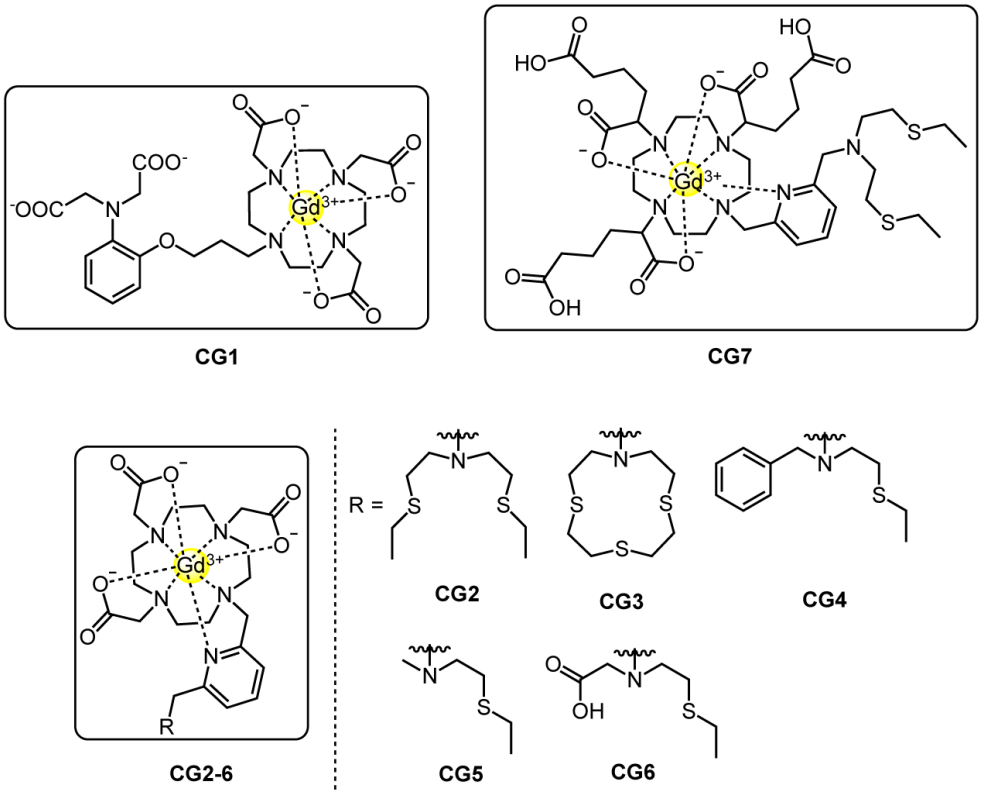

Figure 1-9. Copper selective MR-contrast agents with thioether receptors.

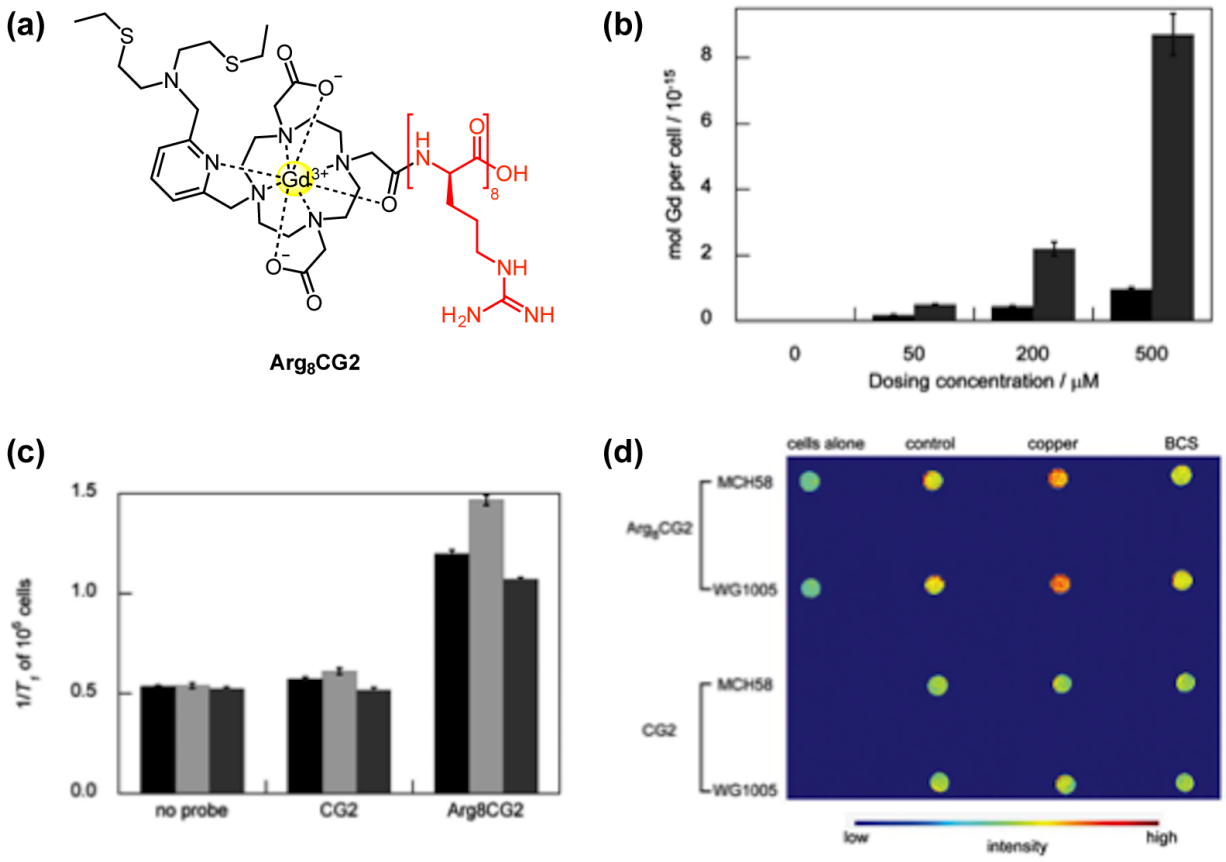

Figure 1-10. (a) Structure of the Arg_8CG2 construct. (b) Cellular uptake of CG2 (black) and Arg_8CG2 (gray) in HEK 293T cells at different dosing concentrations. Cells were lysed with RIPA buffer after probe incubation and analyzed by ICP-MS. (c) Relaxivity measurements of CG2 and Arg_8CG2 in HEK 293T cells. Bars represent the incubation of cells with control vehicle (black), copper (light gray) or BCS (dark grey). (d) T_1-weighed phantom images of MCH58 and WG1005 cells incubated with CG2 or Arg_8CG2.

References

1. Lippard, S. J.; Berg, J. M., *Principles of Bioinorganic Chemistry*. University Science Books: Mill Valley, CA, 1994.
2. Tapiero, H.; Townsend, D. M.; Tew, K. D., Trace elements in human physiology and pathology. Copper. *Biomed. Pharmacother.* **2003,** *57* (9), 386-98.
3. Vulpe, C.; Levinson, B.; Whitney, S.; Packman, S.; Gitschier, J., Isolation of a candidate gene for Menkes disease and evidence that it encodes a copper-transporting ATPase. *Nat. Genet.* **1993,** *3*, 7-13.
4. Kaler, S. G., ATP7A-related copper transport diseases - emerging concepts and future trends. *Nat. Rev. Neurol.* **2011,** *7*, 15-29.
5. La Fontaine, S.; Mercer, J. F., Trafficking of the copper-ATPases, ATP7A and ATP7B: role in copper homeostasis. *Arch. Biochem. Biophys.* **2007,** *463*, 149-167.
6. Lutsenko, S., Atp7b$^{-/-}$ mice as a model for studies of Wilson's disease. *Biochem. Soc. Trans.* **2008,** *36* (Pt 6), 1233-1238.
7. Huster, D.; Hoppert, M.; Lutsenko, S.; Zinke, J.; Lehmann, C.; Mossner, J.; Berr, F.; Caca, K., Defective cellular localization of mutant ATP7B in Wilson's disease patients and hepatoma cell lines. *Gastroenterology* **2003,** *124*, 335-345.
8. Huster, D., Structural and metabolic changes in Atp7b-/- mouse liver and potential for new interventions in Wilson's disease. *Ann. NY Acad. Sci.* **2014,** *1314*, 37-44.
9. Ayton, S.; Lei, P.; Bush, A. I., Metallostasis in Alzheimer's disease. *Free Radic. Biol. Med.* **2013,** *62*, 76-89.
10. Barnham, K. J.; Masters, C. L.; Bush, A. I., Neurodegenerative diseases and oxidative stress. *Nat. Rev. Drug Discov.* **2004,** *3* (3), 205-214.
11. Savelieff, M. G.; Lee, S.; Liu, Y.; Lim, M. H., Untangling amyloid-b, tau, and metals in Alzheimer's disease. *ACS Chem. Biol.* **2013,** *8*, 856-865.
12. Matlack, K. E.; Tardiff, D. F.; Narayan, P.; Hamamichi, S.; Caldwell, K. A.; Caldwell, G. A.; Lindquist, S., Clioquinol promotes the degradation of metal-dependent amyloid-b (Ab) oligomers to restore endocytosis and ameliorate Ab toxicity. *Proc. Natl. Acad. Sci. USA* **2014,** *111*, 4013-4018.
13. Vonk, W. I.; Kakkar, V.; Bartuzi, P.; Jaarsma, D.; Berger, R.; Hofker, M. H.; Klomp, L. W.; Wijmenga, C.; Kampinga, H. H.; van de Sluis, B., The Copper Metabolism MURR1 domain protein 1 (COMMD1) modulates the aggregation of misfolded protein species in a client-specific manner. *PLoS One* **2014,** *9*, e92408.
14. Xiao, G.; Fan, Q.; Wang, X.; Zhou, B., Huntington disease arises from a combinatory toxicity of polyglutamine and copper binding. *Proc. Natl. Acad. Sci. USA* **2013,** *110*, 14995-15000.
15. Burkhead, J. L.; Lutsenko, S., The role of copper as a modifier of lipid metabolism. In *Lipid Metabolism*, Baez, R. V., Ed. InTech: 2013; DOI: 10.5772/51819.
16. Huster, D.; Purnat, T. D.; Burkhead, J. L.; Ralle, M.; Fiehn, O.; Stuckert, F.; Olson, N. E.; Teupser, D.; Lutsenko, S., High copper selectively alters lipid metabolism and cell cycle machinery in the mouse model of Wilson disease. *J. Biol. Chem.* **2007,** *282*, 8343-8355.
17. Huster, D.; Lutsenko, S., Wilson disease: not just a copper disorder. Analysis of a Wilson disease model demonstrates the link between copper and lipid metabolism. *Mol. Biosyst.* **2007,** *3*, 816-824.

18. Dodani, S. C.; Domaille, D. W.; Nam, C. I.; Miller, E. W.; Finney, L. A.; Vogt, S.; Chang, C. J., Calcium-dependent copper redistributions in neuronal cells revealed by a fluorescent copper sensor and X-ray fluorescence microscopy. *Proc. Natl. Acad. Sci. USA* **2011,** *108* (15), 5980-5985.
19. Dodani, S. C.; Firl, A.; Chan, J.; Nam, C. I.; Aron, A. T.; Onak, C. S.; Ramos-Torres, K. M.; Paek, J.; Webster, C. M.; Feller, M. B.; Chang, C. J., Copper is an endogenous modulator of neural circuit spontaneous activity. *Proc. Natl. Acad. Sci. USA* **2014,** *111*, 16280-16285.
20. Krishnamoorthy, L.; Cotruvo, J. A. J.; Chan, J.; Kaluarachchi, H.; Muchenditsi, A.; Pendyala, V. S.; Jia, S.; Aron, A. T.; Vander Wal, M. N.; Guan, T.; Smaga, L. P.; Farhi, S. S.; New, E. J.; Lutsenko, S.; Chang, C. J., Copper regulates cyclic AMP-dependent lipolysis. *Nat. Chem. Biol.* **2016,** *12*, 586-592.
21. Turski, M. L.; Brady, D. C.; Kim, H. J.; Kim, B. E.; Nose, Y.; Counter, C. M.; Winge, D. R.; Thiele, D. J., A novel role for copper in Ras/mitogen-activated protein kinase signaling. *Mol. Cell. Biol.* **2012,** *32*, 1284-1295.
22. Brady, D. C.; Crowe, M. S.; Turski, M. L.; Hobbs, G. A.; Yao, X.; Chaikuad, A.; Knapp, S.; Xiao, K.; Campbell, S. L.; Thiele, D. J.; Counter, C. M., Copper is required for oncogenic BRAF signalling and tumorigenesis. *Nature* **2014,** *509*, 492-496.
23. Que, E. L. D., D. W. ; Chang, C. J. , Metals in neurobiology: Probing their chemistry and biology with molecular imaging. *Chem. Rev.* **2008,** *108* (5), 1517-1549.
24. Domaille, D. W. Q., E. L. ; Chang, C. J., Synthetic Fluorescent Sensors for Studying the Cell Biology of Metals. *Nat. Chem. Biol.* **2008,** *4*, 168-175.
25. Chan, J.; Dodani, S. C.; Chang, C. J., Reaction-based small-molecule fluorescent probes for chemoselective bioimaging. *Nature Chem.* **2012,** *4*, 973-984.
26. Go, Y. M.; Jones, D. P., Redox compartmentalization in eukaryotic cells. *Biochim. Biophys. Acta* **2008,** *1780* (11), 1273-1290.
27. Lutsenko, S., Human copper homeostasis: a network of interconnected pathways. *Curr. Opin. Chem. Biol.* **2010,** *14* (2), 211-217.
28. Hatori, Y.; Lutsenko, S., An expanding range of functions for the copper chaperone/antioxidant protein Atox1. *Antioxid. Redox Signal.* **2013,** *19*, 945-957.
29. Culotta, V. C.; Klomp, L. W. J.; Strain, J.; Casareno, R. L. B.; Krems, B.; Gitlin, J. D., The copper chaperone for superoxide dismutase. *J. Biol. Chem.* **1997,** *272*, 23469-23472.
30. Rae, T. D.; Schmidt, P. J.; Pufahl, R. A.; Culotta, V. C.; O'Halloran, T. V., Undetectable intracellular free copper: the requirement of a copper chaperone for superoxide dismutase. *Science* **1999,** *284* (5415), 805-808.
31. Leary, S. C. C., P. A.; Kaufman, B. A.; Guercin, G. H.; Mattman, A.; Palaty, J.; Lockitch, G.; Winge, D. R.; Rustin, P.; Horvath, R.; Shoubridge, E. A. , The Human Cytochrome c Oxidase Assembly Factors SCO1 and SCO2 Have Regulatory Roles in the Maintenance of Cellular Copper Homeostasis. *Cell. Metab.* **2007,** *5* (1), 9-20.
32. Punter, F. A.; Adams, D. L.; Glerum, D. M., Characterization and localization of human COX17, a gene involved in mitochondrial copper transport. *Hum. Genet.* **2000,** *107* (1), 69-74.
33. Pearson, R. G., Hard and soft acids and bases. *J. Am. Chem. Soc.* **1963,** *85* (22), 3533-3539.
34. Ahrland, S.; Chatt, J.; Davies, N. R., The relative affinites of ligand atoms for acceptor molecules and ions. *Quarterly Reviews* **1958,** *12* (3), 265-276.

35. Westerby, B. C.; Juntunen, K. L.; Leggett, G. H.; Pett, V. B.; Koenigbauer, M. J.; Purgett, M. D.; Taschner, M. J.; Ochrymowycz, L. A.; Rorabacher, D. B., Macrocyclic polyamino polythiaether ligands with NxS4-x and NxS5-x donor sets - protonation constants, stability-constants, and kinetics of complex-formation with the aquocopper(ii) ion. *Inor. Chem.* **1991,** *30* (9), 2109-2120.
36. Reedijk, J., Plasticity in the copper-thioether bond: manifestation in blue Cu proteins and in synthetic analogs. *J. Inorg. Biochem.* **2012,** *115*, 182-185.
37. Davis, A. V.; O'Halloran, T. V., A place for thioether chemistry in cellular copper ion recognition and trafficking. *Nat. Chem. Biol.* **2008,** *4*, 148-151.
38. Colman, P. M.; Freeman, H. C.; Guss, J. M.; Murata, M.; Norris, V. A.; Ramshaw, J. A. M.; Venkatappa, M. P., X-ray crystal-structure analysis of plastocyanin at 2.7 A resolution *Nature* **1978,** *272* (5651), 319-324.
39. Nar, H.; Messerschmidt, A.; Huber, R.; Vandekamp, M.; Canters, G. W., Crystal-structure analysis of oxidized pseudomonas-aeruginosa azurin at pH 5.5 and pH 9.0 - a pH-induced conformational transition involves a peptide-bond flip. *J. Mol. Biol.* **1991,** *221* (3), 765-772.
40. Tsukihara, T.; Aoyama, H.; Yamashita, E.; Tomizaki, T.; Yamaguchi, H.; Shinzawaitoh, K.; Nakashima, R.; Yaono, R.; Yoshikawa, S., Structures of metal sites of oxidized bovine heart cytochrome-c-oxidase at 2.8 Angstrom. *Science* **1995,** *269* (5227), 1069-1074.
41. Lamb, A. L.; Wernimont, A. K.; Pufahl, R. A.; O'Halloran, T. V.; Rosenzweig, A. C., Crystal structure of the second domain of the human copper chaperone for superoxide dismutase. *Biochemistry* **2000,** *39* (7), 1589-1595.
42. Lamb, A. L.; Wernimont, A. K.; Pufahl, R. A.; Culotta, V. C.; O'Halloran, T. V.; Rosenzweig, A. C., Crystal structure of the copper chaperone for superoxide dismutase. *Nat. Struct. Biol.* **1999,** *6*, 724-729.
43. Wernimont, A. K.; Huffman, D. L.; Lamb, A. L.; O'Halloran, T. V.; Rosenzweig, A. C., Structural basis for copper transfer by the metallochaperone for the Menkes/Wilson disease proteins. *Nat. Struct. Biol.* **2000,** *7*, 766-771.
44. Anastassopoulou, I.; Banci, L.; Bertini, I.; Cantini, F.; Katsari, E.; Rosato, A., Solution structure of the Apo and copper(I)-loaded human metallochaperone HAH1. *Biochemistry* **2004,** *43* (41), 13046-13053.
45. Hamza, I. S., M. ; Klomp, L. W. ; Gitlin, J. D. , Interaction of the copper chaperone HAH1 with the Wilson disease protein is essential for copper homeostasis. *Proc. Nat. Acad. Sci. USA* **1999,** *96*, 13363-13368.
46. Larin, D.; Mekios, C.; Das, K.; Ross, B.; Yang, A. S.; Gilliam, T. C., Characterization of the interaction between the Wilson and Menkes disease proteins and the cytoplasmic copper chaperone, HAH1p. *J. Biol. Chem.* **1999,** *274* (40), 28497-28504.
47. Walker, J. M.; Tsivkovskii, R.; Lutsenko, S., Metallochaperone Atox1 transfers copper to the NH2-terminal domain of the Wilson's disease protein and regulates its catalytic activity. *J. Biol. Chem.* **2002,** *277* (31), 27953-27959.
48. Banci, L.; Bertini, I.; Ciofi-Baffoni, S.; Huffman, D. L.; O'Halloran, T. V., Solution structure of the yeast copper transporter domain Ccc2a in the apo and Cu(I)-loaded states. *J. Biol. Chem.* **2001,** *276* (11), 8415-8426.

49. Banci, L.; Bertini, I.; Del Conte, R.; D'Onofrio, M.; Rosato, A., Solution structure and backbone dynamics of the Cu(I) and apo forms of the second metal-binding domain of the Menkes protein ATP7A. *Biochemistry* **2004,** *43* (12), 3396-3403.
50. DeSilva, T. M.; Veglia, G.; Opella, S. J., Solution structures of the reduced and Cu(I) bound forms of the first metal binding sequence of ATP7A associated with Menkes disease. *Proteins* **2005,** *61* (4), 1038-1049.
51. Puig, S.; Lee, J.; Lau, M.; Thiele, D. J., Biochemical and genetic analyses of yeast and human high affinity copper transporters suggest a conserved mechanism for copper uptake. *J. Biol. Chem.* **2002,** *277*, 26021-26030.
52. Rubino, J. T.; Riggs-Gelasco, P.; Franz, K. J., Methionine motifs of copper transport proteins provide general and flexible thioether-only binding sites for Cu(I) and Ag(I). *J. Biol. Inorg. Chem.* **2010,** *15*, 1033-1049.
53. Pope, C. R.; Flores, A. G.; Kaplan, J. H.; Unger, V. M., Structure and function of copper uptake transporters. *Curr. Top. Membr.* **2012,** *69*, 97-112.
54. De Feo, C. J.; Aller, S. G.; Siluvai, G. S.; Blackburn, N. J.; Unger, V. M., Three-dimensional structure of the human copper transporter hCTR1. *Proc. Nat. Acad. Sci. USA* **2009,** *106* (11), 4237-4242.
55. Rensing, C.; Fan, B.; Sharma, R.; Mitra, B.; Rosen, B. P., CopA: An Escherichia coli Cu(I)-translocating P-type ATPase. *Proc. Nat. Acad. Sci. USA* **2000,** *97* (2), 652-656.
56. Paulsen, I. T.; Park, J. H.; Choi, P. S.; Saier, M. H., Jr., A family of gram-negative bacterial outer membrane factors that function in the export of proteins, carbohydrates, drugs and heavy metals from gram-negative bacteria. *FEMS Microbiol. Lett.* **1997,** *156* (1), 1-8.
57. Long, F.; Su, C. C.; Zimmermann, M. T.; Boyken, S. E.; Rajashankar, K. R.; Jernigan, R. L.; Yu, E. W., Crystal structures of the CusA efflux pump suggest methionine-mediated metal transport. *Nature* **2010,** *467* (7314), 484-488.
58. Bagai, I.; Liu, W.; Rensing, C.; Blackburn, N. J.; McEvoy, M. M., Substrate-linked conformational change in the periplasmic component of a Cu(I)/Ag(I) efflux system. *J. Biol. Chem.* **2007,** *282* (49), 35695-35702.
59. Kulathila, R.; Kulathila, R.; Indic, M.; van den Berg, B., Crystal Structure of Escherichia coli CusC, the Outer Membrane Component of a Heavy Metal Efflux Pump. *Plos One* **2011,** *6* (1), 7.
60. Franke, S.; Grass, G.; Rensing, C.; Nies, D. H., Molecular analysis of the copper-transporting efflux system CusCFBA of Escherichia coli. *J. Bacteriol.* **2003,** *185* (13), 3804-3812.
61. Loftin, I. R.; Franke, S.; Blackburn, N. J.; McEvoy, M. M., Unusual Cu(I)/Ag(I) coordination of Escherichia coli CusF as revealed by atomic resolution crystallography and X-ray absorption spectroscopy. *Protein Sci.* **2007,** *16* (10), 2287-2293.
62. Xue, Y.; Davis, A. V.; Balakrishnan, G.; Stasser, J. P.; Staehlin, B. M.; Focia, P.; Spiro, T. G.; Penner-Hahn, J. E.; O'Halloran, T. V., Cu(I) recognition via cation-pi and methionine interactions in CusF. *Nat. Chem. Biol.* **2008,** *4*, 107-109.
63. Peariso, K.; Huffman, D. L.; Penner-Hahn, J. E.; O'Halloran, T. V., The PcoC copper resistance protein coordinates Cu(I) via novel S-methionine interactions. *J. Am. Chem. Soc.* **2003,** *125*, 342-343.

64. Arnesano, F.; Banci, L.; Bertini, I.; Mangani, S.; Thompsett, A. R., A redox switch in CopC: An intriguing copper trafficking protein that binds copper(I) and copper(II) at different sites. *Proc. Nat. Acad. Sci. USA* **2003,** *100* (7), 3814-3819.
65. Arnesano, F.; Banci, L.; Bertini, I.; Thompsett, A. R., Solution structure of CopC: A cupredoxin-like protein involved in copper homeostasis. *Structure* **2002,** *10* (10), 1337-1347.
66. Arnesano, F.; Banci, L.; Bertini, I.; Felli, I. C.; Luchinat, C.; Thompsett, A. R., A strategy for the NMR characterization of type II copper(II) proteins: the case of the copper trafficking protein CopC from Pseudomonas syringae. *J. Am. Chem. Soc.* **2003,** *125* (24), 7200-7208.
67. Zhang, L.; Koay, M.; Maher, M. J.; Xiao, Z.; Wedd, A. G., Intermolecular transfer of copper ions from the CopC protein of Pseudomonas syringae. Crystal structures of fully loaded Cu(I)Cu(II) forms. *J. Am. Chem. Soc.* **2006,** *128* (17), 5834-5850.
68. Murray, S. G.; Hartley, F. R., Coordination chemistry of thioethers, selenoethers, and telluroethers in transition-metal complexes. *Chem. Rev.* **1981,** *81* (4), 365-414.
69. Cooper, S. R., Crown thioether chemistry. *Acc. Chem. Res.* **1988,** *21* (4), 141-146.
70. Cooper, S. R.; Rawle, S. C., Crown thioether chemistry. *Struct. Bond.* **1990,** *72*, 1-72.
71. Guss, J. M.; Freeman, H. C., Structure of oxidized polar plastocyanin at 1.6 A resolution *J. Mol. Biol.* **1983,** *169* (2), 521-563.
72. Adman, E. T.; Stenkamp, R. E.; Sieker, L. C.; Jensen, L. H., Crystallographic model for azurin at 3-A resolution. *J. Mol. Biol.* **1978,** *123* (1), 35-47.
73. Rorabacher, D. B.; Martin, M. J.; Koenigbauer, M. J.; Malik, M.; Schroeder, R. R.; Endicott, J. F.; Ochrymowycz, L. A., Structural Effects on Cu(II)/Cu(I) Potentials and Electron Transfer Kinetics as Well as Related Physical Peoperties in Polythiaether and Polyaminothiaether Complexes. In *Copper Coordination Chemistry: Biochemical and Inorganic Perspectives*, Karlin, K. D.; Zubieta, J., Eds. Adenine Press: Guilderland, NY, 1983; p 167.
74. Diaddario, L. L.; Dockal, E. R.; Glick, M. D.; Ochrymowycz, L. A.; Rorabacher, D. B., Structural changes accompanying electron transfer in copper(II)/copper(I) complexes involving related open-chain and cyclic tetrathia ether ligands. *Inorg. Chem.* **1985,** *24* (3), 356-363.
75. Bernardo, M. M.; Heeg, M. J.; Schroeder, R. R.; Ochrymowycz, L. A.; Rorabacher, D. B., Comparison of the influence of saturated nitrogen and sulfur donor atoms on the properties of copper(II/I)-macrocyclic polyamino polythiaether ligand complexes: redox potentials and protonation and stability constants of $Cu^{I}L$ species and new structural data. *Inorg. Chem.* **1992,** *31*, 191-198.
76. Ambundo, E. A.; Ochrymowycz, L. A.; Rorabacher, D. B., Electron-transfer kinetics of tris(2-(methylthioethyl))aminecopper(II/I). A tripodal ligand complex exhibiting virtual C-3v symmetry. *Inorganic Chemistry* **2001,** *40* (20), 5133-5138.
77. Ambundo, E. A.; Yu, Q. Y.; Ochrymowycz, L. A.; Rorabacher, D. B., Electron-transfer kinetics of copper(II/I) tripodal ligand complexes. *Inorg. Chem.* **2003,** *42* (17), 5267-5273.
78. Cotruvo, J. A.; Aron, A. T.; Ramos-Torres, K. M.; Chang, C. J., Synthetic fluorescent probes for studying copper in biological systems. *Chem. Soc. Rev.* **2015,** *44* (13), 4400-4414.
79. Aron, A. T.; Ramos-Torres, K. M.; Cotruvo, J. A.; Chang, C. J., Recognition- and Reactivity-Based Fluorescent Probes for Studying Transition Metal Signaling in Living Systems. *Acc. Chem. Res.* **2015,** *48* (8), 2434-2442.

80. Fahrni, C. J., Synthetic fluorescent probes for monovalent copper. *Curr. Opin. Chem. Biol.* **2013,** *17*, 656-662.
81. de Silva, A. P.; Gunaratne, H. Q. N.; Gunnlaugsson, T.; Huxley, A. J. M.; McCoy, C. P.; Rademacher, J. T.; Rice, T. E., Signaling Recognition Events with Fluorescent Sensors and Switches. *Chem. Rev.* **1997,** *97*, 1515-1566.
82. de Silva, A. P.; Moody, T. S.; Wright, G. D., Fluorescent PET (photoinduced electron transfer) sensors as potent analytical tools. *Analyst* **2009,** *134* (12), 2385-93.
83. Valeur, B.; Leray, I., Design principles of fluorescent molecular sensors for cation recognition. *Coord. Chem. Rev.* **2000,** *205* (1), 3-40.
84. Chandross, E. A.; Thomas, H. T., Intramolecular exciplex formation in naphthylalkylamines. *Chem. Phys. Lett.* **1971,** *9* (5), 393-396.
85. Zeng, L.; Miller, E. W.; Pralle, A.; Isacoff, E. Y.; Chang, C. J., A selective turn-on fluorescent sensor for imaging copper in living cells. *J. Am. Chem. Soc.* **2006,** *128*, 10-11.
86. Yang, L.; McRae, R.; Henary, M. M.; Patel, R.; Lai, B.; Vogt, S.; Fahrni, C. J., Imaging of the intracellular topography of copper with a fluorescent sensor and by synchrotron x-ray fluorescence microscopy. *Proc. Natl. Acad. Sci. USA* **2005,** *102* (32), 11179-11184.
87. Price, K. A.; Hickey, J. L.; Xiao, Z.; Wedd, A. G.; James, S. A.; Liddell, J. R.; Crouch, P. J.; White, A. R.; Donnelly, P. S., The challenges of using a copper fluorescent sensor (CS1) to track intracellular distributions of copper in neuronal and glial cells. *Chem. Sci.* **2012,** *3*, 2748-2759.
88. Espirito Santo, C.; Lam, E. W.; Elowsky, C. G.; Quaranta, D.; Domaille, D. W.; Chang, C. J.; Grass, G., Bacterial killing by dry metallic copper surfaces. *Appl. Environ. Microbiol.* **2011,** *77*, 794-802.
89. Bernal, M.; Casero, D.; Singh, V.; Wilson, G. T.; Grande, A.; Yang, H.; Dodani, S. C.; Pellegrini, M.; Huijser, P.; Connolly, E. L.; Merchant, S. S.; Kramer, U., Transcriptome sequencing identifies SPL7-regulated copper acquisition genes FRO4/FRO5 and the copper dependence of iron homeostasis in Arabidopsis. *Plant Cell* **2012,** *24*, 738-761.
90. Beaudoin, J.; Ioannoni, R.; López-Maury, L.; Bähler, J.; Ait-Mohand, S.; Guérin, B.; Dodani, S. C.; Chang, C. J.; Labbé, S., Mfc1 is a novel forespore membrane copper transporter in meiotic and sporulating cells. *J. Biol. Chem.* **2011,** *286*, 34356-34372.
91. Cusick, K. D.; Minkin, S. C.; Dodani, S. C.; Chang, C. J.; Wilhelm, S. W.; Sayler, G. S., Inhibition of copper uptake in yeast reveals the copper transporter Ctr1p as a potential molecular target of saxitoxin. *Environ. Sci. Technol.* **2012,** *46*, 2959-2966.
92. Quaranta, D.; Krans, T.; Espirito Santo, C.; Elowsky, C. G.; Domaille, D. W.; Chang, C. J.; Grass, G., Mechanisms of contact-mediated killing of yeast cells on dry metallic copper surfaces. *Appl. Environ. Microbiol.* **2011,** *77*, 416-426.
93. Ohrvik, H.; Nose, Y.; Wood, L. K.; Kim, B. E.; Gleber, S. C.; Ralle, M.; Thiele, D. J., Ctr2 regulates biogenesis of a cleaved form of mammalian Ctr1 metal transporter lacking the copper- and cisplatin-binding ecto-domain. *Proc. Natl. Acad. Sci. USA* **2013,** *110*, E4279-E4288.
94. Huang, C. P.; Fofana, M.; Chan, J.; Chang, C. J.; Howell, S. B., Copper transporter 2 regulates intracellular copper and sensitivity to cisplatin. *Metallomics* **2014,** *6*, 654-661.
95. Ding, X.; Xie, H.; Kang, Y. J., The significance of copper chelators in clinical and experimental application. *J. Nutr. Biochem.* **2011,** *22*, 301-310.

96. Polishchuk, E. V.; Concilli, M.; Iacobacci, S.; Chesi, G.; Pastore, N.; Piccolo, P.; Paladino, S.; Baldantoni, D.; van Ijzendoorn, S. C.; Chan, J.; Chang, C. J.; Amoresano, A.; Pane, F.; Pucci, P.; Tarallo, A.; Parenti, G.; Brunetti-Pierri, N.; Settembre, C.; Ballabio, A.; Polishchuk, R. S., Wilson disease protein ATP7B utilizes lysosomal exocytosis to maintain copper homeostasis. *Dev. Cell* **2014**, *29* (6), 686-700.
97. Hong-Hermesdorf, A.; Miethke, M.; Gallaher, S. D.; Kropat, J.; Dodani, S. C.; Chan, J.; Barupala, D.; Domaille, D. W.; Shirasaki, D. I.; Loo, J. A.; Weber, P. K.; Pett-Ridge, J.; Stemmler, T. L.; Chang, C. J.; Merchant, S. S., Sub-cellular metal imaging identifies dynamic sites of Cu accumulation in *Chlamydomonas*. *Nat. Chem. Biol.* **2014,** *10*, 1034-1042.
98. Whitaker, J. E.; Haugland, R. P.; Ryan, D.; Hewitt, P. C.; Haugland, R. P.; Prendergast, F. G., Fluorescent rhodol derivatives: versatile, photostable labels and tracers. *Anal. Biochem.* **1992,** *207*, 267-279.
99. Dodani, S. C.; Leary, S. C.; Cobine, P. A.; Winge, D. R.; Chang, C. J., A targetable fluorescent sensor reveals that copper-deficient SCO1 and SCO2 patient cells prioritize mitochondrial copper homeostasis. *J. Am. Chem. Soc.* **2011,** *133* (22), 8606-8616.
100. Murphy, M. P.; Smith, R. A., Targeting antioxidants to mitochondria by conjugation to lipophilic cations. *Annu. Rev. Pharmacol. Toxicol.* **2007,** *47*, 629-656.
101. Chaudhry, A. F.; Verma, M.; Morgan, M. T.; Henary, M. M.; Siegel, N.; Hales, J. M.; Perry, J. W.; Fahrni, C. J., Kinetically controlled photoinduced electron transfer switching in Cu(I)-responsive fluorescent probes. *J. Am. Chem. Soc.* **2010,** *132* (2), 737-747.
102. Hirayama, T.; Van de Bittner, G. C.; Gray, L. W.; Lutsenko, S.; Chang, C. J., Near-infrared fluorescent sensor for in vivo copper imaging in a murine Wilson disease model. *Proc. Natl. Acad. Sci. USA* **2012,** *109* (7), 2228-2233.
103. Brewer, G. J., Zinc and tetrathiomolybdate for the treatment of Wilson's disease and the potential efficacy of anticopper therapy in a wide variety of diseases. *Metallomics* **2009,** *1*, 199-206.
104. Kuhn, W., NMR Microscopy—Fundamentals, Limits and Possible Applications. *Angew. Chem. Int. Ed. Engl.* **1990,** *29* (1), 1-19.
105. Raymond, K. N.; Pierre, V. C., Next generation, high relaxivity gadolinium MRI agents. *Bioconjugate Chem.* **2005,** *16* (1), 3-8.
106. Caravan, P.; Ellison, J. J.; McMurry, T. J.; Lauffer, R. B., Gadolinium(III) chelates as MRI contrast agents: Structure, dynamics, and applications. *Chem. Rev.* **1999,** *99* (9), 2293-2352.
107. Yoo, B.; Pagel, M. D., An overview of responsive MRI contrast agents for molecular imaging. *Front. Biosci.* **2008,** *13*, 1733-1752.
108. Major, J. L.; Meade, T. J., Bioresponsive, cell-penetrating, and multimeric MR contrast agents. *Acc. Chem. Res.* **2009,** *42* (7), 893-903.
109. Que, E. L.; Chang, C. J., Responsive magnetic resonance imaging contrast agents as chemical sensors for metals in biology and medicine. *Chem. Soc. Rev.* **2010,** *39* (1), 51-60.
110. Moats, R. A.; Fraser, S. E.; Meade, T. J., A "smart" magnetic resonance imaging agent that reports on specific enzymatic activity. *Angew. Chem. Int. Ed. Engl.* **1997,** *36* (7), 726-728.
111. Louie, A. Y.; Huber, M. M.; Ahrens, E. T.; Rothbacher, U.; Moats, R.; Jacobs, R. E.; Fraser, S. E.; Meade, T. J., In vivo visualization of gene expression using magnetic resonance imaging. *Nat. Biotechnol.* **2000,** *18* (3), 321-325.

112. Que, E. L.; Chang, C. J., A smart magnetic resonance contrast agent for selective copper sensing. *J. Am. Chem. Soc.* **2006,** *128* (50), 15942-15943.
113. Que, E. L.; Gianolio, E.; Baker, S. L.; Wong, A. P.; Aime, S.; Chang, C. J., Copper-Responsive Magnetic Resonance Imaging Contrast Agents. *J. Am. Chem. Soc.* **2009,** *131* (24), 8527-8536.
114. Que, E. L.; Gianolio, E.; Baker, S. L.; Aime, S.; Chang, C. J., A copper-activated magnetic resonance imaging contrast agent with improved turn-on relaxivity response and anion compatibility. *Dalton Trans.* **2010,** *39* (2), 469-476.
115. Que, E. L.; New, E. J.; Chang, C. J., A cell-permeable gadolinium contrast agent for magnetic resonance imaging of copper in a Menkes disease model. *Chem. Sci.* **2012,** *3* (6), 1829-1834.

Chapter 2:

Development of a Color Palette of Cu^{+} Responsive Probes Based on Center-Atom Substitution of the Rhodol Core

Portions of this work were performed in collaboration with the following persons:

Synthesis and *in vitro* characterization of CSF1 was performed by Shang Jia. Synthesis and *in vitro* characterization of CPF1 was performed by Dr. Safacan Kolemen.

Abstract

Multicolor, multi-analyte imaging experiments pose an attractive approach to the study and understanding of complex biological processes. To this end, the development of fluorescent sensors with a variety of excitation profiles via synthetic modification of the fluorophore reporters has proven to be an appropriate strategy. This Chapter summarizes the design, synthesis and application of a new family of copper probes based on center-atom substitution of the rhodol fluorophore platform. Application of this method afforded a palette of probes with distinctive optical features and selective turn-on responses upon Cu^+ binding. Additionally, confocal microscopy experiments revealed that this new scaffold is capable of detecting changes in the labile copper levels of different cell types.

Introduction

Visualization of ion fluxes in living cells with the use of fluorescent sensors has proven to be a well-suited approach to study the roles of metals, such as copper, in essential physiological functions.[1,2] Additionally, the involvement of these ions in more complex multi-component processes can be potentially evaluated with these chemical tools, as optical microscopy tolerates the simultaneous use of multiple probes as long as spectral bleeding of the incorporated chromophores is sufficiently minimized.[1,3-6] Against this backdrop, there is substantial motivation for the development and application of a variety of fluorophores to serve as reporters of bio-analyte function. Use of fluorogenic molecules that span the ultraviolet (UV), visible and near-infrared (NIR) spectrum in metal-sensing applications generates a versatile toolbox of probes that can be combined with other small-molecule or protein-based fluorescent reporters in multicolor imaging experiments.

The available collection of small-molecule copper sensors (Scheme 2-1) offers dyes that can be excitable in various regions of the energy spectrum.[7,8] Pyrazoline-based sensors CTAP-1[9] and CTAP-2,[10] as well as coumarin-based ACu1,[11] present absorption features in the UV range, while visible excitation profiles in different color regions are observed by fluorescein-based FluTPA1 (blue), BODIPY-based CS1,[12] CS3[13] and Mito-CS1[14] (green), rhodol-based CR3[15] and CF3[15] (green) and silicon rhodol based CSR1[16] (orange-red). Additionally, the cyanine fluorophore platform has been used to develop Probe 3[17] and CS790[18] as NIR sensors for copper. However, the spectral region between green and red excitation has been underutilized in the development of copper-responsive fluorogenic molecules.

The advantages gained by the implementation of xanthene-based dyes for copper detection, including enhanced hydrophilicity, high brightness, good quantum yield, sensitivity, etc., when compared to other established fluorophore scaffolds like BODIPY dyes, make this fluorophore core an exciting platform for molecular imaging applications.[15,16] In order to expand upon these improvements and fill the gap of excitation profiles available in the copper probe arsenal, we have implemented two common strategies to afford yellow-excitable sensors. First, we employed the substitution of the xanthene oxygen, a proven strategy that elicits red-shifts in the spectra of xanthene fluorophores.[19-29] Particularly, substitution with a quaternary carbon produces a 50-nm bathochromic shift in the excitation energy.[20] Secondly, use of a hybrid fluorescein-rhodamine dye – the rhodol platform – provides improved hydrophilicity, good optical brightness, photostability,

and insensitivity to changes in the physiological pH range, as well as a uniquely tunable scaffold.[30] Introduction of different amine substituents on the xanthene core leads to slightly altered optical features;[15,31] this results in a strategy that can be used for fine tuning of the spectral properties for specific applications. Therefore, we envisioned the construction of a small palette of probes bearing the quaternary carbon substitution in combination with two different amine substituents (Scheme 2-3) as a means to evaluate the properties of this new class of sensors.

Results and Discussion

Synthesis of Carbo-rhodol Based Copper Sensors. Inspired on the carbofluorescein dye platform, we sought to develop a palette of copper probes through the attachment of an arylmetal species that features a copper-binding receptor to a carboxanthone derivative. To that end, we combined the previously reported synthesis of anthrone **4**[23] with a substitution method to produce the rhodol functionality, as shown in Scheme 2-1. Briefly, Negishi cross-coupling of methyl 2-bromo-5-methoxybenzoate with 4-methoxybenzylzinc chloride provided methyl benzylbenzoate **1**, to which addition of methylmagnesium bromide afforded the alcohol derivative **2**. Demethylation and concomitant ring formation with BBr_3 to form **3**, followed by DDQ-mediated oxidation provided dihydroxy-carboxanthone **4** in good yields. Conversion to the corresponding ditriflate **5** allowed for subsequent nucleophilic aromatic substitution with stoichiometric cyclic amines (morpholine or piperidine) to produce mono-amino carboxanthones **6** and **7**. One-pot protecting group transformation through hydrolysis of the triflate with tetraethylammonium hydroxide, followed by protection of the phenol with *tert*-butyldimethylsilyl chloride yielded the protected-monoamino anthrones **8** and **9**.

Construction of the final copper probes, depicted in Scheme 2-2, proceeded through lithium halogen exchange of **12** to form an aryl lithium species featuring the thioether-rich metal binding domain and subsequent addition to appropriate xanthones **8** and **9** to afford the Copper Carbo-Rhodol analogues **CCR1** and **CCR4**, respectively. Additionally, the probe family was expanded with the replacement of the methyl substituent on the bottom aryl ring of **CCR1** and **CCR4** with a trifluoromethyl (CF_3) group. We have previously shown that introduction of this substitution leads to enhancements in the dynamic range and optical brightness of rhodol-based copper probes by (i) decreasing the available non-radiative decay pathways by rotational motions about the aryl-aryl bond and (ii) favoring PeT quenching in the unbound probe by withdrawing electron density from the receptor containing aryl ring.[15] This modification led to the synthesis of Copper Carbo-Fluor counterparts **CCF1** and **CCF4**.

Spectroscopic Properties of Carbo-rhodol Copper Sensors. Evaluation of the spectroscopic properties of the carbo-rhodol probes in aqueous conditions showed optical features parallel to the canonical rhodol-platform. Central-atom substitution of the xanthene core with a quaternary carbon indeed produces copper probes with red-shifted spectra. *Apo*-sensors exhibit broad absorption bands ($\lambda_{abs\ (apo)}$ 529 nm, $\varepsilon = 4.91 \times 10^3\ M^{-1}cm^{-1}$ for **CCR1,** $\lambda_{abs\ (apo)}$ 530 nm, $\varepsilon = 7.56 \times 10^3\ M^{-1}cm^{-1}$ for **CCR4**), similar to CopperRhodol analogues **CR1** and **CR4**. A typical 50-nm bathochromic shift in the absorption features, when compared to the classic rhodol sensors, is observed in the copper bound states ($\lambda_{abs\ (Cu)}$ 564 nm, $\varepsilon = 7.46 \times 10^3\ M^{-1}cm^{-1}$ for **CCR1,** $\lambda_{abs\ (Cu)}$ 586 nm, $\varepsilon = 2.23 \times 10^4\ M^{-1}cm^{-1}$ for **CCR4**). (Figures 2-1, 2-6) Additionally, lower energy fluorescence emission ($\lambda_{fl\ (Cu)}$ 602 nm for **CCR1**, ($\lambda_{fl\ (Cu)}$ 607 nm for **CCR4**) is enhanced with

addition of one equivalent of Cu^+ by 4.5- and 17.4-fold for the respective probes. (Figures 2-2, 2-7) The turn-on fluorescence responses of both sensors show high metal ion and oxidation state selectivity for Cu^+ over physiologically relevant metal ion concentrations (2 mM Mg^{2+}, Ca^{2+} and Zn^{2+} and 50 μM Mn^{2+}, Fe^{2+}, Co^{2+}, Ni^{2+}, Cu^{2+}). Finally, examination of the complexes formed showed a 1:1 Cu^+:sensor stoichiometry with apparent dissociation constants in the 10^{-13} M range. (Figures 2-4, 2-5, 2-9, 2-10)

Furthermore, characterization of the **CCF1** and **CCF4** probes allowed for analysis of the effects imparted by the aryl ring CF_3 modification on their spectroscopic features. Introduction of the electron-deficient CF_3 substituent triggered an additional 10-nm bathochromic shift on the absorption bands of the metal-bound species ($\lambda_{abs\ (Cu)}$ 580 nm, $\varepsilon = 164 \times 10^4\ M^{-1}cm^{-1}$ for **CCF1,** $\lambda_{abs\ (Cu)}$ 594 nm for **CCR4**). (Figures 2-11, 2-16) Notably, this consistent shift in the absorption features allows for deliberate adjustment of a sensor's spectral properties in order to produce dyes whose excitation profiles lie closer to available laser lines for fluorescence microscopy applications. Improved turn-on responses for **CCF1** and **CCF4** (13.6- and 29.0-fold, respectively; Figures 2-12, 2-17) aligned with our speculation that alteration of the sterics and electronic density of the aryl ring containing the metal-binding domain would lead to more efficient and brighter dyes. Moreover, this substitution did not alter the selectivity, binding stoichiometry or affinity for copper.

Live-cell Imaging of Carbo-rhodol Copper Sensors with Confocal Microscopy. We next sought to investigate the ability of these new probes to visualize biological copper in cell culture applications. Because there is no one-size-fits-all probe that can be generally applied to all cell systems, we decided to characterize these probes in various cell lines. Recent identification of a role for copper in lipid metabolism in 3T3-L1 adipocytes[16] motivated us to evaluate the capability of these probes to observe copper dynamics in this system. Confocal imaging experiments with cells stained with 2 μM **CCR1**, **CCR4** or **CCF4** for 10 min at 37 ºC showed an even cytosplasmic distribution of fluorescence. Subsequent on-stage supplementation of 50 μM $CuCl_2$ for 2 h resulted in fluorescence enhancement values that parallel the dynamic range of each probe. (Figure 2-18) Moreover, similar experiments with **CCF4** in RAW 264.7 macrophages displayed significant increased fluorescence upon copper treatments for 1.5 h. (Figure 2-19)

Furthermore, we established that **CCF1** is proficient in detecting fluctuations in labile, intracellular copper pools in live human embryonic kidney cells (HEK 293T). Cells incubated with 5 μM **CCF1** for 15 min at 37 ºC showed characteristic intracellular fluorescence as observed by confocal microscopy. Cells grown with 50 μM $CuCl_2$, supplemented in the growth medium overnight, exhibited an increase of intracellular fluorescence upon staining with **CCF1**. (Figure 2-20b) Additionally, in order to test if this chemical tool could image intracellular, exchangeable Cu^+ at basal levels, we depleted cells of their endogenous copper stores by culturing them in media containing the membrane-impermeable chelator bathocuproine disulfonate (BCS). This treatment has been shown to reduce copper levels in mammalian cells without jeopardizing their viability.[32] Accordingly, cells were grown in media containing 500 μM BCS for 18 h, stained with 5 μM **CCF1**, and subsequently imaged. (Figure 2-20c) Cells grown in chelator-containing media presented distinctly lower fluorescence signals compared to control cells grown in normal media, indicating that **CCF1** can report on changes in endogenous levels of labile Cu^+ in this cell line.

Additional center-atom substitutions lead to an extended color palette. We last investigated the effect of other center-atom substitutions in order to create a broader color palette for potential multicolor imaging experiments. In order to maintain a higher tendency for hydrophilicity, the morpholino substituent was selected as the amine group to produce the rhodol platform. Additionally, the *ortho*-CF_3 substitution was implemented to yield sensors with high brightness and sensitivity. With these two considerations, we set out to introduce silicon and phosphorus substitutions on the xanthene oxygen position, since these modifications have been previously shown to red-shift the excitation profiles to different degrees.[24,29] To this end, the corresponding Si- or P-xanthone derivatives were synthesized according to published methods,[16,29] and coupled to the copper-binding domain through standard addition of an aryl lithium species, derived from **13**, to the appropriate xanthone to afford the Copper Silica-Fluor and Copper Phospha-Fluor analogues, **CSF1** and **CPF1**, respectively. Spectroscopic characterization of these two probes indeed showed bathochromic-shifts in their spectra, with **CSF1** presenting excitation wavelengths in the red spectral region ($\lambda_{abs\ (Cu)}$ 616 nm) and **CPF1** a close to NIR excitation energy ($\lambda_{abs\ (Cu)}$ 640 nm). Furthermore, addition of copper causes fluorescence enhancements of 16- and 3-fold for the respective probes.

Finally, application of these probes in confocal imaging experiments allowed us to evaluate their capability to sense variations in labile copper HEK 293T cells. Control cells incubated with 5 μM **CSF1** or **CPF1** for 15 min at 37 ºC showed lower intracellular fluorescence in comparison to cells supplemented with 50 μM $CuCl_2$ overnight. Moreover, both sensors were able to report on changes in labile, endogenous pools of copper as cells grown in media containing 500 μM BCS for 18 h presented lowered **CSF1** or **CPF1** fluorescence when compared to cells grown in normal media. (Figures 2-21, 2-22) These promising results suggest that further characterization of the CXF1 family of copper probes in various systems could lead to their application, combined with other fluorescent reporters, in exciting multicolor experiments to evaluate more complex biological processes.

Concluding Remarks

We have presented the design, synthesis and application of a new family of copper probes based on center-atom substitution of the rhodol fluorophore. Permutations in modifications to the xanthene oxygen position, the amine groups on the rhodol scaffold and the *ortho*-substituent on the pendant aryl ring afforded sensors with a variety of excitation profiles and fluorescent responses to copper binding. Imaging experiments with the resulting probe palette established their suitability to evaluate dynamics of labile copper in different cell types. Future efforts to characterize the sensors' responses in more complex systems could lead to their application in multicolor, multi-analyte imaging experiments to understand possible crosstalk of bio-analytes in important biological processes.

Experimental Section

Synthetic Materials and Methods. All reactions were carried out under a dry N_2 atmosphere and stirred magnetically unless stated otherwise. All reactions using air- or moisture-sensitive reagents were performed in oven- and flame-dried glassware under an atmosphere of dry N_2. THF used for

anhydrous reactions was dried and stored over 3-Å molecular sieves. Compounds **1** – **4**,[23] **12**,[15] and **13**[15] were synthesized according to literature procedures. Compounds **CSF1** and **CPF1** were synthesized by Shang Jia and Dr. Safacan Kolemen, respectively. Unless otherwise noted, all chemicals were used as received. Silica gel P60 (SiliCycle) and activated basic aluminum oxide (Brockmann) were used for column chromatography. Flash chromatography was performed on an automated purification system using pre-packed silica gel columns. SiliCycle 60 F254 silica gel (precoated sheets, 0.25 mm thick) was used for analytical TLC, visualized with UV light and/or staining with p-anisaldehyde or $KMNO_4$. ^1H and ^{13}C NMR spectra were collected in $CDCl_3$ (Cambridge Isotope Laboratories, Cambridge, MA) at 25 °C on a Bruker AV-300, Bruker AVB-400 or Bruker AVQ-400 spectrometer at the College of Chemistry NMR Facility at the University of California, Berkeley. All chemical shifts are reported in the standard notation of parts per million using the peak of residual proton or carbon signals of $CDCl_3$ as an internal reference.

Synthesis.

9,9-Dimethyl-10-oxo-9,10-dihydroanthracene-2,7-diyl bis(trifluoromethanesulfonate) (5). A solution of compound **4** (4.0 g, 15.90 mmol), $NPhTf_2$ (17.04 g, 47.69 mmol, 3 eq) and DIPEA (16.61 mL, 95.38 mmol, 6 eq) in anhydrous DMF (159 mL, 0.1 M) was stirred for 16 h at room temperature. The reaction mixture was then diluted with H_2O, and extracted with EtOAc (x2). The combined organic layers were washed with brine, dried with Na_2SO_4 and concentrated under reduced pressure. Flash column chromatography on silica gel (0-10 % EtOAc/hexanes, linear gradient) afforded 5.69 g (69 %) of **5** as an off-white solid. ^1H NMR (300 MHz, $CDCl_3$) δ 8.46 (d, J = 8.8 Hz, 2H), 7.58 (d, J = 2.4 Hz, 2H), 7.38 (dd, J = 8.8, 2.4 Hz, 2H), 1.78 (s, 6H). ^{13}C NMR (75 MHz, $CDCl_3$) δ 180.60, 153.14, 152.46, 130.64, 129.18, 120.81, 120.30, 119.81, 116.56, 38.53, 32.64. LRESI-MS calculated for [M+H] 519.0, found 519.6.

9,9-Dimethyl-7-morpholino-10-oxo-9,10-dihydroanthracen-2-yl trifluoromethanesulfonate (6). A solution of compound **5** (1.13 g, 2.18 mmol) in DMSO (10.9 mL, 0.2 M) was preheated to 85 ºC and charged with morpholine (188.1 µL, 2.18 mmol, 1 eq). After 16 h, the reaction mixture was cooled to room temperature, poured into brine and extracted with EtOAc (x3). The combined organic layers were washed with brine, dried with Na_2SO_4 and concentrated under reduced pressure. The crude residue was purified via flash column chromatography on silica gel (0-50 % EtOAc/hexanes, linear gradient) to yield 0.49 g (49 %) of **6** as a yellow solid. ^1H NMR (400 MHz, $CDCl_3$) δ 8.44 (d, J = 8.7 Hz, 1H), 8.26 (d, J = 8.8 Hz, 1H), 7.53 (d, J = 2.4 Hz, 1H), 7.31 (dd, J = 8.7, 2.4 Hz, 1H), 6.96 (d, J = 7.8 Hz, 2H), 3.89 (t, J = 4.7 Hz, 4H), 3.39 (t, J = 4.8 Hz, 4H), 1.72 (s, 6H). ^{13}C NMR (101 MHz, $CDCl_3$) δ 180.38, 154.67, 152.81, 152.33, 151.76, 130.11, 129.91, 129.60, 120.90, 120.20, 119.45, 117.00, 113.49, 110.01, 66.36, 47.29, 38.22, 32.91.

9,9-Dimethyl-10-oxo-7-(piperidin-1-yl)-9,10-dihydroanthracen-2-yl trifluoromethanesulfonate (7). A solution of compound **5** (0.50 g, 0.96 mmol) in DMSO (4.8 mL, 0.2 M) was preheated to 85 ºC and charged with piperidine (95.3 µL, 0.96 mmol, 1 eq). After 16 h, the reaction mixture was cooled to room temperature, poured into brine and extracted with EtOAc (x3). The combined organic layers were washed with brine, dried with Na_2SO_4 and concentrated under reduced pressure. The crude residue was purified via flash column chromatography on silica gel (0-10 % EtOAc/hexanes, linear gradient) to yield 0.21 g (48 %) of **7** as a yellow solid. ^1H NMR (400 MHz, $CDCl_3$) δ 8.45 (d, J = 8.7 Hz, 1H), 8.23 (d, J = 9.3 Hz, 1H), 7.52 (d, J = 2.4 Hz, 1H), 7.30 (dd, J =

8.7, 2.4 Hz, 1H), 6.96 (d, *J* = 7.9 Hz, 2H), 3.44 (t, *J* = 5.1 Hz, 4H), 1.78 – 1.67 (m, 12H). ^{13}C NMR (101 MHz, $CDCl_3$) δ 180.26, 154.91, 152.91, 152.29, 151.90, 130.43, 129.94, 129.78, 120.30, 119.70, 119.47, 119.40, 117.11, 113.75, 109.94, 48.54, 38.26, 33.07, 25.37, 24.26.

3-Hydroxy-10,10-dimethyl-6-morpholinoanthracen-9(10*H*)-one (8). A solution of **6** (0.36 g, 0.80 mmol) in dioxane (7.5 mL, 0.107 M) was charged with Et_4NOH (25 % in MeOH, 1.6 mL, 3.0 eq) and the reaction mixture was stirred for 2 h at room temperature. Upon completion of the reaction, judged by TLC, volatiles were removed under reduced pressure to afford a yellow solid crude that was used further without purification. LRESI-MS calculated for [M+H] 323.2, found 323.8.

3-Hydroxy-10,10-dimethyl-6-(piperidin-1-yl)anthracen-9(10*H*)-one (9). A solution of **7** (0.18 g, 0.39 mmol) in dioxane (3.6 mL, 0.107 M) was charged with Et_4NOH (25 % in MeOH, 515.4 μL, 3.0 eq) and the reaction mixture was stirred for 2 h at room temperature. Upon completion of the reaction, judged by TLC, volatiles were removed under reduced pressure to afford a dark yellow solid crude that was used further without purification.

3-((*Tert*-butyldimethylsilyl)oxy)-10,10-dimethyl-6-morpholinoanthracen-9(10*H*)-one (10). Crude compound **8** (0.17 g, 0.52 mmol) was dissolved in anhydrous CH_2Cl_2 (12.8 mL, 0.04 M) and subjected to imidazole (0.10 g, 1.53 mmol, 3 eq). Reaction mixture was cooled to 0 ºC, treated with *tert*-butyldimethylsilyl chloride (0.15 g, 1.02 mmol, 2 eq) and stirred at room temperature for 3 h. Upon completion of the reaction, judged by TLC, volatiles were removed under reduced pressure and crude residue was purified via flash column chromatography on silica gel (0-25 % EtOAc/hexanes, linear gradient) to afford 0.20 g (92 %) of **10** as a pale yellow solid. ^{1}H NMR (400 MHz, $CDCl_3$) δ 8.26 (dd, *J* = 8.7, 3.2 Hz, 2H), 7.02 (dd, *J* = 12.3, 2.4 Hz, 2H), 6.91 (ddd, *J* = 29.7, 8.8, 2.4 Hz, 2H), 3.89 (t, *J* = 4.9 Hz, 4H), 3.36 (t, *J* = 4.9 Hz, 4H), 1.68 (s, 6H), 1.01 (s, 9H), 0.26 (s, 6H). ^{13}C NMR (101 MHz, $CDCl_3$) δ 181.51, 159.91, 154.22, 152.57, 152.13, 129.44, 129.27, 124.43, 122.10, 118.95, 117.34, 113.42, 110.60, 66.58, 47.78, 37.92, 33.18, 25.61, 18.25, -4.33.

3-((*Tert*-butyldimethylsilyl)oxy)-10,10-dimethyl-6-(piperidin-1-yl)anthracen-9(10*H*)-one (11). Crude compound **9** (0.12 g, 0.39 mmol) was dissolved in anhydrous CH_2Cl_2 (9.7 mL, 0.04 M) and subjected to imidazole (0.26 g, 3.87 mmol, 10 eq). Reaction mixture was cooled to 0 ºC, treated with *tert*-butyldimethylsilyl chloride (0.17 g, 1.16 mmol, 3 eq) and stirred at room temperature for 3 h. Upon completion of the reaction, judged by TLC, volatiles were removed under reduced pressure and crude residue was purified via flash column chromatography on silica gel (0-10 % EtOAc/hexanes, linear gradient) to afford 0.12 g (72 %) of **11** as a pale orange solid. ^{1}H NMR (400 MHz, $CDCl_3$) δ 8.26 (d, *J* = 8.6 Hz, 1H), 8.23 (d, *J* = 8.8 Hz, 1H), 7.04 (d, *J* = 2.3 Hz, 1H), 6.97 (d, *J* = 2.3 Hz, 1H), 6.94 (dd, *J* = 8.8, 2.4 Hz, 1H), 6.87 (dd, *J* = 8.6, 2.3 Hz, 1H), 3.39 (t, *J* = 5.3 Hz, 4H), 1.77 – 1.61 (m, 12H), 1.01 (s, 9H), 0.26 (s, 6H). ^{13}C NMR (101 MHz, $CDCl_3$) δ 181.44, 159.72, 154.59, 152.63, 152.17, 129.35, 129.28, 124.60, 120.77, 118.82, 117.34, 113.67, 110.59, 99.90, 48.85, 33.20, 25.63, 24.28, 18.26, 17.96, -4.32.

10-(4-((Bis(2-((2-(ethylthio)ethyl)thio)ethyl)amino)methyl)-2-methylphenyl)-9,9-dimethyl-7-morpholinoanthracen-2(9*H*)-one (14, CCR1). A flame-dried three-neck round-bottom flask was charged with **12** (56.7 mg, 0.11 mmol, 2 eq) and anhydrous THF (1.0 mL, 0.10 M in **12**). The solution was cooled to -78 ºC and then *tert*-butyllithium (1.7 M in pentane, 64 μL, 0.11 mmol, 1.9

eq) was added dropwise. After stirring at the same temperature for 12 min, a solution of compound **11** (25.0 mg, 0.06 mmol) in anhydrous TFH (4.0 mL, 0.01 M in **11**) was added dropwise. The reaction was warmed to room temperature, stirred for 1 h and subsequently quenched with addition of aq. HCl (1 M, 3 mL). After 1 h, the reaction was poured into a 1:1 mixture of sat. $NaHCO_3$ and EtOAc. Layers were separated and aqueous layer was further extracted with EtOAc (x2). The combined organic layers were washed with brine, dried with Na_2SO_4 and concentrated under reduced pressure. The crude residue was purified via column chromatography on silica gel (2.0 % MeOH/CH_2Cl_2) to afford **CCR1** as a purple solid (4.6 mg, 11 %). ^{1}H NMR (400 MHz, $CDCl_3$) δ 7.32 – 7.30 (m, 2H), 7.10 – 7.07 (m, 3H), 6.95 (d, *J* = 10.0 Hz, 1H), 6.81 (d, *J* = 8.8 Hz, 1H), 6.65 (dd, *J* = 7.6, 2.4 Hz, 1H), 6.32 (dd, *J* = 8.0, 2.0 Hz, 1H), 3.87 (t, *J* = 4.4 Hz, 4H), 3.35 (t, *J* = 4.8 Hz, 4H), 2.55 (q, *J* = 7.6 Hz, 4H), 2.06 (s, 3H), 1.69 (s, 3H), 1.64 (s, 3H), 1.26 (t, *J* = 7.6 Hz, 6H). HRESI-MS calculated for [M+H] 723.3068, found 723.3133.

10-(4-((Bis(2-((2-(ethylthio)ethyl)thio)ethyl)amino)methyl)-2-methylphenyl)-9,9-dimethyl-7-(piperidin-1-yl)anthracen-2(9*H*)-one (15, CCR4). A flame-dried three-neck round-bottom flask was charged with **12** (57.0 mg, 0.11 mmol, 2 eq) and anhydrous THF (1.0 mL, 0.10 M in **12**). The solution was cooled to -78 ºC and then *tert*-butyllithium (1.7 M in pentane, 128 µL, 0.11 mmol, 1.9 eq) was added dropwise. After stirring at the same temperature for 12 min, a solution of compound **11** (25.0 mg, 0.06 mmol) in anhydrous TFH (4.0 mL, 0.01 M in **11**) was added dropwise. The reaction was warmed to room temperature, stirred for 1 h and subsequently quenched with addition of aq. HCl (1 M, 3 mL). After 1 h, the reaction was poured into a 1:1 mixture of sat. $NaHCO_3$ and EtOAc. Layers were separated and aqueous layer was further extracted with EtOAc (x2). The combined organic layers were washed with brine, dried with Na_2SO_4 and concentrated under reduced pressure. The crude residue was purified via column chromatography on silica gel (5.0 % MeOH/CH_2Cl_2) to afford **CCR4** as a purple solid (27.9 mg, 67 %). ^{1}H NMR (400 MHz, $CDCl_3$) δ 7.31 – 7.28 (m, 2H), 7.07 – 7.06 (m, 2H), 6.92 (d, *J* = 9.6 Hz, 1H), 6.77 – 6.75 (m, 2H), 6.63 (d, *J* = 6.4 Hz, 1H), 6.30 (dd, *J* = 7.6, 2.0 Hz, 1H), 3.71 (s, 2H), 3.40 (m, 4H), 2.83 – 2.79 (m, 4H), 2.73 – 2.68 (m, 12H), 2.56 (q, *J* = 7.6 Hz, 4H), 2.05 (s, 3H), 1.67 – 1.63 (m, 12H), 1.25 (t, *J* = 7.6 Hz, 6H). ^{13}C NMR (101 MHz, $CDCl_3$) δ 186.02, 156.19, 153.11, 150.68, 137.82, 136.24, 135.33, 132.48, 130.28, 129.32, 126.10, 125.90, 124.02, 121.54, 120.60, 112.45, 111.33, 58.21, 53.93, 48.50, 39.91, 34.35, 32.75, 32.41, 31.75, 29.98, 26.04, 25.41, 24.25, 19.57, 14.78. HRESI-MS calculated for [M+H] 721.3275, found 721.3337.

10-(4-((Bis(2-((2-(ethylthio)ethyl)thio)ethyl)amino)methyl)-2-(trifluoromethyl)phenyl)-9,9-dimethyl-7-morpholinoanthracen-2(9*H*)-one (16, CCF1). A flame-dried three-neck round-voibottom flask was charged with **13** (214.9 mg, 0.39 mmol, 2 eq) and anhydrous THF (1.3 mL, 0.30 M in **13**). The solution was cooled to -78 ºC and then *tert*-butyllithium (1.7 M in pentane, 0.46 mL, 0.78 mmol, 4 eq) was added dropwise. After stirring at the same temperature for 12 min, a solution of compound **10** (85.4 mg, 0.20 mmol) in anhydrous TFH (6.5 mL, 0.03 M in **10**) was added dropwise. The reaction was warmed to room temperature, stirred for 1 h and subsequently quenched with addition of aq. HCl (1 M, 3 mL). After 1 h, the reaction was poured into a 1:1 mixture of sat. $NaHCO_3$ and EtOAc. Layers were separated and aqueous layer was further extracted with EtOAc (x2). The combined organic layers were washed with brine, dried with Na_2SO_4 and concentrated under reduced pressure. The crude residue was purified via column chromatography on silica gel (2.5 % MeOH/CH_2Cl_2) to afford **CCF1** as a purple solid (81.1 mg, 53 %). ^{1}H NMR (400 MHz, $CDCl_3$) δ 7.87 (d, *J* = 1.5 Hz, 1H), 7.73 (d, *J* = 7.8 Hz, 1H), 7.25 (d,

J = 8.3 Hz, 1H), 7.09 (d, *J* = 1.7 Hz, 1H), 6.82 – 6.74 (m, 2H), 6.65 (s, 2H), 6.30 (dd, *J* = 9.7, 1.9 Hz, 1H), 3.92 – 3.78 (m, 6H), 3.40 – 3.29 (m, 4H), 2.86 – 2.83 (m, 4H), 2.76 – 2.72 (m, 12H), 2.56 (q, *J* = 7.4 Hz, 4H), 1.73 (s, 3H), 1.57 (s, 3H), 1.25 (t, *J* = 7.4 Hz, 6H). ^{13}C NMR (75 MHz, $CDCl_3$) δ 186.12, 155.78, 152.63, 149.56, 148.87, 140.81, 137.77, 133.86, 132.18, 131.50, 131.37, 129.45, 126.44, 124.42, 122.99, 122.59, 112.12, 111.04, 66.41, 57.75, 53.78, 53.38, 47.28, 39.97, 35.72, 32.42, 31.67, 30.32, 30.10, 25.98, 14.72. HRESI-MS calculated for [M+H] 777.2785, found 777.2845.

10-(4-((Bis(2-((2-(ethylthio)ethyl)thio)ethyl)amino)methyl)-2-(trifluoromethyl)phenyl)-9,9-dimethyl-7-(piperidin-1-yl)anthracen-2(9*H*)-one (17, CCF4). A flame-dried three-neck round-bottom flask was charged with **13** (126.2 mg, 0.23 mmol, 2 eq) and anhydrous THF (1.0 mL, 0.10 M in **13**). The solution was cooled to -78 ºC and then *tert*-butyllithium (1.7 M in pentane, 128 µL, 0.22 mmol, 1.9 eq) was added dropwise. After stirring at the same temperature for 12 min, a solution of compound **11** (50.0 mg, 0.11 mmol) in anhydrous TFH (4.0 mL, 0.01 M in **11**) was added dropwise. The reaction was warmed to room temperature, stirred for 1 h and subsequently quenched with addition of aq. HCl (1 M, 3 mL). After 1 h, the reaction was poured into a 1:1 mixture of sat. $NaHCO_3$ and EtOAc. Layers were separated and aqueous layer was further extracted with EtOAc (x2). The combined organic layers were washed with brine, dried with Na_2SO_4 and concentrated under reduced pressure. The crude residue was purified via column chromatography on silica gel (2.5 % MeOH/CH_2Cl_2) to afford **CCF4** as a purple solid (4.9 mg, 5.5 %). ^{1}H NMR (400 MHz, $CDCl_3$) δ 7.86 (s, 1H), 7.69 (d, *J* = 7.6 Hz, 1H), 7.25 (d, *J* = 8.3 Hz, 1H), 7.08 (s, 1H), 6.79 – 6.75 (m, 2H), 6.62 (s, 2H), 6.29 (dd, *J* = 7.6, 2.0 Hz, 1H), 3.81 (s, 2H), 3.40 (m, 4H), 2.84 – 2.81 (m, 4H), 2.75 – 2.72 (m, 12H), 2.57 (q, *J* = 7.2 Hz, 4H), 1.73 – 1.68 (m, 12H), 1.26 (t, *J* = 7.6 Hz, 6H). HRESI-MS calculated for [M+H] 775.2993, found 775.3074.

Spectroscopic Materials and Methods. Millipore water was used to prepare all aqueous solutions. All final spectroscopic measurements were performed in HEPES or MOPS buffer. Absorption spectra were recorded using a Varian Cary 50 spectrophotometer (Walnut Creek, CA) and fluorescence spectra were recorded using a Photon Technology International Quanta Master 4 L-format scan spectrofluorometer (Lawrenceville, NJ) equipped with an LPS-220B 75-W xenon lamp and power supply, A-1010B lamp housing with integrated igniter, switchable 814 photocounting/analog photomultiplier detection unit, and MD5020 motor driver. Samples for absorption and emission measurements were contained in 1-cm quartz cuvettes (1.4-mL volume, Starna, Atascadero, CA). Cu^+ was delivered in the form of $[Cu(MeCN)_4][PF_6]$ from an acetonitrile stock solution (2 mM). For **CCR1** excitation was provided at 564 nm and collected emission was integrated from 570-700 nm. For **CCR4** excitation was provided at 586 nm and collected emission was integrated from 595-700 nm. For **CCF1** excitation was provided at 580 nm and collected emission was integrated from 598-618 nm. For **CCF4** excitation was provided at 594 nm.

Cell Culture. 3T3-L1 preadipocytes (CL 173, ATCC, authenticated by short tandem repeat analysis and tested to confirm absence of *Mycoplasma* by Hoechst staining) were cultured in DMEM containing 10% newborn calf serum and grown to confluence. Cells were then differentiated by the addition of insulin, dexamethasone, and IMBX as described.[33] Adipocytes were maintained at 37 °C and 5% CO_2. RAW264.7 macrophages were cultured in Dulbecco's Modified Eagle Medium (DMEM) containing high glucose with GlutaMAX (Invitrogen, Carlsbad,

CA) and supplemented with 10% Fetal Bovine Serum (FBS, Hyclone). HEK 293T cells were cultured in Dulbecco's Modified Eagle Medium (DMEM, Invitrogen, Carlsbad, CA) supplemented with 10% Fetal Bovine Serum (FBS, Invitrogen), glutamine (2mM) and penicillin/streptomycin (50 mg/mL, Invitrogen). One day before imaging, cells were passed and plated on 18-mm glass coverslips coated with poly-L-lysine (50 mg/mL, Sigma, St. Louis, MO). Immediately before the experiments, cells were washed with DMEM buffer and imaged. Unless otherwise noted, experiments to assess copper uptake were performed in the same media supplemented with the additives at the indicated concentrations.

Live-Cell Imaging. Confocal fluorescence imaging was performed with a Zeiss LSM 710 laser-scanning microscope and a 20x objective lens. Excitation of **CCR1** and **CCR4** loaded cells at 543 nm was carried out with a He-Ne laser, and emission was collected using a META detector between 550 and 733 nm. Excitation of **CCF1** and **CCF4** loaded cells at 594 nm was carried out with a He-Ne laser, and emission was collected using a META detector between 600 and 733 nm. Excitation of **CSF1** and **CPF1** loaded cells at 633 nm was carried out **with** a He-Ne laser, and emission was collected using a META detector between 640 and 733 nm. Probe (2 μM or 5 μM for CXF1 probes in DMEM) was incubated with live cells samples for 10 (or 15 for CXF1 probes) min at 37 °C. Cells were washed with DMEM (1 x 450 μL) and then imaged. Images were analyzed using ImageJ.

Schemes and Figures

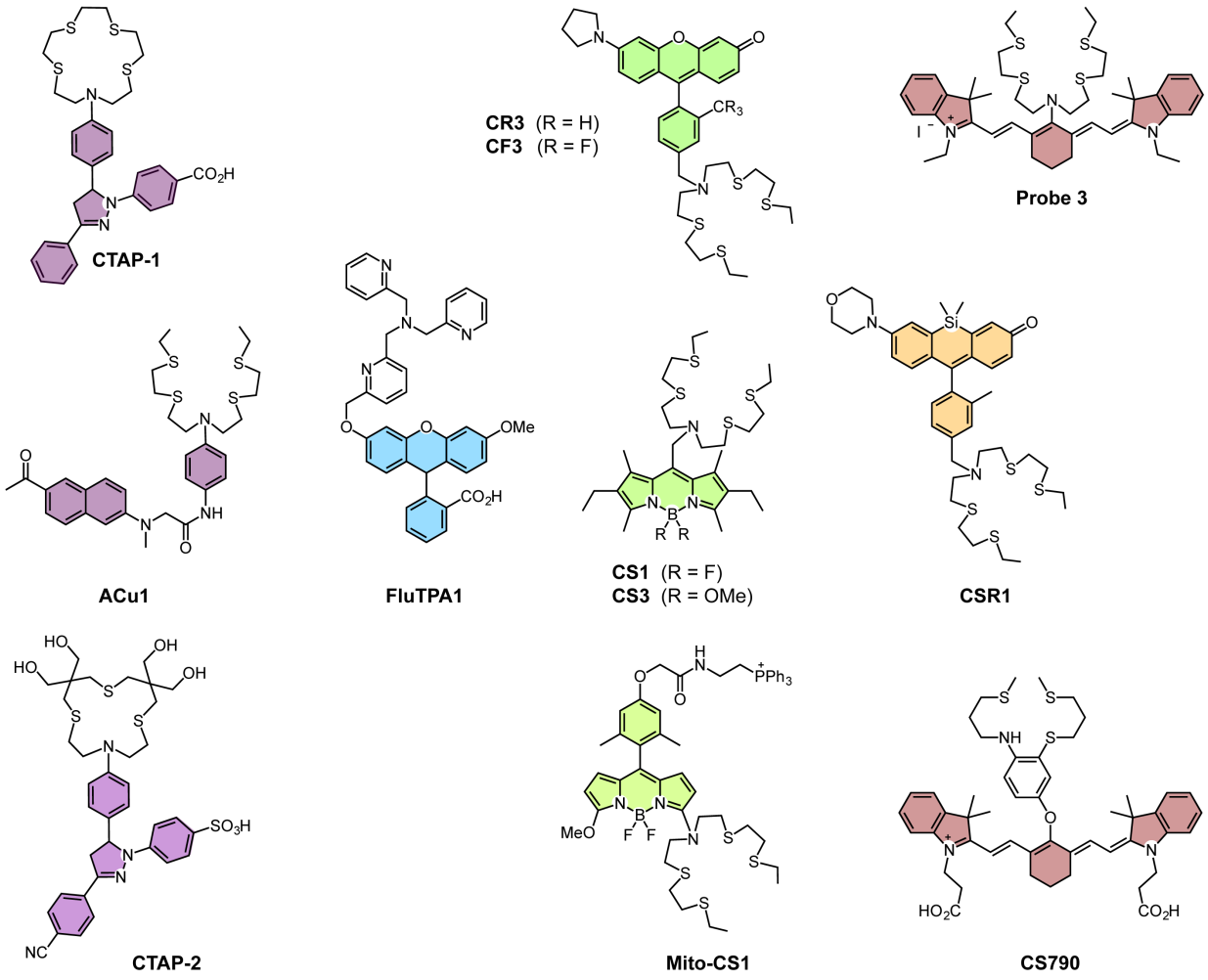

Scheme 2-1. Available probes for sensing copper (I)

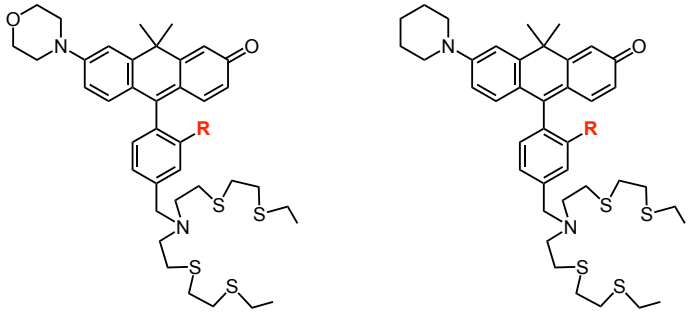

Scheme 2-2. Targets for carbo-rhodol probes for sensing copper (I)

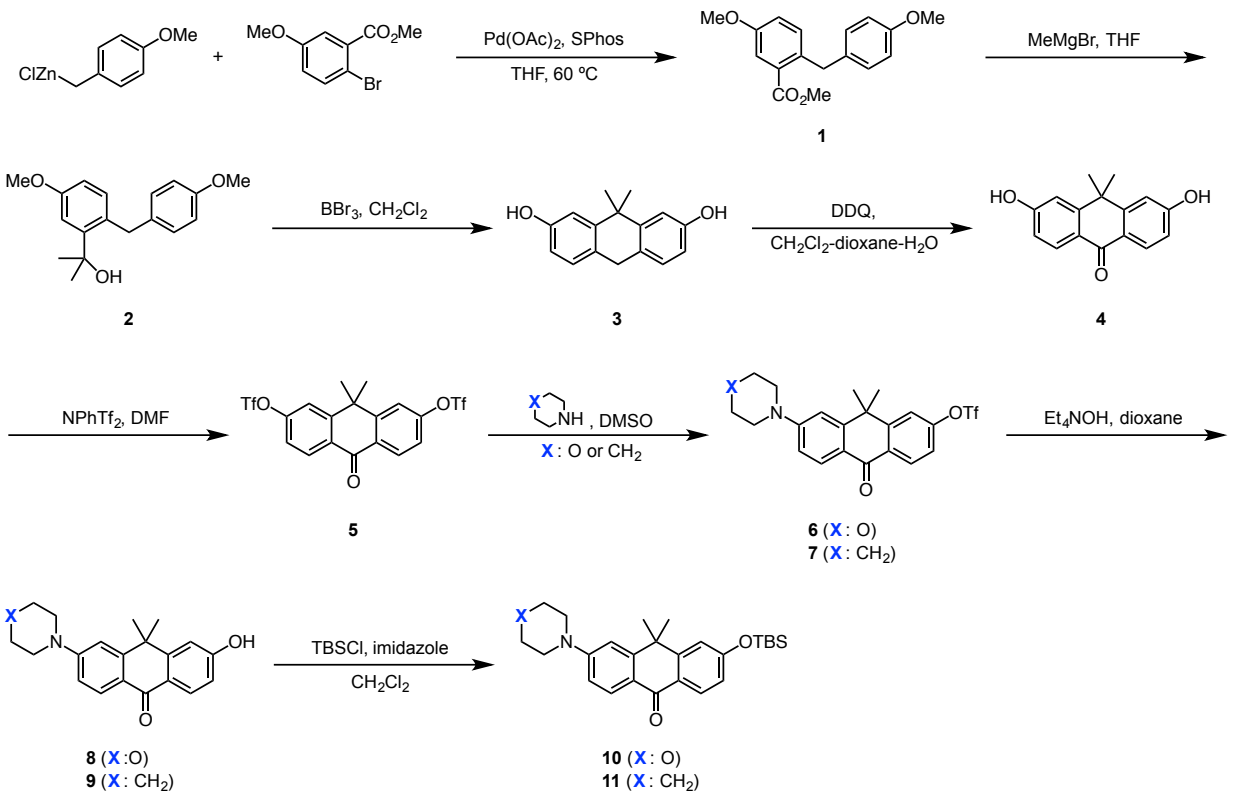

Scheme 2-3. Synthesis of carbo-xanthones.

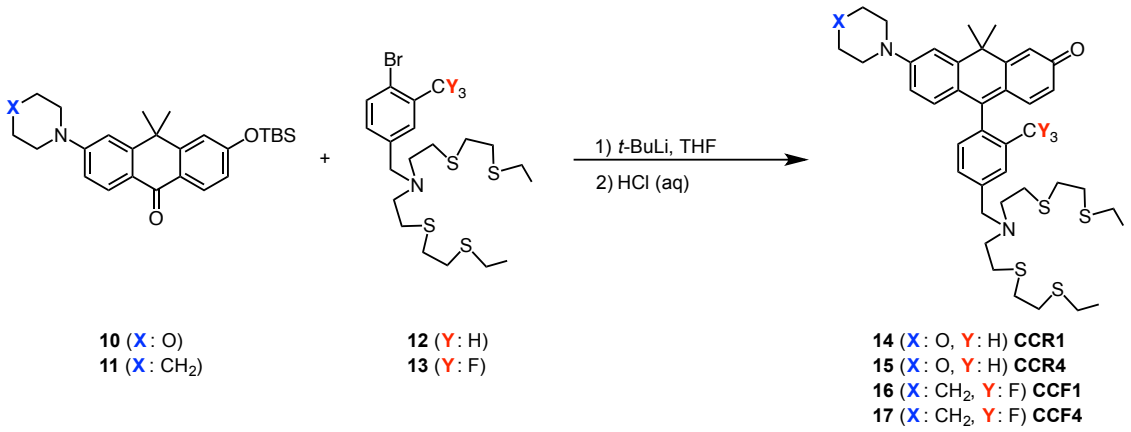

10 (**X**: O)
11 (**X**: CH_2)

12 (**Y**: H)
13 (**Y**: F)

14 (**X**: O, **Y**: H) **CCR1**
15 (**X**: O, **Y**: H) **CCR4**
16 (**X**: CH_2, **Y**: F) **CCF1**
17 (**X**: CH_2, **Y**: F) **CCF4**

Scheme 2-4. Synthesis of carbo-rhodol probes.

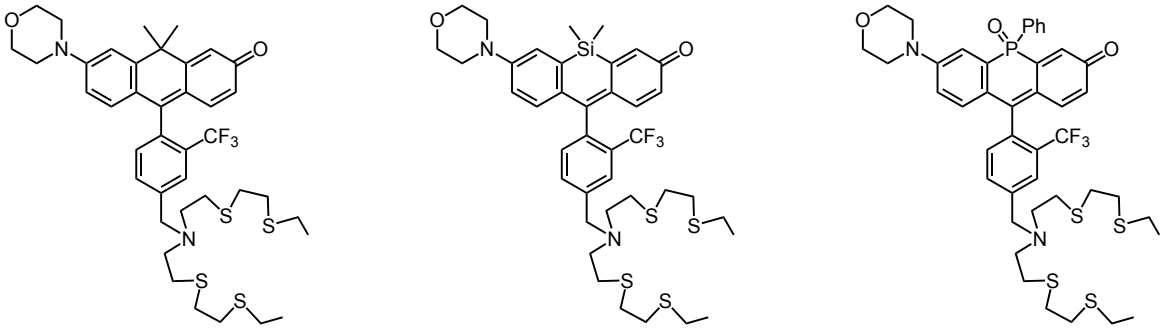

Scheme 2-5. Targets for rhodol probes with center-atom substitution to expand the available color palette.

	Cu(I)	λ_{abs} (nm)	λ_{fl} (nm)	F_f/F_i	ε ($M^{-1}cm^{-1}$)	Φ	K_d (M)
CCR1	-	529 (broad)	605		4.91×10^3	0.061	
	+	564	602	4.5	7.46×10^3	0.241	1.12×10^{-13}
CCR4	-	530 (broad)	608		7.56×10^3	0.011	
	+	586	607	17.4	2.23×10^4	0.046	7.65×10^{-13}
CCF1	-	546 (broad)	606		1.09×10^4	0.107	
	+	580	607	13.6	1.64×10^4	0.772	4.67×10^{-13}
CCF4	-	532 (broad)	616		n.d.	n.d	
	+	594	615	29.0	n.d.	n.d.	n.d.

Table 2-1. Summary of spectroscopic properties of carbo-rhodol copper sensors.

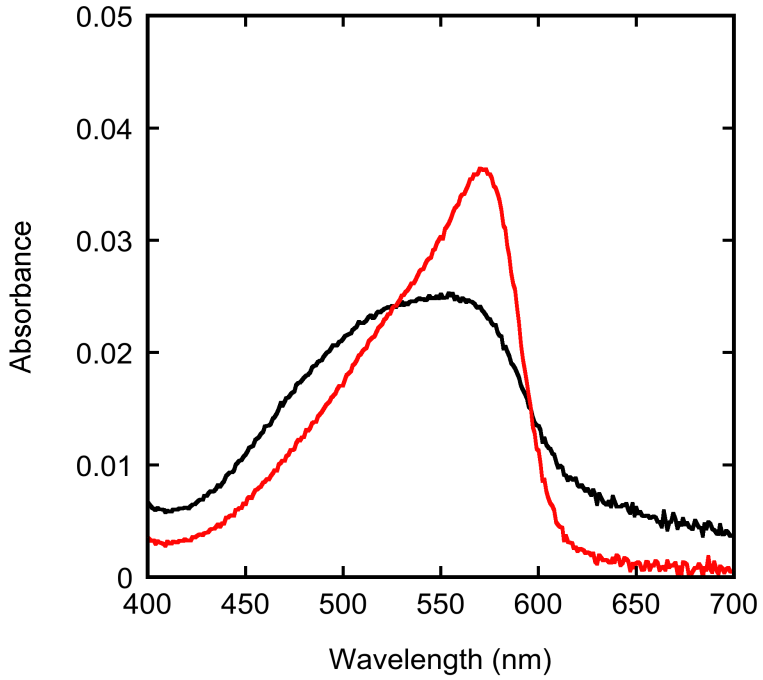

Figure 2-1. Absorbance spectra of 5 μM **CCR1**. Spectra shown are for buffered [Cu^{+}] of 0.0 (black trace) and 5.0 (red trace) μM. Spectra were acquired in 20 mM HEPES, pH 7.4.

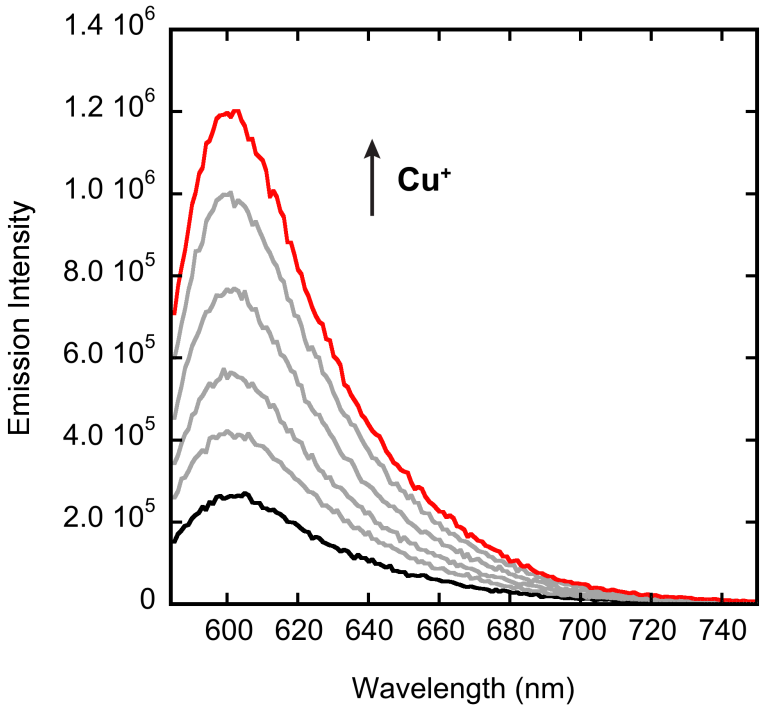

Figure 2-2. Fluorescence response of 2 μM **CCR1** to Cu^+. Spectra shown are for buffered [Cu^+] of 0.0, 0.4, 0.8, 1.2, 1.6, and 2.0 μM. Spectra were acquired in 20 mM HEPES, pH 7.4 with excitation at 564 nm.

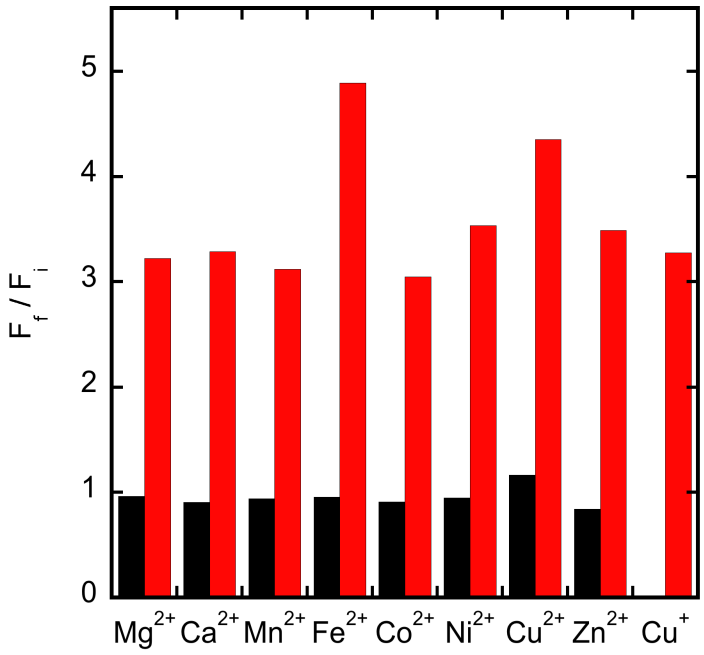

Figure 2-3. Fluorescence response of **CCR1** to various metal ions. Bars represent the final integrated fluorescence response (F_f) over the initial integrated emission (F_i). Spectra were acquired in 20 mM HEPES, pH 7.4. Black bars represent the addition of an excess of the appropriate metal ion (2 mM for Mg^{2+}, Ca^{2+}, and Zn^{2+}, 50 μM for all other cations) to a 2 μM solution of **CCR1**. Red bars represent the subsequent addition of 2 μM Cu^{+} to the solution. Excitation was provided at 564 nm, and the collected emission was integrated over 570 to 700 nm.

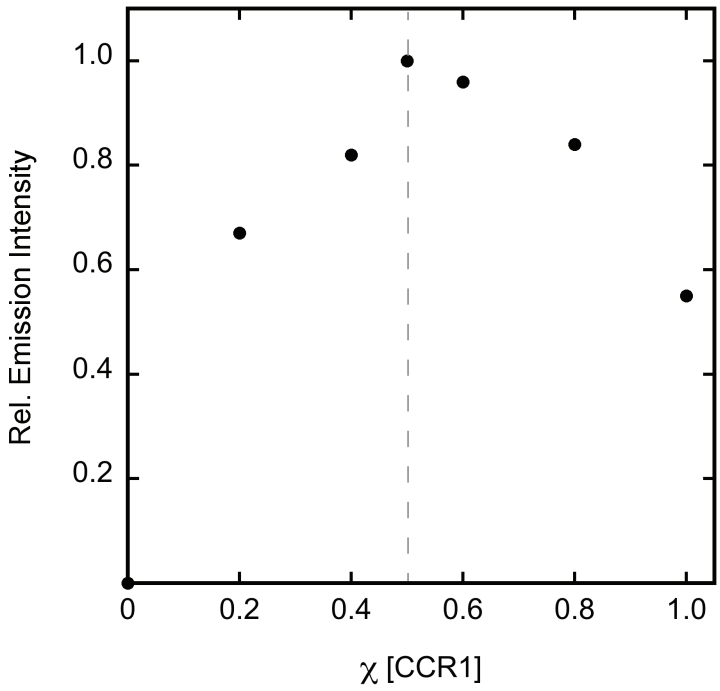

Figure 2-4. Job's plot of CCR1 and Cu^{+}. The total concentration of **CCR1** and Cu^{+} was kept at a constant 5.25 μM. Excitation was provided at 564 nm and the collected emission intensity was integrated from 570 to 700 nm. Spectra were acquired in 20 mM HEPES pH 7.4. The maximum fluorescence response at 0.50 mol fraction of **CCR1** indicates formation of a 1:1 Cu^{+}:**CCR1** complex.

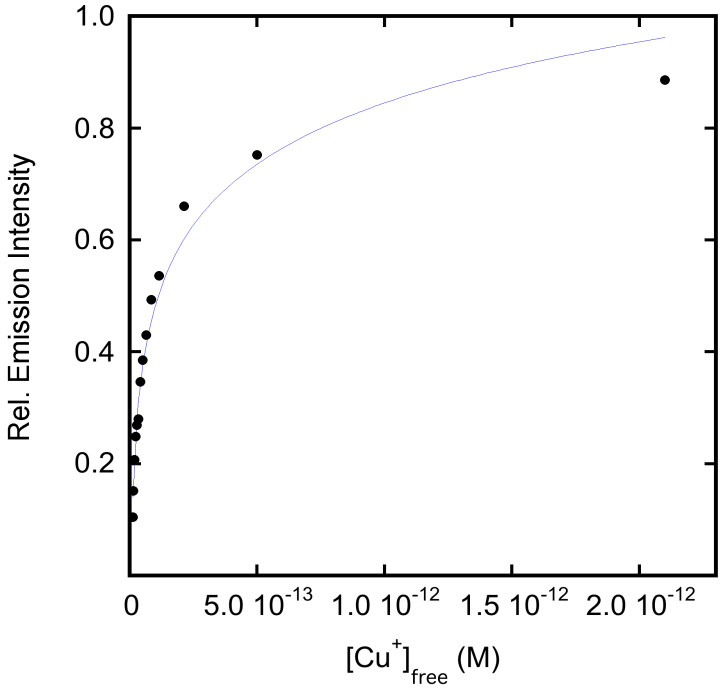

Figure 2-5. Normalized fluorescence response of 3.5 μM **CCR1** to thiourea buffered Cu^+ solutions for K_d value determination. Excitation was provided at 565 nm and the collected emission was integrated from 570 to 700 nm. Spectra were acquired in 20 mM HEPES, pH 7.4. The points shown are for free Cu^+ buffered at 11.4, 14.3, 18.3, 22.7, 27.1, 32.8, 40.2, 50.2, 64.0, 83.9, 114, 212, 500 and 2100 fM, respectively. The observed K_d value is 1.12×10^{-13} M.

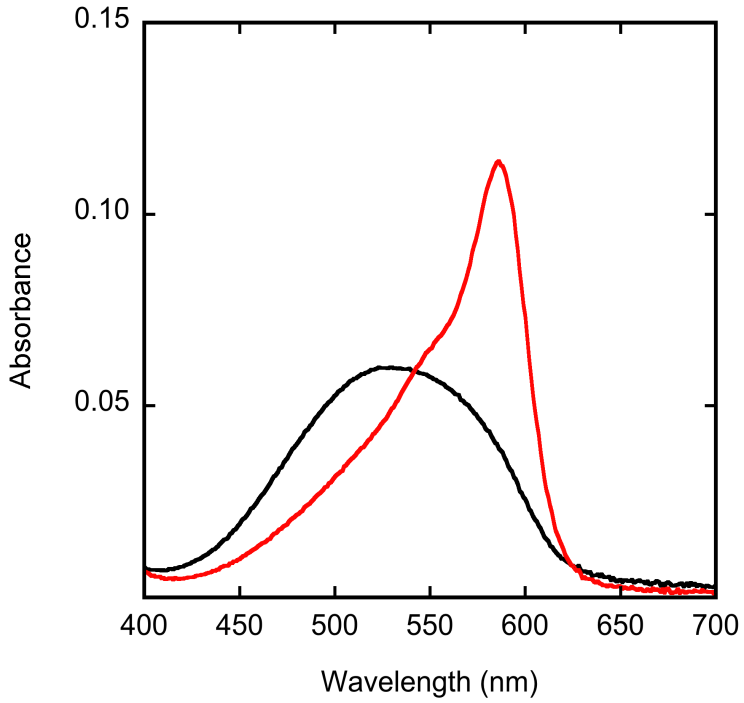

Figure 2-6. Absorbance spectra of 5 μM **CCR4**. Spectra shown are for buffered [Cu^{+}] of 0.0 (black trace) and 5.0 (red trace) μM. Spectra were acquired in 50 mM HEPES, pH 7.4.

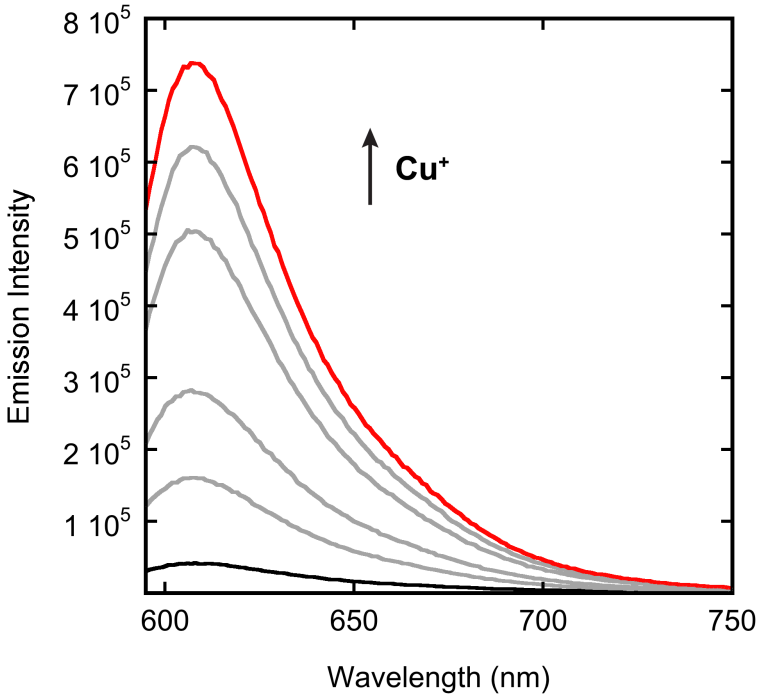

Figure 2-7. Fluorescence response of 2 μM **CCR4** to Cu^+. Spectra shown are for buffered [Cu^+] of 0.0, 0.4, 0.8, 1.2, 1.6, and 2.0 μM. Spectra were acquired in 50 mM HEPES, pH 7.4 with excitation at 586 nm.

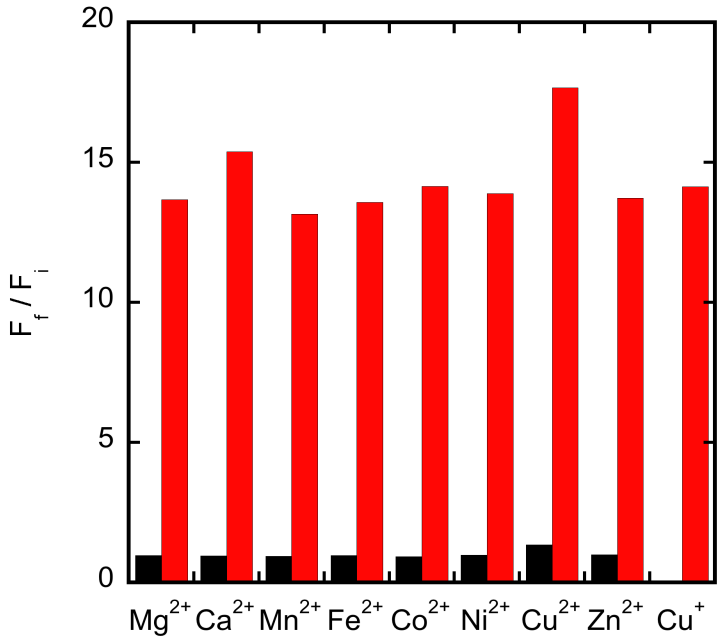

Figure 2-8. Fluorescence response of **CCR4** to various metal ions. Bars represent the final integrated fluorescence response (F_f) over the initial integrated emission (F_i). Spectra were acquired in 50 mM HEPES, pH 7.4. Black bars represent the addition of an excess of the appropriate metal ion (2 mM for Mg^{2+}, Ca^{2+}, and Zn^{2+}, 50 μM for all other cations) to a 2 μM solution of **CCR4**. Red bars represent the subsequent addition of 2 μM Cu^{+} to the solution. Excitation was provided at 586 nm, and the collected emission was integrated over 595 to 700 nm.

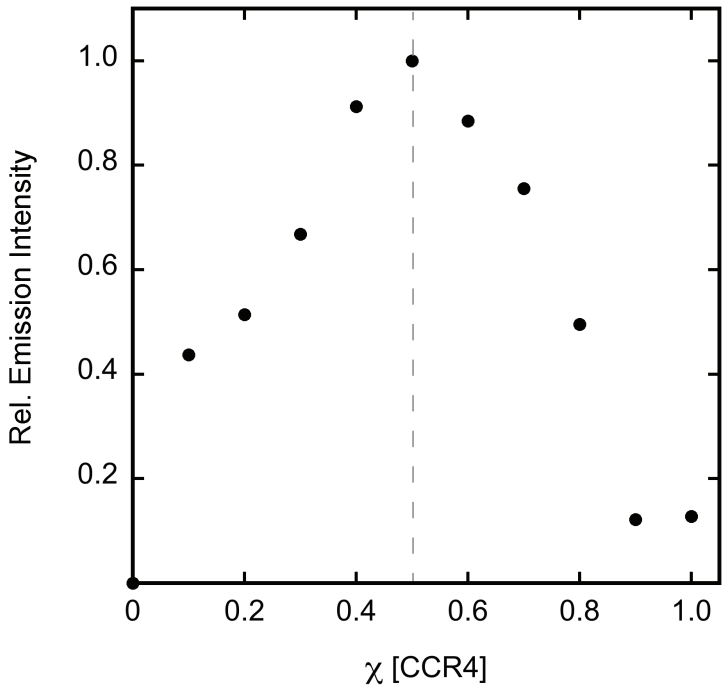

Figure 2-9. Job's plot of **CCR4** and Cu^{+}. The total concentration of **CCR4** and Cu^{+} was kept at a constant 2 μM. Excitation was provided at 586 nm and the collected emission intensity was integrated from 595 to 700 nm. Spectra were acquired in 50 mM HEPES pH 7.4. The maximum fluorescence response at 0.50 mol fraction of **CCR4** indicates formation of a 1:1 Cu^{+}:**CCR4** complex.

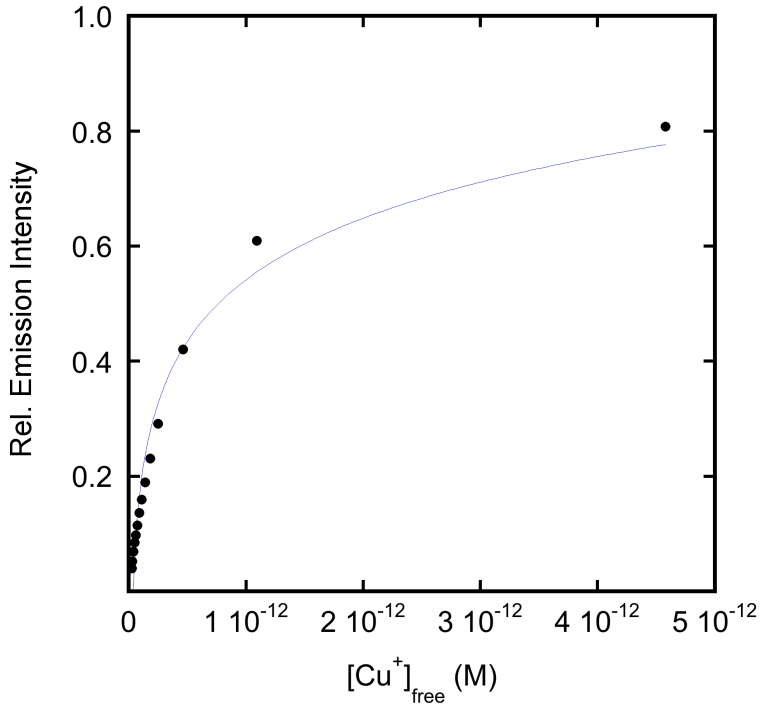

Figure 2-10. Normalized fluorescence response of 2 μM **CCR4** to thiourea buffered Cu^+ solutions for K_d value determination. Excitation was provided at 586 nm and the collected emission was integrated from 595 to 700 nm. Spectra were acquired in 50 mM HEPES, pH 7.4. The points shown are for free Cu^+ buffered at 24.8, 31.1, 39.9, 49.6, 59.2, 71.5, 87.6, 109, 140, 183, 249, 462, 1090 and 4576 fM, respectively. The observed K_d value is 7.65 x 10^{-13} M.

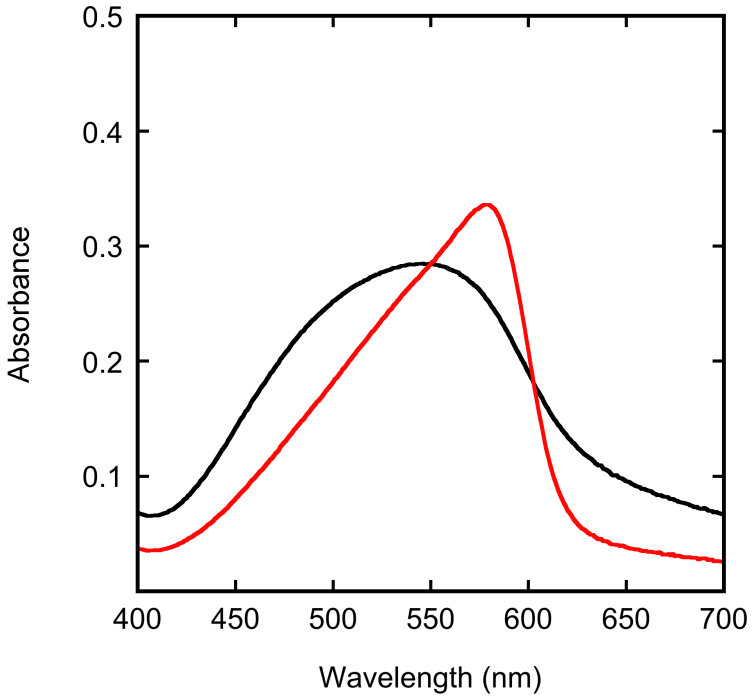

Figure 2-11. Absorbance spectra of 10 μM **CCF1**. Spectra shown are for buffered [Cu^{+}] of 0.0 (black trace) and 10.0 (red trace) μM. Spectra were acquired in 50 mM MOPS, pH 7.4.

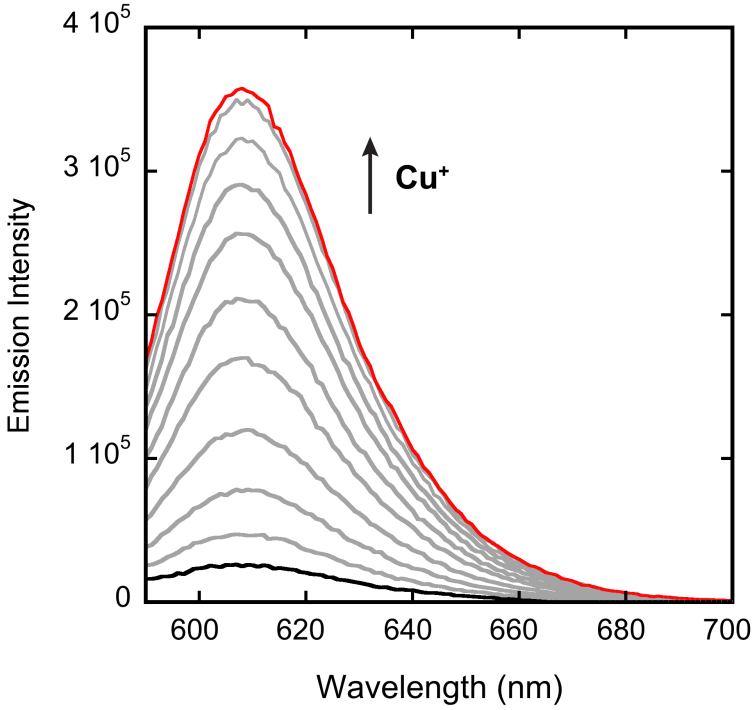

Figure 2-12. Fluorescence response of 4 μM **CCF1** to Cu^+. Spectra shown are for buffered [Cu^+] of 0.0, 0.4, 0.8, 1.2, 1.6, 2.0, 2.4, 2.8, 3.2, 3.6 and 4.0 μM. Spectra were acquired in 50 mM MOPS, pH 7.4 with excitation at 580 nm.

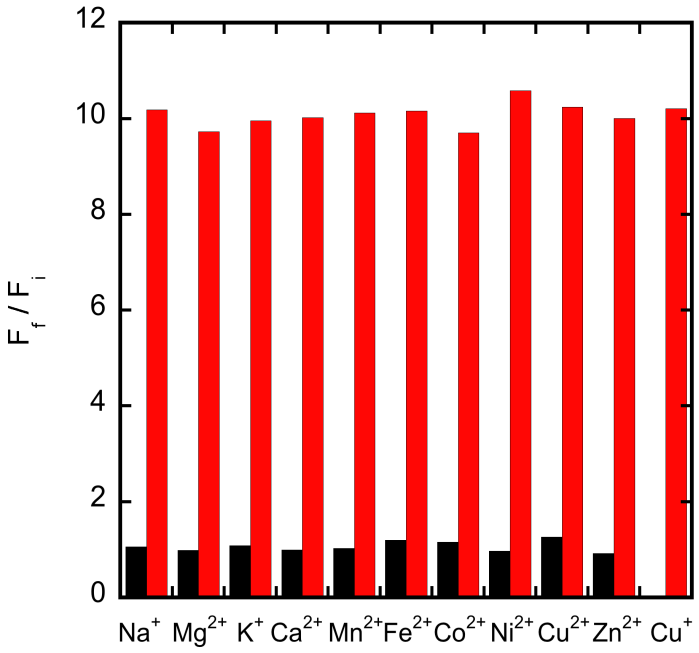

Figure 2-13. Fluorescence response of **CCF1** to various metal ions. Bars represent the final integrated fluorescence response (F_f) over the initial integrated emission (F_i). Spectra were acquired in 50 mM MOPS, pH 7.4. Black bars represent the addition of an excess of the appropriate metal ion (2 mM for Na^+, Mg^{2+}, K^+, Ca^{2+}, and Zn^{2+}, 50 μM for all other cations) to a 2 μM solution of CCF1. Red bars represent the subsequent addition of 2 μM Cu^+ to the solution. Excitation was provided at 580 nm, and the collected emission was integrated over 598 to 618 nm.

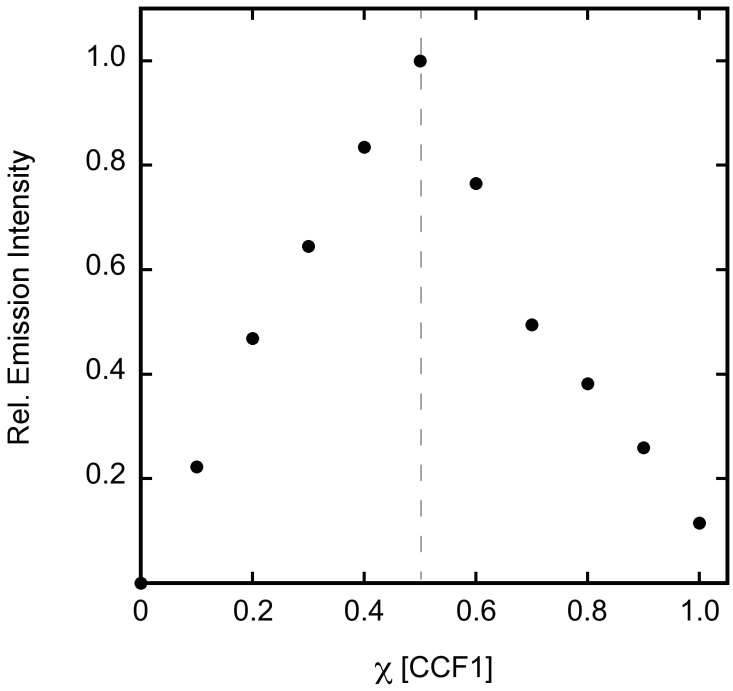

Figure 2-14. Job's plot of **CCF1** and Cu^+. The total concentration of **CCF1** and Cu^+ was kept at a constant 4 μM. Excitation was provided at 580 nm and the collected emission intensity was integrated from 598 to 618 nm. Spectra were acquired in 50 mM MOPS pH 7.4. The maximum fluorescence response at 0.50 mol fraction of **CCF1** indicates formation of a 1:1 Cu^+:**CCF1** complex.

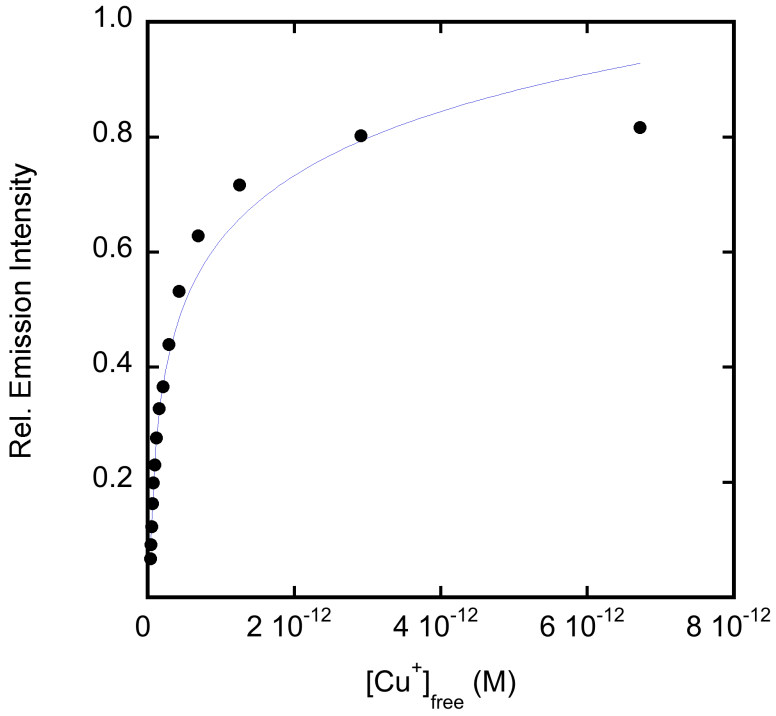

Figure 2-15. Normalized fluorescence response of 2 μM **CCF1** to thiourea buffered Cu^+ solutions for K_d value determination. Excitation was provided at 580 nm and the collected emission was integrated from 598 to 618 nm. Spectra were acquired in 50 mM MOPS, pH 7.4. The points shown are for free Cu^+ buffered at 28.5, 36.6, 43.0, 51.1, 61.4, 74.9, 93.0, 118, 153, 205, 287, 425, 684, 1253, 2913 and 6720 fM, respectively. The observed K_d value is 4.67 x 10^{-13} M.

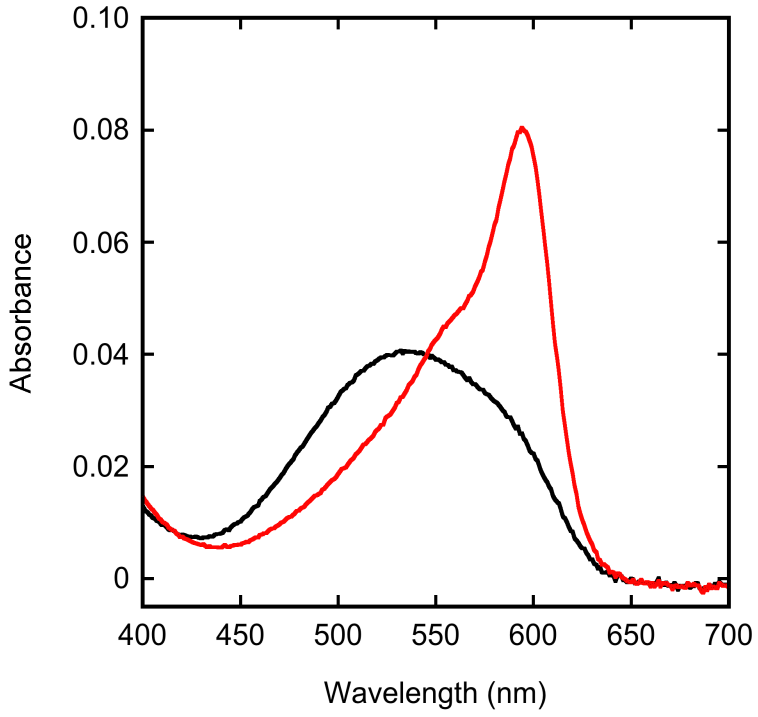

Figure 2-16. Absorbance spectra of 5 μM **CCF4**. Spectra shown are for buffered [Cu^{+}] of 0.0 (black trace) and 5.0 (red trace) μM. Spectra were acquired in 50 mM HEPES, pH 7.4.

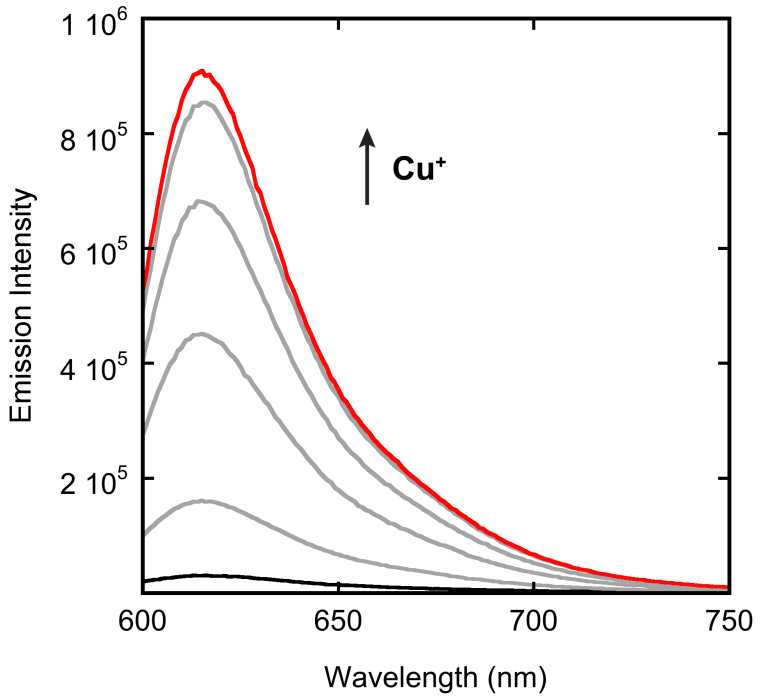

Figure 2-17. Fluorescence response of 5 μM **CCF4** to Cu^+. Spectra shown are for buffered [Cu^+] of 0.0, 1.0, 2.0, 3.0, 4.0, and 5.0 μM. Spectra were acquired in 50 mM HEPES, pH 7.4 with excitation at 594 nm.

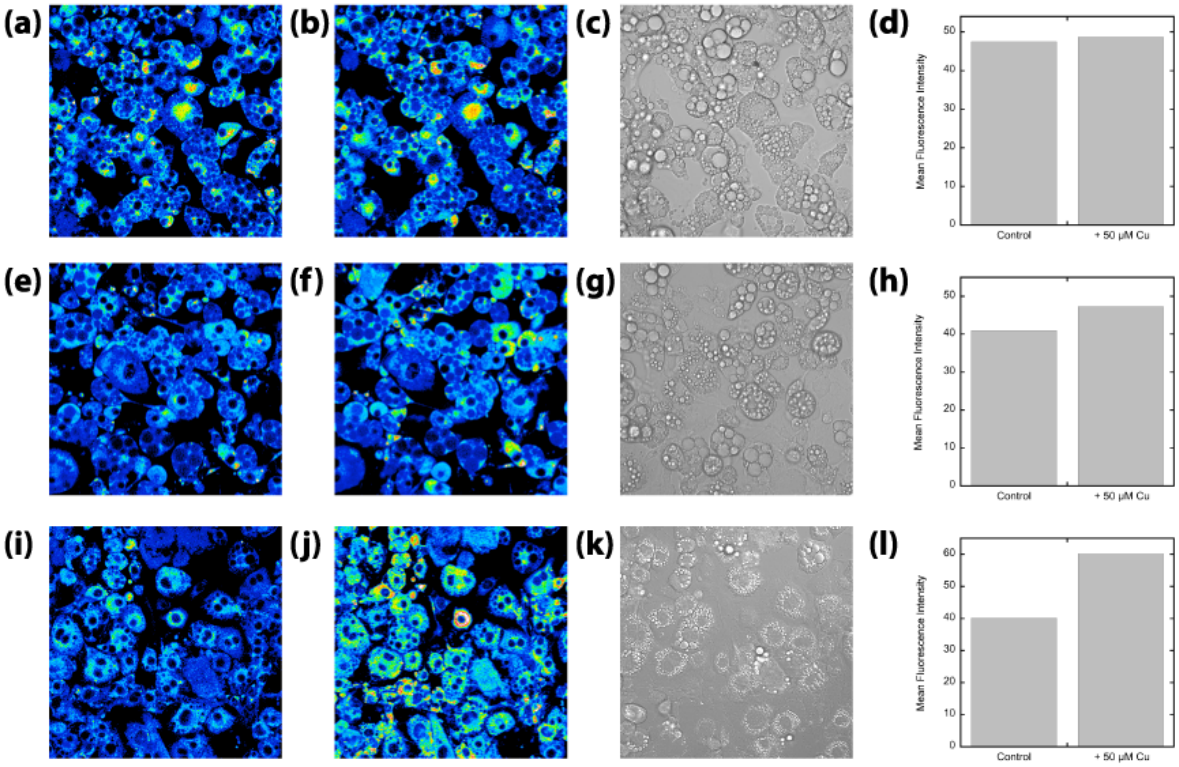

Figure 2-18. Imaging of copper-supplemented 3T3-L1 adipocytes with carborhodol probes. (a) Adipocytes incubated with 2 µM **CCR1** for 10 min at 37 ºC in DMEM, (b) on-stage treatment with 50 µM $CuCl_2$, (c) brightfield image of cells in (b) to show viability and (d) quantification of mean fluorescence intensity of each condition. (e) Adipocytes incubated with 2 µM **CCR4** for 10 min at 37 ºC in DMEM, (f) on-stage treatment with 50 µM $CuCl_2$, (g) brightfield image of cells in (f) to show viability and (h) quantification of mean fluorescence intensity of each condition. (i) Adipocytes incubated with 2 µM **CCF4** for 10 min at 37 ºC in DMEM, (j) on-stage treatment with 50 µM $CuCl_2$, (k) brightfield image of cells in (j) to show viability and (l) quantification of mean fluorescence intensity of each condition.

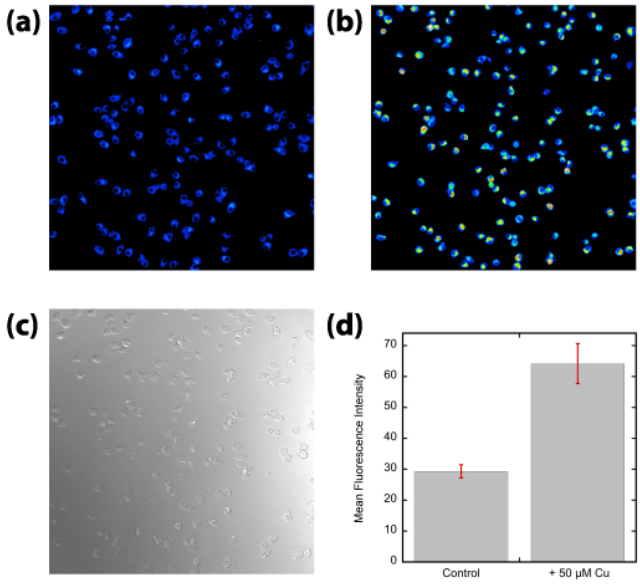

Figure 2-19. Molecular imaging of labile copper in RAW 264.7 macrophages with **CCF4**. Cells were stained with 2 µM **CCF4** for 10 min at 37 ºC in DMEM. Images show (a) control macrophages, (b) on-stage supplementation with 50 µM $CuCl_2$ and (c) brightfield image of cells in (b) to show viability. (d) Quantification of mean fluorescence intensity of each condition (n = 5 fields of cells per condition). Error bars represent SEM.

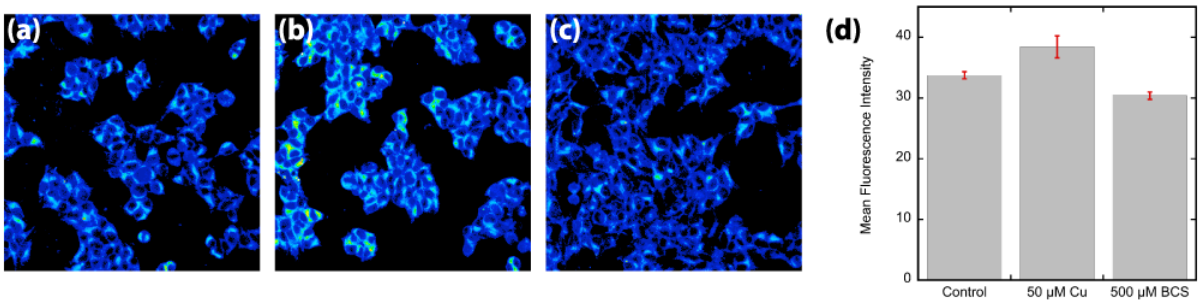

Figure 2-20. Molecular imaging of labile copper in HEK 293T cells with **CCF1**. (a) Control HEK 293T cells, HEK 293T cells supplemented with (b) 50 μM $CuCl_2$ or (c) 500 μM BCS in the growth medium for 18 h at 37 ºC were stained with 5 μM **CCF1** for 15 min at 37 ºC in DMEM. (d) Quantification of mean fluorescence intensity of each condition (n = 5 fields of cells per condition). Error bars represent SEM.

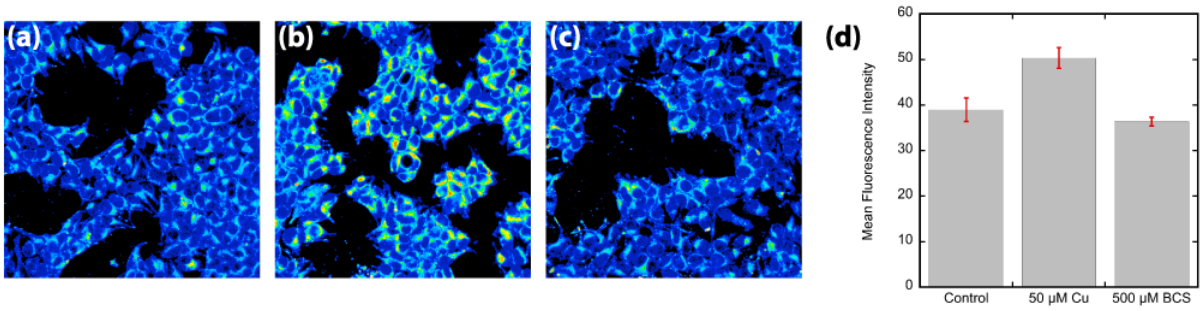

Figure 2-21. Molecular imaging of labile copper in HEK 293T cells with **CSF1**. (a) Control HEK 293T cells, HEK 293T cells supplemented with (b) 50 μM $CuCl_2$ or (c) 500 μM BCS in the growth medium for 18 h at 37 ºC were stained with 5 μM **CSF1** for 15 min at 37 ºC in DMEM. (d) Quantification of mean fluorescence intensity of each condition (n = 5 fields of cells per condition). Error bars represent SEM.

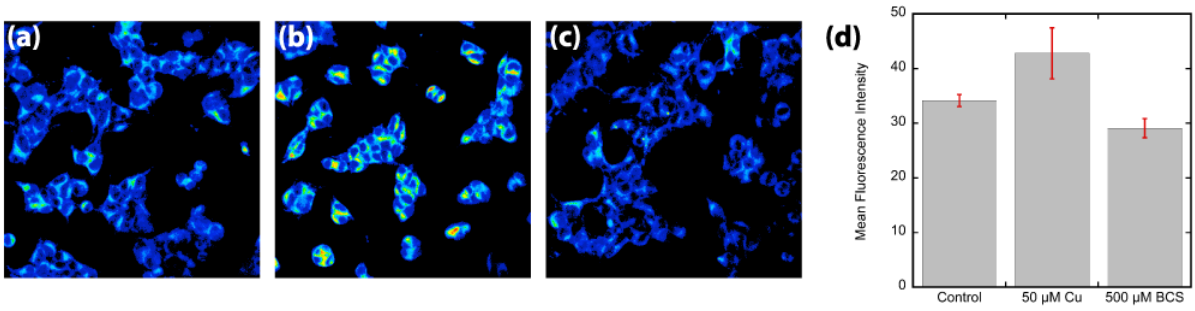

Figure 2-22. Molecular imaging of labile copper in HEK 293T cells with **CPF1**. (a) Control HEK 293T cells, HEK 293T cells supplemented with (b) 50 μM $CuCl_2$ or (c) 500 μM BCS in the growth medium for 18 h at 37 ºC were stained with 5 μM **CPF1** for 15 min at 37 ºC in DMEM. (d) Quantification of mean fluorescence intensity of each condition (n = 5 fields of cells per condition). Error bars represent SEM.

References

1. Domaille, D. W.; Que, E. L.; Chang, C. J., Synthetic fluorescent sensors for studying the cell biology of metals. *Nat. Chem. Biol.* **2008,** *4*, 168-175.
2. Aron, A. T.; Ramos-Torres, K. M.; Cotruvo, J. A.; Chang, C. J., Recognition- and Reactivity-Based Fluorescent Probes for Studying Transition Metal Signaling in Living Systems. *Acc. Chem. Res.* **2015,** *48* (8), 2434-2442.
3. Shaner, N. C.; Steinbach, P. A.; Tsien, R. Y., A guide to choosing fluorescent proteins. *Nat. Methods* **2005,** *2* (12), 905-909.
4. Giepmans, B. N.; Adams, S. R.; Ellisman, M. H.; Tsien, R. Y., The fluorescent toolbox for assessing protein location and function. *Science* **2006,** *312* (5771), 217-24.
5. Terai, T.; Nagano, T., Fluorescent probes for bioimaging applications. *Curr. Opin. Chem. Biol.* **2008,** *12* (5), 515-521.
6. Lavis, L. D.; Raines, R. T., Bright ideas for chemical biology. *ACS Chem. Biol.* **2008,** *3*, 142-155.
7. Cotruvo, J. A.; Aron, A. T.; Ramos-Torres, K. M.; Chang, C. J., Synthetic fluorescent probes for studying copper in biological systems. *Chem. Soc. Rev.* **2015,** *44* (13), 4400-4414.
8. Fahrni, C. J., Synthetic fluorescent probes for monovalent copper. *Curr. Opin. Chem. Biol.* **2013,** *17*, 656-662.
9. Yang, L.; McRae, R.; Henary, M. M.; Patel, R.; Lai, B.; Vogt, S.; Fahrni, C. J., Imaging of the intracellular topography of copper with a fluorescent sensor and by synchrotron x-ray fluorescence microscopy. *Proc. Natl. Acad. Sci. USA* **2005,** *102* (32), 11179-11184.
10. Morgan, M. T.; Bagchi, P.; Fahrni, C. J., Designed to dissolve: suppression of colloidal aggregation of Cu(I)-selective fluorescent probes in aqueous buffer and in-gel detection of a metallochaperone. *J. Am. Chem. Soc.* **2011,** *133*, 15906-15909.
11. Lim, C. S.; Han, J. H.; Kim, C. W.; Kang, M. Y.; Kang, D. W.; Cho, B. R., A copper(I)-ion selective two-photon fluorescent probe for in vivo imaging. *Chem. Commun. (Camb.)* **2011,** *47*, 7146-7148.
12. Zeng, L.; Miller, E. W.; Pralle, A.; Isacoff, E. Y.; Chang, C. J., A selective turn-on fluorescent sensor for imaging copper in living cells. *J. Am. Chem. Soc.* **2006,** *128*, 10-11.
13. Dodani, S. C.; Domaille, D. W.; Nam, C. I.; Miller, E. W.; Finney, L. A.; Vogt, S.; Chang, C. J., Calcium-dependent copper redistributions in neuronal cells revealed by a fluorescent copper sensor and X-ray fluorescence microscopy. *Proc. Natl. Acad. Sci. USA* **2011,** *108* (15), 5980-5985.
14. Dodani, S. C.; Leary, S. C.; Cobine, P. A.; Winge, D. R.; Chang, C. J., A targetable fluorescent sensor reveals that copper-deficient SCO1 and SCO2 patient cells prioritize mitochondrial copper homeostasis. *J. Am. Chem. Soc.* **2011,** *133* (22), 8606-8616.
15. Dodani, S. C.; Firl, A.; Chan, J.; Nam, C. I.; Aron, A. T.; Onak, C. S.; Ramos-Torres, K. M.; Paek, J.; Webster, C. M.; Feller, M. B.; Chang, C. J., Copper is an endogenous modulator of neural circuit spontaneous activity. *Proc. Natl. Acad. Sci. USA* **2014,** *111*, 16280-16285.
16. Krishnamoorthy, L.; Cotruvo, J. A. J.; Chan, J.; Kaluarachchi, H.; Muchenditsi, A.; Pendyala, V. S.; Jia, S.; Aron, A. T.; Vander Wal, M. N.; Guan, T.; Smaga, L. P.; Farhi, S. S.; New, E. J.; Lutsenko, S.; Chang, C. J., Copper regulates cyclic AMP-dependent lipolysis. *Nat. Chem. Biol.* **2016,** *12*, 586-592.

17. Cao, X.; Lin, W.; Wan, W., Development of a near-infrared fluorescent probe for imaging of endogenous Cu^+ in live cells. *Chem. Commun. (Camb.)* **2012,** *48*, 6247-6249.
18. Hirayama, T.; Van de Bittner, G. C.; Gray, L. W.; Lutsenko, S.; Chang, C. J., Near-infrared fluorescent sensor for in vivo copper imaging in a murine Wilson disease model. *Proc. Natl. Acad. Sci. USA* **2012,** *109* (7), 2228-2233.
19. Ohulchanskyy, T. Y.; Donnelly, D. J.; Detty, M. R.; Prasad, P. N., Heteroatom Substitution Induced Changes in Excited-State Photophysics and Singlet Oxygen Generation in Chalcogenoxanthylium Dyes: Effect of Sulfur and Selenium Substitutions. *J. Phys. Chem. B* **2004,** *108* (25), 8668-8672.
20. Arden-Jacob, J.; Frantzeskos, J.; Kemnitzer, N. U.; Zilles, A.; Drexhage, K. H., New fluorescent markers for the red region. *Spectrochim. Acta Mol. Biomol. Spectrosc.* **2001,** *57* (11), 2271-2283.
21. Kolmakov, K.; Belov, V. N.; Bierwagen, J.; Ringemann, C.; Muller, V.; Eggeling, C.; Hell, S. W., Red-emitting rhodamine dyes for fluorescence microscopy and nanoscopy. *Chemistry* **2010,** *16* (1), 158-166.
22. Kolmakov, K.; Wurm, C.; Sednev, M. V.; Bossi, M. L.; Belov, V. N.; Hell, S. W., Masked red-emitting carbopyronine dyes with photosensitive 2-diazo-1-indanone caging group. *Photochem. Photobiol. Sci.* **2012,** *11* (3), 522-532.
23. Grimm, J. B.; Sung, A. J.; Legant, W. R.; Hulamm, P.; Matlosz, S. M.; Betzig, E.; Lavis, L. D., Carbofluoresceins and Carborhodamines as Scaffolds for High-Contrast Fluorogenic Probes. *ACS Chem. Biol.* **2013,** *8* (6), 1303-1310.
24. Egawa, T.; Koide, Y.; Hanaoka, K.; Komatsu, T.; Terai, T.; Nagano, T., Development of a fluorescein analogue, TokyoMagenta, as a novel scaffold for fluorescence probes in red region. *Chem. Commun. (Camb.)* **2011,** *47* (14), 4162-4164.
25. Koide, Y.; Urano, Y.; Hanaoka, K.; Terai, T.; Nagano, T., Evolution of group 14 rhodamines as platforms for near-infrared fluorescence probes utilizing photoinduced electron transfer. *ACS Chem. Biol.* **2011,** *6* (6), 600-608.
26. Kushida, Y.; Hanaoka, K.; Komatsu, T.; Terai, T.; Ueno, T.; Yoshida, K.; Uchiyama, M.; Nagano, T., Red fluorescent scaffold for highly sensitive protease activity probes. *Bioorg. Med. Chem. Lett.* **2012,** *22* (12), 3908-3911.
27. Lukinavicius, G.; Umezawa, K.; Olivier, N.; Honigmann, A.; Yang, G.; Plass, T.; Mueller, V.; Reymond, L.; Correa, I. R., Jr.; Luo, Z. G.; Schultz, C.; Lemke, E. A.; Heppenstall, P.; Eggeling, C.; Manley, S.; Johnsson, K., A near-infrared fluorophore for live-cell super-resolution microscopy of cellular proteins. *Nat. Chem.* **2013,** *5* (2), 132-139.
28. Calitree, B.; Donnelly, D. J.; Holt, J. J.; Gannon, M. K.; Nygren, C. L.; Sukumaran, D. K.; Autschbach, J.; Detty, M. R., Tellurium Analogues of Rosamine and Rhodamine Dyes: Synthesis, Structure, 125Te NMR, and Heteroatom Contributions to Excitation Energies. *Organometallics* **2007,** *26* (25), 6248-6257.
29. Fukazawa, A.; Suda, S.; Taki, M.; Yamaguchi, E.; Grzybowski, M.; Sato, Y.; Higashiyama, T.; Yamaguchi, S., Phospha-fluorescein: a red-emissive fluorescein analogue with high photobleaching resistance. *Chem. Commun. (Camb.)* **2016,** *52* (6), 1120-1123.
30. Whitaker, J. E.; Haugland, R. P.; Ryan, D.; Hewitt, P. C.; Haugland, R. P.; Prendergast, F. G., Fluorescent rhodol derivatives: versatile, photostable labels and tracers. *Anal. Biochem.* **1992,** *207*, 267-279.

31. Grimm, J. B.; English, B. P.; Chen, J.; Slaughter, J. P.; Zhang, Z.; Revyakin, A.; Patel, R.; Macklin, J. J.; Normanno, D.; Singer, R. H.; Lionnet, T.; Lavis, L. D., A general method to improve fluorophores for live-cell and single-molecule microscopy. *Nat. Methods* **2015,** *12* (3), 244-250.
32. Hamza, I.; Prohaska, J.; Gitlin, J. D., Essential role of Atox1 in the copper-mediated intracellular trafficking of the Menkes ATPase. *Proc. Natl. Acad. Sci. USA*. **2003,** *100*, 1215-1220.
33. Stephens, J. M.; Lee, J.; Pilch, P. F., Tumor necrosis factor-alpha-induced insulin resistance in 3T3-L1 adipocytes is accompanied by a loss of insulin receptor substrate-1 and GLUT4 expression without a loss of insulin receptor-mediated signal transduction. *J. Biol. Chem.* **1997,** *272* (2), 971-976.

Chapter 3:

Development of a Xanthene Based Family of Cu^{+} Responsive Probes with a Novel Tripodal NS_3 Receptor

Abstract

Development of fluorescent copper probes with a wide range of binding affinities is desired in order to be able to access different cellular metal pools. This Chapter summarizes the design, synthesis and application of a novel tripodal NS_3 receptor for visualizing biological copper. Combination of this new binding moiety with an array of xanthene-based chromophores afforded a palette of probes with varying turn-on responses upon Cu^+ binding and good selectivity for Cu^+ over other biologically relevant metal ions in aqueous solution. Additionally, confocal microscopy experiments show that this platform is suitable for sensing endogenous copper pools in living cells.

Introduction

The design of an ideal small-molecule sensor for the detection of bio-relevant analytes generally includes addressing properties like a selective turn-on response to the analyte of interest, high brightness, high quantum yield, and biocompatibility. Furthermore, in the development of recognition-based probes, tuning the affinity of the binding-platform to the analyte, so that it lies within the appropriate range for the intended application, is a key element to address. Considering that cellular copper is associated with a variety of ligands with different binding strengths, it is desirable to be able to access probes with a range of binding affinities in hopes of studying different biological pools of this metal. In order to report on the dynamics of cellular copper, fluorescent sensors must be capable of metal exchange with native copper ligands that exhibit picomolar (10^{-12} M) to subfemtomolar ($< 10^{-15}$ M)[1] affinities for the cation. While current available probes for copper typically present dissociation constant values in the modest 10^{-11} to 10^{-13} M range,[2-4] visualization of endogenous copper levels in various systems,[5-8] as well as interesting copper dynamics involved in transition metal signaling,[5,7,8] has been possible. Nevertheless, expansion of the available copper probe toolbox to access a more complete array of binding strengths could lead to the discovery of new roles for copper by probing previously inaccessible pools of the metal.

Approaches to modulate the binding affinities of fluorescent sensors for the metal of interest involve alterations to the fluorophore reporter or to the metal-binding receptor. Although the use of more electron-rich fluorophores can lead to an improvement in the metal binding properties of the sensor,[5] dye variations usually lead to lesser adjustments of these values. In order to more directly influence the binding affinity, changes to the metal binding framework are necessary. Established strategies to modulate cation binding by receptor platforms include affecting the strength of individual metal-ligand (M-L) bonds[9,10] (by electronic or steric effects), changing the number of total M-L interactions[11] and introducing differences in the coordination sphere[11-15] by varying the donor set. Additionally, chelator strength has been shown to depend on the binding geometry,[16,17] the chelate ring size[15,17] and the ligand architecture[18-21].

Tripodal ligand topologies that better accommodate tetrahedral coordination geometries when compared to macrocyclic or acyclic constructions have been shown to form favorable Cu^+ complexes.[21,22] Here we present the development of a novel NS_3-based receptor for Cu^+ and its application in a palette of sensors for biological application. Since thioether coordination has been proven to impart selectivity in binding of soft Cu^+ over other biologically relevant metals,[23,24] we have included three thioether motifs in the design of this metal-binding platform. The final donor

of the coordination unit, the amino moiety, serves as the traditional photoinduced electron transfer (PeT) on/off switch for sensing as well as the bridgehead for the tripodal architecture of the ligand.

Results and Discussion

Synthesis of a Tripodal NS_3 Metal Binding Domain for the Sensing Copper. The construction of a copper binding domain with an NS_3 coordination sphere and a true tripodal ligand architecture is outlined in Scheme 3-1. Briefly, insertion of the first thioether donor via nucleophilic aromatic substitution of **1** with sodium thiomethoxide afforded methylthio-substituted benzoic acid **2**, which was subsequently reduced to alcohol **3**. The corresponding benzyl chloride **4** was accessed by reaction with thionyl chloride in anhydrous dichloromethane. Finally, incorporation of bis(2-(ethylthio)ethyl)amine **5** via nucleophilic displacement of the benzyl chloride allowed for the introduction of the amino-bridgehead and the two final thioether donors of bromobenzene tripodal receptor **6**. Furthermore, this synthetic approach involving the displacement of a modified benzyl chloride unit allows for the facile introduction of a variety of amino-bridged binding domains, giving access to the possible evaluation of the effect of altered coordination units as well as chelate ring size effects of corresponding donor sets.

Synthesis and Spectroscopic Characterization of a First Generation of Xanthene-Based Copper Probes with Novel Tripodal NS_3 Receptor. Model tripodal NS_3 receptor **6** was incorporated to well established xanthene-based fluorophore platforms to develop first generation probes for copper sensing. The general syntheses for probes **CR3 TT-556** and **TG TT-556** proceeded through addition of an aryl lithium species, derived from lithium halogen exchange of **6**, to appropriate xanthones **7** and **8** to afford the CopperRhodol and TokyoGreen analogues, respectively. Spectroscopic characterization of both probes, performed in 50 mM MOPS buffered at pH 7.4, showed characteristic optical features of xanthene-based dyes. *Apo*-**CR3 TT-556** presents a broad absorption band at 530 nm, and fluorescence emission centered at 557 nm. (Figures 3-1, 3-2) Upon copper binding to the receptor, interruption of non-radiative relaxation pathways allows for an increase of the excited-state lifetime, which results in a narrowing of the absorption bandwidth and a bathochromic shift of the peak maximum ($\lambda_{abs\ (Cu)}$ 535 nm). Additionally, a 2.2-fold enhancement in the fluorescence intensity at 557 nm is observed with the addition of one equivalent of Cu^+. **TG TT-556** exhibits parallel features to **CR3 TT-556** – a hypsochromic-shifted absorption for both *apo*- and *holo*-configurations ($\lambda_{abs\ (apo/Cu)}$ 495 nm) and a 2.1-fold increase in emission at 520 nm upon copper binding. (Figures 3-4, 3-5) Moreover, the selectivity for the response to Cu^+ of the new tripodal NS_3 binding motif over a variety of biologically relevant cations (Mg^{2+}, Ca^{2+}, Mn^{2+}, Fe^{2+}, Co^{2+}, Ni^{2+}, Cu^{2+}, and Zn^{2+}) was established with competition experiments using **CR3 TT-556** as a model probe. (Figure 3-3)

Electron-rich Fluorophore Scaffolds for the Synthesis of More Responsive TT-556 Copper Sensors. Although the first generation of xanthene-based copper probes with the tripodal receptor scaffold showed a promising turn-on response upon copper binding, further characterization of the binding mode and affinity to copper could not be accurately completed because of the modest dynamic range observed. In order to address this limitation, we sought to evaluate more closely the electronics of the modified electron-donor (tripodal NS_3 receptor **6**) and its ability to modulate fluorescence via a PeT quenching mechanism when combined with traditional xanthene-based electron-acceptors. For this purpose, we calculated and compared the HOMO energy for

compounds **A** (model compound for tripodal NS_3 receptor **6)** and **B** (model compound for a commonly used copper receptor[5,7,8,25]). Nagano and coworkers have previously established that HOMO energies of the electron donors that lie between – 0.20 and – 0.22 hartrees are most appropriate for PeT modulation in TokyoGreen, rhodamine and rhodol-based systems.[26,27] Consequently, electron donors with HOMO energy values that fall out of this range are not suitable partners for the construction of PeT-based sensors with these common fluorophore platforms. Density functional theory (DFT) calculation of the HOMO energy of model compound **A** showed a higher energy value (– 0.1793 hartree), that lies out of the desired range for PeT-assisted fluorescence modulation, when compared to model compound **B** (– 0.2210 hartree). (Figure 3-6) This result suggested that increasing the electron density of the fluorophore acceptor would lead to a better electronic matching with electron donor **6** and thus improve the fluorescence enhancement that results from PeT modulation.

Use of more electron-rich alkyl-substituted xanthones **9** and **10** afforded the corresponding probes, **Me2TG TT-556** and **EtTG TT-556**. In aqueous conditions, *apo*-**Me2TG TT-556** exhibits two major absorption peaks at 499 nm and 540 nm, with a fluorescence emission band at 543 nm. (Figures 3-7, 3-8) Upon copper binding, a decrease in intensity of the absorption bands at 499 nm and 540 nm is observed in combination with the appearance of an intense feature at 519 nm. Additionally, a 10.0-fold fluorescence enhancement with no shift in the emission maximum ($\lambda_{fl\ (Cu)}$ 540 nm) is detected with addition of one equivalent of Cu^+. **EtTG TT-556** presents a similar optical profile with absorption peaks at 478 nm and 512 nm in the *apo*-state, and a single band at 508 nm in the Cu-bound form. A fluorescence band at 530 nm is observed for both configurations, with a 5.5-fold enhancement of the emission intensity upon addition of one equivalent of Cu^+.

Although the use of more electron-rich fluorophores allowed for expansion of the available dynamic range, further characterization of these second-generation probes was not successful. Identification of the binding stoichiometry for the probe:Cu^+ complexes formed was not achieved due to irreproducible time-dependent variations in the fluorescence of the probes. Observation of increased background fluorescence over time, that can be slowed down at lower temperatures, in the *apo*-state of the probes led us to hypothesize that the added electron-richness of the fluorophore allows for oxidation-based degradation of the sensor, thus complicating the complete characterization of binding stoichiometry and affinity of the new tripodal NS_3 receptor framework.

Live-cell Imaging of Xanthene-based TT-556 Copper Sensors with Confocal Microscopy. We next sought to investigate if the tripodal NS_3 receptor allowed for visualization of endogenous levels of labile copper. Live human embryonic kidney cells (HEK 293T) incubated with 2 μM **Me2TG TT-556** or **EtTG TT-556** for 10 min at 37 ºC showed intracellular fluorescence as observed by confocal microscopy. Cells grown with either 50 or 200 μM $CuCl_2$, supplemented in the growth medium overnight, exhibit an increase of intracellular fluorescence upon staining with the second-generation probes. (Figures 3-11b, 3-12b, 3-13b, 3-14b) Overnight treatments with 200 or 500 μM of the cell-impermeable copper chelator bathocuproinedisulfonic acid (BCS) afforded decreases in the fluorescence levels, indicating that the probes are able to sense endogenous pools of labile copper in this cell line. (Figures 3-11c, 3-12c, 3-13c, 3-14c) Quantification of these experiments show comparable responses for **Me2TG TT-556** and **EtTG TT-556** at lower treatment concentrations, but a more sensitive response of **Me2TG TT-556** at higher treatment

concentrations that corresponds to the larger dynamic range observed *in vitro*. (Figures 3-11e, 3-12e, 3-13e, 3-14e)

Concluding Remarks

In this report, we have presented the design and synthesis of a novel tripodal NS_3 receptor for the detection of biological copper. Combination of this metal-binding platform with an assortment of xanthene-based fluorophores allowed for the development of a palette of probes with visible excitation and emission profiles and a range of selective, turn-on responses upon copper binding. Confocal microscopy experiments with the more sensitive probes showed that they are suitable for visualizing changes in the endogenous labile copper pools of living cells. Future efforts for assay development to characterize the identity of the probe:Cu^+ complexes formed and the binding affinity towards copper will lead to a better understanding of the effects of the ligand topology, donor set and coordination geometry on the ability to sense biological copper.

Experimental Section

Synthetic Materials and Methods. All reactions were carried out under a dry N_2 atmosphere and stirred magnetically unless stated otherwise. All reactions using air- or moisture-sensitive reagents were performed in oven- and flame-dried glassware under an atmosphere of dry N_2. THF used for anhydrous reactions was dried and stored over 3-Å molecular sieves. Compounds **7**[28] and **8**[7] were synthesized according to literature procedures. Compounds **9** and **10** were synthesized by Samouil Farhi. Unless otherwise noted, all chemicals were used as received. Silica gel P60 (SiliCycle) and activated basic aluminum oxide (Brockmann) were used for column chromatography. Flash chromatography was performed on an automated purification system using pre-packed silica gel columns. SiliCycle 60 F254 silica gel (precoated sheets, 0.25 mm thick) was used for analytical TLC, visualized with UV light and/or staining with p-anisaldehyde or $KMNO_4$. ^1H and ^{13}C NMR spectra were collected in $CDCl_3$ (Cambridge Isotope Laboratories, Cambridge, MA) at 25 °C on a Bruker AV-300, Bruker AVB-400 or Bruker AVQ-400 spectrometer at the College of Chemistry NMR Facility at the University of California, Berkeley. All chemical shifts are reported in the standard notation of parts per million using the peak of residual proton or carbon signals of $CDCl_3$ as an internal reference.

Synthesis.

Methyl 4-bromo-2-fluorobenzoate (1). A solution of 4-bromo-2-fluorobenzoic acid (10.0 g, 45.66 mmol) in MeOH (97.1 mL, 0.47 M) was charged with con. HCl (1.41 mL, 17.08 mmol, 0.37 eq) and stirred for 16 h at reflux. The reaction mixture was cooled to room temperature, and MeOH was removed under reduced pressure. The resulting white solid residue was dissolved in a EtOAc and H_2O mixture and layers were then separated. The combined organic layers were washed with sat. $NaHCO_3$, then brine, dried with Na_2SO_4 and concentrated under reduced pressure. Resulting white solid (9.99 g, 94 %) was used without further purification. ^1H NMR (400 MHz, $CDCl_3$) δ 7.82 (dd, J = 8.7, 7.7 Hz, 1H), 7.39 – 7.32 (m, 2H), 3.93 (s, 3H).

4-Bromo-2-(methylthio)benzoic acid (2). A solution of **1** (9.74 g, 41.79 mmol) in DMF (64.3 mL, 0.65 M) was treated with a solution of $NaSCH_3$ (3.0 M in H_2O, 69.9 mL, 5 eq). The reaction mixture was heated to 80 ºC and stirred at this temperature for 16 h. Upon completion, reaction mixture was cooled to 0 ºC and the pH was adjusted to ~ 2-3 using conc. HCl. The mixture was then extracted with EtOAc (x3). The combined organic layers were washed with brine, dried with Na_2SO_4 and concentrated under reduced pressure. The crude residue was purified via flash column chromatography on silica gel (0-100 % EtOAc/hexanes, linear gradient) to yield 3.92 g (38 %) of **2** as a white solid. ^{1}H NMR (400 MHz, $CDCl_3$) δ 7.98 (d, *J* = 8.4 Hz, 1H), 7.39 (d, *J* = 1.9 Hz, 1H), 7.32 (dd, *J* = 8.4, 1.8 Hz, 1H), 2.47 (s, 3H).

(4-Bromo-2-(methylthio)phenyl)methanol (3). A solution of benzoic acid **2** (0.68 g, 2.74 mmol) in anhydrous THF (6.0 mL, 0.46 M) was cooled to -40 ºC using a dry ice/acetone bath. A BH_3-THF complex solution (1.0 M in THF, 5.5 mL, 2 eq) was then added dropwise. Upon addition, reaction was heated to 50 ºC and stirred for 1.5 h. Reaction was then quenched with careful addition of MeOH at 0 ºC and concentrated under reduced pressure. Crude was purified via flash column chromatography on silica gel (0-25 % EtOAc/hexanes, linear gradient) to afford 0. 44 g (68 %) of **3** as a white solid. ^{1}H NMR (400 MHz, $CDCl_3$) δ 7.24 – 7.21 (m, 1H), 7.21 – 7.18 (m, 1H), 7.14 (d, *J* = 8.0 Hz, 1H), 4.54 (s, 2H), 3.39 (s, 1H), 2.42 (s, 3H).

(5-Bromo-2-(chloromethyl)phenyl)(methyl)sulfane (4). Alcohol **3** (0.44 g, 1.88 mmol) was dissolved in anhydrous CH_2Cl_2 (18.8 mL, 0.10 M) and charged with thionyl chloride (0.31 mL, 4.32 mmol, 2.3 eq). Reaction was stirred at room temperature for 4 h. Upon completion, as judged by TLC, the reaction was quenched with careful addition of sat. $NaHCO_3$ and then washed with CH_2Cl_2 (x3). The combined organic layers dried with Na_2SO_4 and concentrated under reduced pressure. After purification via flash column chromatography on silica gel (0-10 % EtOAc/hexanes, linear gradient) **4** (0.34 g, 73 %) was attained as a colorless oil. ^{1}H NMR (400 MHz, $CDCl_3$) δ 7.39 (d, *J* = 1.9 Hz, 1H), 7.31 (dd, *J* = 8.2, 2.0 Hz, 1H), 7.25 (d, *J* = 8.2 Hz, 1H), 4.68 (s, 2H), 2.54 (s, 3H). ^{13}C NMR (101 MHz, $CDCl_3$) δ 140.64, 133.84, 131.16, 128.62, 128.14, 123.17, 43.51, 15.93.

Bis(2-(ethylthio)ethyl)amine (5). A flame-dried three-necked round-bottom flask was charged with ethanol (560.3 mL, 1.0 M in sodium). Under a dry N_2 atmosphere, sodium (12.88 g, 560.26 mmol, 5 eq) was carefully added in small portions. After all the sodium has dissolved, ethanethiol (24.9 mL, 336.15 mmol, 3 eq) was added dropwise to the sodium ethoxide solution. Reaction mixture was heated to reflux and then a solution of bis(2-chloroethyl)amine hydrochloride (20.0 g, 112.1 mmol) in ethanol (280.1 mL, 0.4 M in amine) was added dropwise. Upon completion of addition, reaction mixture was stirred at reflux for 2 h. Reaction was then cooled to room temperature and ethanol was removed under reduced pressure. Residue was taken up in chloroform and washed with H_2O (x3). Organic layer was dried with Na_2SO_4 and concentrated under reduced pressure. Crude was purified via vacuum distillation to afford 13.29 g (61 %) of **5** as a pale yellow oil. ^{1}H NMR (400 MHz, $CDCl_3$) δ 2.81 (t, *J* = 6.6 Hz, 4H), 2.68 (t, *J* = 6.6 Hz, 4H), 2.53 (q, *J* = 7.4 Hz, 4H), 1.78 (s, 1H), 1.25 (t, *J* = 7.4 Hz, 6H). ^{13}C NMR (101 MHz, $CDCl_3$) δ 48.28, 31.86, 25.80, 14.84.

***N*-(4-Bromo-2-(methylthio)benzyl)-2-(ethylthio)-*N*-(2-(ethyltho)ethyl)ethan-1-amine (6).** A solution of **4** (0.18 g, 0.71 mmol), **5** (0.28 g, 1.43 mmol, 2 eq), K_2CO_3 (0.99 g, 7.14 mmol, 10 eq) and KI (0.24 g, 1.43 mmol, 2 eq) in anhydrous acetonitrile (7.1 mL, 0.10 mmol) was stirred at 45

ºC for 16 h. Upon completion, reaction mixture was concentrated under reduced pressure. Resulting residue was dissolved in EtOAc and washed with brine (x2). Organic layer was dried with Na_2SO_4 and concentrated under reduced pressure. Purification via flash column chromatography on silica gel (0-10 % EtOAc/hexanes, linear gradient) afforded 0.25 g (87 %) of **6** as a colorless oil. ^{1}H NMR (400 MHz, $CDCl_3$) δ 7.29 (d, *J* = 8.1 Hz, 1H), 7.25 (d, *J* = 1.9 Hz, 1H), 7.21 (dd, *J* = 8.1, 2.0 Hz, 1H), 3.61 (s, 2H), 2.74 – 2.68 (m, 4H), 2.63 – 2.57 (m, 4H), 2.47 (q, *J* = 7.4 Hz, 4H), 2.42 (s, 3H), 1.20 (t, *J* = 7.4 Hz, 6H). ^{13}C NMR (101 MHz, $CDCl_3$) δ 140.46, 135.86, 130.50, 127.36, 127.33, 121.36, 55.71, 53.95, 29.14, 26.10, 15.77, 14.83.

9-(4-((Bis(2-(ethylthio)ethyl)amino)methyl)-3-(methylthio)phenyl)-6-(pyrrolidin-1-yl)-3*H*-xanthen-3-one (11, CR3 TT-556). A flame-dried three-neck round-bottom flask was charged with **6** (143.1 mg, 0.35 mmol, 2 eq) and anhydrous THF (1.2 mL, 0.30 M in **6**). The solution was cooled to -78 ºC and then *tert*-butyllithium (1.7 M in pentane, 412.6 µL, 0.70 mmol, 4 eq) was added dropwise. After stirring at the same temperature for 12 min, a solution of compound **7** (69.3 mg, 0.18 mmol) in anhydrous TFH (5.8 mL, 0.03 M in **7**) was added dropwise. The reaction was warmed to room temperature, stirred for 1 h and subsequently quenched with addition of aq. HCl (1 M, 3 mL). After 1 h, the reaction was poured into a 1:1 mixture of sat. $NaHCO_3$ and EtOAc. Layers were separated and aqueous layer was further extracted with EtOAc (x2). The combined organic layers were washed with brine, dried with Na_2SO_4 and concentrated under reduced pressure. The crude residue was purified via column chromatography on silica gel (5 % MeOH/CH_2Cl_2) to afford **CR3 TT-556** as an orange solid (11.7 mg, 11%). ^{1}H NMR (400 MHz, $CDCl_3$) δ 7.65 (d, *J* = 8.2 Hz, 1H), 7.16 – 7.03 (m, 4H), 6.59 (dd, *J* = 9.6, 2.1 Hz, 1H), 6.49 (td, *J* = 7.7, 7.1, 2.3 Hz, 3H), 3.79 (s, 2H), 3.43 (d, *J* = 6.7 Hz, 4H), 2.87 – 2.80 (m, 4H), 2.70 (dd, *J* = 9.4, 5.7 Hz, 4H), 2.54 (q, *J* = 7.4 Hz, 4H), 2.42 (s, 3H), 2.13 – 2.04 (m, 4H), 1.24 (t, *J* = 7.4 Hz, 6H). ^{13}C NMR (101 MHz, $CDCl_3$) δ 159.05, 155.67, 152.11, 139.00, 138.13, 132.54, 130.80, 130.16, 128.93, 127.13, 125.43, 125.23, 114.67, 111.19, 111.06, 104.98, 99.91, 96.98, 77.21, 55.90, 54.00, 48.09, 29.20, 26.17, 25.30, 15.64, 14.87. HRESI-MS calculated for [M+H] 593.2252, found 593.2314.

9-(4-((Bis(2-(ethylthio)ethyl)amino)methyl)-3-(methylthio)phenyl)-6-hydroxy-3*H*-xanthen-3-one (12, TG TT-556). A flame-dried three-neck round-bottom flask was charged with **6** (77.6 mg, 0.19 mmol, 2 eq) and anhydrous THF (0.6 mL, 0.30 M in **6**). The solution was cooled to -78 ºC and then *tert*-butyllithium (1.7 M in pentane, 223.5 µL, 0.34 mmol, 4 eq) was added dropwise. After stirring at the same temperature for 12 min, a solution of compound **8** (43.4 mg, 0.09 mmol) in anhydrous TFH (3.2 mL, 0.03 M in **8**) was added dropwise. The reaction was warmed to room temperature, stirred for 1 h and subsequently quenched with addition of aq. HCl (1 M, 3 mL). After 1 h, the reaction was poured into a 1:1 mixture of sat. $NaHCO_3$ and EtOAc. Layers were separated and aqueous layer was further extracted with EtOAc (x2). The combined organic layers were washed with brine, dried with Na_2SO_4 and concentrated under reduced pressure. The crude residue was purified via column chromatography on silica gel (10 % MeOH/CH_2Cl_2) to afford **TG TT-556** as an orange solid (18.1 mg, 35%). ^{1}H NMR (400 MHz, $CDCl_3$) δ 7.70 (d, *J* = 8.1 Hz, 1H), 7.28 (d, *J* = 9.2 Hz, 2H), 7.13 (d, *J* = 6.5 Hz, 2H), 6.92 – 6.84 (m, 4H), 3.80 (s, 2H), 2.85 – 2.82 (m, 4H), 2.71 – 2.68 (m, 4H), 2.53 (q, *J* = 7.4 Hz, 4H), 2.41 (s, 3H), 1.24 (t, *J* = 7.4 Hz, 6H). HRESI-MS calculated for [M+H] 540.1623, found 540.1687.

9-(4-((Bis(2-(ethylthio)ethyl)amino)methyl)-3-(methylthio)phenyl)-6-hydroxy-2,4,5,7-tetramethyl-3*H*-xanthen-3-one (13, Me2TG TT-556). A flame-dried three-neck round-bottom flask was charged with **6** (100.0 mg, 0.24 mmol, 2 eq) and anhydrous THF (0.8 mL, 0.30 M in **6**). The solution was cooled to -78 ºC and then *tert*-butyllithium (1.7 M in pentane, 288.0 µL, 0.49 mmol, 4 eq) was added dropwise. After stirring at the same temperature for 12 min, a solution of compound **9** (62.8 mg, 0.12 mmol) in anhydrous TFH (4.1 mL, 0.03 M in **9**) was added dropwise. The reaction was warmed to room temperature, stirred for 1 h and subsequently quenched with addition of aq. HCl (1 M, 3 mL). After 1 h, the reaction was poured into a 1:1 mixture of sat. $NaHCO_3$ and EtOAc. Layers were separated and aqueous layer was further extracted with EtOAc (x2). The combined organic layers were washed with brine, dried with Na_2SO_4 and concentrated under reduced pressure. The crude residue was purified via column chromatography on silica gel (5 % MeOH/CH_2Cl_2) and the resulting product was triturated with MeOH to afford **Me2TG TT-556** as an orange solid (13.5 mg, 19%). ^{1}H NMR (400 MHz, $CDCl_3$) δ 7.68 (s, 1H), 7.09 (d, *J* = 5.7 Hz, 2H), 6.86 (s, 2H), 3.85 (s, 2H), 2.87 (d, *J* = 8.0 Hz, 4H), 2.73 (dd, *J* = 9.3, 5.7 Hz, 4H), 2.55 (q, *J* = 7.4 Hz, 4H), 2.43 (s, 3H), 2.39 (s, 6H), 2.17 (s, 6H), 1.25 (t, *J* = 7.4 Hz, 6H). ^{13}C NMR (101 MHz, $CDCl_3$) δ 170.92, 152.75, 147.14, 138.93, 133.45, 129.05, 126.39, 125.82, 125.67, 115.73, 111.67, 77.31, 77.20, 77.00, 76.77, 76.68, 55.98, 54.13, 29.09, 26.20, 16.79, 15.77, 14.90, 8.36. HRESI-MS calculated for [M+H] 596.2249, found 596.2315.

9-(4-((Bis(2-(ethylthio)ethyl)amino)methyl)-3-(methylthio)phenyl)-2,7-diethyl-6-hydroxy-3*H*-xanthen-3-one (14, EtTG TT-556). A flame-dried three-neck round-bottom flask was charged with **6** (134.6 mg, 0.33 mmol, 2 eq) and anhydrous THF (1.0 mL, 0.30 M in **6**). The solution was cooled to -78 ºC and then *tert*-butyllithium (1.7 M in pentane, 390.0 µL, 0.67 mmol, 4 eq) was added dropwise. After stirring at the same temperature for 12 min, a solution of compound **10** (122.6 mg, 0.24 mmol) in anhydrous TFH (8.0 mL, 0.03 M in **10**) was added dropwise. The reaction was warmed to room temperature, stirred for 1 h and subsequently quenched with addition of aq. HCl (1 M, 3 mL). After 1 h, the reaction was poured into a 1:1 mixture of sat. $NaHCO_3$ and EtOAc. Layers were separated and aqueous layer was further extracted with EtOAc (x2). The combined organic layers were washed with brine, dried with Na_2SO_4 and concentrated under reduced pressure. The crude residue was purified via column chromatography on silica gel (5 % MeOH/CH_2Cl_2) and the resulting product was triturated with MeOH to afford **EtTG TT-556** as an orange solid (13.8 mg, 10%). ^{1}H NMR (400 MHz, $CDCl_3$) δ 9.10 (s, 1H), 7.71 (d, *J* = 8.0 Hz, 1H), 7.18 – 7.10 (m, 2H), 7.08 (s, 2H), 6.87 (s, 2H), 3.85 (s, 2H), 2.87 (dd, *J* = 9.4, 5.9 Hz, 4H), 2.72 (dd, *J* = 9.3, 5.8 Hz, 4H), 2.61 (q, *J* = 7.4 Hz, 4H), 2.55 (q, *J* = 7.4 Hz, 5H), 1.26 (t, *J* = 7.4 Hz, 6H), 1.12 (t, *J* = 7.4 Hz, 6H). ^{13}C NMR (101 MHz, $CDCl_3$) δ 173.96, 156.76, 139.06, 138.46, 136.75, 132.51, 129.01, 127.58, 125.62, 114.63, 102.73, 77.32, 77.00, 76.68, 56.09, 54.22, 29.23, 26.18, 23.32, 15.78, 14.91, 13.60. HRESI-MS calculated for [M+H] 596.2249, found 596.2314.

Spectroscopic Materials and Methods. Millipore water was used to prepare all aqueous solutions. All final spectroscopic measurements were performed in MOPS buffer. Absorption spectra were recorded using a Varian Cary 50 spectrophotometer (Walnut Creek, CA) and fluorescence spectra were recorded using a Photon Technology International Quanta Master 4 L-format scan spectrofluorometer (Lawrenceville, NJ) equipped with an LPS-220B 75-W xenon lamp and power supply, A-1010B lamp housing with integrated igniter, switchable 814

photocounting/analog photomultiplier detection unit, and MD5020 motor driver. Samples for absorption and emission measurements were contained in 1-cm quartz cuvettes (1.4-mL volume, Starna, Atascadero, CA). Cu^+ was delivered in the form of $[Cu(MeCN)_4][PF_6]$ from an acetonitrile stock solution (2 mM). Excitation was provided at 535 nm and collected emission was integrated from 540-700 nm for CR3 TT-556, 495 nm and collected emission was integrated from 501-700 nm for TG TT-556, 519 nm and collected emission was integrated from 525-700 nm for Me2TG TT-556, and 508 nm and collected emission was integrated from 515-700 nm for EtTG TT-556.

Cell Culture. HEK 293T cells were cultured in Dulbecco's Modified Eagle Medium (DMEM, Invitrogen, Carlsbad, CA) supplemented with 10% Fetal Bovine Serum (FBS, Invitrogen), glutamine (2mM) and penicillin/streptomycin (50 mg/mL, Invitrogen). One day before imaging, cells were passed and plated on 18-mm glass coverslips coated with poly-L-lysine (50 mg/mL, Sigma, St. Louis, MO). Immediately before the experiments, cells were washed with DMEM buffer and imaged. Experiments to assess copper uptake were performed in the same media supplemented with the additives at the indicated concentrations.

Live-Cell Imaging. Confocal fluorescence imaging was performed with a Zeiss LSM 710 laser-scanning microscope and a 20x objective lens. Excitation of **Me2TG TT-556** or **EtTG TT-556** loaded cells at 514 nm was carried out with a He-Ne laser, and emission was collected using a META detector between 520 and 733 nm. Probe (2 μM in DMEM) was incubated with live cells samples for 10 min at 37 °C. Staining solution was exchanged with fresh DMEM and cells were imaged. Images were analyzed using ImageJ.

Schemes and Figures

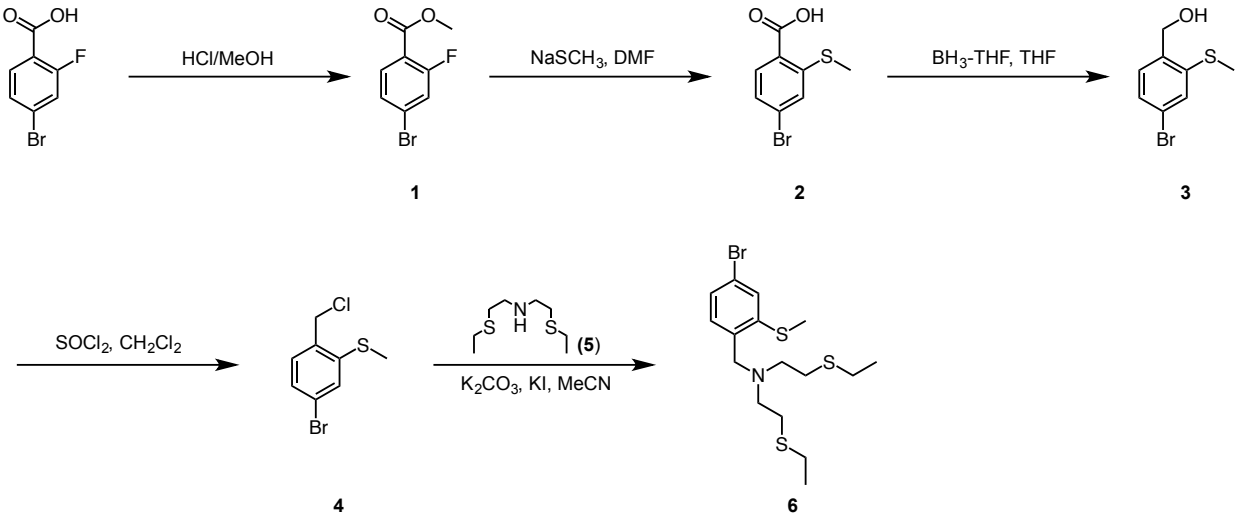

Scheme 3-1. Synthesis of novel tripodal NS_3 receptor for copper (I) sensing

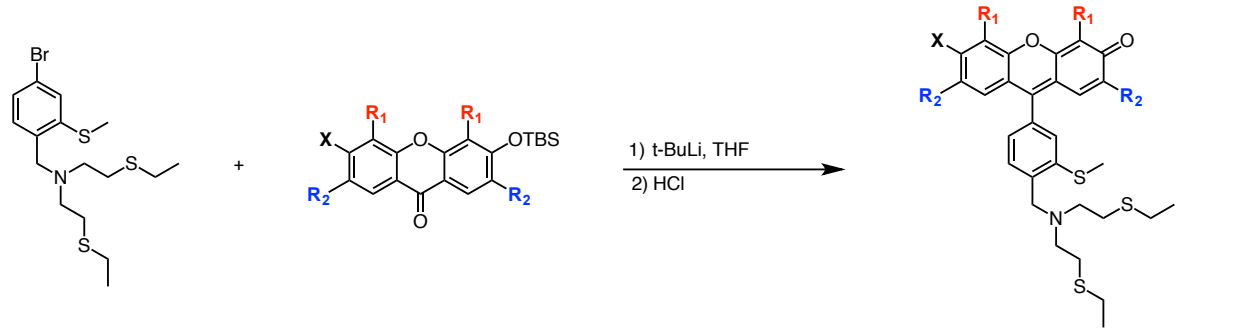

6

7 (**X**: pyrrolidine, R_1: H, R_2: H)
8 (**X**: OTBS, R_1: H, R_2: H)
9 (**X**: OTBS, R_1: CH_3, R_2: CH_3)
10 (**X**: OTBS, R_1: H, R_2: CH_2CH_3)

11 (**X**: pyrrolidine, R_1: H, R_2: H) **CR3 TT-556**
12 (**X**: OH, R_1: H, R_2: H) **TG TT-556**
13 (**X**: OH, R_1: CH_3, R_2: CH_3) **Me2TG TT-556**
14 (**X**: OH, R_1: H, R_2: CH_2CH_3) **EtTG TT-556**

Scheme 3-2. Synthesis of xanthene-based probes with novel tripodal NS_3 receptor for copper (I) sensing

Probe	Cu(I)	λ_{abs} (nm)	λ_{fl} (nm)	F_f / F_i
CR3 TT-556	-	530		
	+	535	557	2.2
TG TT-556	-	495		
	+	495	520	2.1
Me2TG TT-556	-	499, 540		
	+	519	543	10.0
EtTG TT-556	-	478, 512		
	+	508	530	5.5

Table 3-1. Photophysical properties of xanthene-based NS_3 probes.

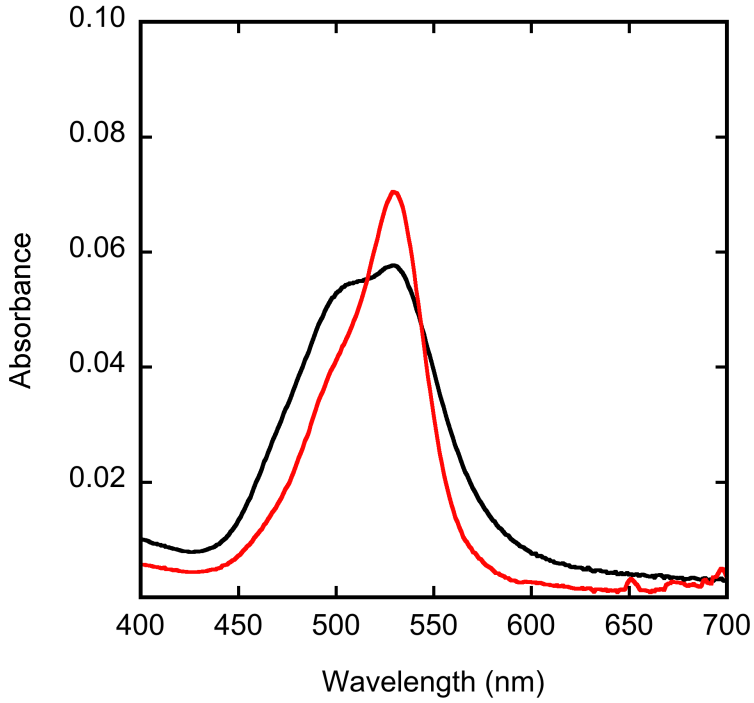

Figure 3-1. Absorbance spectra of 1.2 µM **CR3 TT-556**. Spectra shown are for buffered [Cu^+] of 0.0 (black trace) and 1.2 (red trace) µM. Spectra were acquired in 50 mM MOPS, pH 7.4.

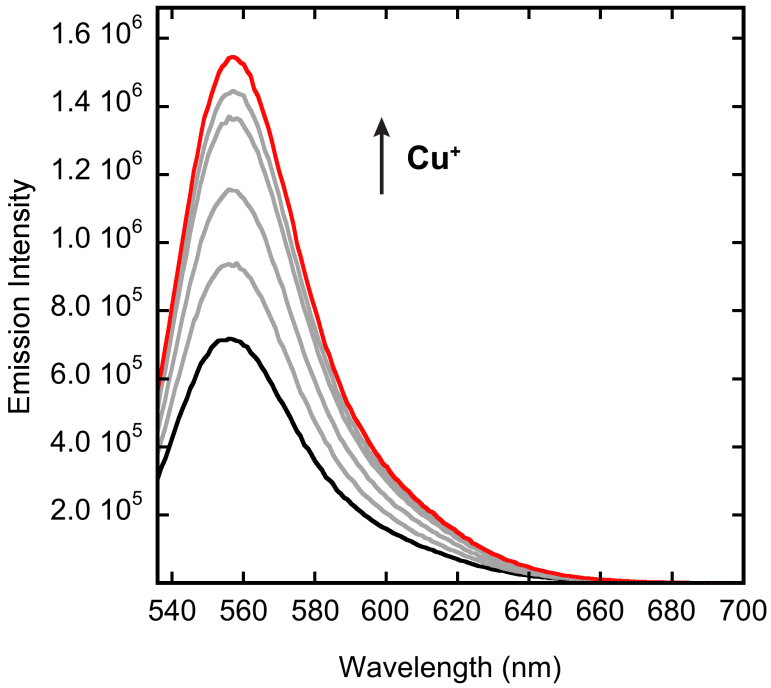

Figure 3-2. Fluorescence response of 1.2 μM **CR3 TT-556** to Cu^+. Spectra shown are for buffered [Cu^+] of 0.00 (black trace), 0.24, 0.48, 0.72, 0.96, and 1.2 μM (red trace). Spectra were acquired in 50 mM MOPS, pH 7.4 with excitation at 535 nm.

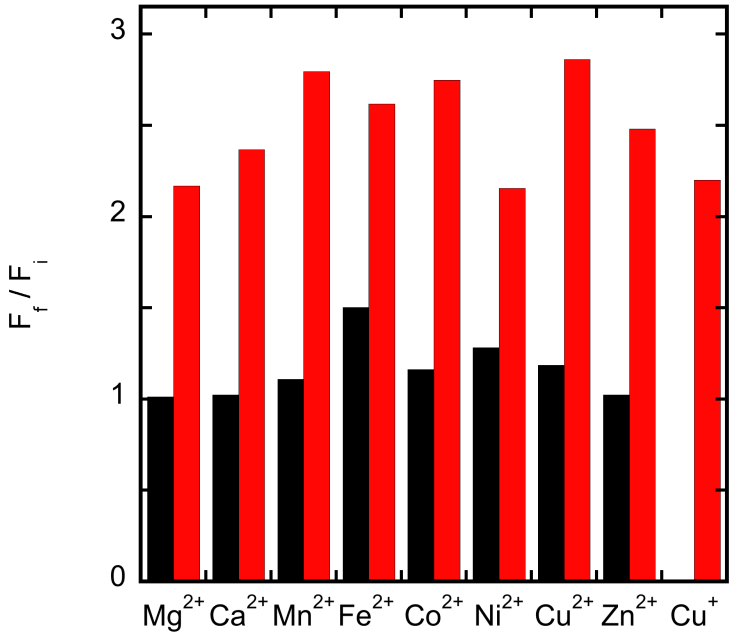

Figure 3-3. Fluorescence response of **CR3 TT-556** to various metal ions. Bars represent the final integrated fluorescence response (F_f) over the initial integrated emission (F_i). Spectra were acquired in 50 mM MOPS, pH 7.4. Black bars represent the addition of an excess of the appropriate metal ion (2 mM for Mg^{2+}, Ca^{2+}, and Zn^{2+}, 50 μM for all other cations) to a 2 μM solution of **CR3 TT-556**. Red bars represent the subsequent addition of 2 μM Cu^+ to the solution. Excitation was provided at 535 nm, and the collected emission was integrated over 540 to 700 nm.

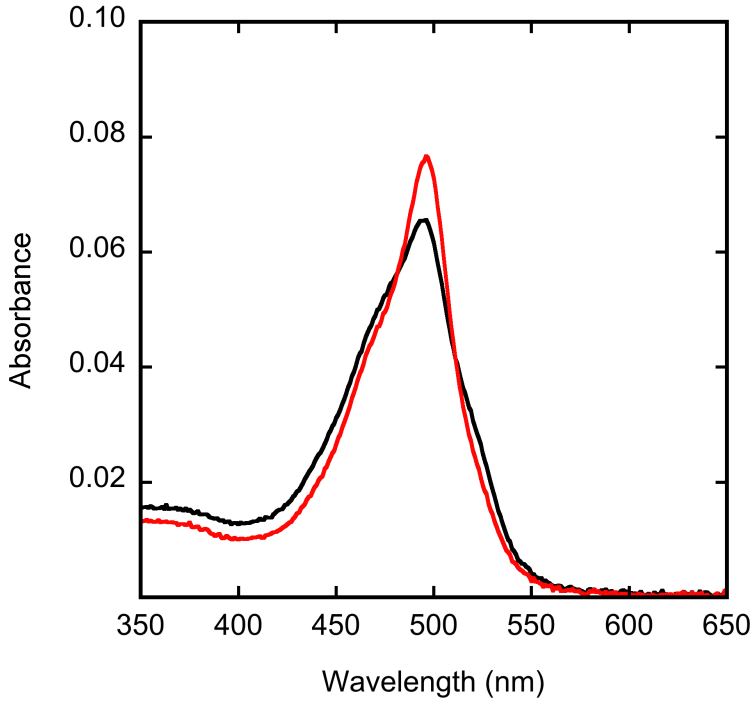

Figure 3-4. Absorbance spectra of 2 μM **TG TT-556**. Spectra shown are for buffered [Cu^+] of 0.0 (black trace) and 2.0 (red trace) μM. Spectra were acquired in 50 mM MOPS, pH 7.4.

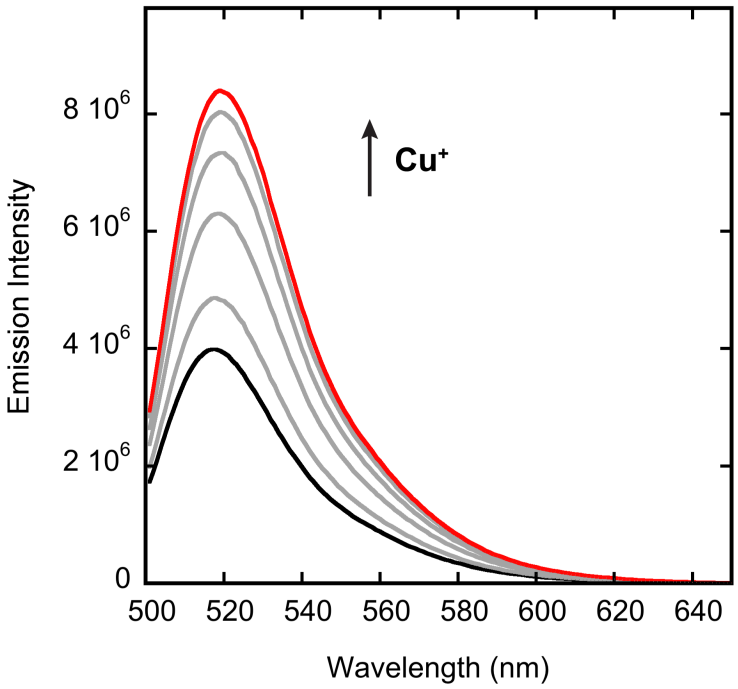

Figure 3-5. Fluorescence response of 2 μM **TG TT-556** to Cu^+. Spectra shown are for buffered [Cu^+] of 0.0 (black trace), 0.4, 0.8, 1.2, 1.6, and 2.0 μM (red trace). Spectra were acquired in 50 mM MOPS, pH 7.4 with excitation at 495 nm.

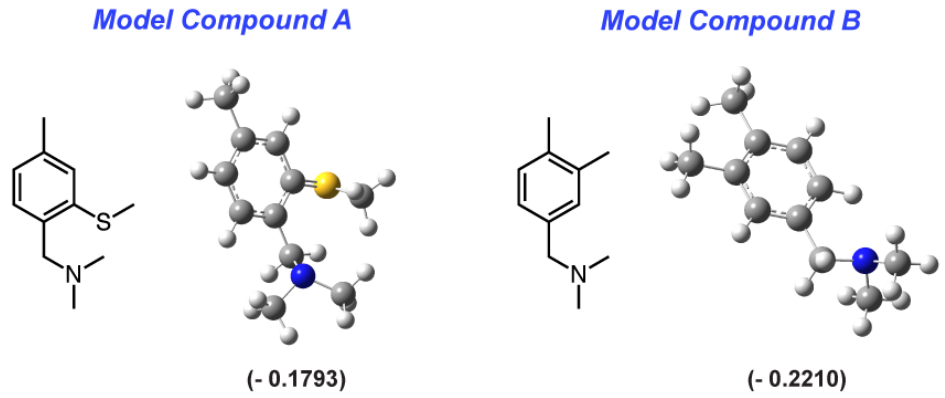

Figure 3-6. Density functional theory HOMO energy calculations of electron-donor model compounds. Geometry optimization and energy calculations were performed at the B3LYP/6-31G* level using the *Gaussian 03* software. Energy values shown in hartrees.

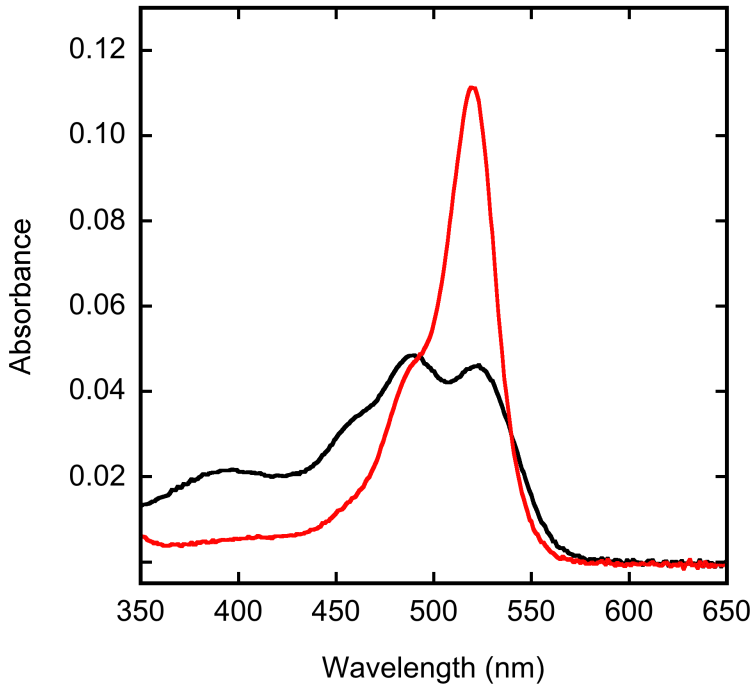

Figure 3-7. Absorbance spectra of 2.8 μM **Me2TG TT-556**. Spectra shown are for buffered [Cu^+] of 0.0 (black trace) and 2.8 (red trace) μM. Spectra were acquired in 50 mM MOPS, pH 7.4.

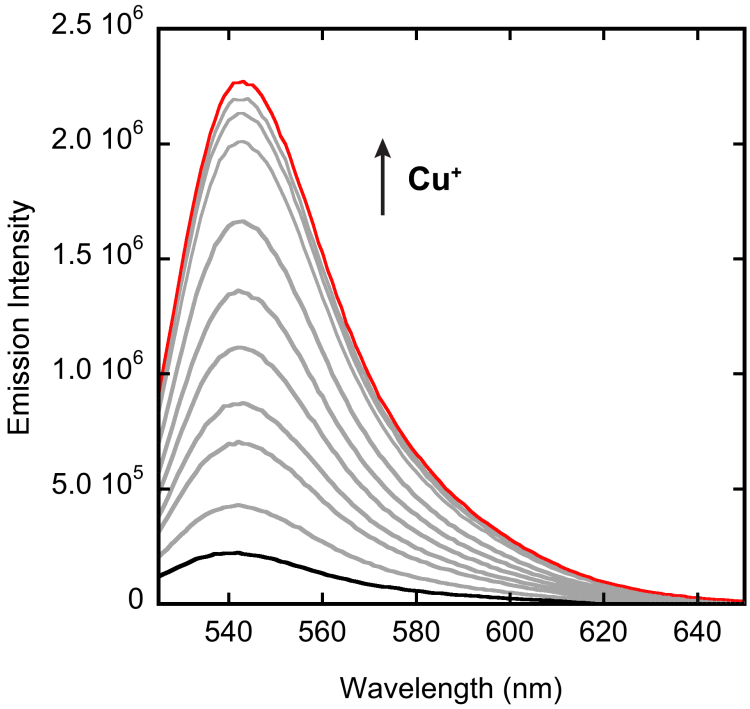

Figure 3-8. Fluorescence response of 2.4 μM **Me2TG TT-556** to Cu^+. Spectra shown are for buffered [Cu^+] of 0.0 (black trace), 0.24, 0.72, 0.96, 1.20, 1.44, 1.68, 1.92, 2.16, and 2.40 μM (red trace). Spectra were acquired in 50 mM MOPS, pH 7.4 with excitation at 519 nm.

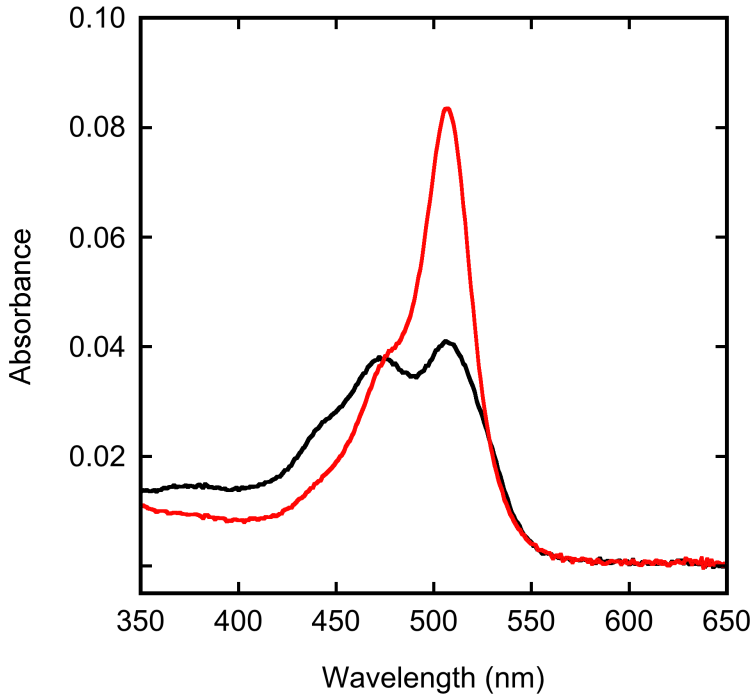

Figure 3-9. Absorbance spectra of 2.4 μM **EtTG TT-556**. Spectra shown are for buffered [Cu^+] of 0.0 (black trace) and 2.4 (red trace) μM. Spectra were acquired in 50 mM MOPS, pH 7.4.

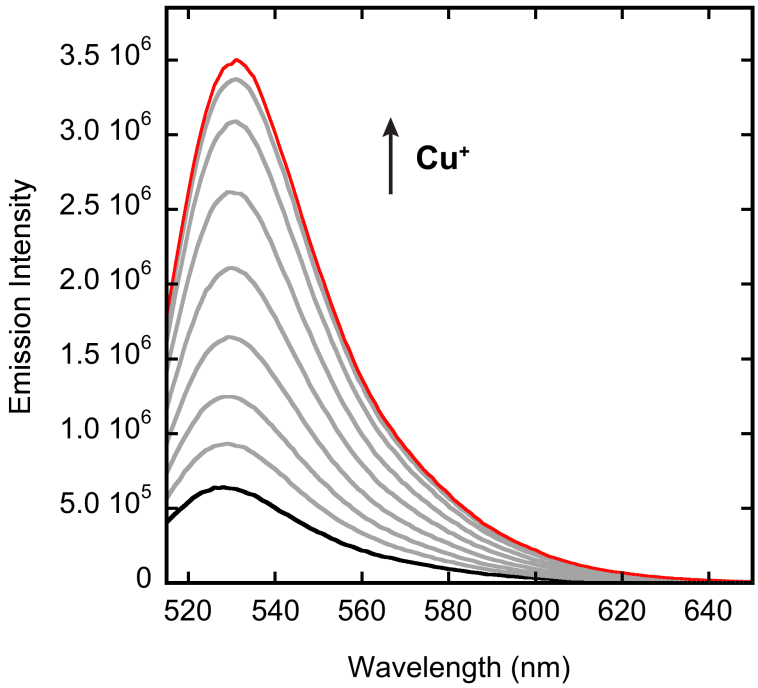

Figure 3-10. Fluorescence response of 3.2 μM **EtTG TT-556** to Cu^+. Spectra shown are for buffered [Cu^+] of 0.0 (black trace), 0.4, 0.8, 1.2, 1.6, 2.0, 2.4, 2.8 and 3.2 μM (red trace). Spectra were acquired in 50 mM MOPS, pH 7.4 with excitation at 508 nm.

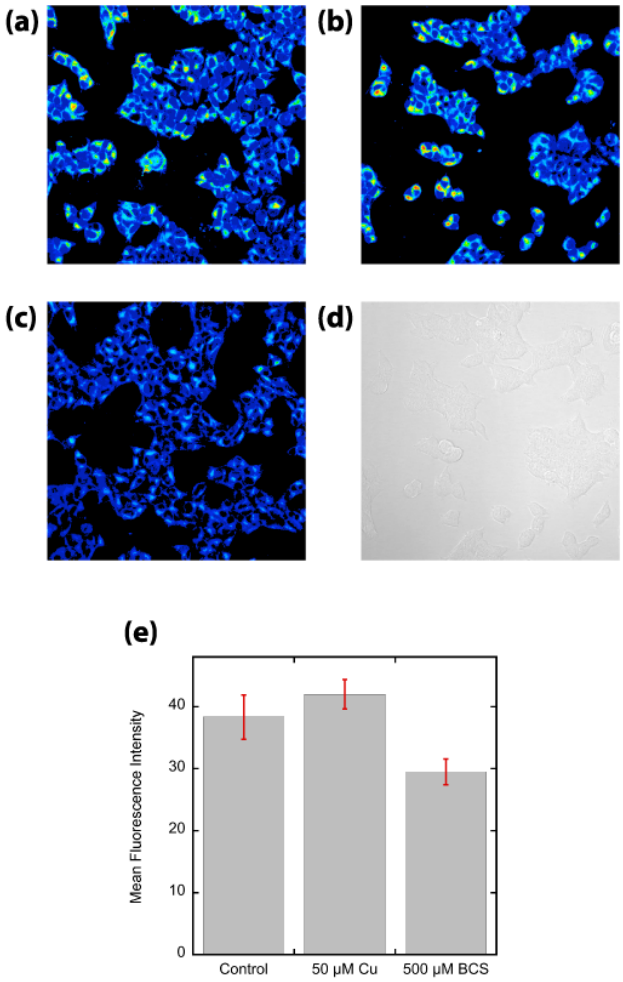

Figure 3-11. Molecular imaging of labile copper in HEK 293T cells with **Me2TG TT-556**. (a) Control HEK 293T cells, HEK 293T cells supplemented with (b) 50 µM $CuCl_2$ or (c) 500 µM BCS in the growth medium for 18 h at 37 ºC were stained with 2 µM **Me2TG TT-556** for 10 min at 37 ºC in DMEM. (d) Brightfield image of cells in (b) to show viability. (e) Quantification of mean fluorescence intensity of each condition (n = 5 fields of cells per condition). Error bars represent SEM.

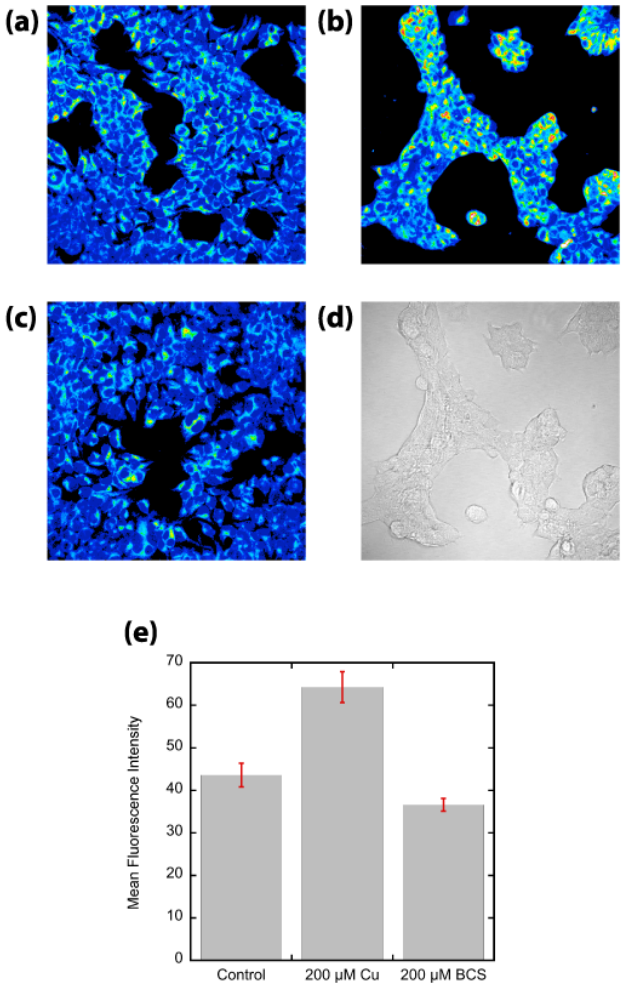

Figure 3-12. Molecular imaging of labile copper in HEK 293T cells with **Me2TG TT-556**. (a) Control HEK 293T cells, HEK 293T cells supplemented with (b) 200 µM $CuCl_2$ or (c) 200 µM BCS in the growth medium for 22 h at 37 ºC were stained with 2 µM **Me2TG TT-556** for 10 min at 37 ºC in DMEM. (d) Brightfield image of cells in (b) to show viability. (e) Quantification of mean fluorescence intensity of each condition (n = 5 fields of cells per condition). Error bars represent SEM.

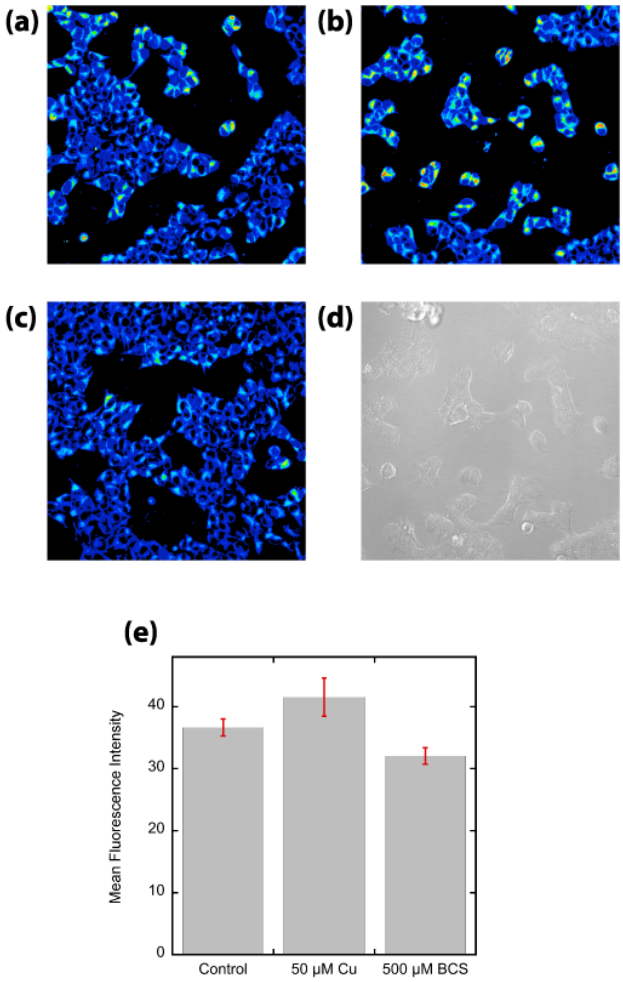

Figure 3-13. Molecular imaging of labile copper in HEK 293T cells with **EtTG TT-556**. (a) Control HEK 293T cells, HEK 293T cells supplemented with (b) 50 µM $CuCl_2$ or (c) 500 µM BCS in the growth medium for 18 h at 37 ºC were stained with 2 µM **EtTG TT-556** for 10 min at 37 ºC in DMEM. (d) Brightfield image of cells in (b) to show viability. (e) Quantification of mean fluorescence intensity of each condition (n = 5 fields of cells per condition). Error bars represent SEM.

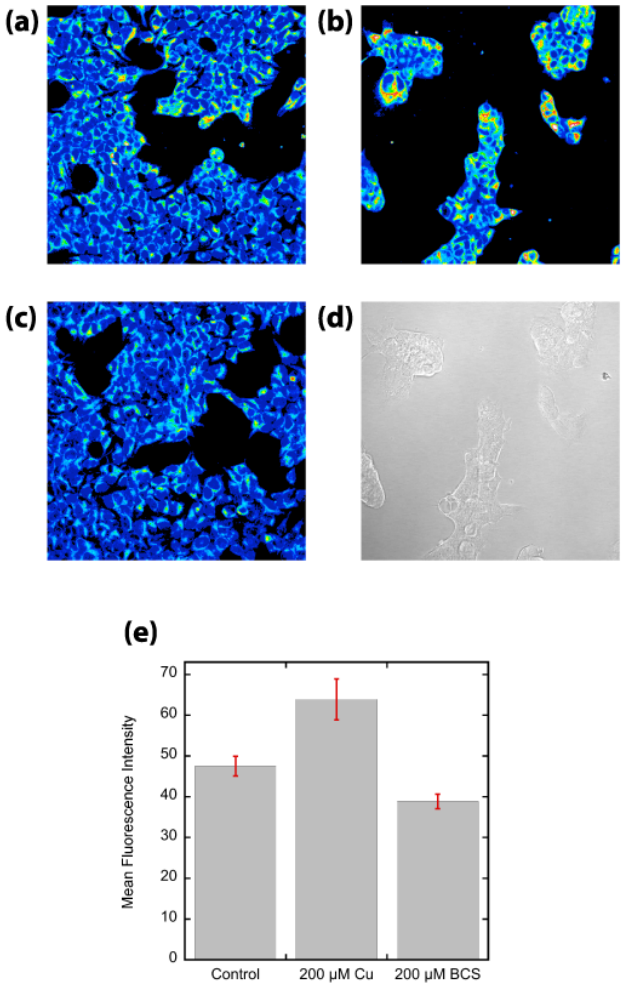

Figure 3-14. Molecular imaging of labile copper in HEK 293T cells with **EtTG TT-556**. (a) Control HEK 293T cells, HEK 293T cells supplemented with (b) 200 µM $CuCl_2$ or (c) 200 µM BCS in the growth medium for 22 h at 37 ºC were stained with 2 µM **EtTG TT-556** for 10 min at 37 ºC in DMEM. (d) Brightfield image of cells in (b) to show viability. (e) Quantification of mean fluorescence intensity of each condition (n = 5 fields of cells per condition). Error bars represent SEM.

References

1. Banci, L.; Bertini, I.; Ciofi-Baffoni, S.; Kozyreva, T.; Zovo, K.; Palumaa, P., Affinity gradients drive copper to cellular destinations. *Nature* **2010,** *465* (7298), 645-648.
2. Fahrni, C. J., Synthetic fluorescent probes for monovalent copper. *Curr. Opin. Chem. Biol.* **2013,** *17*, 656-662.
3. Cotruvo, J. A. J.; Aron, A. T.; Ramos-Torres, K. M.; Chang, C. J., Synthetic fluorescent probes for studying copper in biological systems. *Chem. Soc. Rev.* **2015,** *44* (13), 4400-4414.
4. Aron, A. T.; Ramos-Torres, K. M.; Cotruvo, J. A.; Chang, C. J., Recognition- and Reactivity-Based Fluorescent Probes for Studying Transition Metal Signaling in Living Systems. *Acc. Chem. Res.* **2015,** *48* (8), 2434-2442.
5. Dodani, S. C.; Domaille, D. W.; Nam, C. I.; Miller, E. W.; Finney, L. A.; Vogt, S.; Chang, C. J., Calcium-dependent copper redistributions in neuronal cells revealed by a fluorescent copper sensor and X-ray fluorescence microscopy. *Proc. Natl. Acad. Sci. USA* **2011,** *108* (15), 5980-5985.
6. Dodani, S. C.; Leary, S. C.; Cobine, P. A.; Winge, D. R.; Chang, C. J., A targetable fluorescent sensor reveals that copper-deficient SCO1 and SCO2 patient cells prioritize mitochondrial copper homeostasis. *J. Am. Chem. Soc.* **2011,** *133* (22), 8606-8616.
7. Dodani, S. C.; Firl, A.; Chan, J.; Nam, C. I.; Aron, A. T.; Onak, C. S.; Ramos-Torres, K. M.; Paek, J.; Webster, C. M.; Feller, M. B.; Chang, C. J., Copper is an endogenous modulator of neural circuit spontaneous activity. *Proc. Natl. Acad. Sci. USA* **2014,** *111*, 16280-16285.
8. Krishnamoorthy, L.; Cotruvo, J. A. J.; Chan, J.; Kaluarachchi, H.; Muchenditsi, A.; Pendyala, V. S.; Jia, S.; Aron, A. T.; Vander Wal, M. N.; Guan, T.; Smaga, L. P.; Farhi, S. S.; New, E. J.; Lutsenko, S.; Chang, C. J., Copper regulates cyclic AMP-dependent lipolysis. *Nat. Chem. Biol.* **2016,** *12*, 586-592.
9. Goldsmith, C. R.; Lippard, S. J., 6-Methylpyridyl for Pyridyl Substitution Tunes the Properties of Fluorescent Zinc Sensors of the Zinpyr Family. *Inorg. Chem.* **2006,** *45* (2), 555-561.
10. Komatsu, K.; Kikuchi, K.; Kojima, H.; Urano, Y.; Nagano, T., Selective Zinc Sensor Molecules with Various Affinities for Zn^{2+}, Revealing Dynamics and Regional Distribution of Synaptically Released Zn^{2+} in Hippocampal Slices *J. Am. Chem. Soc.* **2005,** *127* (29), 10197-10204.
11. Nolan, E. M.; Jaworski, J.; Okamoto, K.-I.; Hayashi, Y.; Sheng, M.; Lippard, S. J., QZ1 and QZ2: Rapid, Reversible Quinoline-Derivatized Fluoresceins for Sensing Biological Zn(II). *J. Am. Chem. Soc.* **2005,** *127* (48), 16812-16823.
12. Rorabacher, D. B.; Martin, M. J.; Koenigbauer, M. J.; Malik, M.; Schroeder, R. R.; Endicott, J. F.; Ochrymowycz, L. A., Structural Effects on Cu(II)/Cu(I) Potentials and Electron Transfer Kinetics as Well as Related Physical Peoperties in Polythiaether and Polyaminothiaether Complexes. In *Copper Coordination Chemistry: Biochemical and Inorganic Perspectives*, Karlin, K. D.; Zubieta, J., Eds. Adenine Press: Guilderland, NY, 1983; p 167.
13. Chaka, G.; Kandegedara, A.; Heeg, M. J.; Rorabacher, D. B., Comparative study of donor atom effects on the thermodynamic and electron-transfer kinetic properties of copper(II/I) complexes with sexadentate macrocyclic ligands. [CuII/I([18]aneS4N2)] and [CuII/I([18]aneS4O2)]. *Dalton Trans. (Camb.)* **2007,** (4), 449-458.

14. Bernardo, M. M.; Heeg, M. J.; Schroeder, R. R.; Ochrymowycz, L. A.; Rorabacher, D. B., Comparison of the influence of saturated nitrogen and sulfur donor atoms on the properties of copper(II/I)-macrocyclic polyamino polythiaether ligand complexes: redox potentials and protonation and stability constants of $Cu^{I}L$ species and new structural data. *Inorg. Chem.* **1992,** *31*, 191-198.
15. Westerby, B. C.; Juntunen, K. L.; Leggett, G. H.; Pett, V. B.; Koenigbauer, M. J.; Purgett, M. D.; Taschner, M. J.; Ochrymowycz, L. A.; Rorabacher, D. B., Macrocyclic polyamino polythiaether ligands with NxS4-x and NxS5-x donor sets - protonation constants, stability-constants, and kinetics of complex-formation with the aquocopper(ii) ion. *Inorg. Chem.* **1991,** *30* (9), 2109-2120.
16. Ambundo, E. A.; Deydier, M.-V.; Grall, A. J.; Aguera-Vega, N.; Dressel, L. T.; Cooper, T. H.; Heeg, M. J.; Ochrymowycz, L. A.; Rorabacher, D. B., Influence of Coordination Geometry upon Copper(II/I) Redox Potentials. Physical Parameters for Twelve Copper Tripodal Ligand Complexes. *Inorg. Chem.* **1999,** *38* (19), 4233-4242.
17. Blomenkemper, M.; Schröder, H.; Pape, T.; Hahn, F. E., Copper(I) complexes of N-centered aliphatic tripodal trithioether ligands – Adjustment of complex geometry by variation of spacer lengths. *Inorg. Chim. Acta* **2011,** *366* (1), 76-80.
18. Addison, A. W., Is ligand topology an influence on the redox potentials of copper complexes? *Inorg. Chim. Acta* **1989,** *162* (2), 217-220.
19. Dunn, B. C.; Wijetunge, P.; Vyvyan, J. R.; Howard, T. A.; Grall, A. J.; Ochrymowycz, L. A.; Rorabacher, D. B., Electron-Transfer Kinetics and Thermodynamic Characterization of Copper(II/I) Complexes with Acyclic Tetrathiaethers in Aqueous Solution. *Inorg. Chem.* **1997,** *36* (20), 4484-4489.
20. Dockal, E. R.; Jones, T. E.; Sokol, W. F.; Engerer, R. J.; Rorabacher, D. B.; Ochrymowycz, L. A., Redox properties of copper-thiaether complexes. Comparison to blue copper protein behavior. *J. Am. Chem. Soc.* **1976,** *98* (14), 4322-4324.
21. Ambundo, E. A.; Yu, Q. Y.; Ochrymowycz, L. A.; Rorabacher, D. B., Electron-transfer kinetics of copper(II/I) tripodal ligand complexes. *Inorg. Chem.* **2003,** *42* (17), 5267-5273.
22. Ambundo, E. A.; Ochrymowycz, L. A.; Rorabacher, D. B., Electron-transfer kinetics of tris(2-(methylthioethyl))aminecopper(II/I). A tripodal ligand complex exhibiting virtual C-3v symmetry. *Inorg. Chem.* **2001,** *40* (20), 5133-5138.
23. Reedijk, J., Plasticity in the copper-thioether bond: manifestation in blue Cu proteins and in synthetic analogs. *J. Inorg. Biochem.* **2012,** *115*, 182-185.
24. Davis, A. V.; O'Halloran, T. V., A place for thioether chemistry in cellular copper ion recognition and trafficking. *Nat. Chem. Biol.* **2008,** *4*, 148-151.
25. Zeng, L.; Miller, E. W.; Pralle, A.; Isacoff, E. Y.; Chang, C. J., A selective turn-on fluorescent sensor for imaging copper in living cells. *J. Am. Chem. Soc.* **2006,** *128*, 10-11.
26. Urano, Y.; Kamiya, M.; Kando, K.; Ueno, T.; Hirose, K.; Nagano, T., Evolution of fluorescein as a platform for finely tunable fluorescence probes. *J. Am. Chem. Soc.* **2005,** *127*, 4888-4894.
27. Koide, Y.; Urano, Y.; Hanaoka, K.; Terai, T.; Nagano, T., Evolution of Group 14 Rhodamines as Platforms for Near-Infrared Fluorescence Probes Utilizing Photoinduced Electron Transfer. *ACS Chem. Biol.* **2011,** *6* (6), 600-608.
28. Shieh, P.; Hangauer, M. J.; Bertozzi, C. R., Fluorogenic azidofluoresceins for biological imaging. *J. Am. Chem. Soc.* **2012,** *134* (42), 17428-17431.

Chapter 4:

Synthesis and Characterization of NS_6' Based Probes for Cu^+ Sensing

Abstract

Construction of a palette of fluorescent sensors with an ample assortment of binding affinities is necessary for the study of different cellular copper pools. This Chapter summarizes the design, synthesis and characterization of a novel NS_6' receptor for visualizing biological copper. Combination of this new binding platform with BODIPY and rhodol-based fluorophores afforded **CS1-NS_6'** and **CF4-NS_6'**, two copper probes with different turn-on responses upon Cu^+ binding and good selectivity for Cu^+ over other biologically relevant metal ions in aqueous solution. Additionally, the effects of the alteration of the metal-binding framework on the apparent binding affinities for these probes were evaluated and showed no major improvement of the copper binding properties.

Introduction

Application of fluorescent molecules as chemical tools to visualize metal dynamics in a cellular environment benefits from the tunable nature of small-molecule sensors.[1-4] The development of probes with a range of photophysical and binding properties results in expansion of the available toolbox for sensing these analytes in a variety of biologically relevant applications. Particularly, the construction of sensors with a range of binding affinities allows for the observation of different cellular metal pools, an approach that is significant in the study of metal fluxes involved in physiological processes pertinent to human health. In the case of copper, its association with a plethora of ligands with different binding strengths[5,6] motivates the construction of sensors that can compete for the ion within its biological window, defined by the affinity values of the small-molecule ligands and metalloproteins linked to copper homeostasis.

In this regard, the widespread use of the canonical NS_4 coordination unit as a reporter for copper has resulted in a fluorescent probe arsenal with a narrow range in the binding affinity for the cuprous ion.[7,6,4] Therefore, an adjustment of the metal-binding platform is most likely necessary in order to expand the limits of the sensing window for copper with the use of these small-molecule sensors. Conventional approaches that lead to altered cation binding properties include affecting the strength of individual metal-ligand (M-L) bonds,[8,9] varying the number of total M-L interactions[10] and introducing differences in the coordination sphere by changing the donor set.[9,10] This report presents the application of affinity modulation by the inclusion of a higher number of possible donors in order to decrease the metal dissociation values of established fluorescent sensors for Cu^+. To this end, our design of a novel NS_6 coordination unit relies on statistical effects for improved metal binding; the presence of additional donor atoms conceivably results in increased metal association events and decreased rates of metal release (k_{off}) from the metal-binding framework.

Results and Discussion

Synthesis of a New NS_6' Receptor for Copper Sensing. The design strategy for the construction of a new metal-binding domain with an NS_6 coordination unit, outlined in Scheme 4-1, involves the preparation of a thioether-modified propanethiol synthon as a method to introduce the thioether donors. To that end, chloride displacement of epichlorohydrin with sodium thiomethoxide afforded methylthio-substituted oxirane **1**, which was then converted to its thiirane analogue **2** using

thiourea as the sulfur donor. Subsequent ring opening with sodium thiomethoxide to incorporate the third thioether moiety yielded propanethiol **3**. Combination of **3**, as one of the two metal-binding arms, with bis(chloroethyl)amine resulted in the free amine chelator **4** in good yield. Finally, as a means to form a key intermediate for the integration of this receptor platform to xanthene-based sensors, coupling of **4** via nucleophilic displacement of bromobenzyl chloride **5** allowed for the development of receptor scaffold **6**.

Synthesis of NS_6' Based Copper Sensors. In order to directly compare the characteristics of this new class of copper sensors to a previously established probe, we proposed a direct analog of **CS1**, the first copper-responsive probe with a visible-excitation profile.[11] For this, we synthesized **CS1-NS_6'** as a first-generation sensor with the new receptor motif. Reaction of chloromethyl-modified BODIPY scaffold **7** and free amine metal-binding domain **4** afforded the intended probe. (Scheme 4-2) Additionally, as a means to produce a more hydrophilic equivalent, we pursued the synthesis of **CF4-NS_6'**, a rhodol-based sensor that also displays the NS_6 coordination unit and that is structurally comparable to the validated rhodol-comprising **CF3**[12] probe. Accordingly, addition of an aryl lithium species, derived from lithium halogen exchange of **6**, to xanthone **9** resulted in the second-generation sensor. (Scheme 4-3)

Spectroscopic Properties of NS_6' Based Copper Sensors. Evaluation of the spectroscopic properties of the NS_6' based copper sensors in 25 mM HEPES, buffered at pH 7.4, is summarized in Table 4-1. **CS1-NS_6'** showed characteristic optical features of the BODIPY platform; *apo*-dye presents a main absorption band at 541 nm with an additional significant feature at 514 nm. Upon addition of one equivalent of copper, the intensity of the band at 514 nm decreases and an intensification of the main band is observed ($\lambda_{abs\ (Cu)}$ 540 nm). (Figure 4-1) Additionally, copper binding causes a 6.1-fold increase in fluorescence intensity at 555 nm, with no shift in the emission energy. (Figure 4-2) Competition experiments with a variety of biologically relevant cations (Mg^{2+}, Ca^{2+}, Mn^{2+}, Co^{2+}, Ni^{2+}, Cu^{2+}, and Zn^{2+}) established the selectivity of the response of this new receptor motif for Cu^+. (Figure 4-3) Moreover, the identity of the copper complex formed was assessed by the method of continuous variations (Job's plot) to identify a 1:1 Cu^+:**CS1-NS_6'** binding stoichiometry. (Figure 4-4) This information allowed for the characterization of the binding affinity for Cu^+ via competition assays with thiourea as a competing ligand for the cation. Although we hypothesized that the inclusion of a higher number of thioether donors would result in an increased binding affinity, results showed a $K_d = 4.83 \times 10^{-12}$ M for **CS1-NS_6'** (Figure 4-5), a value that is comparable to its NS_4' analogue ($K_d = 3.6(3) \times 10^{-12}$ M for **CS1**).

Parallel characterization of **CF4-NS_6'** showed similar results to its BODIPY-based counterpart. Absorbance of the *apo*-configuration is centered at 548 nm, with emission at 557 nm. Addition of one equivalent of Cu^+ causes a small shift in the absorbance features ($\lambda_{abs\ (Cu)}$ 545 nm) with a modest 2.4-fold fluorescence enhancement at 557 nm. (Figures 4-6, 4-7) Likewise, the fluorescence response is selective for Cu^+ over a range of biologically relevant cations (Mg^{2+}, Ca^{2+}, Mn^{2+}, Co^{2+}, Ni^{2+}, Cu^{2+}, and Zn^{2+}). (Figure 4-8) Additionally, the copper complex responsible for the fluorescence response is also characterized by a 1:1 Cu^+:**CF4-NS_6'** stoichiometry, (Figure 4-9) with a dissociation constant value $K_d = 1.06 \times 10^{-11}$ M (Figure 4-10). Seemingly, the incorporation of the NS_6' receptor to the rhodol platform decreases the affinity for Cu^+ ($K_d = 3.3 \times 10^{-13}$ M for **CF3**), an effect that we speculate could result from an increased sensor hydrophobicity and/or a

reduced accuracy in the determination of this value due to the modest dynamic range of the response.

Concluding Remarks

In this report, we have presented the design and synthesis of a novel NS_6 metal-binding platform in efforts to enhance the binding affinity of available fluorescent copper sensors. Incorporation of the NS_6' framework to a pair of fluorophores suitable for molecular imaging allowed for the development of two small-molecule probes, **CS1-NS_6'** and **CF4-NS_6'**, with different responses upon copper binding. While we hypothesized that increasing the amount of possible M-L interactions could potentially increase the binding affinity towards the desired metal, we have shown that this is not the case with the developed NS_6' receptor for copper. With this result, we speculate that increased hydrophobicity, as well as steric hindrance in the binding pocket, might be responsible of the somewhat inconsequential effects this modification has on the affinity of the probes towards copper.

Experimental Section

Synthetic Materials and Methods. All reactions were carried out under a dry N_2 atmosphere and stirred magnetically unless stated otherwise. All reactions using air- or moisture-sensitive reagents were performed in oven- and flame-dried glassware under an atmosphere of dry N_2. THF used for anhydrous reactions was dried and stored over 3-Å molecular sieves. Compounds **5**,[12] **7**,[11,13] and **9**[12] were synthesized according to literature procedures. Unless otherwise noted, all chemicals were used as received. Silica gel P60 (SiliCycle) and activated basic aluminum oxide (Brockmann) were used for column chromatography. Flash chromatography was performed on an automated purification system using pre-packed silica gel columns. SiliCycle 60 F254 silica gel (precoated sheets, 0.25 mm thick) was used for analytical TLC, visualized with UV light and/or staining with *p*-anisaldehyde or $KMNO_4$. ^1H and ^{13}C NMR spectra were collected in $CDCl_3$ (Cambridge Isotope Laboratories, Cambridge, MA) at 25 °C on a Bruker AV-300, Bruker AVB-400 or Bruker AVQ-400 spectrometer at the College of Chemistry NMR Facility at the University of California, Berkeley. All chemical shifts are reported in the standard notation of parts per million using the peak of residual proton or carbon signals of $CDCl_3$ as an internal reference.

Synthesis.

2-((Methylthio)methyl)oxirane (1). A solution of epichlorohydrin (10.00 g, 108.08 mmol, 1.0 eq) in CH_2Cl_2 (216.2 mL, 0.50 M) and H_2O (100.0 mL, 1.0 M) was cooled to 0 ºC and treated with sodium thiomethoxide solution (3.0 M in H_2O, 50.4 mL, 1.4 eq) and tetra-n-butylammonium bromide (1.99 g, 6.16 mmol, 0.06 eq). Reaction was stirred at the same temperature for 3 h. The reaction mixture was then partitioned and the organic layer was washed with H_2O (x3), dried with Na_2SO_4 and concentrated under reduced pressure. Crude residue was purified via Kugelrohr distillation (65 ºC) to afford 3.69 g (33 %) of **1** as a colorless liquid. ^1H NMR (400 MHz, $CDCl_3$) δ 3.13 (tt, *J* = 5.6, 3.2 Hz, 1H), 2.84 – 2.76 (m, 1H), 2.68 (dd, *J* = 14.2, 5.5 Hz, 1H), 2.61 – 2.54 (m, 2H), 2.17 (s, 3H). ^{13}C NMR (101 MHz, $CDCl_3$) δ 51.61, 46.61, 36.05, 15.91.

2-((Methylthio)methyl)thiirane (2). A solution of **1** (1.92 g, 18.39 mmol, 1.0 eq) in methanol (42.8 mL, 0.43 M) was subjected to thiourea (2.80 g, 36.78 mmol, 2.0 eq) and was stirred at room temperature for 16 h. Reaction mixture was then concentrated under reduced pressure and the resulting white solid residue was dissolved in H_2O and extracted with CH_2Cl_2 (x3). The combined organic layers were dried with Na_2SO_4 and concentrated under reduced pressure. Crude was purified via Kugelrohr distillation (140 ºC) to afford 1.22 g (55 %) of **2** as a colorless liquid. ^{1}H NMR (400 MHz, $CDCl_3$) δ 3.09 (ddt, *J* = 8.1, 6.0, 5.1 Hz, 1H), 2.99 (ddd, *J* = 13.8, 4.8, 0.9 Hz, 1H), 2.57 (dt, *J* = 6.1, 1.2 Hz, 1H), 2.49 (dd, *J* = 13.7, 8.2 Hz, 1H), 2.23 (dd, *J* = 5.4, 1.4 Hz, 1H), 2.20 (s, 3H). ^{13}C NMR (101 MHz, $CDCl_3$) δ 40.27, 33.69, 25.75, 15.96.

1,3-Bis(methylthio)propane-2-thiol (3). A solution of **2** (0.98 g, 8.14 mmol, 1.0 eq) in methanol (15.0 mL, 0.54 M) was charged with sodium thiomethoxide (0.71 g, 10.18 mmol, 1.25 eq) and was stirred at the room temperature for 45 min. Solvent was then removed under reduced pressure and residue was dissolved in H_2O. Mixture was acidified to pH ~ 3 with conc. HCl causing formation of a white precipitate. This aqueous mixture was extracted with CH_2Cl_2 (x3) and combined organic layers were dried with Na_2SO_4 and concentrated under reduced pressure. Crude residue was purified via Kugelrohr distillation (190 ºC) to afford 0.55 g (40 %) of **3** as a colorless oil. ^{1}H NMR (400 MHz, $CDCl_3$) δ 3.21 (h, *J* = 6.5 Hz, 1H), 2.92 (dd, *J* = 13.5, 6.3 Hz, 2H), 2.78 (dd, *J* = 13.5, 6.7 Hz, 2H), 2.28 (d, *J* = 6.3 Hz, 1H), 2.15 (s, 6H). ^{13}C NMR (101 MHz, $CDCl_3$) δ 41.80, 39.81, 16.37.

Bis(2-((1,3-bis(methylthio)propan-2-yl)thio)ethyl)amine (4). A flame-dried three-necked round-bottom flask was charged with ethanol (9.3 mL, 0.20 M in thiol). Under a dry N_2 atmosphere, sodium (64.2 mg, 2.79 mmol, 1.5 eq) was carefully added in small portions. After all the sodium has dissolved, thiol **3** (313.2 mg, 1.86 mmol, 1.0 eq) was added dropwise to the sodium ethoxide solution. Reaction mixture was heated to reflux and then a solution of bis(2-chloroethyl)amine hydrochloride (109.9 mg, 0.61 mmol, 0.33 eq) in ethanol (1.0 mL, 0.60 M in amine) was added dropwise. Upon completion of addition, reaction mixture was stirred at reflux for 16 h. Reaction was then cooled to room temperature and ethanol was removed under reduced pressure. Residue was taken up in EtOAc and extracted with H_2O and brine. Organic layer was dried with Na_2SO_4 and concentrated under reduced pressure. Flash column chromatography on silica gel (0-10 % MeOH/CH_2Cl_2 with 1% TEA additive, linear gradient) yielded 211.7 mg (81 %) of **4** as a pale brown oil. ^{1}H NMR (400 MHz, $CDCl_3$) δ 2.91 (p, *J* = 6.3 Hz, 2H), 2.86 – 2.70 (m, 12H), 2.66 (t, *J* = 6.3 Hz, 4H) ^{13}C NMR (101 MHz, $CDCl_3$) δ 48.33, 45.25, 38.87, 31.50, 16.45.

2-((1,3-Bis(methylthio)propan-2-yl)thio)-*N*-(2-((1,3-bis(methylthio)propan-2-yl)thio)ethyl)-*N*-(4-bromo-3-(trifluoromethyl)benzyl)ethan-1-amine (6). A solution of **4** (330.6 mg, 0.81 mmol, 2.0 eq), **5** (111.4 mg, 0.41 mmol), K_2CO_3 (0.56 g, 4.10 mmol, 10.0 eq) and KI (0.14 g, 0.81 mmol, 2.0 eq) in anhydrous acetonitrile (4.0 mL, 0.10 mmol) was stirred at 45 ºC for 16 h. Upon completion, reaction mixture was concentrated under reduced pressure. Resulting residue was dissolved in EtOAc and washed with water (x2). Organic layer was dried with Na_2SO_4 and concentrated under reduced pressure. Purification via flash column chromatography on silica gel (0-10 % EtOAc/hexanes, linear gradient) afforded 94.3 mg (36 %) of **6** as a yellow oil. ^{1}H NMR (400 MHz, $CDCl_3$) δ 7.68 (d, *J* = 2.1 Hz, 1H), 7.63 (d, *J* = 8.2 Hz, 1H), 7.42 (dd, *J* = 8.2, 2.2 Hz,

1H), 3.63 (s, 2H), 2.97 – 2.65 (m, 19H), 2.11 (s, 12H). ^{13}C NMR (101 MHz, $CDCl_3$) δ 137.83, 135.05, 133.35, 128.15, 124.00, 121.28, 118.44, 46.60, 45.26, 39.00, 38.77, 35.48, 35.12, 16.49.

2-((1,3-Bis(methylthio)propan-2-yl)thio)-*N*-(2-((1,3-bis(methylthio)propan-2-yl)thio)ethyl)-*N*-((2,8-diethyl-5,5-difluoro-1,3,7,9-tetramethyl-5*H*-4λ^4,5λ^4-dipyrrolo[1,2-*c*:2',1'-*f*][1,3,2]diazaborinin-10-yl)methyl)ethan-1-amine (8, CS1-NS_6′). A solution of **4** (254.7 mg, 0.63 mmol, 1.3 eq), Cl-BODIPY **7** (171.6 mg, 0.49 mmol), K_2CO_3 (86.8 mg, 0.63 mmol, 1.3 eq) and KI (80.0 mg, 0.48 mmol, 1.0 eq) in anhydrous acetonitrile (3.5 mL, 0.14 M) was stirred at 45 ºC for 3 h. Upon completion, reaction mixture was concentrated under reduced pressure. Resulting residue was dissolved in EtOAc and washed with brine (x2). Combined aqueous layers were washed with EtOAc and combined organic layers were dried with Na_2SO_4 and concentrated under reduced pressure. Purification via flash column chromatography on silica gel (0-30 % EtOAc/hexanes, linear gradient) afforded 47.9 mg (14 %) of **CS1-NS_6′** as a dark pink solid. ^{1}H NMR (400 MHz, $CDCl_3$): δ 4.03 (s, 2H), 2.94 – 2.69 (m. 18H), 2.62 (m, 4H), 2.49 (s, 6H), 2.40 (s, 6H), 1.07 (t, J = 7.6 Hz, 6H).

9-(4-((Bis(2-((1,3-bis(methylthio)propan-2-yl)thio)ethyl)amino)methyl)-2-(trifluoromethyl)phenyl)-6-(piperidin-1-yl)-3*H*-xanthen-3-one (10, CF4-NS_6′). A flame-dried three-neck round-bottom flask was charged with **6** (82.4 mg, 0.13 mmol, 1.3 eq) and anhydrous THF (0.4 mL, 0.30 M in **6**). The solution was cooled to -78 ºC and then *tert*-butyllithium (1.7 M in pentane, 150.8 µL, 0.26 mmol, 2.6 eq) was added dropwise. After stirring at the same temperature for 12 min, a solution of compound **9** (40.4 mg, 0.10 mmol) in anhydrous TFH (3.2 mL, 0.03 M in **9**) was added dropwise. The reaction was warmed to room temperature, stirred for 1 h and subsequently quenched with addition of aq. HCl (1 M, 3 mL). After 1 h, the reaction was poured into a 1:1 mixture of sat. $NaHCO_3$ and EtOAc. Layers were separated and aqueous layer was further extracted with EtOAc (x2). The combined organic layers were washed with brine, dried with Na_2SO_4 and concentrated under reduced pressure. The crude residue was purified via column chromatography on silica gel (5 % MeOH/CH_2Cl_2) to afford **CF4-NS_6′** as red film (4.5 mg, 5 %). ^{1}H NMR (400 MHz, $CDCl_3$) δ 7.90 (s, 1H), 7.75 (d, *J* = 7.8 Hz, 1H), 7.27 (m, 1H), 6.79 – 6.70 (m, 4H), 6.54 (dd, *J* = 9.6, 2.1 Hz, 1H), 6.45 (d, *J* = 2.0 Hz, 1H), 3.82 (s, 2H), 3.47 (s, 4H), 3.02 – 2.76 (m, 18H), 2.15 (s, 12H), 1.25 (s, 6H). HRESI-MS calculated for [M+H] 841.2260, found 841.2292.

Spectroscopic Materials and Methods. Millipore water was used to prepare all aqueous solutions. All final spectroscopic measurements were performed in HEPES buffer. Absorption spectra were recorded using a Varian Cary 50 spectrophotometer (Walnut Creek, CA) and fluorescence spectra were recorded using a Photon Technology International Quanta Master 4 L-format scan spectrofluorometer (Lawrenceville, NJ) equipped with an LPS-220B 75-W xenon lamp and power supply, A-1010B lamp housing with integrated igniter, switchable 814 photocounting/analog photomultiplier detection unit, and MD5020 motor driver. Samples for absorption and emission measurements were contained in 1-cm quartz cuvettes (1.4-mL volume, Starna, Atascadero, CA). Cu^+ was delivered in the form of $[Cu(MeCN)_4][PF_6]$ from an acetonitrile stock solution (2 mM). Excitation was provided at 540 nm and 545 nm and collected emission was integrated from 550-700 nm for **CS1-NS_6'** and **CF4-NS_6'**, respectively.

Schemes and Figures

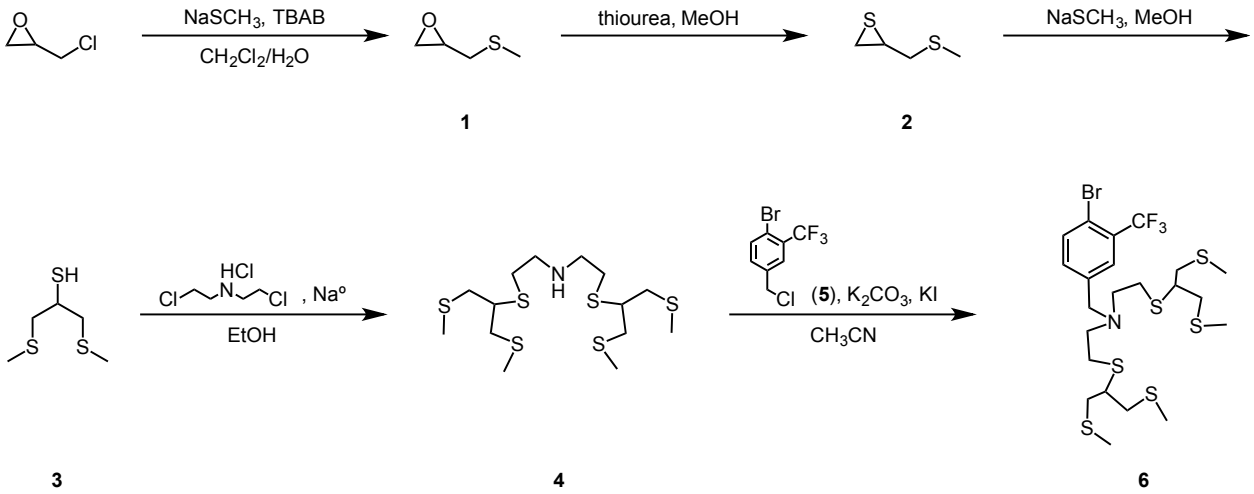

Scheme 4-1. Synthesis of an NS_6' receptor for Cu^+ sensing.

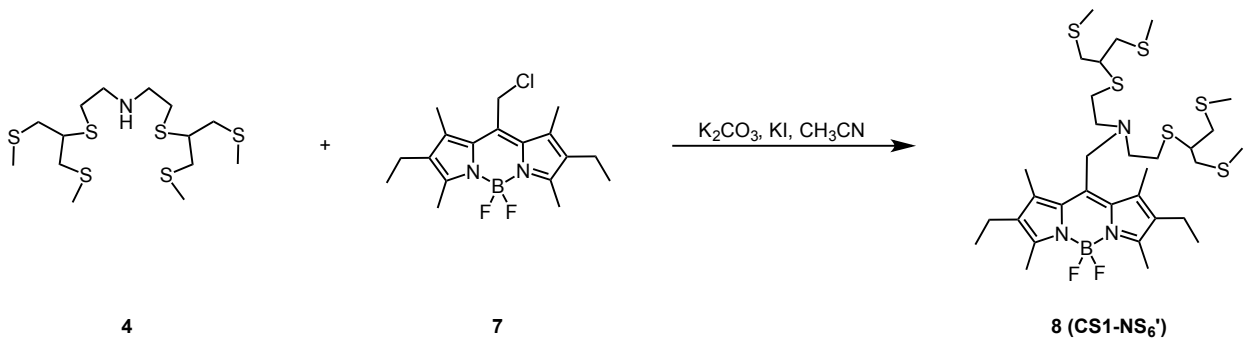

4 **7** **8 (CS1-NS_6')**

Scheme 4-2. Synthesis of BODIPY-based probe **CS1-NS_6'**.

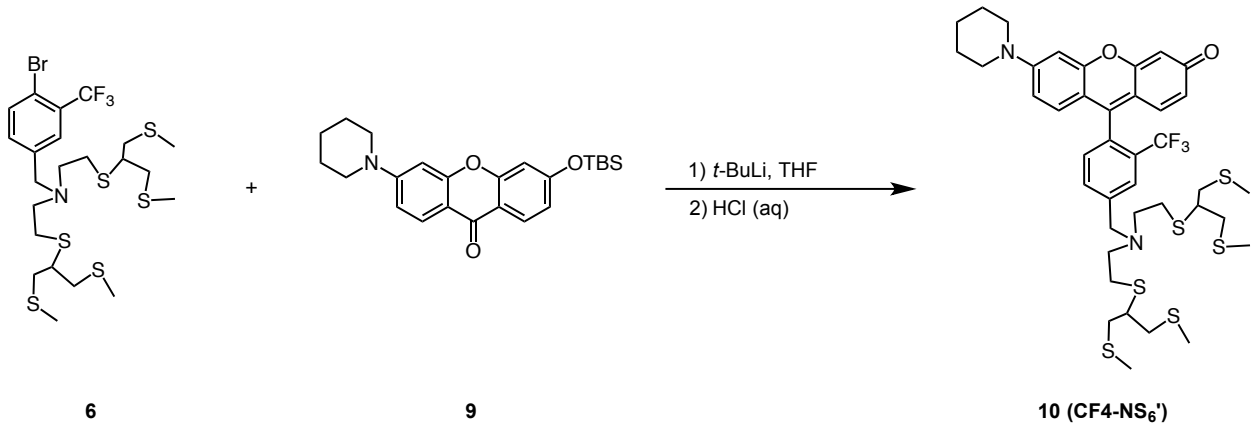

6 **9** **10 (CF4-NS_6')**

Scheme 4-3. Synthesis of rhodol-based probe **CF4-NS_6'**.

Probe	Cu(I)	λ_{abs} (nm)	λ_{fl} (nm)	F_f/F_i	K_d (M)
CS1-NS_6'	-	514, 541	555		
	+	540		6.1	4.83×10^{-12}
CF4-NS_6'	-	505, 548	557		
	+	510, 545	557	2.4	1.06×10^{-11}

Table 4-1. Summary of spectroscopic properties of NS_6' based copper sensors.

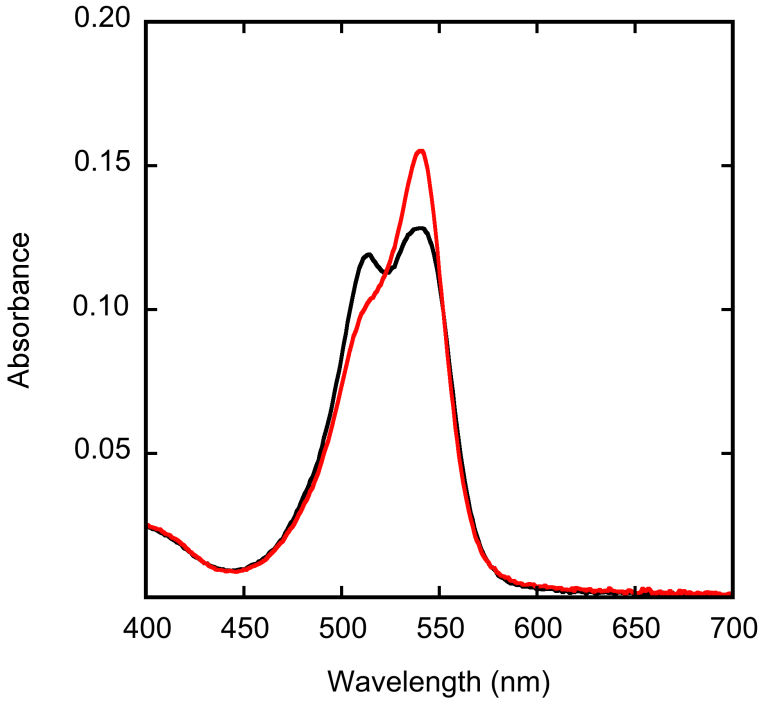

Figure 4-1. Absorbance spectra of 10 μM **CS1-NS_6'**. Spectra shown are for buffered [Cu^+] of 0.0 (black trace) and 10 (red trace) μM. Spectra were acquired in 25 mM HEPES, pH 7.4.

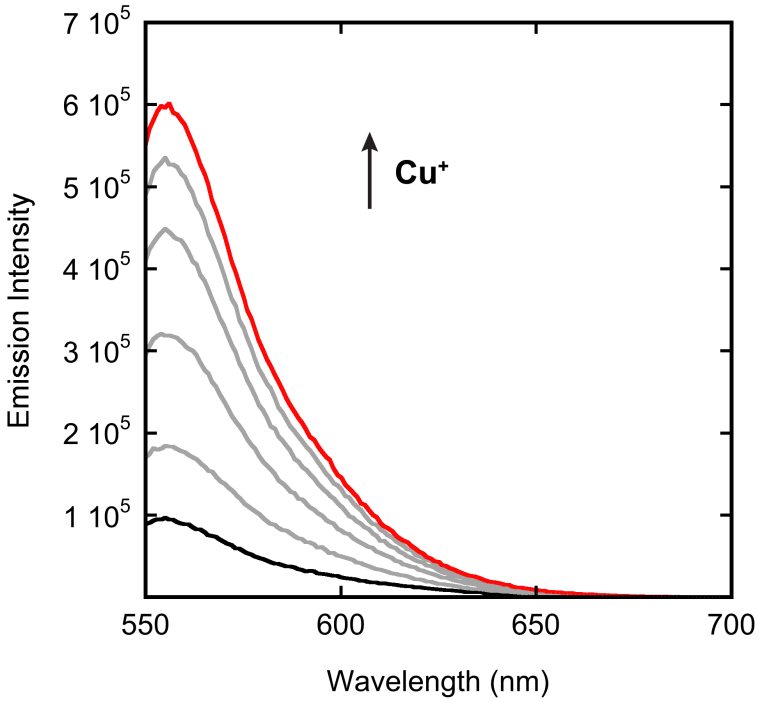

Figure 4-2. Fluorescence response of 2 μM **CS1-NS_6'** to Cu^+. Spectra shown are for buffered [Cu^+] of 0.00 (black trace), 0.4, 0.8, 1.2, 1.6, and 2.0 μM (red trace). Spectra were acquired in 25 mM HEPES, pH 7.4 with excitation at 540 nm.

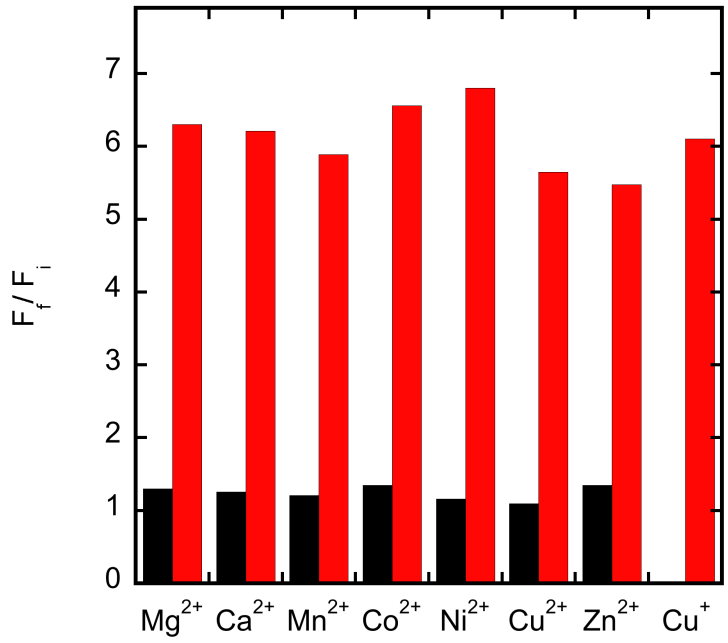

Figure 4-3. Fluorescence response of **CS1-NS_6'** to various metal ions. Bars represent the final integrated fluorescence response (F_f) over the initial integrated emission (F_i). Spectra were acquired in 25 mM HEPES, pH 7.4. Black bars represent the addition of an excess of the appropriate metal ion (2 mM for Mg^{2+}, Ca^{2+}, and Zn^{2+}, 50 μM for all other cations) to a 2 μM solution of **CS1-NS_6'**. Red bars represent the subsequent addition of 2 μM Cu^+ to the solution. Excitation was provided at 540 nm, and the collected emission was integrated over 550 to 700 nm.

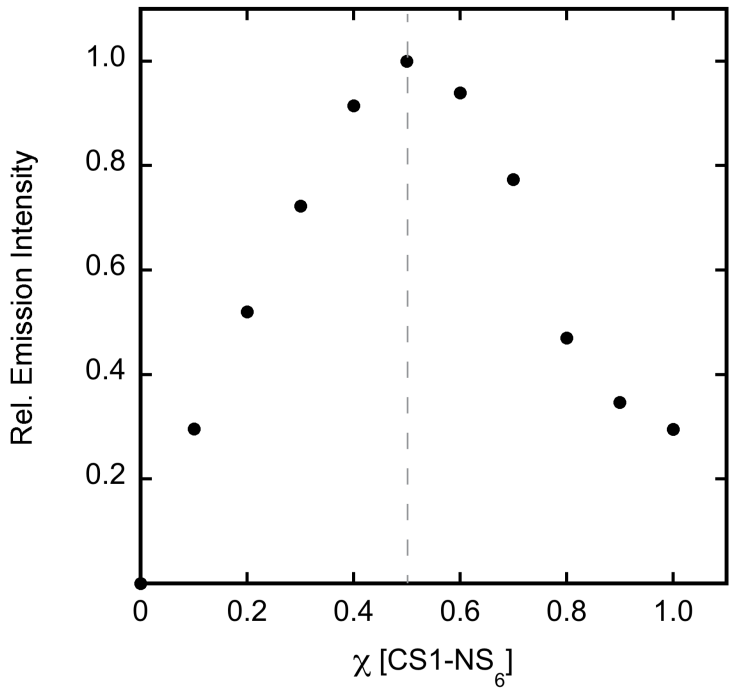

Figure 4-4. Job's plot of **CS1-NS_6'** and Cu^+. The total concentration of **CS1-NS_6'** and Cu^+ was kept at a constant 200 nM. Excitation was provided at 540 nm and the collected emission intensity was integrated from 550 to 700 nm. Spectra were acquired in 25 mM HEPES pH 7.4. The maximum fluorescence response at 0.50 mol fraction of **CS1-NS_6'** indicates formation of a 1:1 Cu^+:**CS1-NS_6'** complex.

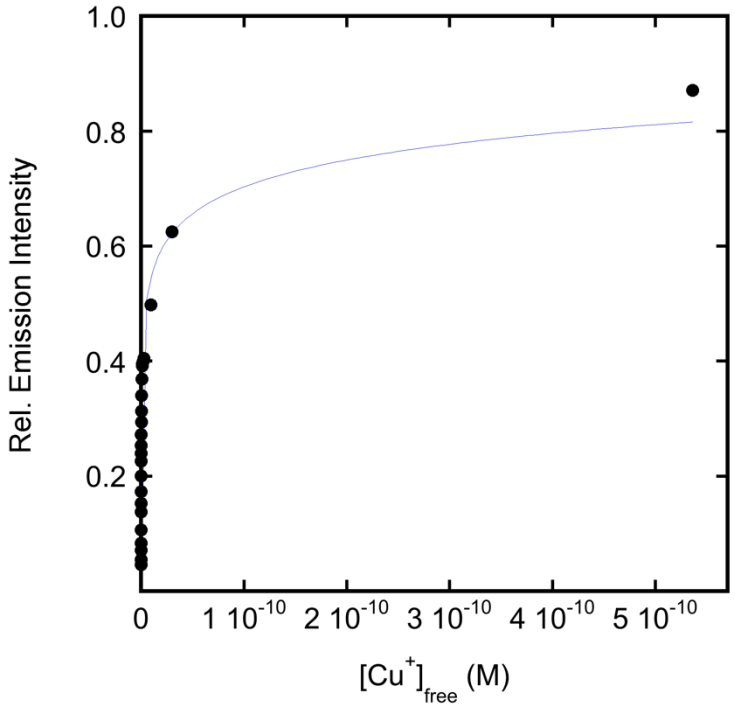

Figure 4-5. Normalized fluorescence response of 1.6 μM **CS1-NS_6'** to thiourea buffered Cu^+ solutions for K_d value determination. Excitation was provided at 540 nm and the collected emission was integrated from 550 to 700 nm. Spectra were acquired in 25 mM HEPES, pH 7.4. The points shown are for free Cu^+ buffered at 3.82, 5.53, 8.42, 11.6, 16.5, 24.8, 31.1, 39.9, 52.6, 71.5, 87.7, 109, 140, 183, 249, 354, 536, 894, 1216, 1740, 2676, 4595, 9551 and 30012 fM respectively. The observed K_d value is 4.83 x 10^{-12} M.

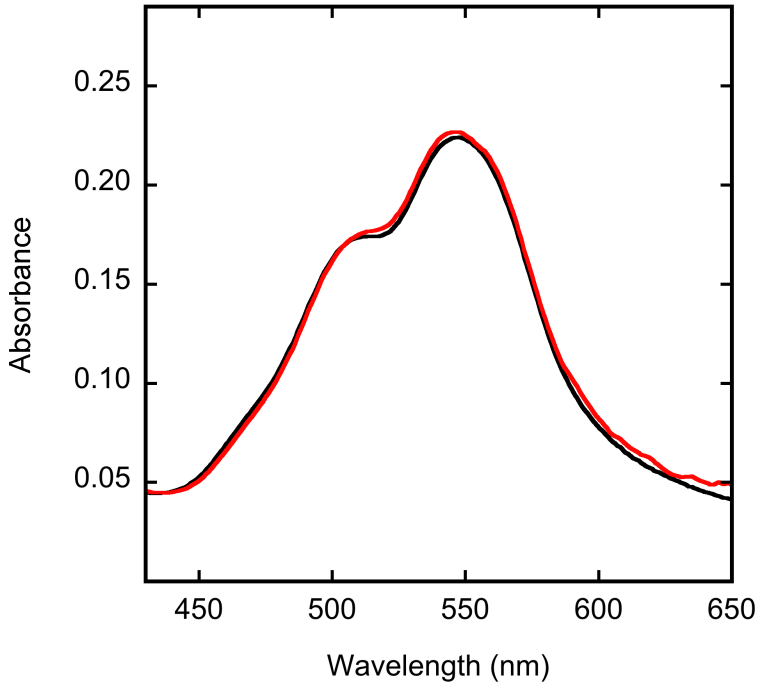

Figure 4-6. Absorbance spectra of 10 μM **CF4-NS_6'**. Spectra shown are for buffered [Cu^+] of 0.0 (black trace) and 10 (red trace) μM. Spectra were acquired in 25 mM HEPES, pH 7.4.

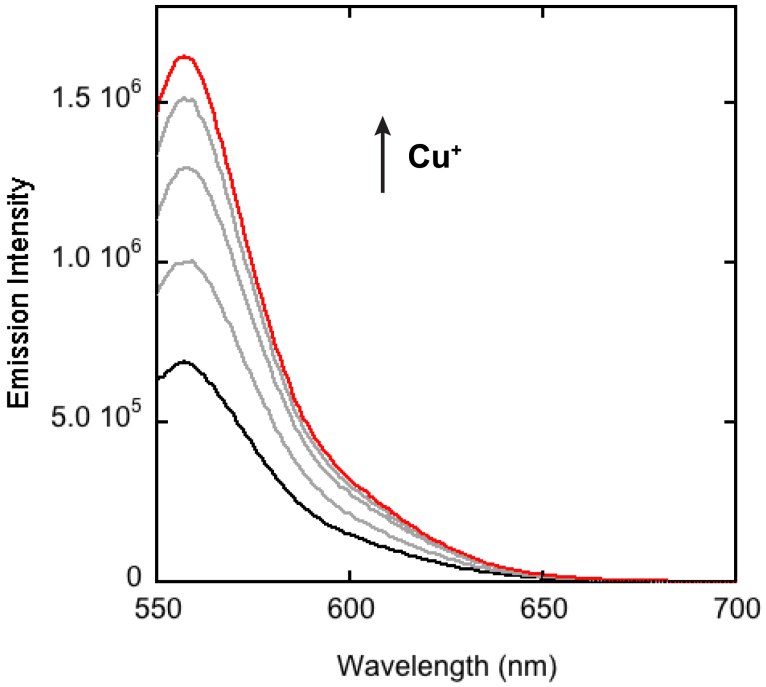

Figure 4-7. Fluorescence response of 1 μM **CF4-NS_6'** to Cu^+. Spectra shown are for buffered [Cu^+] of 0.00 (black trace), 0.25, 0.50, 0.75, and 1.0 μM (red trace). Spectra were acquired in 25 mM HEPES, pH 7.4 with excitation at 545 nm.

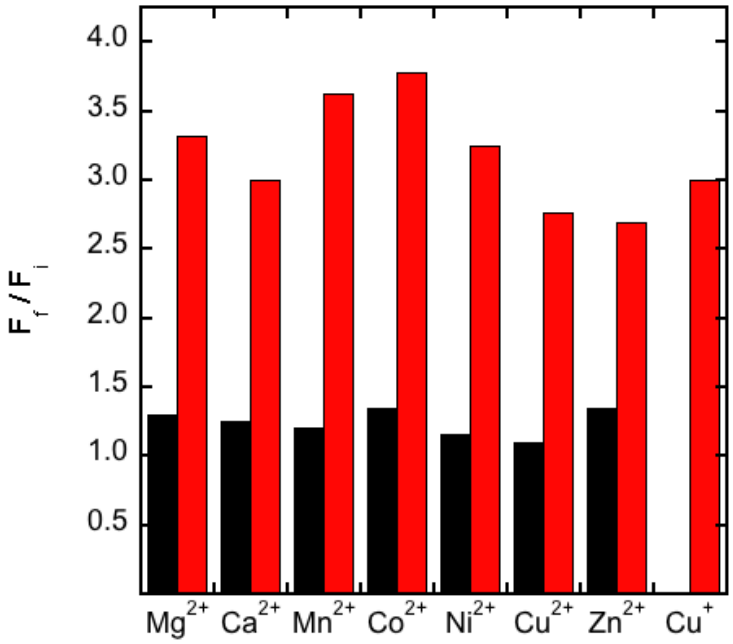

Figure 4-8. Fluorescence response of **CF4-NS_6'** to various metal ions. Bars represent the final integrated fluorescence response (F_f) over the initial integrated emission (F_i). Spectra were acquired in 25 mM HEPES, pH 7.4. Black bars represent the addition of an excess of the appropriate metal ion (2 mM for Mg^{2+}, Ca^{2+}, and Zn^{2+}, 50 μM for all other cations) to a 2 μM solution of **CF4-NS_6'**. Red bars represent the subsequent addition of 2 μM Cu^+ to the solution. Excitation was provided at 545 nm, and the collected emission was integrated over 550 to 700 nm.

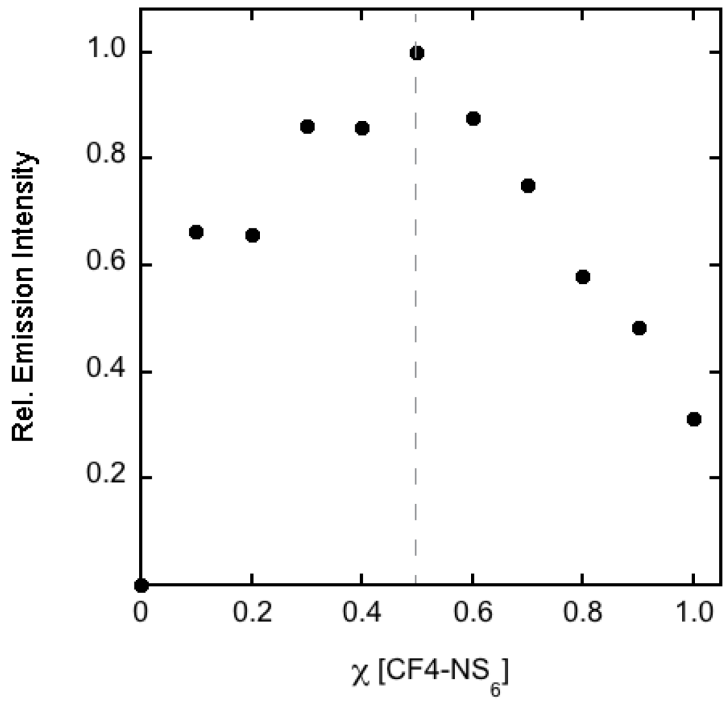

Figure 4-9. Job's plot of **CF4-NS$_6$'** and Cu^+. The total concentration of **CF4-NS$_6$'** and Cu^+ was kept at a constant 2 μM. Excitation was provided at 545 nm and the collected emission intensity was integrated from 550 to 700 nm. Spectra were acquired in 25 mM HEPES pH 7.4. The maximum fluorescence response at 0.50 mol fraction of **CF4-NS$_6$'** indicates formation of a 1:1 Cu^+:**CF4-NS$_6$'** complex.

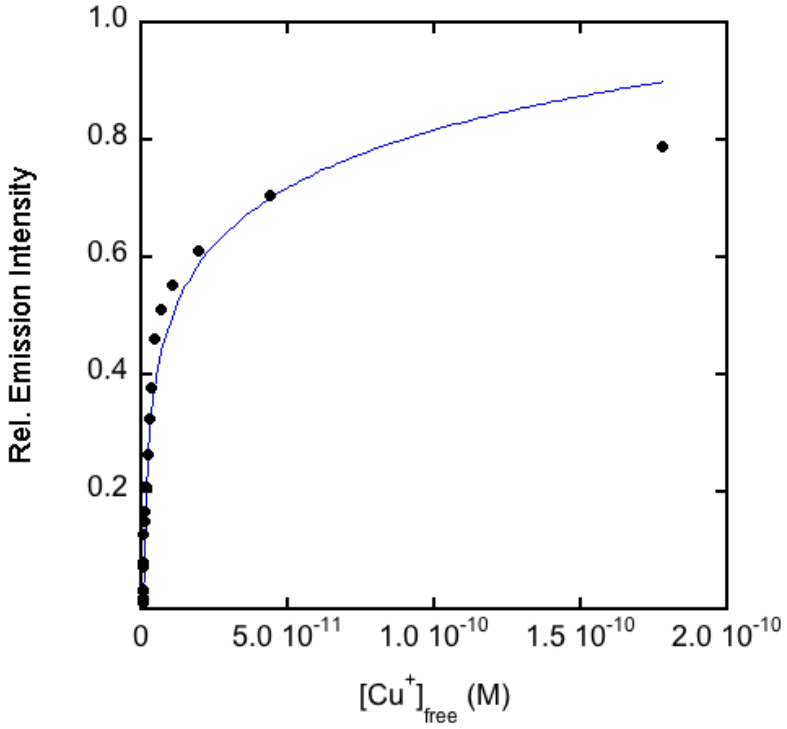

Figure 4-10. Normalized fluorescence response of 1.6 μM **CF4-NS_6'** to thiourea buffered Cu^+ solutions for K_d value determination. Excitation was provided at 545 nm and the collected emission was integrated from 550 to 700 nm. Spectra were acquired in 50 mM HEPES, pH 7.4. The points shown are for free Cu^+ buffered at 0.285, 0.314, 0.347, 0.385, 0.430, 0.482, 0.544, 0.619, 0.709, 0.820, 0.957, 1.13, 1.36, 1.65, 2.06, 2.62, 3.45, 4.73, 6.86, 10.8, 19.4, 43.9 and 178 nM respectively. The observed K_d value is 1.06 x 10^{-11} M.

References

1. Terai, T.; Nagano, T., Fluorescent probes for bioimaging applications. *Curr. Opin. Chem. Biol.* **2008,** *12* (5), 515-521.
2. Domaille, D. W.; Que, E. L.; Chang, C. J., Synthetic fluorescent sensors for studying the cell biology of metals. *Nat. Chem. Biol.* **2008,** *4*, 168-175.
3. Carter, K. P. Y., A. M. ; Palmer, A. E. , Fluorescent Sensors for Measuring Metal Ions in Living Systems. *Chem. Rev.* **2014,** *114*, 4564-4601.
4. Aron, A. T.; Ramos-Torres, K. M.; Cotruvo, J. A.; Chang, C. J., Recognition- and Reactivity-Based Fluorescent Probes for Studying Transition Metal Signaling in Living Systems. *Acc. Chem. Res.* **2015,** *48* (8), 2434-2442.
5. Banci, L.; Bertini, I.; Ciofi-Baffoni, S.; Kozyreva, T.; Zovo, K.; Palumaa, P., Affinity gradients drive copper to cellular destinations. *Nature* **2010,** *465* (7298), 645-648.
6. Cotruvo, J. A. J.; Aron, A. T.; Ramos-Torres, K. M.; Chang, C. J., Synthetic fluorescent probes for studying copper in biological systems. *Chem. Soc. Rev.* **2015,** *44* (13), 4400-4414.
7. Fahrni, C. J., Synthetic fluorescent probes for monovalent copper. *Curr. Opin. Chem. Biol.* **2013,** *17*, 656-662.
8. Goldsmith, C. R.; Lippard, S. J., 6-Methylpyridyl for Pyridyl Substitution Tunes the Properties of Fluorescent Zinc Sensors of the Zinpyr Family. *Inorg. Chem.* **2006,** *45* (2), 555-561.
9. Komatsu, K.; Kikuchi, K.; Kojima, H.; Urano, Y.; Nagano, T., Selective Zinc Sensor Molecules with Various Affinities for Zn2+, Revealing Dynamics and Regional Distribution of Synaptically Released Zn^{2+} in Hippocampal Slices. *J. Am. Chem. Soc.* **2005,** *127* (29), 10197-10204.
10. Nolan, E. M.; Jaworski, J.; Okamoto, K.-I.; Hayashi, Y.; Sheng, M.; Lippard, S. J., QZ1 and QZ2: Rapid, Reversible Quinoline-Derivatized Fluoresceins for Sensing Biological Zn(II). *J. Am. Chem. Soc.* **2005,** *127* (48), 16812-16823.
11. Zeng, L.; Miller, E. W.; Pralle, A.; Isacoff, E. Y.; Chang, C. J., A selective turn-on fluorescent sensor for imaging copper in living cells. *J. Am. Chem. Soc.* **2006,** *128*, 10-11.
12. Dodani, S. C.; Firl, A.; Chan, J.; Nam, C. I.; Aron, A. T.; Onak, C. S.; Ramos-Torres, K. M.; Paek, J.; Webster, C. M.; Feller, M. B.; Chang, C. J., Copper is an endogenous modulator of neural circuit spontaneous activity. *Proc. Natl. Acad. Sci. USA* **2014,** *111*, 16280-16285.
13. Miller, E. W.; Zeng, L.; Domaille, D. W.; Chang, C. J., Preparation and use of Coppersensor-1, a synthetic fluorophore for live-cell copper imaging. *Nat. Protoc.* **2006,** *1*, 824-827.

Appendix 1:
Development of a Modular Synthesis for Organelle-targeted Cu^+ Probes

Portions of this work were performed in collaboration with the following persons:

Synthesis of Golgi-CS and PM-CS was performed by Dr. Jefferson Chan. Imaging experiments were performed with Dr. Jefferson Chan.

Synopsis

The development of fluorescent sensors that are localized to specific subcellular compartments can be valuable tools to study the distribution and homeostasis of different metal pools in the cellular environment. In this regard, we developed a modular synthesis of a BODIPY-based sensor in combination with a thioether-rich binding moiety that includes a carboxylic acid intermediate (**Carboxy-CS2**) as a flexible synthon for the production of a library of targetable probes. This appendix summarizes the synthesis and characterization of an organelle-targeted family of probes for the study of copper in mitochondria, lysosomes, Golgi apparatus and the plasma membrane.

Results and Discussion

Synthesis of Organelle-targeted Copper Sensors. In order to access a library of probes with different subcellular localization, we first sought to develop a modular synthetic pathway for **Carboxy-CS2**, a flexible synthon that can be coupled to different targeting groups for the selective targeting of a desired subcellular locale. Scheme A1-1 outlines the synthetic route to this intermediate. Synthesis of this building block begins with the construction of an aryl-substituted BODIPY core. Commercially available 2,4-dimethyl-3-pyrrolepropionate was deprotected under hydrogenation conditions, followed by an acid-catalyzed decarboxylation to attain **1**. BODIPY **2** was obtained in a one-pot, two-step procedure via asymmetric condensation of pyrrole **1** with 2,4-dimethylpyrrole and 4-(chloromethyl)benzoyl chloride followed by boron insertion with BF_3•OEt_2. Coupling to previously synthesized tetrathiaza receptor **3**[1,2] afforded methylester precursor of **Carboxy-CS2** (**4**), which was then subjected to ester hydrolysis under saponification conditions to yield the carboxylic acid intermediate. The library of organelle-targeted probes was accessed through a canonical peptide bond synthesis between the key intermediate and different known amine substituted targeting groups for selective tagging of mitochondria, lysosomes, Golgi apparatus and plasma membrane. (Scheme A1-2)

Spectroscopic Properties of Organelle-targeted Copper Sensors. Copper sensors were characterized by absorbance and fluorescence spectroscopy. Probes displayed characteristic BODIPY absorbance and emission features with varying fluorescence responses (7-fold turn-on for **Mito-CS2**, 5- turn-on for **Lyso-CS**, 3-fold turn-off for **Golgi-CS**, and 3-fold turn-on for **PM-CS**) upon Cu^+ binding in aqueous buffer. (Figure A1-1) Additionally, **Mito-CS2** and **Lyso-CS** showed good selectivity for Cu^+ over a variety of biologically relevant cations (Ca^{2+}, Mg^{2+}, Mn^{2+}, Fe^{2+}, Co^{2+}, Cu^{2+}, and Zn^{2+}). (Figures A1-2 and A1-3) While further characterization of the **Mito-CS2** analogue was attempted, namely investigation of the binding stoichiometry of the formed copper complex using the method of continuous variations (Job's plot), irreproducible results due to non-copper dependent variations in fluorescence limited the full characterization of the probe.

Live-cell Imaging of Organelle-targeted Copper Sensors with Confocal Microscopy. We next sought to investigate if the modification of **Carboxy-CS2** with different targeting groups resulted in distinctive subcellular localization of the probes. Live human embryonic kidney cells (HEK 293T) incubated with the final probes showed intracellular fluorescence in different subcellular compartments as observed by confocal microscopy. (Figure A1-4) Furthermore, characterization of the subcellular localization of **Mito-CS2** using the mitochondrial dye MitoTracker Deep Red FM showed that **Mito-CS2** indeed presents the characteristic staining pattern for a mitochondrial

dye, as well as decent colocalization with MitoTracker Deep Red FM, as shown by the overlay image in Figure A1-5. Additionally, cells grown with 25 μM $CuCl_2$ supplemented in the growth medium overnight show an increase in intracellular fluorescence upon staining with **Mito-CS2**, (Figure A1-6b) while overnight treatment with 200 μM of the cell-impermeable copper chelator bathocuproine disulfonate (BCS) afforded a decrease in the fluorescence levels, indicating that the probe is able to sense endogenous pools of labile copper in this cell line. (Figure A1-6c)

Conclusion and Future Work

We have investigated the use of a modular synthesis for the development of a family of organelle-targeted copper probes. Even though copper binding of the resulting probes was not fully characterized *in vitro* due to non-copper dependent variations in their fluorescence response, the use of a carboxylic acid-substituted BODIPY scaffold in combination with a variety of targeting groups proved to be an appropriate approach for the synthesis of a family of probes that seem to localize to their intended subcellular compartments. Furthermore, the ability of **Mito-CS2** to respond to changes in Cu^+ levels in live cells is promising for the application of sensors of the like to study copper homeostasis within the cell. Future efforts in enhancing the solubility of the sensors and turn-on responses could lead to improved metal-binding behavior *in vitro*, staining patterns and *in cellulo* responses.

Experimental Section

Synthetic Materials and Methods. All reactions were carried out under a dry N_2 atmosphere and stirred magnetically unless stated otherwise. Silica gel P60 (SiliCycle) and activated basic aluminum oxide (Brockmann) were used for column chromatography. Analytical thin layer chromatography was performed using SiliCycle 60 F254 silica gel (precoated sheets, 0.25 mm thick) and EMD Chemicals 60 F254 basic aluminum oxide. Compound **3**[1,2] was synthesized according to literature procedures. Compounds **Golgi-CS and PM-CS** were synthesized by Dr. Jefferson Chan. Unless otherwise noted, all chemicals were used as received. ^1H and ^{13}C NMR spectra were collected in $CDCl_3$ (Cambridge Isotope Laboratories, Cambridge, MA) at 25 °C on a Bruker AV-300, Bruker AVB-400 or Bruker AVQ-400 spectrometer at the College of Chemistry NMR Facility at the University of California, Berkeley. All chemical shifts are reported in the standard notation of parts per million using the peak of residual proton or carbon signals of $CDCl_3$ as an internal reference.

Synthesis.

Methyl 3-(2,4-dimethyl-1*H*-pyrrol-3-yl)propanoate (1). An oven-dried round-bottom flask was charged with methyl 5-(benzyloxycarbonyl)-2,4-dimethyl-3-pyrrolepropionate (5.00 g, 15.85 mmol, 1.0 eq), 10 % palladium on carbon (0.10 g, 0.09 mmol, 0.006 eq) and acetone (90.0 mL, 0.12 M). Reaction mixture was then placed under a H_2 atmosphere and stirred at room temperature overnight. Upon completion, as judged by TLC, reaction mixture was filtered through Celite to remove Pd/C and washed with additional acetone. The resulting filtrate was concentrated under reduced pressure. Crude was subsequently treated with trifluoroacetic acid (10.0 mL, 130.59 mmol, 8.2 eq), heated to 40 ºC and stirred at this temperature for 10 min. After cooling to room

temperature, reaction mixture was diluted with $CHCl_3$ and washed with H_2O (x2). Aqueous layer was back extracted with $CHCl_3$ and combined organics were washed with sat. $NaHCO_3$, dried with Na_2SO_4 and concentrated under reduced pressure. Purification via column chromatography on silica gel (100% CH_2Cl_2) afforded **1** (1.02 g, 35 %) as a yellow oil. ^{1}H NMR (300 MHz, $CDCl_3$) δ 6.39 (s, 1H), 3.67 (s, 3H), 2.76 – 2.67 (m, 2H), 2.45 (dd, *J* = 9.2, 6.7 Hz, 2H), 2.18 (s, 3H), 2.03 (s, 3H).

Methyl 3-(10-(4-(chloromethyl)phenyl)-8-ethyl-5,5-difluoro-1,3,7,9-tetramethyl-5*H*-4λ^4,5λ^4-dipyrrolo[1,2-*c*:2',1'-*f*][1,3,2]diazaborinin-2-yl)propanoate (2). A solution of pyrrole **1** (1.02 g, 5.62 mmol, 1.2 eq) and kryptopyrrole (695.0 μL, 5.15 mmol, 1.1 eq) in anhydrous CH_2Cl_2 (50.0 mL, 0.09 M) was charged with 4-(chloromethyl)benzoyl chloride (0.86 g, 4.68 mmol, 1.0 eq), heated to 55 ºC and stirred for 1 h. Reaction mixture was then cooled to room temperature and concentrated under reduced pressure. Residue was dissolved in toluene (40.0 mL, 0.12 M), treated with Hünig's base (8.16 mL, 46.83 mmol, 10.0 eq) and stirred for 15 min. BF_3•OEt_2 (5.93 mL, 46.83 mmol, 10.0 eq) was then added and reaction mixture was stirred at 55 ºC for 45 min. Upon completion, solvent was removed under reduced pressure and residue was dissolved in CH_2Cl_2 and washed with H_2O. Organic layer was dried with Na_2SO_4 and concentrated under reduced pressure. Crude was purified via column chromatography on silica gel (25% EtOAc/hexanes) to yield 0.52 g (23 %) of **2** as a purple syrup. ^{1}H NMR (400 MHz, $CDCl_3$) δ 7.56 (d, *J* = 8.1 Hz, 2H), 7.32 (d, *J* = 8.1 Hz, 2H), 4.71 (s, 2H), 3.69 (s, 3H), 2.58 (s, 6H), 2.42 – 2.30 (m, 6H), 1.33 (s, 6H), 1.02 (t, *J* = 7.5 Hz, 3H).

Methyl 3-(10-(4-((bis(2-((2-(ethylthio)ethyl)thio)ethyl)amino)methyl)phenyl)-8-ethyl-5,5-difluoro-1,3,7,9-tetramethyl-5*H*-4λ^4,5λ^4-dipyrrolo[1,2-*c*:2',1'-*f*][1,3,2]diazaborinin-2 yl)propanoate (4). A solution of **2** (0.45 g, 0.92 mmol, 1.0 eq), **3** (0.58 g, 1.84 mmol, 2.0 eq), K_2CO_3 (0.28 g, 2.03 mmol, 2.2 eq) and KI (0.34 g, 2.03 mmol, 2.2 eq) in anhydrous acetonitrile (40.0 mL, 0.02 M) was heated to 65 ºC and stirred protected from light for 2 h. Solvent was then removed under reduced pressure and crude was purified via column chromatography on silica gel (25% EtOAc/hexanes) to afford 0.34 g (48 %) of **4**. ^{1}H NMR (300 MHz, $CDCl_3$) δ 7.46 (d, *J* = 7.6 Hz, 2H), 7.22 (d, *J* = 7.7 Hz, 2H), 3.72 (s, 2H), 3.64 (s, 3H), 2.73 (d, *J* = 7.3 Hz, 18H), 2.61 – 2.48 (m, 12H), 2.32 (dd, *J* = 18.0, 8.0 Hz, 4H), 1.31 – 1.22 (m, 12H), 0.97 (t, *J* = 7.5 Hz, 3H).

3-(10-(4-((Bis(2-((2-(ethylthio)ethyl)thio)ethyl)amino)methyl)phenyl)-8-ethyl-5,5-difluoro-1,3,7,9-tetramethyl-5*H*-4λ^4,5λ^4-dipyrrolo[1,2-*c*:2',1'-*f*][1,3,2]diazaborinin-2-yl)propanoic acid (5, Carboxy-CS2). A solution of **4** (0.74 g, 0.97 mmol, 1.0 eq) in methanol (24.1 mL, 0.04 M) and THF (13.8 mL, 0.07 M) was treated with a NaOH solution (3M, 2.14 mL, 6.6 eq) and stirred protected from light for 16 h. Upon completion, reaction mixture was concentrated under reduced pressure, resulting residue was dissolved in EtOAc and washed with 10% HCl (aq) (x2). Organic layer was dried with Na_2SO_4 and concentrated under reduced pressure. Purification via column chromatography on silica gel (81:17:2% CH_2Cl_2/EtOAc/MeOH) afforded **Carboxy-CS2** (0.16 g, 22 %) as a pink solid. ^{1}H NMR (400 MHz, $CDCl_3$) δ 10.52 (s, 1H), 7.45 (d, *J* = 7.6 Hz, 2H), 7.21 (d, *J* = 7.6 Hz, 2H), 3.73 (s, 2H), 2.79 – 2.63 (m, 18H), 2.63 – 2.47 (m, 12H), 2.36 (t, *J* = 7.9 Hz, 2H), 2.28 (q, *J* = 7.7 Hz, 2H), 1.29 (s, 3H), 1.28 (s, 3H), 1.24 (t, *J* = 7.4 Hz, 6H), 0.96 (t, *J* = 7.5 Hz, 3H).

(3-(10-(4-((Bis(2-((2-(ethylthio)ethyl)thio)ethyl)amino)methyl)phenyl)-8-ethyl-5,5-difluoro-1,3,7,9-tetramethyl-5*H*-4λ^4,5λ^4-dipyrrolo[1,2-*c*:2',1'-*f*][1,3,2]diazaborinin-2-

yl)propanamido)triphenylphosphonium (6, Mito-CS2). A solution of **Carboxy-CS2** (12.0 mg, 0.016 mmol, 1.0 eq), (2-aminoethyl)triphenylphosphonium bromide (12.0 mg, 0.032 mmol, 2.0 eq) and Hünig's base (11.2 µL, 0.064 mmol, 4.0 eq) in anhydrous DMF (1.6 mL, 0.01 M) was charged with HATU (13.0 mg, 0.035 mmol, 2.2 eq) and stirred at room temperature, protected from light for 48 h. Upon completion, reaction mixture was diluted in EtOAc and washed with water and brine (x2). Organic layer was dried with Na_2SO_4 and concentrated under reduced pressure. Crude was purified via column chromatography on silica gel (5% MeOH/CH_2Cl_2) to yield **Mito-CS2** (6.6 mg, 39 %) as a dark pink solid. ^{1}H NMR (400 MHz, CD_3OD) δ 7.76 – 7.65 (m, 15H), 7.49 (d, *J* = 7.9 Hz, 2H), 7.13 (d, *J* = 7.9 Hz, 2H), 3.73 (s, 2H), 3.45 – 3.37 (m, 2H), 2.79 – 2.65 (m, 16H), 2.61 (t, *J* = 7.5 Hz, 2H), 2.54 (q, *J* = 7.4 Hz, 4H), 2.46 (s, 3H), 2.44 (s, 3H), 2.33 (q, *J* = 7.4 Hz, 2H), 2.16 (t, *J* = 7.4 Hz, 2H), 1.33 (s, 3H), 1.30 (s, 3H), 1.24 (s, 6H), 1.22 (s, 2H), 0.99 (t, *J* = 7.5 Hz, 3H).

3-(10-(4-((Bis(2-((2-(ethylthio)ethyl)thio)ethyl)amino)methyl)phenyl)-8-ethyl-5,5-difluoro-1,3,7,9-tetramethyl-5*H*-4λ^4,5λ^4-dipyrrolo[1,2-*c*:2',1'-*f*][1,3,2]diazaborinin-2-yl)-*N*-(2-(dimethylamino)ethyl)propanamide (7, Lyso-CS). A solution of **Carboxy-CS2** (12.0 mg, 0.016 mmol, 1.0 eq), N^1,N^1-dimethylethane-1,2-diamine (3.0 mg, 0.032 mmol, 2.0 eq) and Hünig's base (11.2 µL, 0.064 mmol, 4.0 eq) in anhydrous DMF (1.6 mL, 0.01 M) was charged with HATU (13.0 mg, 0.035 mmol, 2.2 eq) and stirred at room temperature, protected from light for 48 h. Upon completion, reaction mixture was diluted in EtOAc and washed with water and brine (x2). Organic layer was dried with Na_2SO_4 and concentrated under reduced pressure. Crude was purified via column chromatography on activated basic alumina (0-2.5% MeOH/CH_2Cl_2) to yield **Lyso-CS2** (7.6 mg, 58 %) as a dark pink solid. ^{1}H NMR (400 MHz, CD_3OD) δ 7.49 (d, *J* = 7.9 Hz, 2H), 7.13 (d, *J* = 7.9 Hz, 2H), 3.73 (s, 2H), 3.45 – 3.37 (m, 2H), 2.79 – 2.65 (m, 16H), 2.61 (t, *J* = 7.5 Hz, 2H), 2.54 (q, *J* = 7.4 Hz, 4H), 2.46 (s, 3H), 2.44 (s, 3H), 2.33 (q, *J* = 7.4 Hz, 2H), 2.19 (s, 6H), 2.16 (t, *J* = 7.4 Hz, 2H), 1.33 (s, 3H), 1.30 (s, 3H), 1.24 (s, 6H), 1.22 (s, 2H), 0.99 (t, *J* = 7.5 Hz, 3H).

Spectroscopic Materials and Methods. Millipore water was used to prepare all aqueous solutions. All spectroscopic measurements were performed in phosphate buffered saline (1X PBS, pH 7.4, Invitro- gen, Carlsbad, CA). Fluorescence spectra were recorded using a Photon Technology International Quanta Master 4 L-format scan spectrofluorometer (Lawrenceville, NJ) equipped with an LPS-220B 75-W xenon lamp and power supply, A-1010B lamp housing with integrated igniter, switchable 814 photocounting/analog photomultiplier detection unit, and MD5020 motor driver. Samples for emission measurements were contained in 1-cm quartz cuvettes (1.4-mL volume, Starna, Atascadero, CA). Cu^+ was delivered in the form of $[Cu(MeCN)_4][PF_6]$ from an acetonitrile stock solution (2 mM). Excitation was provided at 514 nm and collected emission was integrated from 520-620 nm for **Mito-CS2**, **Lyso-CS**, **Golgi-CS** and **PM-CS**.

Cell Culture. HEK 293T cells were cultured in Dulbecco's Modified Eagle Medium (DMEM, Invitrogen, Carlsbad, CA) supplemented with 10% Fetal Bovine Serum (FBS, Invitrogen), and glutamine (2mM). One day before imaging, cells were passed and plated on 18-mm glass coverslips coated with poly-L-lysine (50 mg/mL, Sigma, St. Louis, MO). Immediately before the experiments, cells were washed with PBS buffer and imaged. Experiments to assess copper uptake

were performed in the same media supplemented with the additives at the indicated concentrations.

Live-Cell Imaging. Confocal fluorescence imaging was performed with a Zeiss LSM 710 laser-scanning microscope and a 40x water-immersion objective lens. Excitation of **Mito-CS2**, **Lyso-CS**, **Golgi-CS** and **PM-CS** loaded cells at 514 nm was carried out with a He-Ne laser, and emission was collected using META detector between 520 and 733 nm. Excitation of MitoTracker Deep Red FM at 633 nm was carried out with a He-Ne laser, and emission was collected using a META detector between 640 and 704 nm. Organelle-targeted probes (1 μM for **Mito-CS2**, **Lyso-CS** and **Golgi-CS**, 18 μM for **PM-CS** in PBS were incubated with live cells samples for 15 min (30 sec for **PM-CS**) at 37 °C. Staining solution was exchanged with fresh PBS and cells were imaged. Images were analyzed using ImageJ.

Schemes and Figures

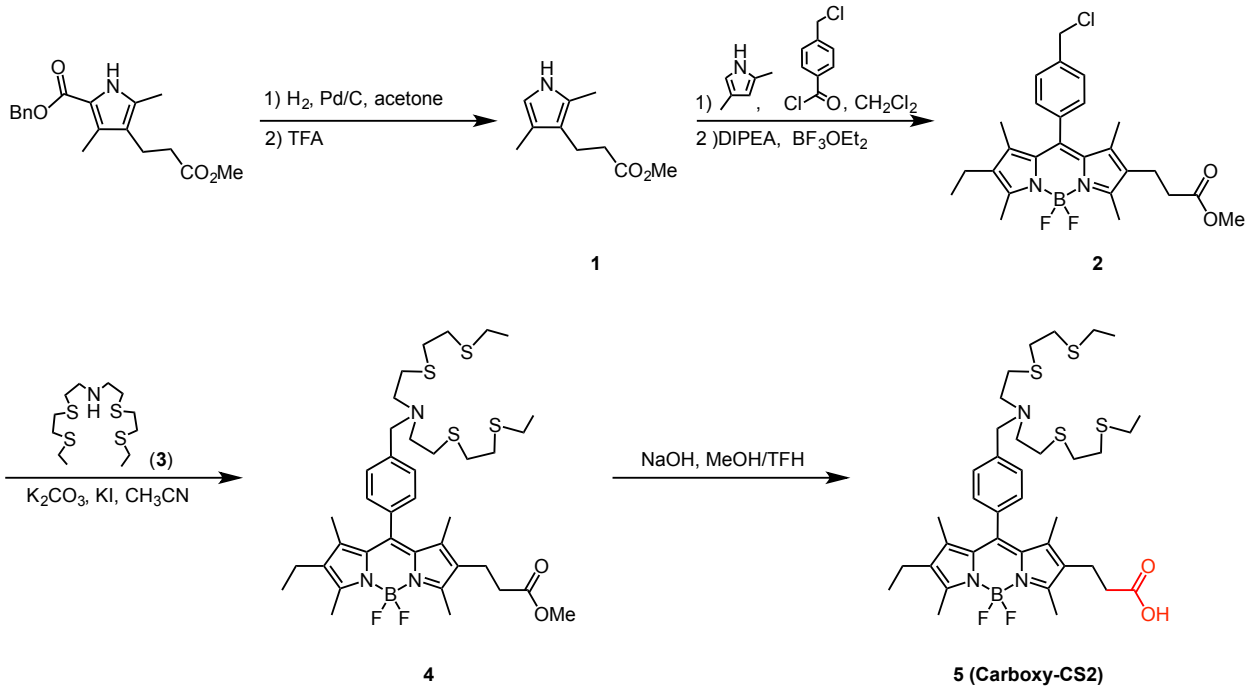

Scheme A1-1. Synthesis of flexible intermediate **Carboxy-CS2**.

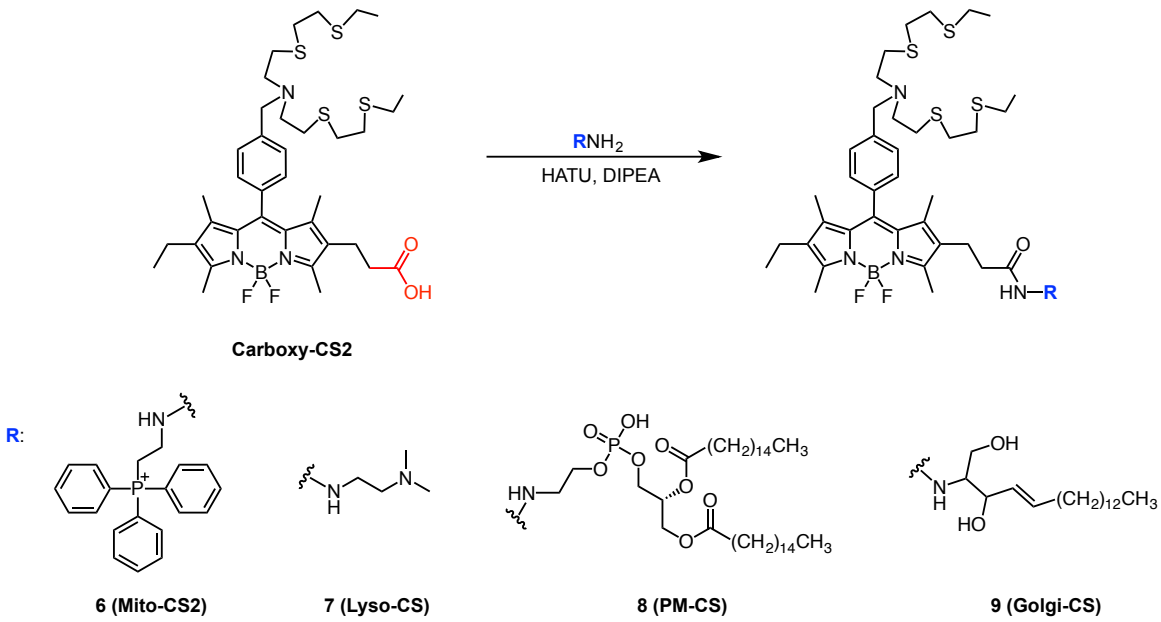

Scheme A1-2. Synthesis of organelle-targeted copper sensors.

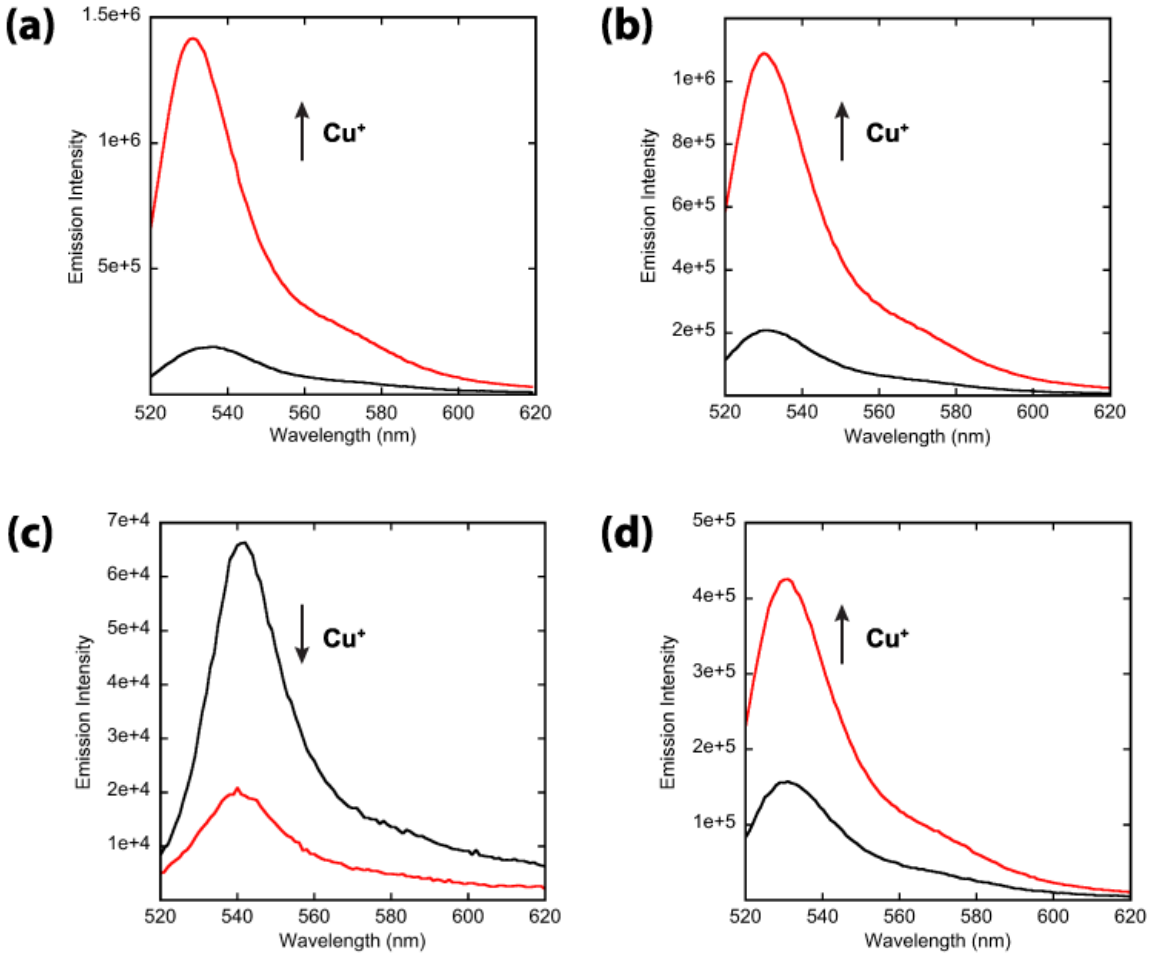

Figure A1-1. Fluorescence response of organelle-targeted probes to Cu^+. Spectra shown are for buffered [Cu^+] of 0.00 (black trace) and 2.0 μM (red trace) for (a) **Mito-CS2**, (b) **Lyso-CS**, (c) **Golgi-CS** and (d) **PM-CS**. Spectra were acquired in PBS buffer, pH 7.4 with excitation at 514 nm.

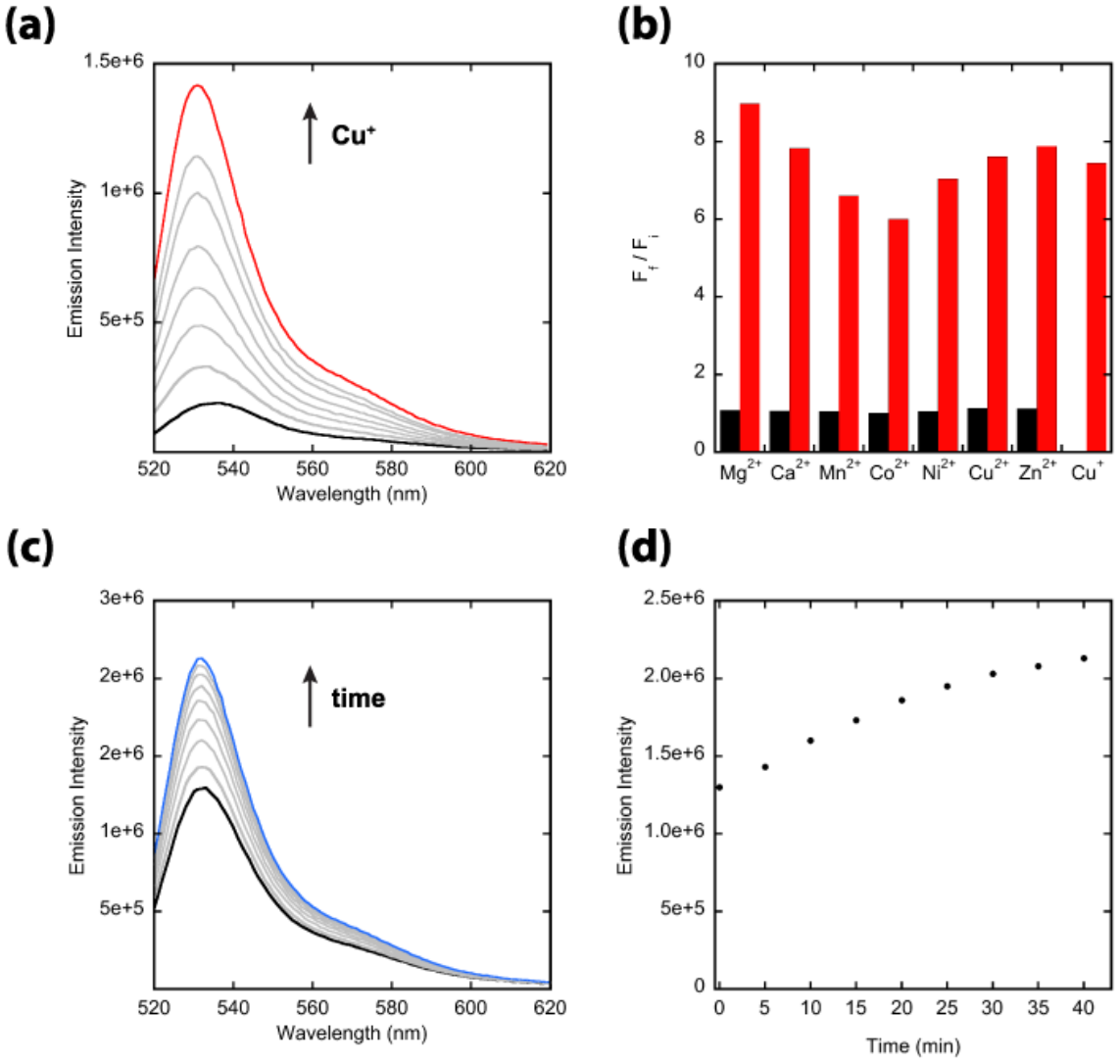

Figure A1-2. *In vitro* characterization of **Mito-CS2**. (a) Fluorescence response of 1.4 μM **Mito-CS2** to Cu^{+}. Spectra shown are for buffered [Cu^{+}] of 0.0 (black trace), 0.2, 0.4, 0.6, 0.8, 1.0, 1.2 and 1.4 μM (red trace). (b) Fluorescence response of **Mito-CS2** to various metal ions. Bars represent the final integrated fluorescence response (F_f) over the initial integrated emission (F_i). Black bars represent the addition of an excess of the appropriate metal ion (2 mM for Mg^{2+}, Ca^{2+}, and Zn^{2+}, 50 μM for all other cations) to a 2 μM solution of **Mito-CS2**. Red bars represent the subsequent addition of 2 μM Cu^{+} to the solution. (c, d) Copper-independent increase in fluorescence intensity of **Mito-CS2** over time. Spectra were acquired in PBS buffer, pH 7.4 with excitation at 514 nm and the collected emission was integrated over 520 to 620 nm.

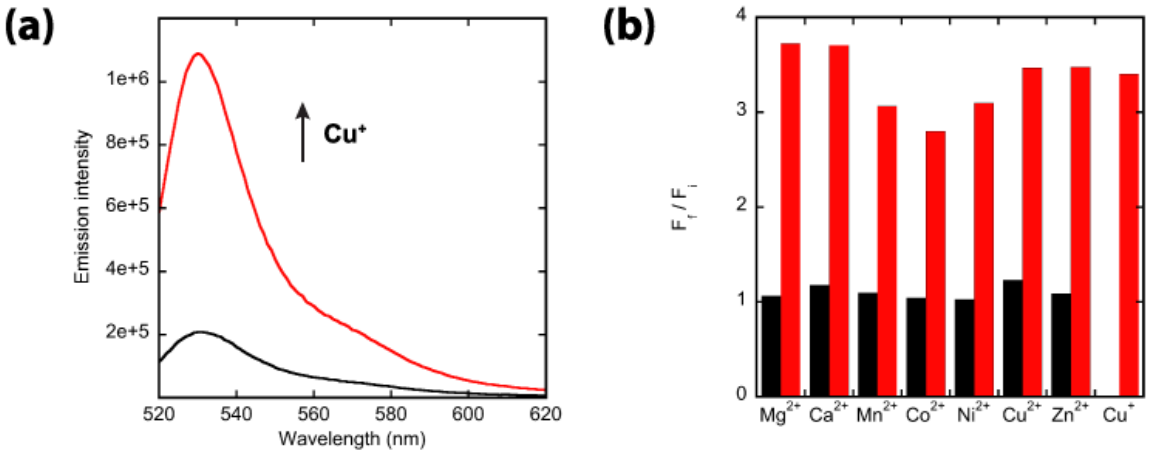

Figure A1-3. *In vitro* characterization of **Lyso-CS**. (a) Fluorescence response of 2.0 μM **Lyso-CS** to Cu^+. Spectra shown are for buffered [Cu^+] of 0.00 (black trace), and 2.0 μM (red trace). (b) Fluorescence response of **Lyso-CS** to various metal ions. Bars represent the final integrated fluorescence response (F_f) over the initial integrated emission (F_i). Black bars represent the addition of an excess of the appropriate metal ion (2 mM for Mg^{2+}, Ca^{2+}, and Zn^{2+}, 50 μM for all other cations) to a 2 μM solution of **Lyso-CS**. Red bars represent the subsequent addition of 2 μM Cu^+ to the solution. Spectra were acquired in PBS buffer, pH 7.4 with excitation at 514 nm and the collected emission was integrated over 520 to 620 nm.

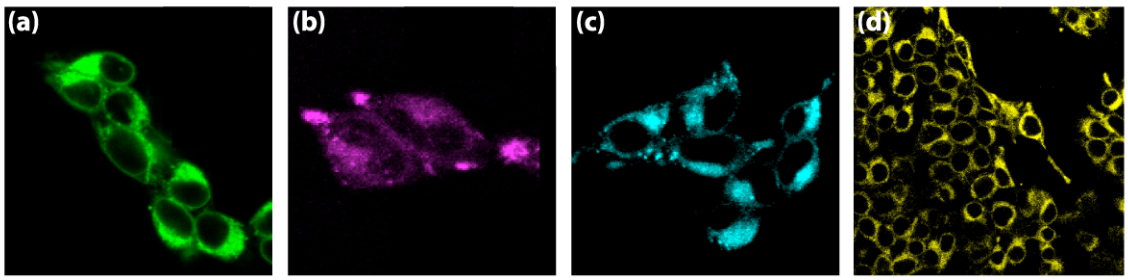

Figure A1-4. Differential subcellular localization of organelle-targeted probes. HEK 293T cells were stained with 1 μM (a) **Mito-CS2**, (b) **Lyso-CS**, (c) **Golgi-CS** for 15 min or (d) 18 μM **PM-CS** for 30 sec at 37 ºC in PBS.

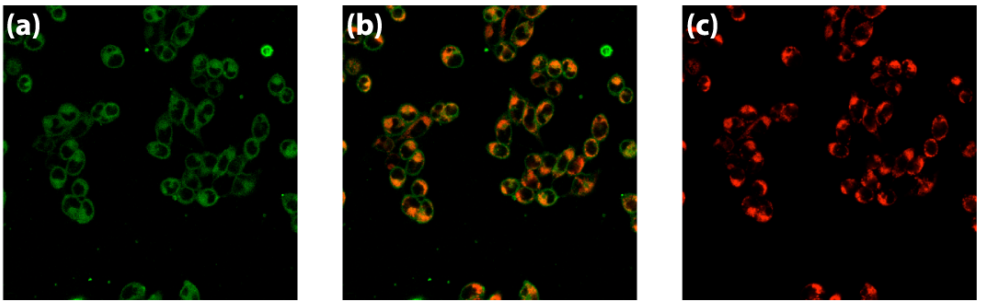

Figure A1-5. Colocalization of **Mito-CS2** and MitoTracker Deep Red FM in HEK 293T cells. Cells were stained with 50 nM MitoTracker Deep Red FM for 15 min at 37 ºC in PBS. Media was then exchanged and cells were subsequently stained with 0.5 μM **Mito-CS2** for 15 min at 37 ºC in PBS. (b) Overlay image of (a) **Mito-CS2** and (c) MitoTracker Deep Red FM staining shows decent colocalization of the mitochondrial probes.

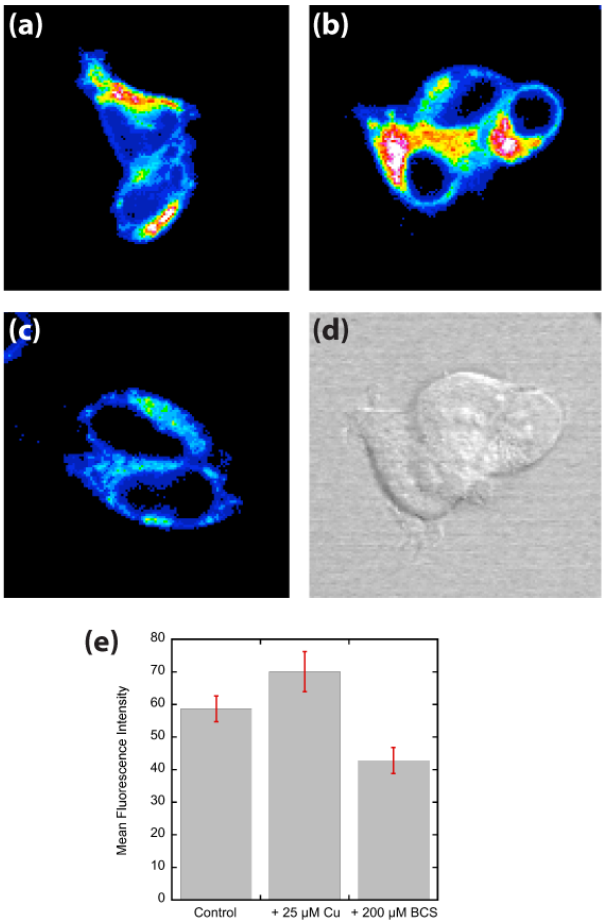

Figure A1-6. Mito-CS2 response to copper supplementation and chelation conditions in HEK 293T cells. (a) Control HEK 293T cells, HEK 293T cells supplemented with (b) 25 µM $CuCl_2$ or (c) 200 µM BCS in the growth medium overnight at 37 ºC were stained with 1 µM **Mito-CS2** for 15 min at 37 ºC in PBS. (d) Brightfield image of cells in (b) to show viability. (e) Quantification of mean fluorescence intensity of each condition (n = 4 fields of cells per condition). Error bars represent SEM.

References

1. Zeng, L.; Miller, E. W.; Pralle, A.; Isacoff, E. Y.; Chang, C. J., A selective turn-on fluorescent sensor for imaging copper in living cells. *J. Am. Chem. Soc.* **2006,** *128*, 10-11.
2. Miller, E. W.; Zeng, L.; Domaille, D. W.; Chang, C. J., Preparation and use of Coppersensor-1, a synthetic fluorophore for live-cell copper imaging. *Nat. Protoc.* **2006,** *1*, 824-827.

Appendix 2:

Efforts Towards the Improvement of the Water Solubility of Cu^{+} Probes Using a More Hydrophylic Receptor

Synopsis

The application of fluorescent dyes as molecular imaging probes for the study of cellular metal homeostasis is dictated by specific properties of the sensor, including a selective turn-on response to the analyte of interest, high brightness and quantum yield, cell permeability and biocompatibility, among others. While the BODIPY fluorophore has been shown to yield Cu^+ responsive sensors,[1-3] the application of the resulting probes to study more complex systems has been limited by their hydrophobic nature, imparted by the high lipophilicity of the fluorophore as well as of the thioether-based metal-ion receptor. Against this backdrop, we sought to balance the hydrophobicity of the BODIPY fluorophore reporter with the use of a known water-soluble thiocrown receptor[4] that is modified with four hydroxymethyl groups to enhance aqueous solubility. This appendix summarizes the synthesis and characterization of two BODIPY-based probes that display a hydroxymethyl-modified NS_3 macrocycle as the Cu^+ receptor in order to improve the biocompatibility of these fluorescent sensors.

Results and Discussion

Synthesis of Hydrophilic Receptor-based Cu^+ Probes. The synthetic route for BODIPY-based probes bearing the NS_3 hydroxymethyl-modified Cu^+ reporter is outlined in Scheme A2-1. Acetonide-protection of 1,3-diols previous to the construction of the aniline-based thiocrown allowed for the synthesis of benzaldehyde macrocyclic receptor **7**, a useful intermediate that can be coupled to a variety of substituted pyrroles for the formation of different BODIPY-based sensors. Synthesis of probe diol-protected probe precursors was achieved via a one-pot, three-step procedure that includes the condensation of kryptopyrrole or 2,4-dimethylpyrrole and benzaldehyde receptor **7**, followed by DDQ oxidation and boron insertion with BF_3•OEt_2. Deprotection of acetonide groups under mild acidic conditions afforded probes **10** and **11**.

Spectroscopic Properties of Cu^+ Probes. The spectroscopic properties of the BODIPY-based dyes were first evaluated in several different solvents, including: phosphate buffered saline (1X PBS), 25 mM HEPES (pH 7.0), 10 mM MOPS (pH 7.2) and methanol. However, due to copper independent fluctuations in the fluorescence of the BODIPY-based probes in aqueous solvents, we chose to examine the behavior of probe **10** and **11** in a more organic environment. Table A2-1 provides a summary of spectroscopic properties of **10** and **11** in methanol. Apo-dye **10** exhibits a major absorption peak at 519 nm, with a fluorescence emission band at 530 nm. (Figures A2-1, A2-2) Upon addition of one equivalent of Cu^+, a 24-fold enhancement in the fluorescence intensity is observed with minimal shifts in absorption ($\lambda_{abs\ (Cu)}$ 521 nm) or emission ($\lambda_{fl\ (Cu)}$ 533 nm) maxima. The increase in the fluorescence intensity does not saturate upon binding one equivalent of the cuprous ion, as addition of up to 25 equivalents of Cu^+ produces corresponding increases in the emission intensity. (Figure A2-2) Response of **10** to Cu^+ over a variety of biologically relevant cations (Mg^{2+}, Ca^{2+}, Mn^{2+}, Fe^{2+}, Co^{2+}, Cu^{2+}, and Zn^{2+}) showed a moderate selectivity towards Cu^+, with interference observed from the s-block metals (Mg^{2+}, Ca^{2+}) possibly due to binding of these cations to the hydroxymethyl receptor modifications. (Figure A2-3) Binding analysis of the formed copper complex using the method of continuous variations (Job's plot), indicated that a 1:3 Cu^+:probe complex is responsible for the enhanced fluorescence response observed for probe **10**. (Figure A2-4) This result seems to suggest a possible dye aggregation in an inverted micelle-like

structure, which we hypothesize to be an effect of a differential hydrophilicity of the water-soluble thiocrown receptor and the lipophilic BODIPY fluorophore.

Spectroscopic characterization of probe **11** in methanol showed an absorption maximum for the apo dye at 498 nm and an emission band at 507 nm, both of which are minimally shifted upon copper addition ($\lambda_{abs\ (Cu)}$ 500 nm, $\lambda_{fl\ (Cu)}$ 506 nm). (Figures A2-5, A2-6) Binding of Cu^+ to **11** triggered an analogous response to **10**, where addition of one equivalent of the metal resulted in a 69-fold fluorescence turn-on that is further increased to up to 187-fold enhancement with addition of 10 equivalents of the cation. (Figure A2-6) Modification of the BODIPY-core did not lead to a change in the selectivity of the response of probe **11** to Cu^+ over other metal cations as quenching of the fluorescence was also observed with Mg^{2+}, Ca^{2+} and Zn^{2+}. (Figure A2-7)

Conclusion and Future Work

We have investigated the use of a hydrophilic thiocrown Cu^+ receptor to improve the water solubility of the BODIPY-based copper probes. However, differential hydrophilicity of the receptor and the fluorophore led to difficulties in the characterization of the probes in aqueous conditions. While preliminary characterization of the probes in organic solvent showed good fluorescence enhancements upon copper binding, 1:3 Cu^+:probe binding suggests possible aggregation that is not ideal for use of these probes in *in cellulo* applications. Therefore, an alteration of the lipophilicity of the fluorophore reporter is needed in order to balance the hydrophilic nature of the hydroxymethyl-modified receptor in order to produce a water-soluble probe.

Experimental Section

Synthetic Materials and Methods. All reactions were carried out under a dry N_2 atmosphere and stirred magnetically unless stated otherwise. Silica gel P60 (SiliCycle) and activated basic aluminum oxide (Brockmann) were used for column chromatography. Analytical thin layer chromatography was performed using SiliCycle 60 F254 silica gel (precoated sheets, 0.25 mm thick) and EMD Chemicals 60 F254 basic aluminum oxide. Compounds **1** – **7**[4] were synthesized according to literature procedures. Unless otherwise noted, all chemicals were used as received. ^1H and ^{13}C NMR spectra were collected in $CDCl_3$ (Cambridge Isotope Laboratories, Cambridge, MA) at 25 °C on a Bruker AV-300, Bruker AVB-400 or Bruker AVQ-400 spectrometer at the College of Chemistry NMR Facility at the University of California, Berkeley. All chemical shifts are reported in the standard notation of parts per million using the peak of residual proton or carbon signals of $CDCl_3$ as an internal reference.

Synthesis.

20-(4-(2,8-Diethyl-5,5-difluoro-1,3,7,9-tetramethyl-5*H*-4λ^4,5λ^4-dipyrrolo[1,2-*c*:2',1'-*f*][1,3,2]diazaborinin-10-yl)phenyl)-3,3,13,13-tetramethyl-2,4,12,14-tetraoxa-8,17,23-trithia-20-azadispiro[5.3.5^{10}.9^6]tetracosane (8). In an oven-dried 2-necked round-bottom, a solution of **7** (85.1 mg, 0.15 mmol, 1.0 eq) in anhydrous CH_2Cl_2 (3.2 mL, 0.048 M) flask in the presence of 2 drops of trifluoroacetic acid was treated with kryptopyrrole (81.8 μL, 0.61 mmol, 3.96 eq) and then stirred at room temperature for 2 h. DDQ (34.8 mg, 0.15 mmol, 1.0 eq) was added in

anhydrous CH_2Cl_2 (1.0 mL), and allowed to react for 1 h. DIPEA (266.7 µL, 1.53 mmol, 10.0 eq) was added dropwise over 10 min and after 20 min BF_3•OEt_2 (194.0 µL, 1.53 mmol, 10.0 eq) was added dropwise and stirred at room temperature protected from light for 16 h. The reaction was quenched with water and extracted with CH_2Cl_2 (x2). The combined organics were dried with Na_2SO_4 and concentrated under reduced pressure and purified by column chromatography on silica gel (0-2 % EtOAC/CH_2Cl_2) to yield 25.2 mg (20 %) of **8** as a dark pink solid. ^{1}H NMR (400 MHz, $CDCl_3$) δ 7.12 (s, 2H), 6.88 (s, 2H), 3.84 – 3.66 (m, 12H), 2.87 (s, 8H), 2.81 (s, 4H), 2.30 (q, *J* = 7.6 Hz, 4H), 1.42 (d, *J* = 9.2 Hz, 12H), 1.35 (s, 6H), 1.25 (s, 6H), 0.98 (t, *J* = 7.5 Hz, 6H).

(4-(4-(2,8-Diethyl-5,5-difluoro-1,3,7,9-tetramethyl-5*H*-4λ^4,5λ^4-dipyrrolo[1,2-*c*:2',1'-*f*][1,3,2]diazaborinin-10-yl)phenyl)-1,7,11-trithia-4-azacyclotetradecane-9,9,13,13-tetrayl)tetramethanol (10). A round-bottom flask containing **8** (25.2 mg, 0.03 mmol, 1.0 eq) was charged with an aqueous solution of acetic acid (12.6 mL, 70 % v/v) and reaction mixture was stirred at room temperature for 16 h. Upon completion, as judged by LC-MS, reaction was quenched with addition of sat. $NaHCO_3$, and washed with CH_2Cl_2 (x3). Combined organics were dried with Na_2SO_4 and concentrated under reduced pressure. Purification via column chromatography on silica gel (0-10 % MeOH/EtOAc) afforded probe **10** (8.4 mg, 37%) as an orange solid. ^{1}H NMR (400 MHz, $CDCl_3$) δ 7.06 (d, *J* = 8.4 Hz, 2H), 6.69 (d, *J* = 8.4 Hz, 2H), 3.77 (m, 4H), 3.63 (q, *J* = 6.4 Hz, 8H), 2.83 (m, 4H), 2.76 (s, 4H), 2.59 (s, 4H), 2.52 (s, 4H), 2.30 (q, *J* = 7.2 Hz, 4H), 1.37 (s, 6H), 0.98 (t, *J* = 7.6 Hz, 6H). LRESI-MS calculated for [M+H] 750.3, found 750.2.

(4-(4-(5,5-Difluoro-1,3,7,9-tetramethyl-5*H*-4λ^4,5λ^4-dipyrrolo[1,2-*c*:2',1'-*f*][1,3,2]diazaborinin-10-yl)phenyl)-1,7,11-trithia-4-azacyclotetradecane-9,9,13,13-tetrayl)tetramethanol (11). In an oven-dried 2-necked round-bottom, a solution of **7** (135.2 mg, 0.24 mmol, 1.0 eq) in anhydrous CH_2Cl_2 (31.2 mL, 0.008 M) flask in the presence of 2 drops of trifluoroacetic acid was treated with 2,4-dimethylpyrrole (55.3 µL, 0.54 mmol, 2.2 eq) and then stirred at room temperature for 2 h. DDQ (60.7 mg, 0.27 mmol, 1.1 eq) was added in anhydrous CH_2Cl_2 (2.0 mL), and allowed to react for 1 h. DIPEA (622.2 µL, 3.58 mmol, 15.0 eq) was added dropwise over 10 min and after 20 min BF_3•OEt_2 (616.4 µL, 4.86 mmol, 20.0 eq) was added dropwise and stirred at room temperature protected from light for 16 h. The reaction was quenched with water and extracted with CH_2Cl_2 (x2). The combined organics were dried with Na_2SO_4 and concentrated under reduced pressure. Purification via column chromatography on silica gel (20 % MeOH/CH_2Cl_2) yielded 27.4 mg (15 %) of probe **11** as a pink solid. ^{1}H NMR (400 MHz, $CDCl_3$) δ 7.05 (d, *J* = 8.5 Hz, 2H), 6.68 (d, *J* = 8.5 Hz, 2H), 5.96 (s, 2H), 3.75 (t, *J* = 7.3 Hz, 4H), 3.67 – 3.56 (m, 8H), 2.81 (t, *J* = 7.2 Hz, 4H), 2.74 (s, 4H), 2.58 (s, 4H), 2.54 (s, 6H), 1.46 (s, 6H).

Spectroscopic Materials and Methods. Millipore water was used to prepare all aqueous solutions. All spectroscopic measurements were performed in neat methanol. Absorption spectra were recorded using a Varian Cary 50 spectrophotometer (Walnut Creek, CA) and fluorescence spectra were recorded using a Photon Technology International Quanta Master 4 L-format scan spectrofluorometer (Lawrenceville, NJ) equipped with an LPS-220B 75-W xenon lamp and power supply, A-1010B lamp housing with integrated igniter, switchable 814 photocounting/analog photomultiplier detection unit, and MD5020 motor driver. Samples for absorption and emission measurements were contained in 1-cm quartz cuvettes (1.4-mL volume, Starna, Atascadero, CA). Cu^+ was delivered in the form of $[Cu(MeCN)_4][PF_6]$ from an acetonitrile stock solution (2 mM).

Excitation was provided at 514 nm or 488 nm (to evaluate response at closest available laser lines for confocal microscopy) and collected emission was integrated from 520-650 nm or 498-620 nm for probes **10** and **11**, respectively.

Schemes and Figures

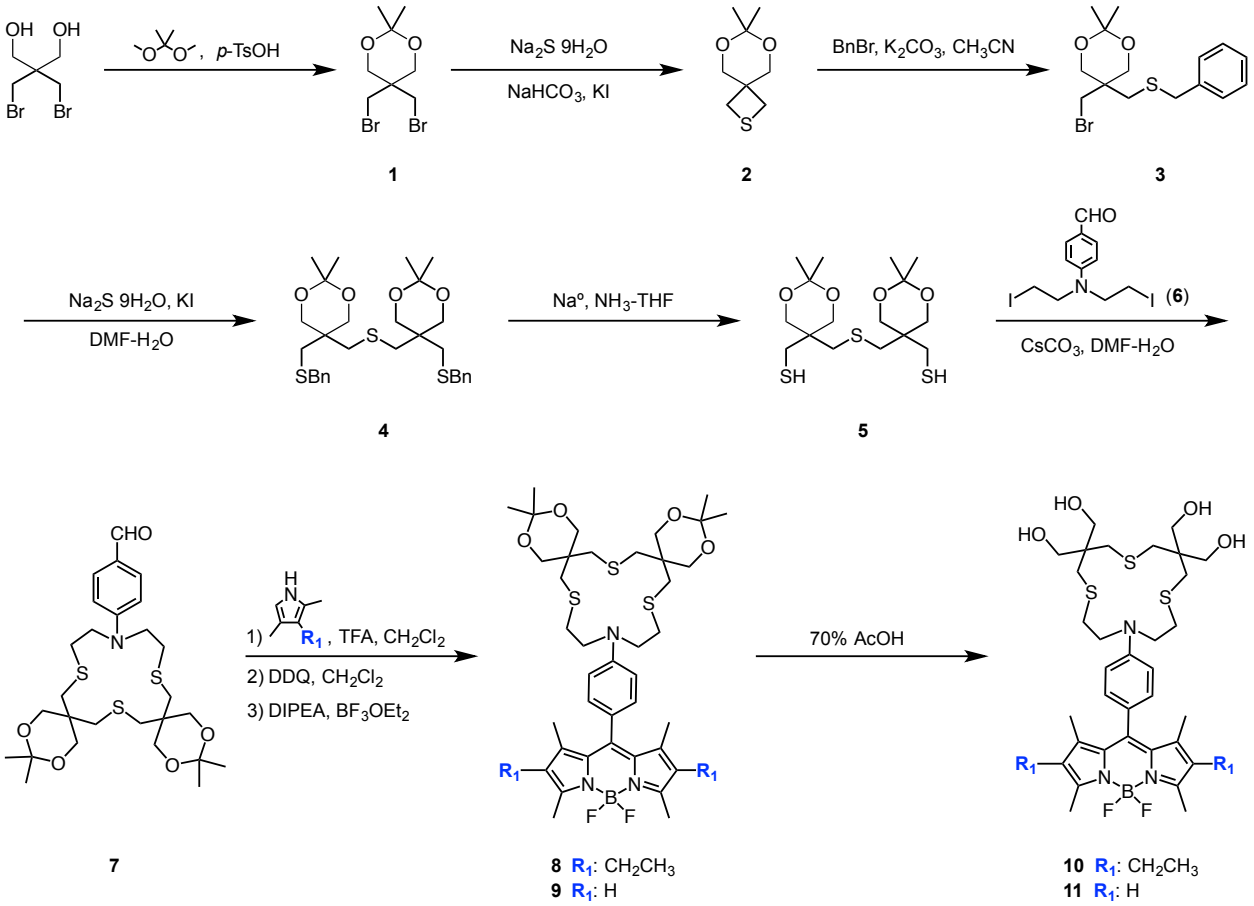

Scheme A2-1. Synthesis of copper sensors with hydrophilic receptor.

Probe	Cu(I)	λ_{abs} (nm)	λ_{fl} (nm)	F_f / F_i (1 eq. Cu^+)
10	-	519	521	
	+	530	533	24
11	-	498	507	
	+	500	506	69

Table A2-1. Photophysical properties of probes **10** and **11** in methanol.

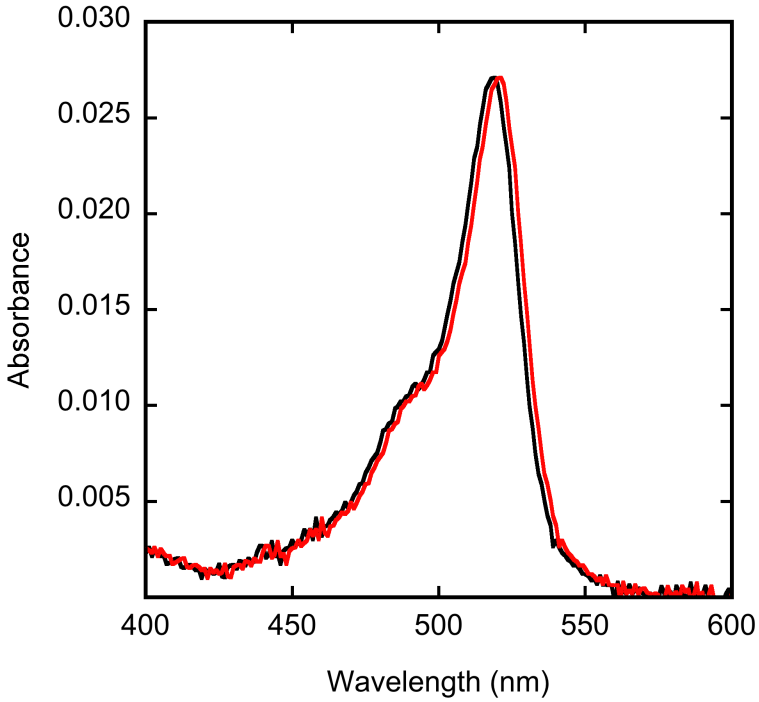

Figure A2-1. Absorbance spectra of 2 μM **10**. Spectra shown are for buffered [Cu^{+}] of 0.0 (black trace) and 2.0 (red trace) μM. Spectra were acquired in methanol

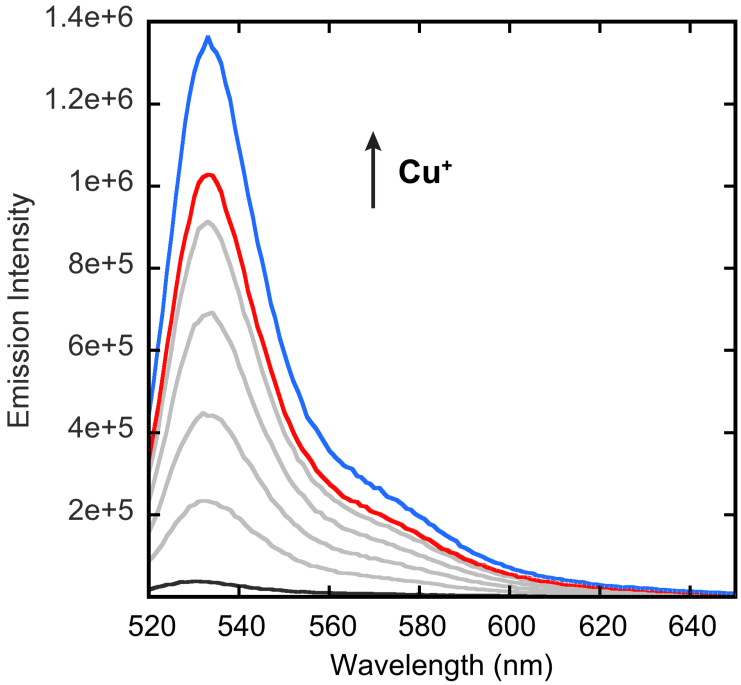

Figure A2-2. Fluorescence response of 2 μM **10** to Cu^+. Spectra shown are for buffered [Cu^+] of 0.0 (black trace) 0.4, 0.8, 1.2, 1.6, 2.0 (red trace) and 50.0 (blue trace) μM. Spectra were acquired in methanol with excitation at 514 nm.

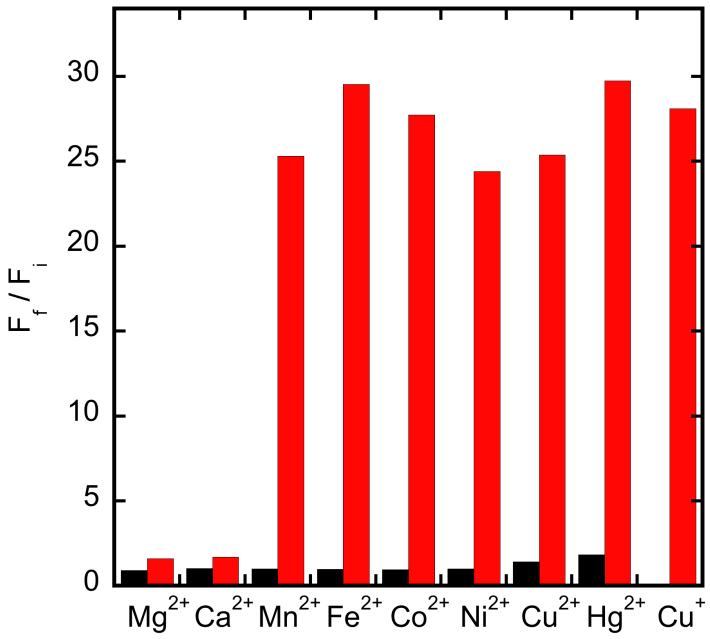

Figure A2-3. Fluorescence response of **10** to various metal ions. Bars represent the final integrated fluorescence response (F_f) over the initial integrated emission (F_i). Spectra were acquired in methanol. Black bars represent the addition of an excess of the appropriate metal ion (2 mM for Mg^{2+}, Ca^{2+}, and Zn^{2+}, 50 μM for all other cations) to a 2 μM solution of **10**. Red bars represent the subsequent addition of 2 μM Cu^{+} to the solution. Excitation was provided at 514 nm, and the collected emission was integrated over 520 to 650 nm.

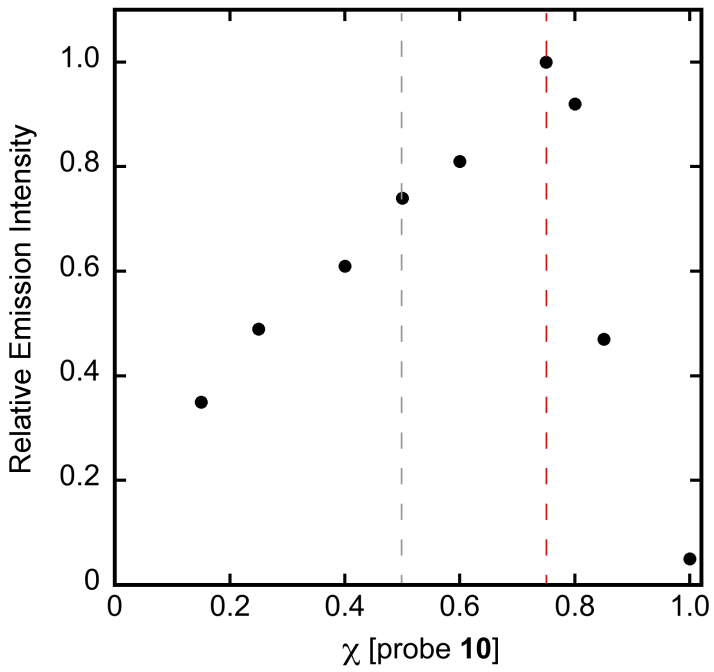

Figure A2-4. Job's plot of **10** and Cu^+. The total concentration of **10** and Cu^+ was kept at a constant 2.0 μM. Excitation was provided at 514 nm and the collected emission intensity was integrated from 520 to 650 nm. Spectra were acquired in methanol. The maximum fluorescence response at 0.75 mol fraction of **10** indicates formation of a 1:3 Cu^+:**10** complex.

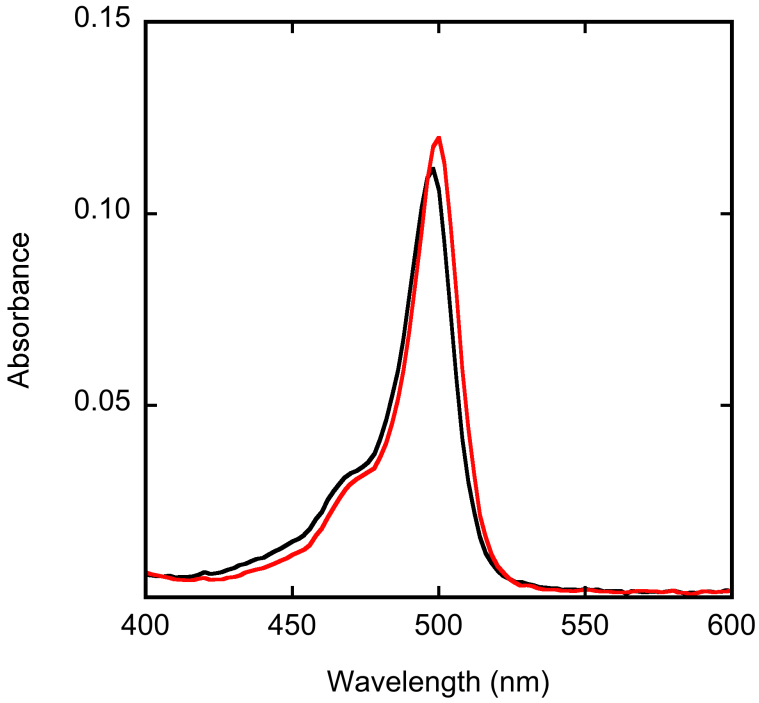

Figure A2-5. Absorbance spectra of 2 μM **11**. Spectra shown are for buffered [Cu^{+}] of 0.0 (black trace) and 2.0 (red trace) μM. Spectra were acquired in methanol.

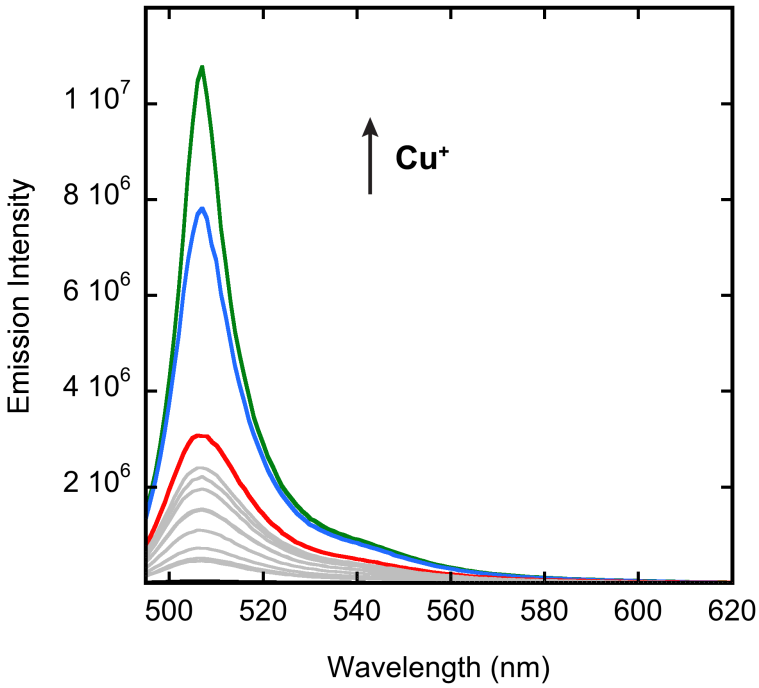

Figure A2-6. Fluorescence response of 2 μM **11** to Cu^+. Spectra shown are for buffered [Cu^+] of 0.0 (black trace) 0.2, 0.4, 0.6, 0.8, 1.0, 1.2, 1.4, 1.6, 2.0 (red trace), 10.0 (blue trace) and 20 (green trace) μM. Spectra were acquired in methanol with excitation at 488 nm.

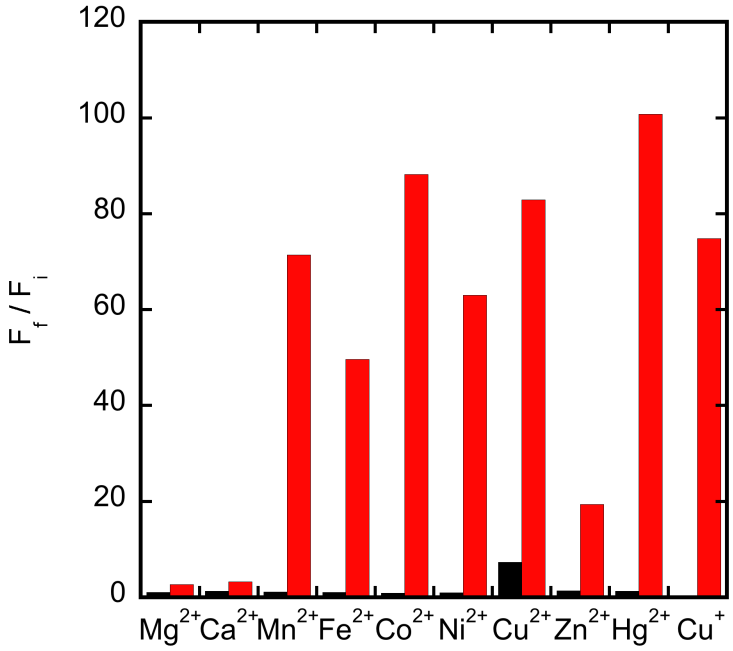

Figure A2-7. Fluorescence response of **11** to various metal ions. Bars represent the final integrated fluorescence response (F_f) over the initial integrated emission (F_i). Spectra were acquired in methanol. Black bars represent the addition of an excess of the appropriate metal ion (2 mM for Mg^{2+}, Ca^{2+}, and Zn^{2+}, 50 μM for all other cations) to a 2 μM solution of **11**. Red bars represent the subsequent addition of 2 μM Cu^{+} to the solution. Excitation was provided at 488 nm, and the collected emission was integrated over 498 to 620 nm.

References

1. Zeng, L.; Miller, E. W.; Pralle, A.; Isacoff, E. Y.; Chang, C. J., A selective turn-on fluorescent sensor for imaging copper in living cells. *J. Am. Chem. Soc.* **2006,** *128*, 10-11.
2. Dodani, S. C.; Domaille, D. W.; Nam, C. I.; Miller, E. W.; Finney, L. A.; Vogt, S.; Chang, C. J., Calcium-dependent copper redistributions in neuronal cells revealed by a fluorescent copper sensor and X-ray fluorescence microscopy. *Proc. Natl. Acad. Sci. USA* **2011,** *108* (15), 5980-5985.
3. Dodani, S. C.; Leary, S. C.; Cobine, P. A.; Winge, D. R.; Chang, C. J., A targetable fluorescent sensor reveals that copper-deficient SCO1 and SCO2 patient cells prioritize mitochondrial copper homeostasis. *J. Am. Chem. Soc.* **2011,** *133* (22), 8606-8616.
4. Morgan, M. T.; Bagchi, P.; Fahrni, C. J., Designed to dissolve: suppression of colloidal aggregation of Cu(I)-selective fluorescent probes in aqueous buffer and in-gel detection of a metallochaperone. *J. Am. Chem. Soc.* **2011,** *133*, 15906-15909.

Appendix 3:

Towards the Enhancement of Photophysical Properties and Hydrophilicity of BODIPY-based Cu^{+} Probes

Synopsis

Use of BODIPY-based Cu^+ probes like **CS1**[1] to study the role of this metal in biological environments has been somewhat limited due to the lipophilic nature of the fluorophore reporter. Additionally, attempts to observe dynamics of endogenous cellular copper pools have been restricted by the relatively low quantum yield of the **CS1**:Cu^+ complex in aqueous environments. Alteration of the BODIPY scaffold by selective substitution of one of the two canonical fluorides in most BODIPY dyes with alkoxy ligands has led to significant improvements in the water solubility of these fluorophores due to the increased out of plane dipole moment these analogues exhibit as opposed to the difluoro counterparts.[2] The high solubility in aqueous environments of the resulting MayaFluors also allows for high quantum yields in water, which is ideal for application in biological studies. Inspired by this improvement to the canonical BODIPY fluorophore, we evaluated the effects of a monoalkoxy substitution to the fluorophore core of **CS1** on its photophysical properties and hydrophilicity. This appendix summarizes the synthesis and characterization of **CS1-OMe**, a monomethoxy BODIPY-based copper sensor as a means to improve the biocompatibility of fluorescent copper probes.

Results and Discussion

Synthesis of Monomethoxy-BODIPY based Copper Probe. Monomethoxy BODIPY-based probe **CS1-OMe** was synthesized as shown in Scheme A3-1 and following published procedures.[1-3] Synthesis of **CS1** as an intermediate was achieved via BODIPY-core construction in a one-pot, two step procedure involving condensation of kryptopyrrole with chloroacetyl chloride followed by boron insertion with BF_3•OEt_2 to afford chloromethyl functionalized BODIPY **1**, which was then coupled to previously synthesized tetrathiaza receptor **2**. Substitution of one of the fluoride substituents for a methoxy moiety on the **CS1** fluorophore by activation of the BODIPY core with TMSOTf and exchange with methanol under basic conditions afforded the desired modified probe **CS1-OMe**.

Spectroscopic Properties of CS1-OMe. The spectroscopic properties of **CS1-OMe** were assessed by absorbance and fluorescence spectroscopy in aqueous buffer to show typical BODIPY features. In its apo form, **CS1-OMe** presents a major absorption band at 557 nm with a fluorescence emission peak at 549 nm. Complexation of one equivalent of Cu^+ causes a more intense and blue-shifted absorption ($\lambda_{abs\ (Cu)}$ 540 nm) as well as a 10.4-fold fluorescence enhancement centered at 551 nm. While modification of the BODIPY core through substitution of one of the electron-withdrawing fluorine atoms for an electron-donating methoxy group has been shown to yield brighter fluorophores,[2] this variation did not lead to an improved fluorescence enhancement upon copper binding (**CS1** exhibits a 10-fold turn-on response to Cu^+). Additionally, no alteration on selectivity of this response or the binding mode between the probe and the cation was observed. Since previous modification by double substitution of the fluoride substituents on **CS1** for methoxy groups to afford **CS3** has shown increased binding affinity for Cu^+ (K_d 3.6(3) x 10^{-12} M for **CS1**[1] vs K_d 8.9(3) x 10^{-14} M for **CS3**[4]) because of the increased electron density on the fluorophore, we were interested in studying how the variation of one of the fluoride positions would alter the affinity for copper. Competition experiments with thiourea resulted in an observed K_d 1.58 x 10^{-12} M, a value that is comparable to the copper affinity of the parent probe. This result

suggests that while introduction of a single electron-donating substituent is enough to alter the photophysical properties through electronic effects, these altered electronics are not sufficient to produce a lower dissociation constant value.

Additionally, preliminary octanol-water partition coefficient (log D) studies to assess altered hydrophilicity showed a slight improvement in water solubility over **CS1**, however because of the high lipophilicity of BODIPY-based probes, accurate values were not determined.

Conclusion and Future Work

We have evaluated the effects of a BODIPY-core modification through single replacement of fluoride substituent for the electron-donating methoxy moiety on the photophysical properties of BODIPY-based copper probes. The monomethoxy adaptation did not show an improved fluorescence response or binding affinity to copper, when compared to parent probe **CS1**. However, substitution with the more hydrophilic methoxy group seems to be a potential strategy to improve the water solubility of the fluorophore.

Experimental Section

Synthetic Materials and Methods. All reactions were carried out under a dry N_2 atmosphere and stirred magnetically unless stated otherwise. All reactions using air- or moisture-sensitive reagents were performed in oven- and flame-dried glassware under an atmosphere of dry N_2. Compounds **1 – 3**[1] were synthesized according to literature procedures. Unless otherwise noted, all chemicals were used as received. Silica gel P60 (SiliCycle) and activated basic aluminum oxide (Brockmann) were used for column chromatography. SiliCycle 60 F254 silica gel (precoated sheets, 0.25 mm thick) was used for analytical TLC, visualized with UV light and/or staining with *p*-anisaldehyde or $KMNO_4$. ^1H and ^{13}C NMR spectra were collected in $CDCl_3$ (Cambridge Isotope Laboratories, Cambridge, MA) at 25 °C on a Bruker AV-300, Bruker AVB-400 or Bruker AVQ-400 spectrometer at the College of Chemistry NMR Facility at the University of California, Berkeley. All chemical shifts are reported in the standard notation of parts per million using the peak of residual proton or carbon signals of $CDCl_3$ as an internal reference.

Synthesis.

***N*-((2,8-Diethyl-5-fluoro-5-methoxy-1,3,7,9-tetramethyl-5*H*-4λ^4,5λ^4-dipyrrolo[1,2-*c*:2',1'-*f*][1,3,2]diazaborinin-10-yl)methyl)-2-((2-(ethylthio)ethyl)thio)-*N*-(2-((2-(ethylthio)ethyl) thio)ethyl)ethan-1-amine (4, CS1-OMe).** In a flame-dried round bottom flask, a solution of **CS1** (102.8 mg, 0.16 mmol, 1.0 eq) in anhydrous dichloromethane (85.9 mL, 0.002 M) was cooled to 0 ºC. A solution of TMSOTf (147.7 µL, 0.82 mmol, 5.0 eq) in anhydrous chloroform (1.5 mL, 10% v/v) was added to cold reaction mixture and allowed to stir for 3 min. Diisopropylethylamine (284.2 µL, 1.63 mmol, 10.0 eq) and methanol (660.3 µL, 16.32 mmol, 100.0 eq) were then added and reaction was stirred for 1 min before quenching with addition of water to partition reaction mixture. Layers were separated and organics were washed with brine (x2), dried with Na_2SO_4 and concentrated under reduced pressure. Purification via column chromatography on silica gel (0-20% EtOAc/hexanes) afforded **CS1-OMe** (10.5 mg, 10 %) as a purple solid. ^1H NMR (400 MHz, $CDCl_3$) δ 4.07 (s, 2H), 2.90 (s, 4H), 2.84 (s, 3H), 2.62 (M, 12H), 2.53 (q, J = 7.4 Hz, 6H), 2.50 (s,

6H), 2.41 (s, 6H), 2.40 (q, *J* = 7.4 Hz, 6H), 1.24 (t, *J* = 7.4 Hz, 6H), 1.05 (t, *J* = 7.5 Hz, 6H). HRESI-MS calculated for [M+H] 642.3182, found 642.3225.

Spectroscopic Materials and Methods. Millipore water was used to prepare all aqueous solutions. All final spectroscopic measurements were performed in HEPES buffer. Absorption spectra were recorded using a Varian Cary 50 spectrophotometer (Walnut Creek, CA) and fluorescence spectra were recorded using a Photon Technology International Quanta Master 4 L-format scan spectrofluorometer (Lawrenceville, NJ) equipped with an LPS-220B 75-W xenon lamp and power supply, A-1010B lamp housing with integrated igniter, switchable 814 photocounting/analog photomultiplier detection unit, and MD5020 motor driver. Samples for absorption and emission measurements were contained in 1-cm quartz cuvettes (1.4-mL volume, Starna, Atascadero, CA). Cu^+ was delivered in the form of $[Cu(MeCN)_4][PF_6]$ from an acetonitrile stock solution (2 mM). Excitation was provided at 540 nm and collected emission was integrated from 545-700 nm for **CS1-OMe**.

Schemes and Figures

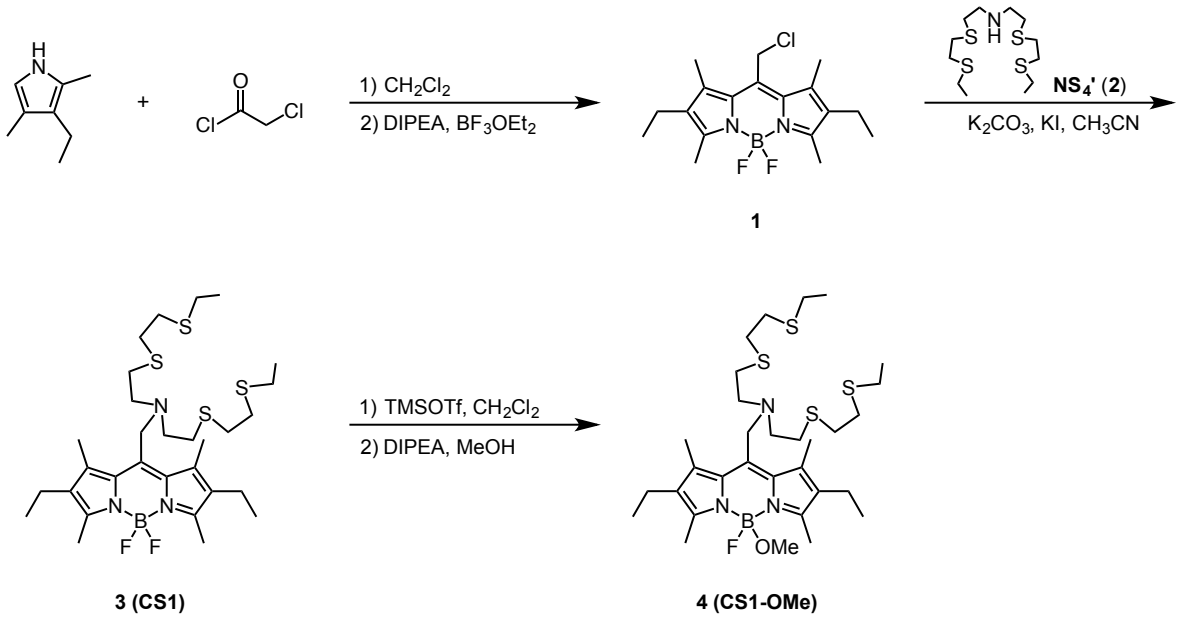

Scheme A3-1. Synthesis of BODIPY-based **CS1-OMe**.

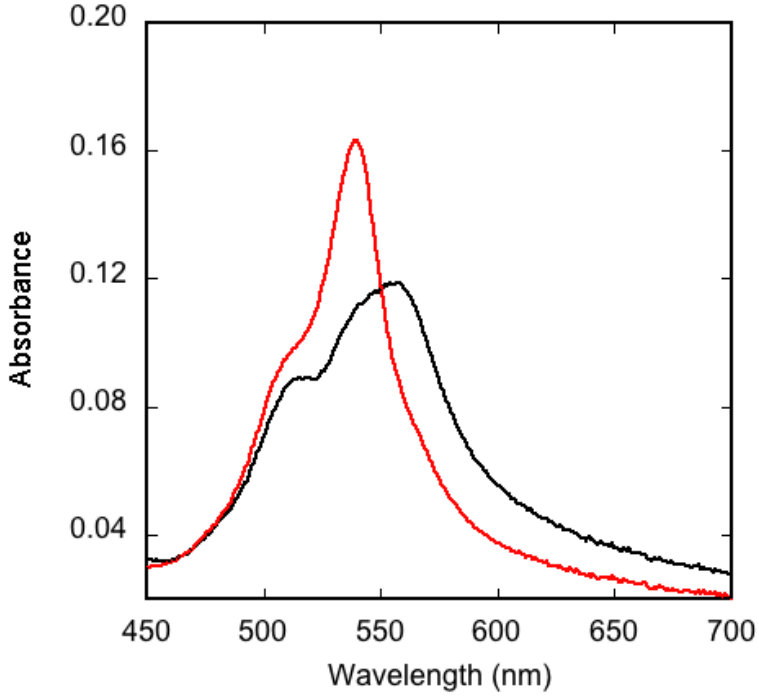

Figure A3-1. Absorbance spectra of 10 μM **CS1-OMe**. Spectra shown are for buffered [Cu^{+}] of 0.0 (black trace) and 10 (red trace) μM. Spectra were acquired in 50 mM HEPES, pH 7.4.

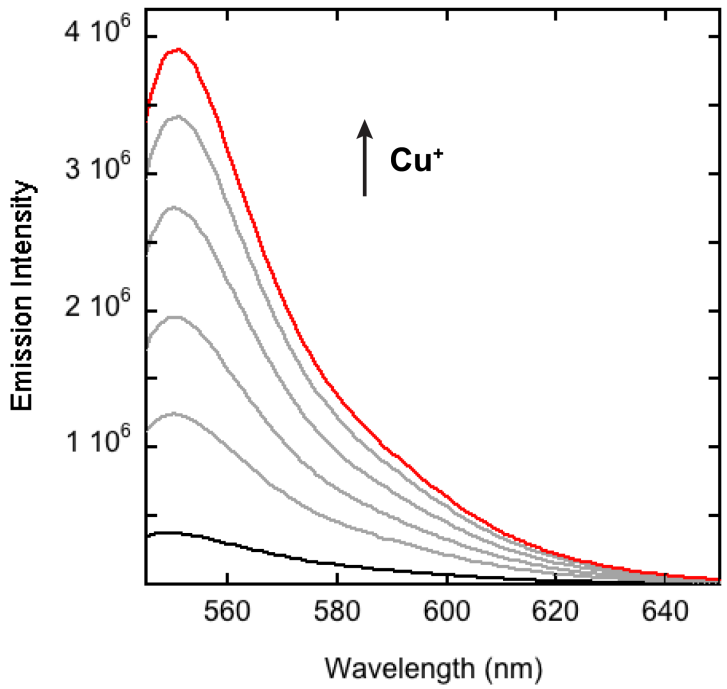

Figure A3-2. Fluorescence response of 2 μM **CS1-OMe** to Cu^+. Spectra shown are for buffered [Cu^+] of 0.00 (black trace), 0.4, 0.8, 1.2, 1.6, and 2.0 μM (red trace). Spectra were acquired in 50 mM HEPES, pH 7.4 with excitation at 540 nm.

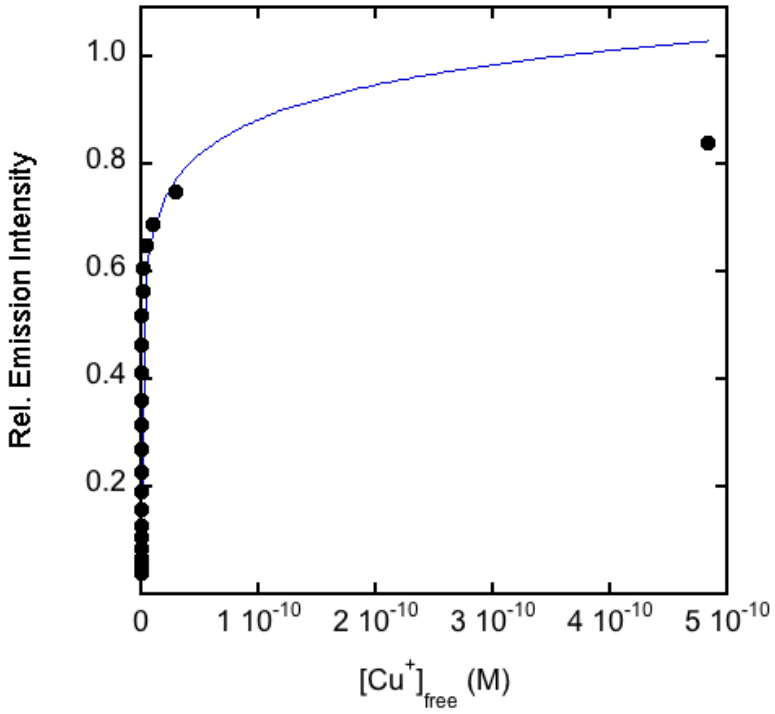

Figure A3-3. Normalized fluorescence response of 2.0 μM **CS1-OMe** to thiourea buffered Cu^+ solutions for K_d value determination. Excitation was provided at 540 nm and the collected emission was integrated from 545 to 700 nm. Spectra were acquired in 50 mM HEPES, pH 7.4. The points shown are for free Cu^+ buffered at 23.7, 27.1, 31.1, 36.0, 42.1, 49.6, 59.2, 71.5, 87.7, 109, 140, 183, 249, 354, 537, 896, 1750, 4620, 9620, 30300 and 54900 fM respectively. The observed K_d value is 1.58×10^{-12} M.

References

1. Zeng, L.; Miller, E. W.; Pralle, A.; Isacoff, E. Y.; Chang, C. J., A selective turn-on fluorescent sensor for imaging copper in living cells. *J. Am. Chem. Soc.* **2006,** *128*, 10-11.
2. Courtis, A. M.; Santos, S. A.; Guan, Y.; Hendricks, J. A.; Ghosh, B.; Szantai-Kis, D. M.; Reis, S. A.; Shah, J. V.; Mazitschek, R., Monoalkoxy BODIPYs—A Fluorophore Class for Bioimaging. *Bioconjugate Chem.* **2014,** *25* (6), 1043-1051.
3. Miller, E. W.; Zeng, L.; Domaille, D. W.; Chang, C. J., Preparation and use of Coppersensor-1, a synthetic fluorophore for live-cell copper imaging. *Nat. Protoc.* **2006,** *1*, 824-827.
4. Dodani, S. C.; Domaille, D. W.; Nam, C. I.; Miller, E. W.; Finney, L. A.; Vogt, S.; Chang, C. J., Calcium-dependent copper redistributions in neuronal cells revealed by a fluorescent copper sensor and X-ray fluorescence microscopy. *Proc. Natl. Acad. Sci. U S A* **2011,** *108* (15), 5980-5985.

Appendix 4:

Development of a Tripodal-like N_2S_2 Receptor-based Probe for Cu^+ Sensing

Synopsis

In the heterogeneous environment of a cell, copper is associated with a plethora of different ligands and proteins.[1,2] This creates specific cellular metal pools – a static pool described by tightly bound copper and a labile pool where copper can be exchanged between more loosely bound ligands – defined by the binding affinities of the metal-ligand partners. Copper trafficking between cellular ligands is dictated by the copper binding strength of these ligands, where transfer occurs from looser binding partners to the tighter binding counterparts.[3] In order to be able to evaluate cellular processes involving metal homeostasis with the use of fluorescent sensors, these must be able to compete for the cation within its biological window. For copper, in mammalian systems, this window is described by ligand affinities that span a range from picomolar (10^{-12} M) to femtomolar (10^{-15} M) dissociation constant values, with some mitochondrial metalloproteins exhibiting tighter binding constants.[3,4]

In order to modulate the affinities of fluorescent sensors, the metal-binding domains can be systematically altered to produce adjustments in the coordination of the metal. Modification of the number and strength of metal-ligand interactions,[5-7] coordination sphere,[6,8-11] ligand topology[12-15] and coordination geometry[16,17] are some of the possible avenues that can be taken to affect the binding properties of a ligand. This appendix summarizes the synthesis and characterization of a rhodol-based probe that makes use of an N_2S_2 metal-binding domain with a tripodal-like architecture for the investigation on the modulation of the copper binding affinities of fluorescent sensors.

Results and Discussion

Synthesis of a New N_2S_2 Tripodal-like Receptor for Copper Sensing. Scheme A4-1 outlines the synthesis of novel tripodal receptor with an N_2S_2 coordination unit and tripodal-like architecture. Tosyl-protection of ethanolamine, followed by tosylate displacement and ring closure under basic conditions affored tosylaziridine **2** as a useful intermediate to build the aminoethyl-arm of the tripodal receptor scaffold. Tosyl-protected tripodal-like receptor **4** was then attained via ring-opening coupling of aziridine **2** with bis(2-(ethylthio)ethyl)amine **3**. Reductive desulfonylation with sodium amalgam[18] produced the free amine tripodal-like N_2S_2 receptor **5** that can be coupled to a variety of fluorophore scaffolds through nucleophilic substitution or reductive amination strategies.

Synthesis of an N_2S_2 Based Copper Sensor. Although coupling of the free amine receptor **5** to a substituted fluorophore scaffold, like a chloromethyl fuctionalized BODIPY dye, via nucleophilic displacement was attempted, the possibility of double substitution presented a valid concern in the synthesis of a functional copper sensor. To avoid complications with multiple substitutions, as well as with hydrophobicity of the final probe due to the lipophilic BODIPY platform, a reductive amination approach was used for the synthesis of a rhodol-based probe. (Scheme A4-2) Briefly, construction of aldehyde functionalized rhodol **10** was achieved by addition of an aryl lithium species, derived from acetonide-protected bromobenzaldehyde **8**, to xanthone **9**. Incorporation of the N_2S_2 binding domain was accomplished via reductive alkylation of the amine under mild conditions to afford the final probe **CF4-N_2S_2**.

Spectroscopic Properties of CF4- N_2S_2 Copper Sensor. Spectroscopic evaluation of **CF4-N_2S_2** was performed in 50 mM HEPES buffered to pH 7.4. The optical features of the probe are characteristic of the piperidine-substituted rhodol platform. In its apo form, **CF4-N_2S_2** exhibits a broad absorption band at 537 nm, with a shoulder at 500 nm and a fluorescence emission feature at 561 nm. (Figures A4-1, A4-2) Addition of one equivalent of Cu^+ results in a slightly blue-shifted decreased absorption ($\lambda_{abs\ (Cu)}$ 535 nm) as well as a 43 % reduction in fluorescence intensity (1.7-fold turn-off) at 559 nm. Emission intensity is further reduced (53 %, 2.1-fold turn-off) by addition of an additional equivalent of Cu^+. (Figure A4-2)

Although the novel N_2S_2 tripodal-like receptor framework did not produce a desirable turn-on response in the presence of Cu^+, we sought to further investigate if this modified coordination unit was able to prompt a response upon complexation to other biologically relevant metal cations. Addition of an excess of a variety of divalent cations (Mg^{2+}, Ca^{2+}, Mn^{2+}, Co^{2+}, Ni^{2+}, Cu^{2+}, Zn^{2+} and Hg^{2+}) to a solution of **CF4-N_2S_2** did not yield a favorable response with any of the metals tested. (Figure A4-3) The most prominent responses were observed with addition of transition metals Mn^{2+}, Ni^{2+} and Zn^{2+} (20 % reduction, 1.6-fold turn-off) and Cu^{2+}, which produced a similar response as the cuprous form (1.6-fold turn-off with 1 eq., 2.3-fold turn-off with excess).

Conclusion and Future Work

We have designed and synthesized a new tripodal-like copper binding moiety with an N_2S_2 coordination unit in order to investigate the effect on the apparent binding affinities of fluorescent copper sensors. Incorporation of this scaffold allowed for the production of rhodol-based probe **CF4-N_2S_2**. Spectroscopic characterization of this probe showed no significant response to the addition of copper or other metal cations. This diminished response could be the result of various scenarios: the lack of metal binding by the receptor, insufficient disruption of the photoinduced electron transfer (PeT) mechanism upon metal binding and/or metal-induced fluorescence quenching of the excited-state fluorophore. Future efforts to produce and study crystals of copper-bound N_2S_2 (compound **5**) could lead to a better understanding of the metal-binding capability of this receptor. Additionally, direct coupling of the copper reporter to the pi-system of the chromophore, so as to induce a change in the intramolecular charge distribution of the fluorophore upon analyte interaction, could lead to a more suitable sensing mechanism for this particular metal-binding domain. (Scheme A4-3) Finally, inclusion of metal-binding scaffolds with lower N-to-S ratios (N/S) might give rise to more selective responses towards the cuprous ion.

Experimental Section

Synthetic Materials and Methods. All reactions were carried out under a dry N_2 atmosphere and stirred magnetically unless stated otherwise. All reactions using air- or moisture-sensitive reagents were performed in oven- and flame-dried glassware under an atmosphere of dry N_2. THF used for anhydrous reactions was dried and stored over 3-Å molecular sieves. Compounds **6**[19], **9**[19] and 2% sodium amalgam[18] were synthesized according to literature procedures. Unless otherwise noted, all chemicals were used as received. Silica gel P60 (SiliCycle) and activated basic aluminum oxide (Brockmann) were used for column chromatography. Flash chromatography was performed on an automated purification system using pre-packed silica gel columns. SiliCycle 60 F254 silica gel

(precoated sheets, 0.25 mm thick) was used for analytical TLC, visualized with UV light and/or staining with *p*-anisaldehyde or $KMNO_4$. ^1H and ^{13}C NMR spectra were collected in $CDCl_3$ (Cambridge Isotope Laboratories, Cambridge, MA) at 25 °C on a Bruker AV-300, Bruker AVB-400 or Bruker AVQ-400 spectrometer at the College of Chemistry NMR Facility at the University of California, Berkeley. All chemical shifts are reported in the standard notation of parts per million using the peak of residual proton or carbon signals of $CDCl_3$ as an internal reference.

Synthesis.

2-((4-Methylphenyl)sulfonamido)ethyl 4-methylbenzenesulfonate (1). A solution of ethanolamine (5.00 g, 81.6 mmol, 1.0 eq) in a 1:1 mixture of pyridine-dichloromethane (75 mL, 1.1 M) was cooled to 0 ºC. Tosyl chloride (39.02 g, 205 mmol, 2.5 eq) was dissolved in a 1:1 mixture of pyridine-dichloromethane (75 mL, 1.1 M) and added via addition funnel over 1.5 h to cold ethanolamine solution. Reaction was stirred at 0 ºC for 16 h. To quench, reaction mixture was carefully poured over a mixture of ice (200 mL) and conc. HCl (100 mL). Once melted, layers were separated and organics were washed with 2M HCl, dried with Na_2SO_4 and concentrated under reduced pressure. Resulting solid was recrystallized from MeOH to yield **1** as an off-white solid (17.97 g, 51 %). ^1H NMR (400 MHz, $CDCl_3$) δ 7.75 (d, J = 8.4 Hz, 2H), 7.70 (d, J = 8.3 Hz, 2H), 7.36 (d, J = 8.0 Hz, 2H), 7.30 (d, J = 7.9 Hz, 2H), 4.78 (s, 1H), 4.05 (t, J = 5.1 Hz, 2H), 3.23 (s, 2H), 2.46 (s, 3H), 2.43 (s, 3H).

1-Tosylaziridine (2). A slurry of **1** (1.21 g, 3.05 mmol, 1.0 eq) in toluene (10.0 mL, 0.31 M) was treated with 20 % KOH (4.0 mL, 4.6 eq) and reaction was stirred at room temperature for 3 h. Reaction mixture was diluted with water, layers separated and organics washed with additional water (x3). Organic layer was dried with Na_2SO_4 and concentrated under reduced pressure to attain **2** as a white solid (0.55 g, 86 %). ^1H NMR (400 MHz, $CDCl_3$) δ 7.83 (d, J = 4.8 Hz, 2H), 7.34 (d, J = 8.0 Hz, 2H), 2.36 (s, 3H), 2.28 (s, 4H). ^{13}C NMR (101 MHz, $CDCl_3$) δ 144.63, 134.77, 129.70, 127.94, 27.38, 21.61.

Bis(2-(ethylthio)ethyl)amine (3). A flame-dried three-necked round-bottom flask was charged with ethanol (560.3 mL, 1.0 M in sodium). Under a dry N_2 atmosphere, sodium (12.88 g, 560.26 mmol, 5.0 eq) was carefully added in small portions. After all the sodium has dissolved, ethanethiol (24.9 mL, 336.15 mmol, 3.0 eq) was added dropwise to the sodium ethoxide solution. Reaction mixture was heated to reflux and then a solution of bis(2-chloroethyl)amine hydrochloride (20.0 g, 112.1 mmol, 1.0 eq) in ethanol (280.1 mL, 0.40 M in amine) was added dropwise. Upon completion of addition, reaction mixture was stirred at reflux for 2 h. Reaction was then cooled to room temperature and ethanol was removed under reduced pressure. Residue was taken up in chloroform and washed with H_2O (x3). Organic layer was dried with Na_2SO_4 and concentrated under reduced pressure. Crude was purified via vacuum distillation to afford 13.29 g (61 %) of **5** as a pale yellow oil. ^1H NMR (400 MHz, $CDCl_3$) δ 2.81 (t, J = 6.6 Hz, 4H), 2.68 (t, J = 6.6 Hz, 4H), 2.53 (q, J = 7.4 Hz, 4H), 1.78 (s, 1H), 1.25 (t, J = 7.4 Hz, 6H). ^{13}C NMR (101 MHz, $CDCl_3$) δ 48.28, 31.86, 25.80, 14.84.

***N*-(2-(Bis(2-(ethylthio)ethyl)amino)ethyl)-4-methylbenzenesulfonamide (4).** Amine **3** (0.44 g, 2.26 mmol, 1.0 eq), was dissolved in anhydrous acetonitrile (20.0 mL, 0.11 M in **3**). A solution of tosylaziridine **2** (0.56 g, 2.83 mmol, 1.2 eq) in anhydrous acetonitrile (8.0 mL, 0.07 M in **2**) was

added dropwise to reaction mixture and stirred for 16 h at room temperature. Upon completion, volatiles were removed under reduced pressure and resulting crude was purified via column chromatography on silica gel (1 % MeOH/CH_2Cl_2 with 1% TEA additive) to afford 0.71 g (80 %) of **4** as a pale yellow oil. ^{1}H NMR (400 MHz, $CDCl_3$) δ 7.70 (d, *J* = 8.4 Hz, 2H), 7.24 (d, *J* = 8.0 Hz, 2H), 5.76 (t, *J* = 5.2 Hz, 1H), 2.86 (q, *J* = 5.6 Hz, 2H), 2.88 – 2.48 (m, 6H), 2.45 – 2.37 (m, 8H), 2.36 (s, 3H), 1.12 (t, *J* = 7.2 Hz, 6H). ^{13}C NMR (101 MHz, $CDCl_3$) δ 142.96, 136.57, 129.36, 126.94, 53.06, 52.08, 40.80, 29.58, 25.93, 21.28, 14.62. LRESI-MS calculated for [M+H] 391.2, found 391.1.

***N*^{1},*N*^{1}-Bis(2-(ethylthio)ethyl)ethane-1,2-diamine (5).** A flame-dried round bottom flask was charged with tosyl-protected amine **4** (0.40 g, 1.02 mmol, 1.0 eq), K_2HPO_4 (1.43 g, 8.19 mmol, 8.0 eq), 2 % Na/Hg amalgam (11.75 g, 10.24 mmol Na, 10.0 eq Na) and anhydrous methanol (11.4 mL, 0.09 M). Reaction was then heated to reflux and stirred for 16 h. Once completed, reaction mixture was cooled to room temperature and the methanolic slurry was decanted. Remaining mercuric pool in flask was washed treated with methanol (7.0 mL) followed by chloroform (7.0 mL), decanting the supernatant each time. Resulting washings and decantate were concentrated under reduced pressure to yield a white solid which was then taken up in chloroform, filtrated and concentrated to afford 0.24 g (99 %) of **5** as a pale yellow oil. ^{1}H NMR (400 MHz, $CDCl_3$) δ 3.15 (t, *J* = 7.2 Hz, 2H), 2.65 – 2.52 (m, 6H), 2.47 – 2.43 (m, 4H), 2.35 (q, *J* = 7.2 Hz, 4H), 1.08 (t, *J* = 7.2 Hz, 6H). ^{13}C NMR ($CDCl_3$, 400 MHz): δ 54.18, 49.86, 39.53, 29.07, 25.77, 14.54.

4-Bromo-3-(trifluoromethyl)benzaldehyde (7). A solution of alcohol **6** (1.93 g, 7.56 mmol, 1.0 eq) in chloroform (18.9 mL, 0.40 M) was treated with manganese dioxide (6.57 g, 75.6 mmol, 10 eq) and stirred at room temperature for 16 h. Upon completion, reaction mixture was filtered through Celite and concentrated under reduced pressure. Resulting residue was purified via flash column chromatography on silica gel (0-25 % EtOAc/hexanes, linear gradient) to afford 0.97 g (51 %) of **7** as a white solid. ^{1}H NMR (400 MHz, $CDCl_3$) δ 10.02 (s, 1H), 8.17 (d, *J* = 1.7 Hz, 1H), 7.94 – 7.87 (m, 2H). ^{13}C NMR ($CDCl_3$, 400 MHz): δ 189.67, 136.03, 135.10, 128.76, 128.71, 120.99, 118.27.

2-(4-Bromo-3-(trifluoromethyl)phenyl)-5,5-dimethyl-1,3-dioxane (8). Aldehyde **7** (0.85 g, 3.36 mmol, 1.0 eq) was dissolved in anhydrous toluene (6.2 mL, 0.54 M) and then subjected to neopentyl glycol (0.39 g, 3.70 mmol, 1.1 eq) and *p*-toluenesulfonic acid (128 mg, 0.07 mmol, 0.02 eq). Reaction mixture was stirred at reflux for 3 h. Once completed, reaction was cooled to room temperature and washed with sat. $NaHCO_3$ and H_2O. The organic layer was then dried with Na_2SO_4 and concentrated under reduced pressure. The crude residue was purified via flash column chromatography on silica gel (0-20 % EtOAc/hexanes, linear gradient) to yield **8** as clear oil. (0.99 g, 87 %). ^{1}H NMR (400 MHz, $CDCl_3$) δ 7.89 – 7.82 (m, 1H), 7.71 (d, *J* = 8.3 Hz, 1H), 7.53 (dd, *J* = 8.2, 2.0 Hz, 1H), 5.38 (s, 1H), 3.78 (d, *J* = 11.1 Hz, 2H), 3.65 (d, *J* = 11.0 Hz, 2H), 1.27 (s, 3H), 0.81 (s, 3H). ^{13}C NMR (101 MHz, $CDCl_3$) δ 138.21, 134.77, 130.73, 125.84, 124.20, 121.49, 120.19, 99.86, 77.59, 30.20, 22.96, 21.77.

4-(3-Oxo-6-(piperidin-1-yl)-3*H*-xanthen-9-yl)-3-(trifluoromethyl)benzaldehyde (10). A flame-dried three-neck round-bottom flask was charged with **8** (238.7 mg, 0.70 mmol, 1.5 eq) and anhydrous THF (2.4 mL, 0.30 M in **8**). The solution was cooled to -78 ºC and then *tert*-butyllithium (1.7 M in pentane, 828.1 µL, 1.41 mmol, 3 eq) was added dropwise. After stirring at the same temperature for 12 min, a solution of compound **9** (192.2 mg, 0.47 mmol) in anhydrous TFH (15.6

mL, 0.03 M in **9**) was added dropwise. The reaction was warmed to room temperature, stirred for 1 h and subsequently quenched with addition of aq. HCl (2 M, 7.0 mL, 20 eq from **8**). Reaction mixture was warmed up to 50 ºC and stirred for 16 h. Reaction was quenched with addition of sat. $NaHCO_3$, and then washed with CH_2Cl_2 (x2). The combined organic layers were washed with brine, dried with Na_2SO_4 and concentrated under reduced pressure. The crude residue was purified via column chromatography on silica gel (5 % MeOH/CH_2Cl_2) to yield **10** as dark red solid (137.7 mg, 65 %). ^{1}H NMR (400 MHz, $CDCl_3$) δ 10.16 (s, 1H), 8.38 (d, *J* = 1.5 Hz, 1H), 8.22 (dd, *J* = 7.8, 1.5 Hz, 1H), 7.53 (d, *J* = 7.7 Hz, 1H), 6.73 (d, *J* = 2.3 Hz, 1H), 6.68 – 6.58 (m, 3H), 6.45 (dd, *J* = 9.6, 2.0 Hz, 1H), 6.37 (d, *J* = 2.0 Hz, 1H), 3.44 (t, *J* = 4.6 Hz, 4H), 1.71 – 1.60 (m, 6H).

9-(4-(((2-(Bis(2-(ethylthio)ethyl)amino)ethyl)amino)methyl)-2-(trifluoromethyl)phenyl)-6-(piperidin-1-yl)-3*H*-xanthen-3-one (11, CF4-N_2S_2). Amine **5** (16.2 mg, 0.07 mmol, 1.0 eq) and aldehyde **10** (30.9 mg, 0.07 mmol, 1.0 eq) were dissolved in 1,2-dichloroethane (1.0 mL, 0.07 M) and stirred for 10 min. Reaction mixture was then treated with glacial AcOH (4.7 µL, 1.2 eq) and sodium triacetoxyborohydride (20.3 mg, 0.10 mmol, 1.4 eq) and stirred at room temperature for 4 h. Reaction was quenched with addition of 1 M NaOH and then washed with CH_2Cl_2 (x3). The combined organic layers were washed with brine, dried with Na_2SO_4 and concentrated under reduced pressure. The crude residue was purified via column chromatography on silica gel (5 % MeOH/CH_2Cl_2) to afford 14.5 mg (31 %) of **CF4-N_2S_2** as dark red solid. ^{1}H NMR (400 MHz, $CDCl_3$) δ 7.93 – 7.88 (m, 1H), 7.74 (t, *J* = 6.6 Hz, 1H), 7.26 (dd, *J* = 7.9, 2.0 Hz, 2H), 6.77 – 6.71 (m, 3H), 6.66 (ddd, *J* = 9.2, 4.6, 2.4 Hz, 1H), 6.50 (dd, *J* = 9.7, 2.0 Hz, 1H), 6.42 (d, *J* = 1.9 Hz, 1H), 4.00 (s, 2H), 3.46 (d, *J* = 5.6 Hz, 5H), 2.79 – 2.71 (m, 6H), 2.65 (dd, *J* = 7.5, 5.5 Hz, 4H), 2.54 (q, *J* = 7.4 Hz, 4H), 1.76 – 1.61 (m, 8H), 1.24 (t, *J* = 7.4 Hz, 6H). ^{13}C NMR (101 MHz, $CDCl_3$) δ 185.35, 158.88, 155.15, 154.47, 151.54, 147.10, 131.67, 131.01, 130.44, 129.53, 128.48, 126.42, 124.82, 116.62, 111.79, 111.42, 105.32, 98.70, 77.21, 63.72, 53.81, 53.14, 53.00, 48.36, 47.21, 29.94, 26.30, 25.33, 24.25, 14.91.

Spectroscopic Materials and Methods. Millipore water was used to prepare all aqueous solutions. All final spectroscopic measurements were performed in HEPES buffer. Absorption spectra were recorded using a Varian Cary 50 spectrophotometer (Walnut Creek, CA) and fluorescence spectra were recorded using a Photon Technology International Quanta Master 4 L-format scan spectrofluorometer (Lawrenceville, NJ) equipped with an LPS-220B 75-W xenon lamp and power supply, A-1010B lamp housing with integrated igniter, switchable 814 photocounting/analog photomultiplier detection unit, and MD5020 motor driver. Samples for absorption and emission measurements were contained in 1-cm quartz cuvettes (1.4-mL volume, Starna, Atascadero, CA). Cu^+ was delivered in the form of $[Cu(MeCN)_4][PF_6]$ from an acetonitrile stock solution (2 mM). Excitation was provided at 536 nm and collected emission was integrated from 541-700 nm.

Schemes and Figures

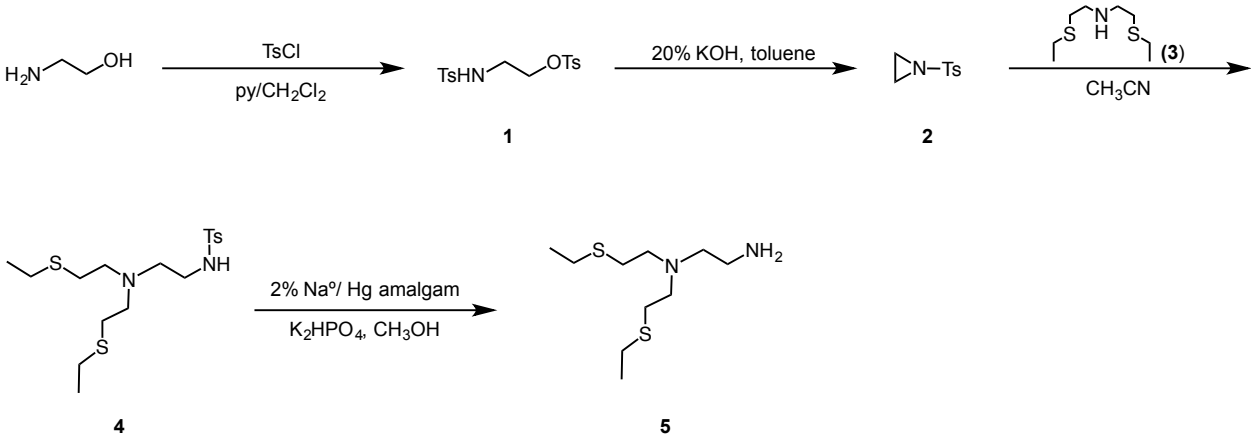

Scheme A4-1. Synthesis of an N_2S_2 tripodal-like receptor for Cu^+ sensing.

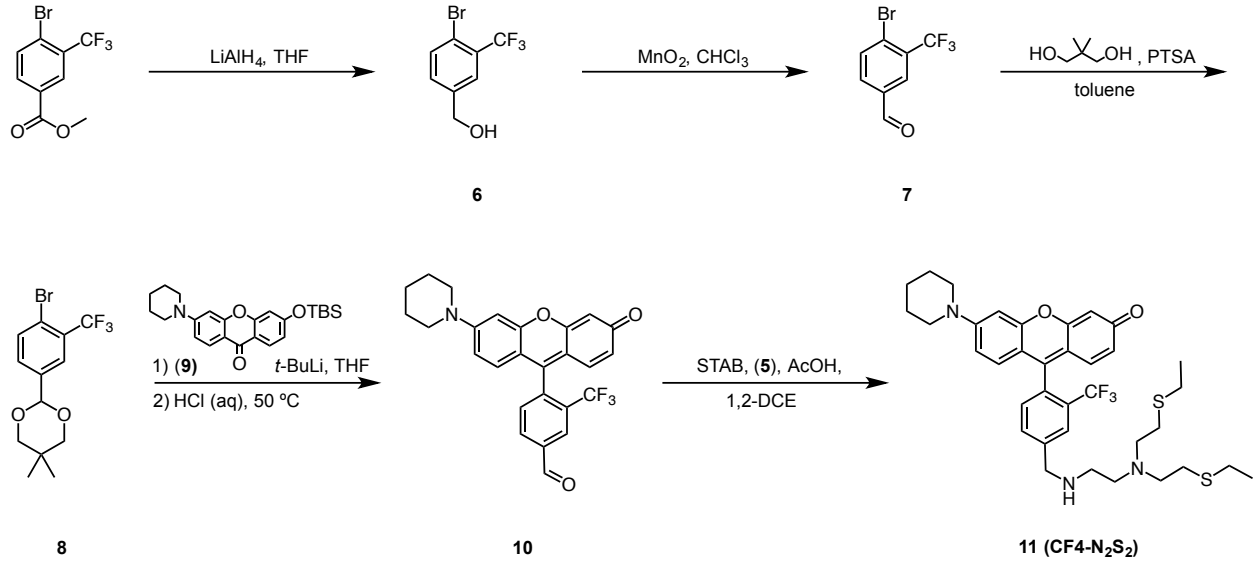

Scheme A4-2. Synthesis of rhodol-based probe **CF4-N_2S_2**.

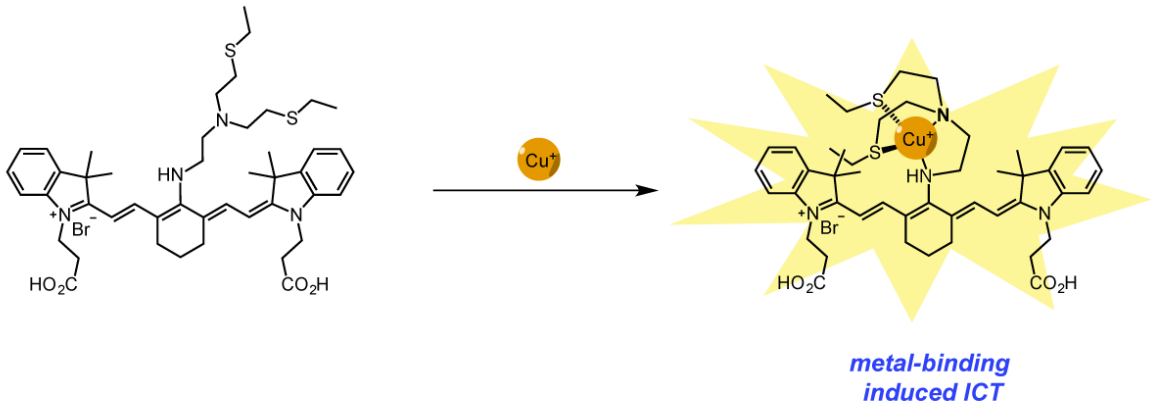

Scheme A4-3. Possible application of the N_2S_2 tripodal-like receptor for metal-binding induced intramolecular charge transfer (ICT) sensing strategy.

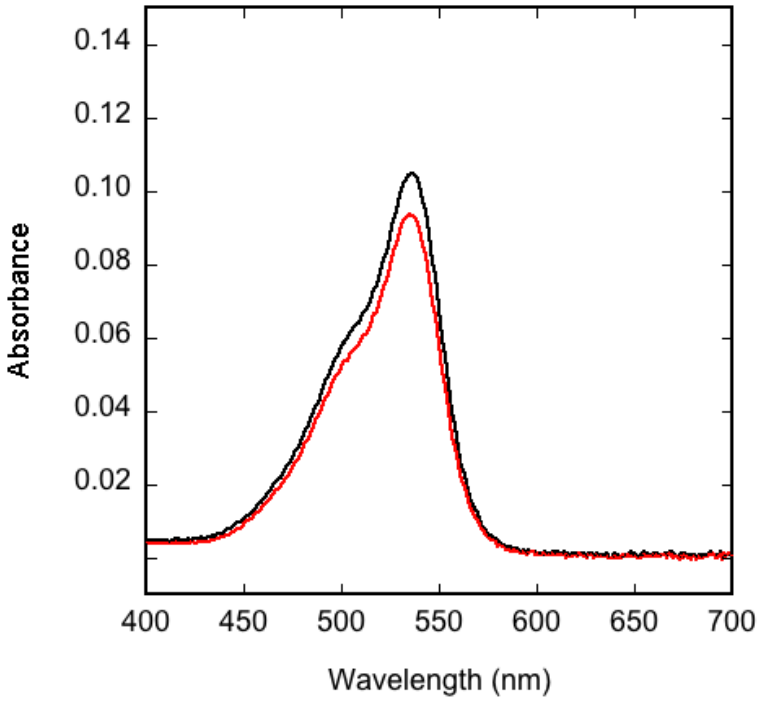

Figure A4-1. Absorbance spectra of 2 μM **CF4-N_2S_2**. Spectra shown are for buffered [Cu^+] of 0.0 (black trace) and 2 (red trace) μM. Spectra were acquired in 50 mM HEPES, pH 7.4.

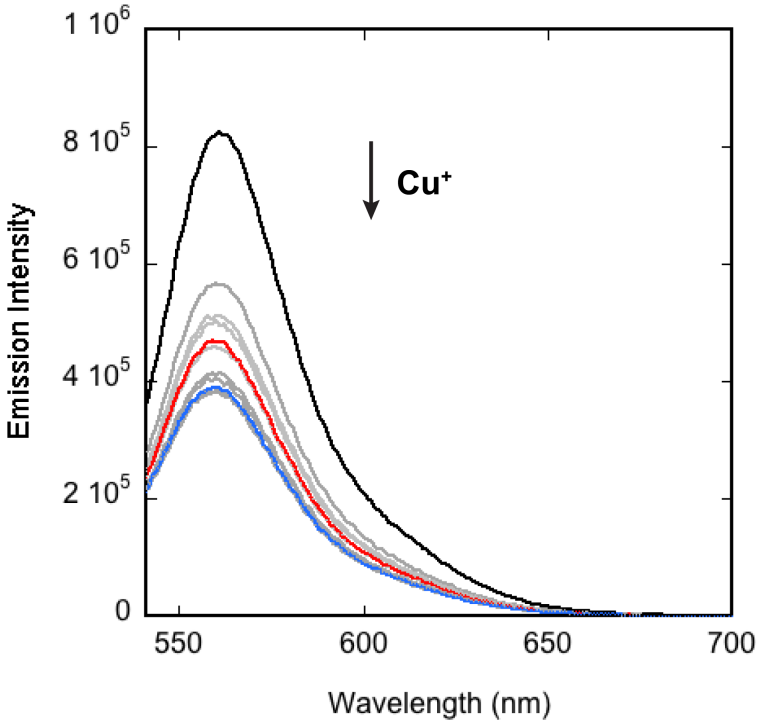

Figure A4-2. Fluorescence response of 2 μM **CF4-N_2S_2** to Cu^+. Spectra shown are for buffered [Cu^+] of 0.00 (black trace), 0.4, 0.8, 1.2, 1.6, 2.0 (red trace), 2.4, 2.8, 3.2, 3.6 and 4.0 (blue trace) μM. Spectra were acquired in 50 mM HEPES, pH 7.4 with excitation at 536 nm.

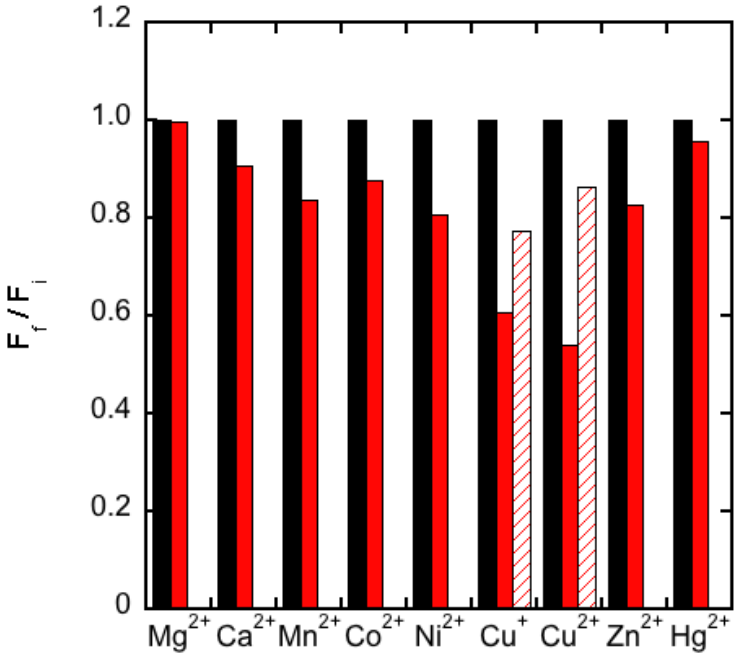

Figure A4-3. Fluorescence response of **CF4-N_2S_2** to various metal ions. Bars represent the final integrated fluorescence response (F_f) over the initial integrated emission (F_i). Spectra were acquired in 50 mM HEPES, pH 7.4. Black bars represent the fluorescence of apo CF4-N_2S_2. Red bars represent the addition of an excess of the appropriate metal ion (2 mM for Mg^{2+}, Ca^{2+}, and Zn^{2+}, 50 μM for all other cations) to a 2 μM solution of **CF4-N_2S_2**. Striped red bars represent the addition of one equivalent of metal cation (2 μM) to the solution. Excitation was provided at 536 nm, and the collected emission was integrated over 541 to 700 nm.

References

1. Boal, A. K.; Rosenzweig, A. C., Structural biology of copper trafficking. *Chem. Rev.* **2009,** *109*, 4760-4779.
2. Lutsenko, S., Human copper homeostasis: a network of interconnected pathways. *Curr. Opin. Chem. Biol.* **2010,** *14* (2), 211-217.
3. Banci, L.; Bertini, I.; Ciofi-Baffoni, S.; Kozyreva, T.; Zovo, K.; Palumaa, P., Affinity gradients drive copper to cellular destinations. *Nature* **2010,** *465* (7298), 645-648.
4. Cotruvo, J. A. J.; Aron, A. T.; Ramos-Torres, K. M.; Chang, C. J., Synthetic fluorescent probes for studying copper in biological systems. *Chem. Soc. Rev.* **2015,** *44* (13), 4400-4414.
5. Goldsmith, C. R.; Lippard, S. J., 6-Methylpyridyl for Pyridyl Substitution Tunes the Properties of Fluorescent Zinc Sensors of the Zinpyr Family. *Inorg. Chem.* **2006,** *45* (2), 555-561.
6. Nolan, E. M.; Jaworski, J.; Okamoto, K.-I.; Hayashi, Y.; Sheng, M.; Lippard, S. J., QZ1 and QZ2: Rapid, Reversible Quinoline-Derivatized Fluoresceins for Sensing Biological Zn(II). *J. Am. Chem. Soc.* **2005,** *127* (48), 16812-16823.
7. Komatsu, K.; Kikuchi, K.; Kojima, H.; Urano, Y.; Nagano, T., Selective Zinc Sensor Molecules with Various Affinities for Zn^{2+}, Revealing Dynamics and Regional Distribution of Synaptically Released Zn^{2+} in Hippocampal Slices. *J. Am. Chem. Soc.* **2005,** *127* (29), 10197-10204.
8. Rorabacher, D. B.; Martin, M. J.; Koenigbauer, M. J.; Malik, M.; Schroeder, R. R.; Endicott, J. F.; Ochrymowycz, L. A., Structural Effects on Cu(II)/Cu(I) Potentials and Electron Transfer Kinetics as Well as Related Physical Peoperties in Polythiaether and Polyaminothiaether Complexes. In *Copper Coordination Chemistry: Biochemical and Inorganic Perspectives*, Karlin, K. D.; Zubieta, J., Eds. Adenine Press: Guilderland, NY, 1983; p 167.
9. Chaka, G.; Kandegedara, A.; Heeg, M. J.; Rorabacher, D. B., Comparative study of donor atom effects on the thermodynamic and electron-transfer kinetic properties of copper(II/I) complexes with sexadentate macrocyclic ligands. [CuII/I([18]aneS4N2)] and [CuII/I([18]aneS4O2)]. *Dalton Trans.* **2007,** (4), 449-458.
10. Bernardo, M. M.; Heeg, M. J.; Schroeder, R. R.; Ochrymowycz, L. A.; Rorabacher, D. B., Comparison of the influence of saturated nitrogen and sulfur donor atoms on the properties of copper(II/I)-macrocyclic polyamino polythiaether ligand complexes: redox potentials and protonation and stability constants of $Cu^{I}L$ species and new structural data. *Inorg. Chem.* **1992,** *31*, 191-198.
11. Westerby, B. C.; Juntunen, K. L.; Leggett, G. H.; Pett, V. B.; Koenigbauer, M. J.; Purgett, M. D.; Taschner, M. J.; Ochrymowycz, L. A.; Rorabacher, D. B., Macrocyclic polyamino polythiaether ligands with NxS4-x and NxS5-x donor sets - protonation constants, stability-constants, and kinetics of complex-formation with the aquocopper(ii) ion. *Inorg. Chem.* **1991,** *30* (9), 2109-2120.
12. Addison, A. W., Is ligand topology an influence on the redox potentials of copper complexes? *Inorg. Chim. Acta* **1989,** *162* (2), 217-220.
13. Dunn, B. C.; Wijetunge, P.; Vyvyan, J. R.; Howard, T. A.; Grall, A. J.; Ochrymowycz, L. A.; Rorabacher, D. B., Electron-Transfer Kinetics and Thermodynamic Characterization of Copper(II/I) Complexes with Acyclic Tetrathiaethers in Aqueous Solution. *Inorg. Chem.* **1997,** *36* (20), 4484-4489.

14. Dockal, E. R.; Jones, T. E.; Sokol, W. F.; Engerer, R. J.; Rorabacher, D. B.; Ochrymowycz, L. A., Redox properties of copper-thiaether complexes. Comparison to blue copper protein behavior. *J. Am. Chem. Soc.* **1976,** *98* (14), 4322-4324.
15. Ambundo, E. A.; Yu, Q. Y.; Ochrymowycz, L. A.; Rorabacher, D. B., Electron-transfer kinetics of copper(II/I) tripodal ligand complexes. *Inorg. Chem.* **2003,** *42* (17), 5267-5273.
16. Ambundo, E. A.; Deydier, M.-V.; Grall, A. J.; Aguera-Vega, N.; Dressel, L. T.; Cooper, T. H.; Heeg, M. J.; Ochrymowycz, L. A.; Rorabacher, D. B., Influence of Coordination Geometry upon Copper(II/I) Redox Potentials. Physical Parameters for Twelve Copper Tripodal Ligand Complexes. *Inorg. Chem.* **1999,** *38* (19), 4233-4242.
17. Blomenkemper, M.; Schröder, H.; Pape, T.; Hahn, F. E., Copper(I) complexes of N-centered aliphatic tripodal trithioether ligands – Adjustment of complex geometry by variation of spacer lengths. *Inorg. Chim. Acta* **2011,** *366* (1), 76-80.
18. Forshee, P. B.; Sibert, J. W., Sodium Amalgam: A Highly Efficient Reagent for the Detosylation of Azathiacrown Ethers. *Synthesis* **2006,** *2006* (05), 756-758.
19. Dodani, S. C.; Firl, A.; Chan, J.; Nam, C. I.; Aron, A. T.; Onak, C. S.; Ramos-Torres, K. M.; Paek, J.; Webster, C. M.; Feller, M. B.; Chang, C. J., Copper is an endogenous modulator of neural circuit spontaneous activity. *Proc. Natl. Acad. Sci. USA* **2014,** *111*, 16280-16285.

Appendix 5:

Efforts Toward the Synthesis and Characterization of Tripodal-like NS_3 Receptors for Cu^+ Sensing

Synopsis

The development of metal-responsive fluorescent sensors that present a variety of binding properties towards the metal of interest is an attractive avenue of research that allows for the potential visualization of different metal pools within the cellular environment. For copper, engineering of small-molecule probes that present a range of binding affinities has been limited by a certain lack of exploration of different binding domains for this application.[1-3] Therefore, the design and synthesis of novel copper binding platforms is desirable in order to investigate their applicability to copper sensing. Nevertheless, the process for the development of new fluorescent sensors that display novel binding sites with the appropriate metal-binding capacities can be a laborious one, as it frequently entails a trial-and-error process of designing new chelators, combining these with appropriate fluorophore reporters and just then characterizing the binding affinities of the resulting probes.

This appendix summarizes the design of a tripodal-like NS_3 platform, with varying linker lengths between the ligand donors, as a prototype for copper binding and for the evaluation of the effects of chelate ring size on the binding affinity for Cu^+. (Figure A5-1) Additionally, we present the synthesis of one analogue, the 5-5-5 chelate ring size configuration, as a model compound for the NS_3 ligand framework. Finally, we review our efforts to characterize the copper binding properties of the model chelator previous to fluorophore conjugation as an attempt to develop a robust assay to screen new metal-binding motifs for the development of a collection of probes with a range of binding affinities for copper.

Results and Discussion

Synthesis of a New Tripodal-like NS_3 Receptor for Copper Sensing. The design for the construction of a new metal-binding platform with an NS_3 donor set and tripodal-like ligand architecture is outlined in Scheme A5-1. The synthesis of a model chelator, with a 5-5-5 chelate ring size configuration, involves the preparation of a thioether-modified propanethiol building block as a means to simultaneously incorporate the three thioether moieties of the donor set. For this purpose, displacement of the epichlorohydrin chloride group was carried out with sodium thiomethoxide to yield methylthio-substituted oxirane **1**, which was subsequently converted to its thiirane equivalent **2** upon reaction with thiourea. Treatment of **2** with sodium thiomethoxide to introduce the last thioether donor afforded the ring-opening product, propanethiol **3**. Formation of the methylthio-thiopropoxide from **3** and subsequent nucleophilic attack of tosyl-aziridine **4** led to a ring-opening coupling to form the tosyl-protected tripodal-like NS_3 receptor **5**. Following reduction of the protecting group with sodium amalgam,[4] the free amine chelator **6** was attained. In order to replicate the typical benzyl amine linkage observed in many fluorescent sensors for copper, we coupled the free amine chelator to *p*-bromobenzaldehyde via reductive amination of the carbonyl species under mild conditions, optimized as shown in Table A5-1, to afford model tripodal-like NS_3 copper receptor **7**.

Efforts to measure the binding affinity of tripodal-like NS_3 receptor via competition assays. The engineering of fluorescent sensors with novel metal-binding receptors would greatly benefit from a method to evaluate the binding properties of the new chelator motifs previous to incorporation to the sensing platforms. Ideally, the synthesis of a library of metal-binding

frameworks would be followed by a screening process to investigate their affinities to the metal of interest and lastly the most promising candidates would be coupled to fluorophore reporters for the construction of new metal-responsive probes. To this end, we set out to develop an assay to measure the dissociation constant values for copper binding as a screening tool to potentially select the most fit chelators for copper sensing.

Traditional determination of the copper binding affinities of fluorescent small-molecule sensors is performed with ligand competition assays, using recognized metal-binders such as thiourea as contesting copper chelators to cause decreases in the probe's emission intensity upon copper release to the competing ligand. Nevertheless, in order to measure the binding affinities of model copper receptors, a fluorescence-based assay is not suitable due to the lack of a fluorescent reporter. Therefore, we envisioned an absorbance-based approach, using well-defined copper complexes as reporters of copper exchange between the established copper chelators and the novel metal-binding platforms. This type of absorbance-based competition assay has been efficiently applied for the evaluation of the binding affinities of copper-binding peptides and metalloproteins. Additionally, and perhaps most importantly, a set of small-molecule chelators and their copper complexes have been extensively characterized as quantitative probes for the study of Cu^+ binding affinities spanning the nanomolar to attomolar range.[5]

Validation of this strategy was attempted with the use of Ferrozine (Fz) as a quantitative probe for Cu^+ binding and the standard NS_4 receptor platform present in most available fluorescent copper sensors.[1-3,6] Briefly, the Fz-Cu complex was formed and aliquots of the competing ligand, NS_4 receptor, were added to the Fz-Cu containing solution. Metal exchange between the Fz probe and the copper receptor was evaluated by a decrease in the absorbance of the Fz-Cu complex at 470 nm. (Figure A5-2) Unfortunately, addition of various concentrations of competing ligand, as well as use of different starting concentrations of the Fz-Cu complex did not produce consistent results that would lead to a characterization of the binding affinity of the copper receptor. Application of this strategy proved to be limited by a combination of (i) the hydrophobicity of the novel copper-binding moieties and (ii) the low molar extinction coefficient of the Fz-Cu complex, as the concentration of ligand needed to cause an observable metal exchange from the Fz probe (at a detectable absorbance from the Fz-Cu complex) would exceed the amount soluble in aqueous solution.

Limitations of the suggested absorbance-based assay for the determination of the copper binding affinity of model copper receptor **7** led us to attempt the partial characterization of this new binding motif through a different strategy. In order to qualitatively assess the copper binding ability of **7**, we attempted a competition assay with established fluorescent copper sensor **CF3**.[7] Cu-complex formation with **CF3**, followed by addition of various concentrations of **7** allowed us to detect possible metal-exchange between the ligands by an observation of decreased fluorescence intensity from the **CF3**-Cu complex. (Figure A5-3) This result suggests that the tripodal-like NS_3 chelator is potentially able to compete for copper in the 10^{-13} M range, however further characterization of this metal-binding framework is needed.

Conclusion and Future Work

We have designed and synthesized a new tripodal-like copper-binding moiety with an NS_3 coordination unit in order to evaluate its binding properties and possible application to copper sensing. Additionally, we attempted to develop an absorbance-based competition assay with Fz, a quantitative probe for Cu^+ binding, as a means to characterize the binding affinity of the NS_3 chelator. Although this strategy was not fruitful, we were able to observe copper-exchange between the developed NS3 receptor and CF3, an established fluorescent copper sensor with a dissociation constant in the 10^{-13} M range. Future efforts in the development of more sensitive assays for the determination of binding affinities could lead to a more rational approach to the synthesis of fluorescent sensors for copper with improved metal-binding characteristics for specific biological applications.

Experimental Section

Synthetic Materials and Methods. All reactions were carried out under a dry N_2 atmosphere and stirred magnetically unless stated otherwise. All reactions using air- or moisture-sensitive reagents were performed in oven- and flame-dried glassware under an atmosphere of dry N_2. Sodium amalgam was synthesized according to literature procedures.[4] Unless otherwise noted, all chemicals were used as received. Flash chromatography was performed on an automated purification system using pre-packed silica gel columns. SiliCycle 60 F254 silica gel (precoated sheets, 0.25 mm thick) was used for analytical TLC, visualized with UV light and/or staining with *p*-anisaldehyde or $KMNO_4$. ^1H and ^{13}C NMR spectra were collected in $CDCl_3$ (Cambridge Isotope Laboratories, Cambridge, MA) at 25 °C on a Bruker AV-300, Bruker AVB-400 or Bruker AVQ-400 spectrometer at the College of Chemistry NMR Facility at the University of California, Berkeley. All chemical shifts are reported in the standard notation of parts per million using the peak of residual proton or carbon signals of $CDCl_3$ as an internal reference.

Synthesis.

2-((Methylthio)methyl)oxirane (1). A solution of epichlorohydrin (10.00 g, 108.08 mmol, 1.0 eq) in CH_2Cl_2 (216.2 mL, 0.50 M) and H_2O (100.0 mL, 1.0 M) was cooled to 0 ºC and treated with sodium thiomethoxide solution (3.0 M in H_2O, 50.4 mL, 1.4 eq) and tetra-n-butylammonium bromide (1.99 g, 6.16 mmol, 0.06 eq). Reaction was stirred at the same temperature for 3 h. The reaction mixture was then partitioned and the organic layer was washed with H_2O (x3), dried with Na_2SO_4 and concentrated under reduced pressure. Crude residue was purified via Kugelrohr distillation (65 ºC) to afford 3.69 g (33 %) of **1** as a colorless liquid. ^1H NMR (400 MHz, $CDCl_3$) δ 3.13 (tt, J = 5.6, 3.2 Hz, 1H), 2.84 – 2.76 (m, 1H), 2.68 (dd, J = 14.2, 5.5 Hz, 1H), 2.61 – 2.54 (m, 2H), 2.17 (s, 3H). ^{13}C NMR (101 MHz, $CDCl_3$) δ 51.61, 46.61, 36.05, 15.91.

2-((Methylthio)methyl)thiirane (2). A solution of **1** (1.92 g, 18.39 mmol) in methanol (42.8 mL, 0.43 M) was subjected to thiourea (2.80 g, 36.78 mmol, 2.0 eq) and was stirred at room temperature for 16 h. Reaction mixture was then concentrated under reduced pressure and the resulting white solid residue was dissolved in H_2O and extracted with CH_2Cl_2 (x3). The combined organic layers were dried with Na_2SO_4 and concentrated under reduced pressure. Crude was purified via Kugelrohr distillation (140 ºC) to afford 1.22 g (55 %) of **2** as a colorless liquid. ^1H NMR (400

MHz, $CDCl_3$) δ 3.09 (ddt, *J* = 8.1, 6.0, 5.1 Hz, 1H), 2.99 (ddd, *J* = 13.8, 4.8, 0.9 Hz, 1H), 2.57 (dt, *J* = 6.1, 1.2 Hz, 1H), 2.49 (dd, *J* = 13.7, 8.2 Hz, 1H), 2.23 (dd, *J* = 5.4, 1.4 Hz, 1H), 2.20 (s, 3H). ^{13}C NMR (101 MHz, $CDCl_3$) δ 40.27, 33.69, 25.75, 15.96.

1,3-Bis(methylthio)propane-2-thiol (3). A solution of **2** (0.98 g, 8.14 mmol) in methanol (15.0 mL, 0.54 M) was charged with sodium thiomethoxide (0.71 g, 10.18 mmol, 1.25 eq) and was stirred at the room temperature for 45 min. Solvent was then removed under reduced pressure and residue was dissolved in H_2O. Mixture was acidified to pH ~ 3 with conc. HCl causing formation of a white precipitate. This aqueous mixture was extracted with CH_2Cl_2 (x3) and combined organic layers were dried with Na_2SO_4 and concentrated under reduced pressure. Crude residue was purified via Kugelrohr distillation (190 ºC) to afford 0.55 g (40 %) of **3** as a colorless oil. ^{1}H NMR (400 MHz, $CDCl_3$) δ 3.21 (h, *J* = 6.5 Hz, 1H), 2.92 (dd, *J* = 13.5, 6.3 Hz, 2H), 2.78 (dd, *J* = 13.5, 6.7 Hz, 2H), 2.28 (d, *J* = 6.3 Hz, 1H), 2.15 (s, 6H). ^{13}C NMR (101 MHz, $CDCl_3$) δ 41.80, 39.81, 16.37.

1-Tosylaziridine (4). A slurry of tosyl-protected ethanolamine (1.21 g, 3.05 mmol, 1.0 eq) in toluene (10.0 mL, 0.31 M) was treated with 20 % KOH (4.0 mL, 4.6 eq) and reaction was stirred at room temperature for 3 h. Reaction mixture was diluted with water, layers separated and organics washed with additional water (x3). Organic layer was dried with Na_2SO_4 and concentrated under reduced pressure to attain **2** as a white solid (0.55 g, 86 %). ^{1}H NMR (400 MHz, $CDCl_3$) δ 7.83 (d, *J* = 4.8 Hz, 2H), 7.34 (d, *J* = 8.0 Hz, 2H), 2.36 (s, 3H), 2.28 (s, 4H). ^{13}C NMR (101 MHz, $CDCl_3$) δ 144.63, 134.77, 129.70, 127.94, 27.38, 21.61.

***N*-(2-((1,3-Bis(methylthio)propan-2-yl)thio)ethyl)-4-methylbenzenesulfonamide (5).** A flame-dried three-necked round-bottom flask was charged with ethanol (12.3 mL, 0.3 M in sodium). Under a dry N_2 atmosphere, sodium (84.9 mg, 3.69 mmol, 1.5 eq) was carefully added in small portions. After all the sodium has dissolved, thiol **3** (414.1 mg, 2.46 mmol, 1.0 eq) was added dropwise to the sodium ethoxide solution and thiolate was allowed to form for 2 h. A solution of tosylaziridine **4** (606.5 mg, 3.07 mmol, 1.2 eq) in ethanol (5.0 mL, 0.60 M in **4**) was added dropwise. Upon completion of addition, reaction mixture was stirred at room temperature for 16 h. Upon completion ethanol was removed under reduced pressure. Residue was dissolved in EtOAc and washed with brine (x2). Organic layer was dried with Na_2SO_4 and concentrated under reduced pressure. Purification via flash column chromatography on silica gel (0-1 % MeOH/CH_2Cl_2 with 1% TEA additive, linear gradient) yielded 619.9 mg (69 %) of **5** as a clear oil. ^{1}H NMR (400 MHz, $CDCl_3$) δ 7.75 (d, *J* = 8.0 Hz, 2H), 7.31 (d, *J* = 8.0 Hz, 2H), 5.46 (t, *J* = 6.3 Hz, 1H), 3.14 (q, *J* = 6.2 Hz, 2H), 2.91 – 2.79 (m, 3H), 2.73 – 2.69 (m, 4H), 2.43 (s, 3H), 2.13 (d, *J* = 0.7 Hz, 6H).

2-((1,3-Bis(methylthio)propan-2-yl)thio)ethan-1-amine (6). A flame-dried round bottom flask was charged with tosyl-protected amine **5** (0.62 g, 1.69 mmol, 1.0 eq), K_2HPO_4 (2.36 g, 13.55 mmol, 8.0 eq), 2 % Na/Hg amalgam (0.39 g, 16.95 mmol Na, 10.0 eq Na) and anhydrous methanol (18.8 mL, 0.09 M). Reaction was then heated to reflux and stirred for 16 h. Once completed, reaction mixture was cooled to room temperature and the methanolic slurry was decanted. Remaining mercuric pool in flask was washed treated with methanol (7.0 mL) followed by chloroform (7.0 mL), decanting the supernatant each time. Resulting washings and decantate were concentrated under reduced pressure to yield a white solid which was then taken up in chloroform,

filtrated and concentrated to afford 0.33 g (92 %) of **6** as a yellow oil. ^{1}H NMR (400 MHz, $CDCl_3$) δ 2.96 (p, *J* = 6.2 Hz, 1H), 2.91 – 2.62 (m, 8H), 2.13 (s, 6H).

2-((1,3-Bis(methylthio)propan-2-yl)thio)-*N*-(4-bromobenzyl)ethan-1-amine (7). Amine **6** (215.8 mg, 1.02 mmol, 3.0 eq) and *p*-bromobenzaldehyde (63.0 mg, 0.34 mmol, 1.0 eq) were dissolved in anhydrous methanol (1.4 mL, 0.25 M) and stirred for 24 h. Reaction mixture was then treated sodium triacetoxyborohydride (115.4 mg, 0.54 mmol, 1.6 eq) and stirred at room temperature for 1 h. Reaction was quenched with addition of 1 M NaOH and then washed with CH_2Cl_2 (x3). The combined organic layers were washed with brine, dried with Na_2SO_4 and concentrated under reduced pressure. The crude residue was purified via flash column chromatography on silica gel (0-10 % MeOH/CH_2Cl_2) to afford 90.7 mg (70 %) of **7** as yellow oil. ^{1}H NMR (400 MHz, $CDCl_3$) δ 7.40 (d, *J* = 8.0 Hz, 2H), 7.18 (d, *J* = 8.0 Hz, 2H), 3.72 (s, 2H), 2.97 – 2.70 (m, 9H), 2.10 (s, 6H).

Spectroscopic Materials and Methods. Millipore water was used to prepare all aqueous solutions. Binding assays with Fz were conducted in an anaerobic chamber (Vacuum Atmospheres Company) with 90% nitrogen, 10% hydrogen atmosphere (<1 ppm O_2), unless otherwise noted. Buffers and other solutions used for biochemical assays were deoxygenated by three cycles of evacuation (>30 min) and refilling with argon or nitrogen and stored in the anaerobic chamber. Absorption spectra were recorded using a Varian Cary 50 spectrophotometer (Walnut Creek, CA). Samples for absorption measurements were contained in 1-cm quartz cuvettes (1.4-mL volume, Starna, Atascadero, CA). Cu^+ was delivered in the form of $[Cu(MeCN)_4][PF_6]$ from an acetonitrile stock solution (2 mM). For fluorescence-based assay with CF3, excitation was provided at 534 nm and collected emission was integrated from 540-700 nm.

Schemes and Figures

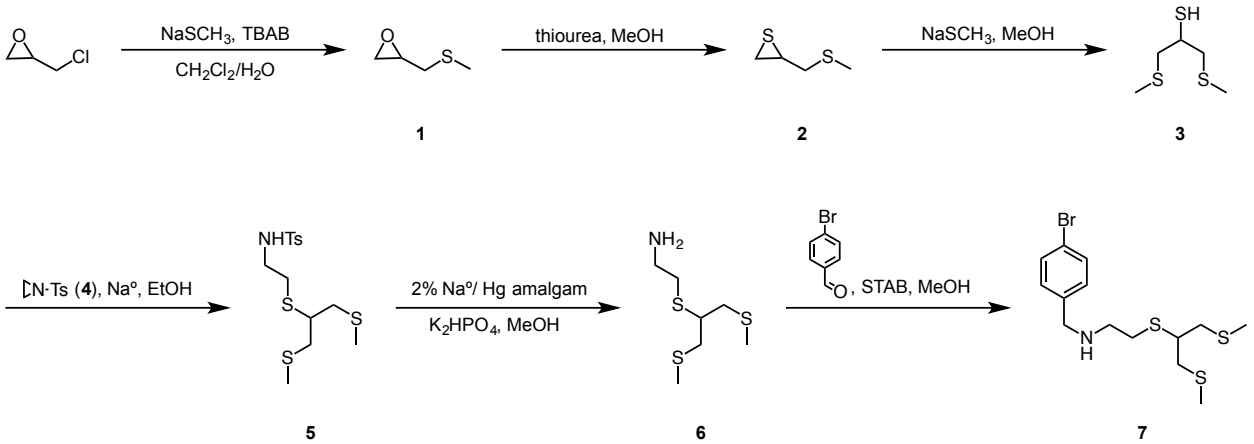

Scheme A5-1. Synthesis of a tripodal-like NS_3 receptor for Cu^+ sensing.

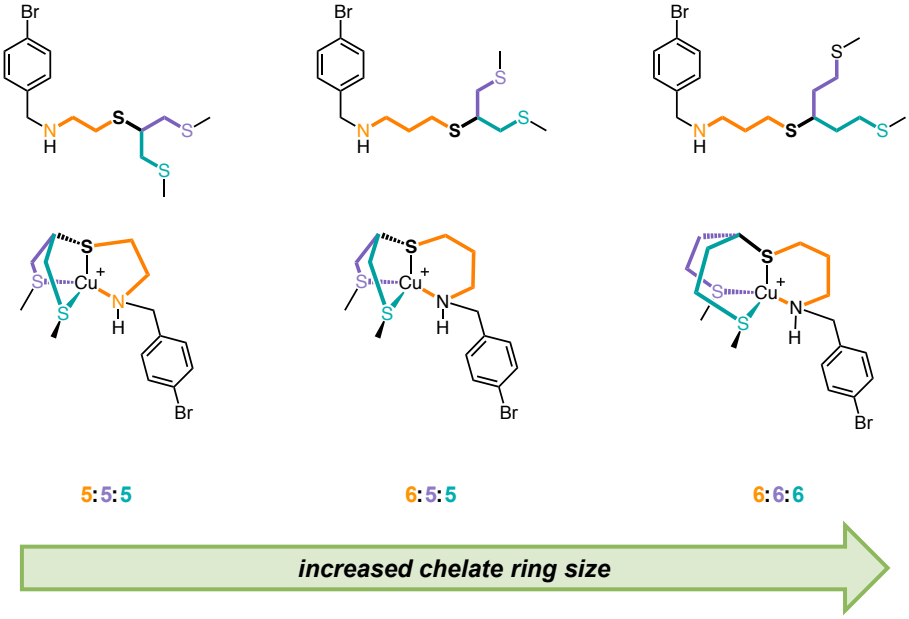

Figure A5-1. Possible tripodal-like NS_3 receptors for Cu^+ sensing.

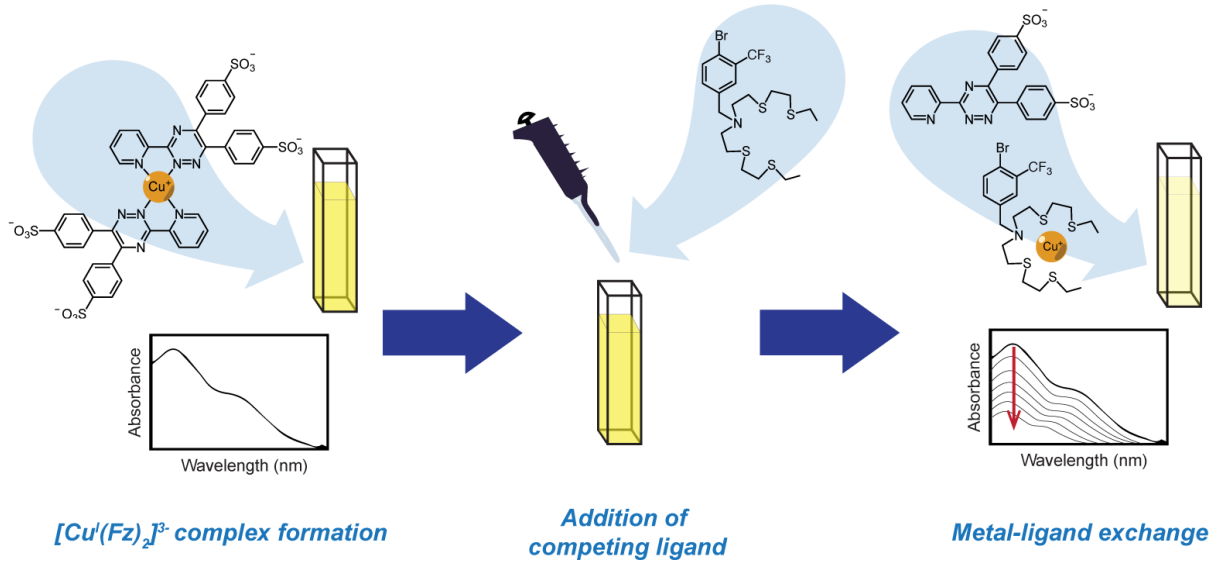

Figure A5-2. Absorbance-based competition assay for evaluation of binding affinity of copper chelators.

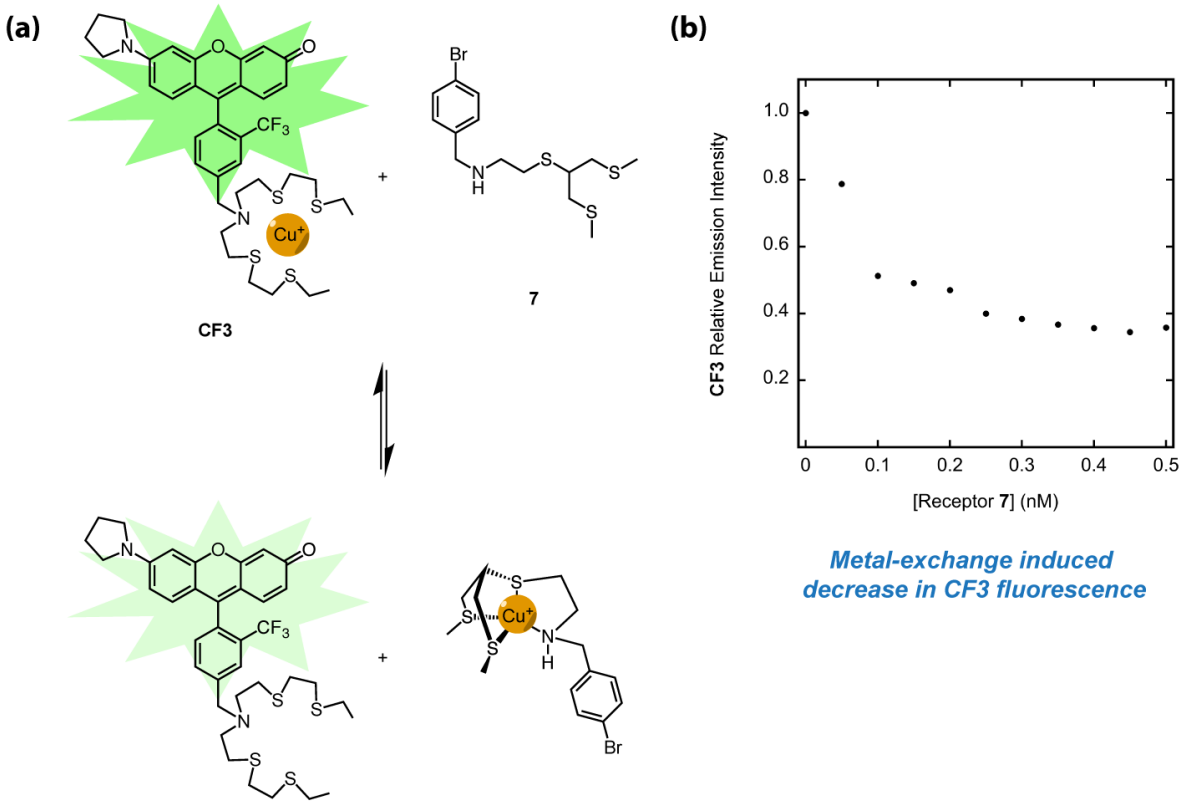

Figure A5-3. Model copper chelator **7** presents metal exchange with established fluorescent copper probe **CF3**. (a) Proposed metal exchange between **CF3** and **7** observed by fluorescence-based assay. (b) Decreased **CF3** fluorescence is observed upon addition of competing ligand **7**.

Entry	Conditions (1:1 stoichiometry of RNH_2:CHO except when noted)					Result
	Solvent	Reducing Agent	AcOH	T (°C)	Rxn time	
1	1,2-DCE	STAB (1.4 eq)	1.2 eq	RT	30 min[a], 2 h[b]	reduction to alcohol
2	1,2-DCE	STAB (1.2 eq)	1.2 eq	RT	30 min[a] , 1 h[b]	reduction to alcohol
3	MeOH	N/A	N/A	RT	18 h[a]	0.35:1 imine:CHO[c]
4	MeOH	N/A	N/A	RT	90 h[a]	0.38:1 imine:CHO[c]
5	MeOH	N/A	1.2 eq	RT	18 h[a]	0.33:1 imine:CHO[c]
6	MeOH	N/A	N/A	50 °C	30 h[a]	0.40:1 imine:CHO[c]
7[d]	MeOH	$NaBH_4$ (1.6 eq)	N/A	RT	21 h[a], 1 h[b]	1.00:0 imine:CHO[c] (mixture of pdt & red. to alcohol)
8[d]	MeOH	STAB (1.6 eq)	N/A	RT	23 h[a], 1 h[b]	1.00:0 imine:CHO[c] 70% isolated pdt

[a] Mixing of amine and aldehyde for imine formation.
[b] After reducing agent is added.
[c] Imine formation was monitored by ^{1}H-NMR in MeOD
[d] 3:1 RNH_2:CHO

Table A5-1. Optimization of reaction conditions for synthesis of receptor **7**.

References

1. Fahrni, C. J., Synthetic fluorescent probes for monovalent copper. *Curr. Opin. Chem. Biol.* **2013,** *17*, 656-662.
2. Cotruvo, J. A. J.; Aron, A. T.; Ramos-Torres, K. M.; Chang, C. J., Synthetic fluorescent probes for studying copper in biological systems. *Chem. Soc. Rev.* **2015,** *44* (13), 4400-4414.
3. Aron, A. T.; Ramos-Torres, K. M.; Cotruvo, J. A.; Chang, C. J., Recognition- and Reactivity-Based Fluorescent Probes for Studying Transition Metal Signaling in Living Systems. *Acc. Chem. Res.* **2015,** *48* (8), 2434-2442.
4. Forshee, P. B.; Sibert, J. W., Sodium Amalgam: A Highly Efficient Reagent for the Detosylation of Azathiacrown Ethers. *Synthesis* **2006,** *2006* (05), 756-758.
5. Xiao, Z.; Gottschlich, L.; van der Meulen, R.; Udagedara, S. R.; Wedd, A. G., Evaluation of quantitative probes for weaker Cu(i) binding sites completes a set of four capable of detecting Cu(i) affinities from nanomolar to attomolar. *Metallomics* **2013,** *5* (5), 501-513.
6. Krishnamoorthy, L.; Cotruvo, J. A. J.; Chan, J.; Kaluarachchi, H.; Muchenditsi, A.; Pendyala, V. S.; Jia, S.; Aron, A. T.; Vander Wal, M. N.; Guan, T.; Smaga, L. P.; Farhi, S. S.; New, E. J.; Lutsenko, S.; Chang, C. J., Copper regulates cyclic AMP-dependent lipolysis. *Nat. Chem. Biol.* **2016,** *12*, 586-592.
7. Dodani, S. C.; Firl, A.; Chan, J.; Nam, C. I.; Aron, A. T.; Onak, C. S.; Ramos-Torres, K. M.; Paek, J.; Webster, C. M.; Feller, M. B.; Chang, C. J., Copper is an endogenous modulator of neural circuit spontaneous activity. *Proc. Natl. Acad. Sci. U. S. A.* **2014,** *111*, 16280-16285.

Appendix 6:

Efforts Towards the Development of a Coumarin-based Probe for Sensing Cu^{+}

Synopsis

The lack of a one-size-fits-all sensor for the investigation of biological roles for copper continuously motivates the evaluation of new fluorophore and metal-binding platforms for selective and sensitive metal detection. The application of a variety of fluorophores, as well as the construction of different binding moieties with varying donor sets, binding geometries and ligand topologies can lead to a possible library of probes with a range in photophysical and metal-sensing features. Considering copper sensing, the available collection of small-molecule probes for its detection mainly relies on a photoinduced electron transfer (PeT) quenching mechanism to afford intensity-based responses upon metal complex formation.[1-3] Remarkably, the use of other analyte-sensing mechanisms has been marginally applied in the development of new probes, resulting in a lack of chemodosimeter molecules for ratiometric detection of copper.

This appendix summarizes the synthesis and characterization of a coumarin-based probe that makes use of an NS_3 metal-binding domain with a tripodal ligand architecture for the investigation of the coumarin dye as a possible fluorogenic platform for the ratiometric detection of copper. Given that this chromophore has been previously implemented in the design of analyte-selective chemodosimeters,[4] we envisioned that the direct attachment of one of the donor atoms of the NS_3 coordination unit to the coumarin core would be a suitable approach to provoke a metal-binding dependent shift in the spectral features of the sensor in a ratiometric fashion.

Results and Discussion

Synthesis of a Coumarin-based Probe with an NS_3 Tripodal Receptor for Copper Sensing. Scheme A6-1 outlines the synthesis of a coumarin-based probe that presents a tripodal receptor with an NS_3 coordination unit. Briefly, the synthesis of probe **4** began with nucleophilic aromatic substitution of chloro-modified formyl-aminocoumarin **1** with ethanethiol in order to introduce the first thioether donor group. Next, reductive amination of the resulting ethylthio-substituted coumarin **2** with bis(2-(ethylthio)ethyl)amine afforded the final probe **4** in decent yield. This synthetic design tolerates the introduction of an assortment of amino-bridged metal-binding platforms, allowing for investigation of the effects of altered coordination spheres, as well as chelate ring size effects of corresponding donor sets, on the response of the resulting sensors.

Spectroscopic Properties of Coumarin-Based Copper Sensor. Spectroscopic characterization of probe **4** was performed in 50 mM MOPS buffered to pH 7.4. *Apo*-probe **4** exhibits two main optical features in the visible region of the spectrum: a high energy absorption band at 262 nm and a more prominent resonance at 435 nm. Upon addition of copper, a shift in the maxima of these bands is observed ($\lambda_{abs\ (Cu)}$ 265 nm and 446 nm), accompanied with a decreased absorption. (Figure A6-1) The emission profile of probe **4** is dependent on the excitation energy. For the *apo*-configuration, excitation at 265 nm affords a narrow emission band at 545 nm, while a 446 nm excitation presents a broader fluorescence feature centered at 538 nm. Copper addition causes minor shifts in the emission energies ($\lambda_{fl\ (Cu)}$ 545 nm and 540 nm, respectively), as well as a reduction in fluorescence intensity – 2.4-fold turn-off at $\lambda_{ex\ (Cu)}$ 265 nm and 1.3-fold turn-off at $\lambda_{ex\ (Cu)}$ 446 nm. (Figure A6-2)

Even though the combination of the NS_3 receptor framework with a coumarin platform did not result in a desirable turn-on response upon copper addition, we had speculated that direct attachment of one of the donor atoms to the conjugated fluorophore system could lead to a ratiometric response upon metal-binding. While a shift in the absorbance features is observed upon copper addition, more notably at the lower energy band, the change in intensity and excitation wavelength was not linearly dependent on the copper concentration. Additionally, the lack of an isosbestic point in the probe spectra did not allow for the characterization of the sensor's response as ratiometric.

Conclusion and Future Work

We have designed and synthesized a coumarin-based sensor that displays an NS_3 coordination unit with tripodal ligand architecture for the detection of copper. Spectroscopic characterization of this probe showed minor turn-off responses and no significant ratiometric character upon the addition of copper. We speculate that the reduced response to Cu^+, in comparison to combinations of the NS_3 motif with other fluorophore platforms, could result from (i) diminished metal-binding capacity, (ii) inefficient interruption of the PeT quenching mechanism upon copper binding and/or (iii) metal-induced quenching of the fluorophore excited-state. Additionally, we hypothesize that the absence of a substantial ratiometric response as a result of metal interaction is possibly due to ineffective modulation of the intramolecular charge distribution in the presence of copper. Although we anticipated that direct introduction of a thioether donor on the fluorophore platform would lead to a ratiometric response via an internal charge transfer (ICT)-dependent mechanism, the position for this substitution does not seem to be suitable for this sensing approach. Therefore, future efforts to incorporate ligand donors on more effective positions of the fluorophore core could lead to ratiometric sensors for copper. We envision that synthesis of a thiocoumarin-based probe, as shown in Scheme A6-2, would provide a superior donor substitution and might result in a fluorescent chemodosimeter for copper, as previous reports on analogous sensors for zinc[5] have shown significant ratiometric responses with metal interaction at the coumarin carbonyl position.

Experimental Section

Synthetic Materials and Methods. All reactions were carried out under a dry N_2 atmosphere and stirred magnetically unless stated otherwise. All reactions using air- or moisture-sensitive reagents were performed in oven- and flame-dried glassware under an atmosphere of dry N_2. Compound **1** was synthesized by Thomas Brewer. Unless otherwise noted, all chemicals were used as received. Flash chromatography was performed on an automated purification system using pre-packed silica gel columns. SiliCycle 60 F254 silica gel (precoated sheets, 0.25 mm thick) was used for analytical TLC, visualized with UV light and/or staining with *p*-anisaldehyde or $KMNO_4$. ^1H and ^{13}C NMR spectra were collected in $CDCl_3$ (Cambridge Isotope Laboratories, Cambridge, MA) at 25 °C on a Bruker AV-300, Bruker AVB-400 or Bruker AVQ-400 spectrometer at the College of Chemistry NMR Facility at the University of California, Berkeley. All chemical shifts are reported in the standard notation of parts per million using the peak of residual proton or carbon signals of $CDCl_3$ as an internal reference.

Synthesis.

9-(Ethylthio)-11-oxo-2,3,6,7-tetrahydro-1*H*,5*H*,11*H*-pyrano[2,3-*f*]pyrido[3,2,1-*ij*]quinoline-10-carbaldehyde (2). A solution of **1** (200 mg, 0.70 mmol) in DMF (7.0 mL, 0.10 M) was charged with K_2CO_3 (384.8 mg, 2.78 mmol, 4.0 eq) and ethanethiol (51.5 µL, 0.70 mmol, 1.0 eq) and stirred for 16 h at room temperature. The reaction mixture was diluted with EtOAc and washed with brine (x3). The organic layer was dried with Na_2SO_4 and concentrated under reduced pressure. Purification via flash column chromatography on silica gel (5 % EtOAc/CH_2Cl_2) afforded 114.7 mg (50 %) of **2** as a red solid. ^{1}H NMR (400 MHz, $CDCl_3$) δ 10.31 (s, 1H), 7.67 (s, 1H), 3.34 (dt, *J* = 8.7, 5.7 Hz, 4H), 3.02 (q, *J* = 7.4 Hz, 2H), 2.84 (t, *J* = 6.4 Hz, 2H), 2.77 (t, *J* = 6.3 Hz, 2H), 1.96 (h, *J* = 6.5 Hz, 4H), 1.24 (t, *J* = 7.4 Hz, 3H). ^{13}C NMR (101 MHz, $CDCl_3$) δ 188.28, 160.78, 160.71, 150.91, 148.97, 125.54, 119.39, 112.57, 110.14, 105.67, 50.24, 49.78, 32.48, 27.52, 21.05, 20.08, 14.82.

Bis(2-(ethylthio)ethyl)amine (3). A flame-dried three-necked round-bottom flask was charged with ethanol (560.3 mL, 1.0 M in sodium). Under a dry N_2 atmosphere, sodium (12.88 g, 560.26 mmol, 5.0 eq) was carefully added in small portions. After all the sodium has dissolved, ethanethiol (24.9 mL, 336.15 mmol, 3.0 eq) was added dropwise to the sodium ethoxide solution. Reaction mixture was heated to reflux and then a solution of bis(2-chloroethyl)amine hydrochloride (20.0 g, 112.1 mmol, 1.0 eq) in ethanol (280.1 mL, 0.4 M in amine) was added dropwise. Upon completion of addition, reaction mixture was stirred at reflux for 2 h. Reaction was then cooled to room temperature and ethanol was removed under reduced pressure. Residue was taken up in chloroform and washed H_2O (x3). Organic layer was dried with Na_2SO_4 and concentrated under reduced pressure. Crude was purified via vacuum distillation to afford 13.29 g (61 %) of **3** as a pale yellow oil. ^{1}H NMR (400 MHz, $CDCl_3$) δ 2.81 (t, *J* = 6.6 Hz, 4H), 2.68 (t, *J* = 6.6 Hz, 4H), 2.53 (q, *J* = 7.4 Hz, 4H), 1.78 (s, 1H), 1.25 (t, *J* = 7.4 Hz, 6H). ^{13}C NMR (101 MHz, $CDCl_3$) δ 48.28, 31.86, 25.80, 14.84.

10-((Bis(2-(ethylthio)ethyl)amino)methyl)-9-(ethylthio)-2,3,6,7-tetrahydro-1*H*,5*H*,11*H*-pyrano[2,3-*f*]pyrido[3,2,1-*ij*]quinolin-11-one (4). A solution of **2** (57.8 mg, 0.18 mmol) and **3** (33.9 mg, 0.18 mmol, 1.0 eq) in 1,2-dichloroethane (5.8 mL, 0.03 M) was treated with $NaBH(OAc)_3$ (74.3 mg, 0.35 mmol, 2.0 eq). The reaction mixture was stirred at room temperature for 16 h. To quench excess reductant, sat. Na_2CO_3 was added and reaction was stirred for 30 min. The mixture was partitioned and the aqueous layer was extracted with CH_2Cl_2 (x2). The combined organic layers were washed with brine, dried with Na_2SO_4 and concentrated under reduced pressure. The crude residue was purified via flash column chromatography on silica gel (0-10 % EtOAc/CH_2Cl_2, linear gradient) to yield 34.6 mg (39 %) of **4** as a dark yellow solid. ^{1}H NMR (400 MHz, $CDCl_3$) δ 7.41 (s, 1H), 3.88 (s, 2H), 3.24 (dt, *J* = 10.4, 5.6 Hz, 4H), 2.87 (q, *J* = 7.0 Hz, 4H), 2.82 – 2.74 (m, 6H), 2.71 – 2.64 (m, 4H), 2.51 (q, *J* = 7.4 Hz, 4H), 1.96 (h, *J* = 5.7 Hz, 4H), 1.24 – 1.18 (m, 9H). ^{13}C NMR (101 MHz, $CDCl_3$) δ 161.81, 151.78, 149.87, 145.60, 124.69, 123.38, 118.18, 109.39, 106.37, 53.72, 51.25, 49.87, 49.45, 31.18, 28.99, 27.70, 26.01, 21.53, 20.61, 20.43, 15.16, 14.89.

Spectroscopic Materials and Methods. Millipore water was used to prepare all aqueous solutions. All final spectroscopic measurements were performed in MOPS buffer. Absorption spectra were recorded using a Varian Cary 50 spectrophotometer (Walnut Creek, CA) and

fluorescence spectra were recorded using a Photon Technology International Quanta Master 4 L-format scan spectrofluorometer (Lawrenceville, NJ) equipped with an LPS-220B 75-W xenon lamp and power supply, A-1010B lamp housing with integrated igniter, switchable 814 photocounting/analog photomultiplier detection unit, and MD5020 motor driver. Samples for absorption and emission measurements were contained in 1-cm quartz cuvettes (1.4-mL volume, Starna, Atascadero, CA). Cu^+ was delivered in the form of $[Cu(MeCN)_4][PF_6]$ from an acetonitrile stock solution (2 mM). Excitation was provided at 265 nm or 446 nm and collected emission was integrated from 270-700 nm or 455-700 nm for **4**.

Schemes and Figures

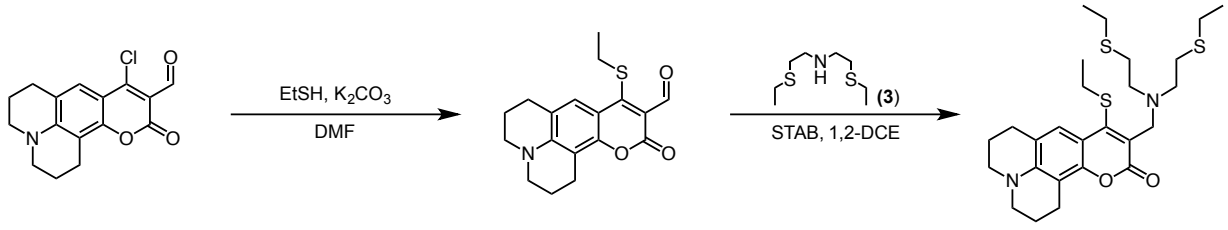

1 **2** **4**

Scheme A6-1. Synthesis of coumarin-based copper (I) probe with tripodal NS_3 receptor

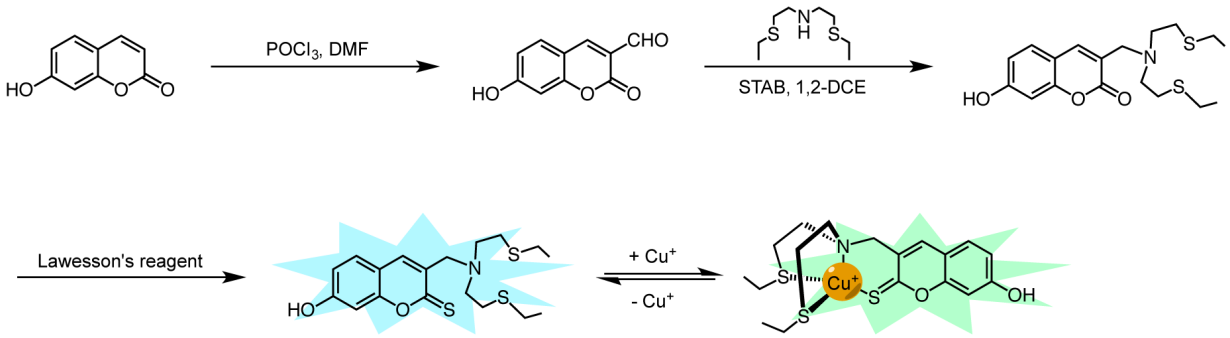

Scheme A6-2. Synthetic approach towards a thiocoumarin-based copper (I) probe with tripodal NS_3 receptor.

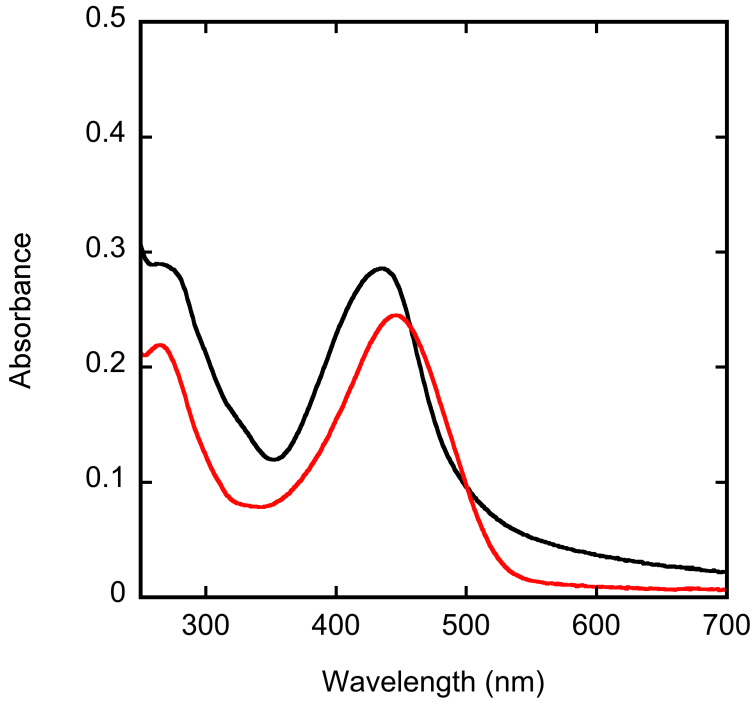

Figure A6-1. Absorbance spectra of 10 µM **4**. Spectra shown are for buffered [Cu^{+}] of 0.0 (black trace) and 10 (red trace) µM. Spectra were acquired in 50 mM MOPS, pH 7.4.

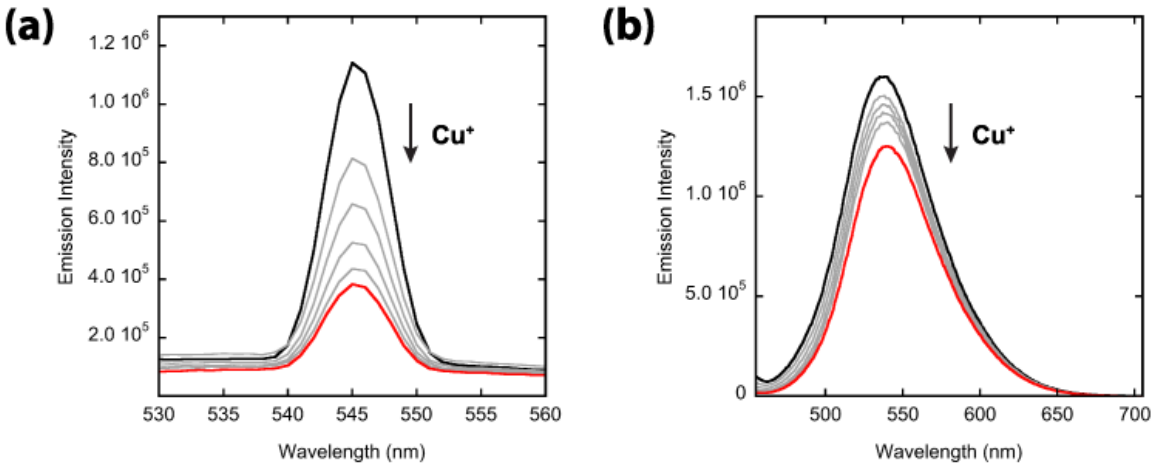

Figure A6-2. Fluorescence response of 10 μM **4** to Cu^+. Spectra shown are for buffered [Cu^+] of 0.00 (black trace), 2.0, 4.0, 6.0, 8.0 and 10.0 (red trace) μM. Spectra were acquired in 50 mM MOPS, pH 7.4 with excitation at (a) 265 nm or (b) 446 nm.

References

1. Fahrni, C. J., Synthetic fluorescent probes for monovalent copper. *Curr. Opin. Chem. Biol.* **2013,** *17*, 656-662.
2. Cotruvo, J. A. J.; Aron, A. T.; Ramos-Torres, K. M.; Chang, C. J., Synthetic fluorescent probes for studying copper in biological systems. *Chem. Soc. Rev.* **2015,** *44* (13), 4400-4414.
3. Aron, A. T.; Ramos-Torres, K. M.; Cotruvo, J. A.; Chang, C. J., Recognition- and Reactivity-Based Fluorescent Probes for Studying Transition Metal Signaling in Living Systems. *Acc. Chem. Res.* **2015,** *48* (8), 2434-2442.
4. Song, Y. X.; Chen, Z.; Li, H. Q., Advances in Coumarin-Derived Fluorescent Chemosensors for Metal Ions. *Curr. Org. Chem.* **2012,** *16* (22), 2690-2707.
5. Lim, N. C.; Schuster, J. V.; Porto, M. C.; Tanudra, M. A.; Yao, L.; Freake, H. C.; Brückner, C., Coumarin-Based Chemosensors for Zinc(II): Toward the Determination of the Design Algorithm for CHEF-Type and Ratiometric Probes. *Inorg. Chem.* **2005,** *44* (6), 2018-2030.

Appendix 7:

Protocol for Drying THF for Li-X Exchange Reactions in the Synthesis of Fluorophores and Fluorescent probes

Synopsis

This appendix describes an experimental protocol for drying THF. This protocol should produce ~ 800 mL of THF of good quality for the Li-halogen exchange reaction needed in the synthesis of fluorophores and fluorescent probes.

Protocol

Materials:

2 1L 2/3-necked round bottom flasks
1 1L Strauss flask
3Å molecular sieves
double-ended needle (cannula)
heating plate
heating block
lab Jack

Procedure:

Day 1

1. In a 1 L 2/3-necked round bottom flask, add 150 g of 3Å molecular sieves and dry overnight at 150 ºC in oven.

Day 2

1. Remove flask (Flask 1) from oven and cool to room temperature under inert N_2 atmosphere.
2. Add ~ 800 mL of low water content THF to flask.
3. Allow THF to sit in activated molecular sieves under N_2 atmosphere and covered from light with foil for 24 h.
4. Prepare another 1 L 2/3-necked round bottom flask (Flask 2) with 150 g of 3Å molecular sieves and dry overnight at 150 ºC in oven.

Day 3: THF transfer

1. Remove Flask 2 from oven and cool to room temperature under inert N_2 atmosphere.
2. Once at room temperature, evacuate and backfill flask with N_2 three times.
3. Under a steady flow of N_2 insert one end of the cannula into Flask 2 and allow inert gas to flow through the cannula for 2-3 min to purge it.
4. Insert the other end of the cannula into Flask 1 (under N_2 pressure) avoiding the tip of the needle to touch the THF.
5. Add a "bleed needle" to Flask 2 to relieve pressure and close access to N_2.
6. Using a lab Jack, raise Flask 1 to a higher level than Flask 2 in order to help the cannula transfer.
7. Lower the end of the cannula in Flask 1 until it is submerged in the liquid.
8. If needed, induce transfer by attaching a syringe onto bleed needle and pulling a slight vacuum. Remove syringe right away, keeping bleed needle; transfer of liquid should begin shortly.

9. Once all of the THF has been transferred, lift both ends of the cannula so that no part of it touches the liquid.
10. Open Flask 2 to N_2, remove bleed needle and then remove the cannula.
11. Cover Flask 2 from light using foil and let sit for 24 h under N_2 atmosphere.

Day 3: Strauss flask preparation

1. While cannula transfer is occurring, add 150 g of 3Å molecular sieves into 1 L Strauss flask.
2. In order to activate sieves, place Strauss flask under high vacuum.
3. Using the heating plate and heat block, activate sieves at 300 ºC for 24 h.

Day 4

1. Remove Strauss flask from heating and cool to room temperature under inert N_2 atmosphere.
2. Once at room temperature, under a heavy stream of N_2, remove plastic stopper and replace with an inverted 14/20 septum. (See Figure A7-1) Evacuate and backfill flask with N_2 three times.
3. For THF transfer, follow steps 3 to 9 in section *Day 3: THF transfer*.
4. Open Strauss flask to **heavy** stream of N_2, remove bleed need and then cannula.
5. After producing a saturated atmosphere of N_2, exchange septum for stopper under a **heavy** stream of inert gas.
6. After 2-3 min of N_2 flow into Strauss flask (enough to create an inert atmosphere), completely close neck of Strauss flask with stopper and evacuate/backfill neck three times.
7. Allow THF to sit under N_2 atmosphere and covered from light with foil for at least 24 h before use.

Collecting THF from Strauss flask

1. Before collecting THF from Strauss flask, evacuate air and backfill neck of flask with N_2 three times. Make sure to trap vacuum pump using liquid N_2 in order to avoid any solvent accumulation in pump.
2. Under a very **heavy** stream of N_2 (to create positive pressure), replace stopper for inverted 14/20 septum.
3. Using a syringe and needle that has been primed with N_2, collect desired amount of THF.
4. When done collecting THF, replace septum with stopper under a **heavy** stream of N_2 and create inert atmosphere in flask.
5. Completely close neck of Strauss flask with stopper and evacuate/backfill neck three times.

Figures

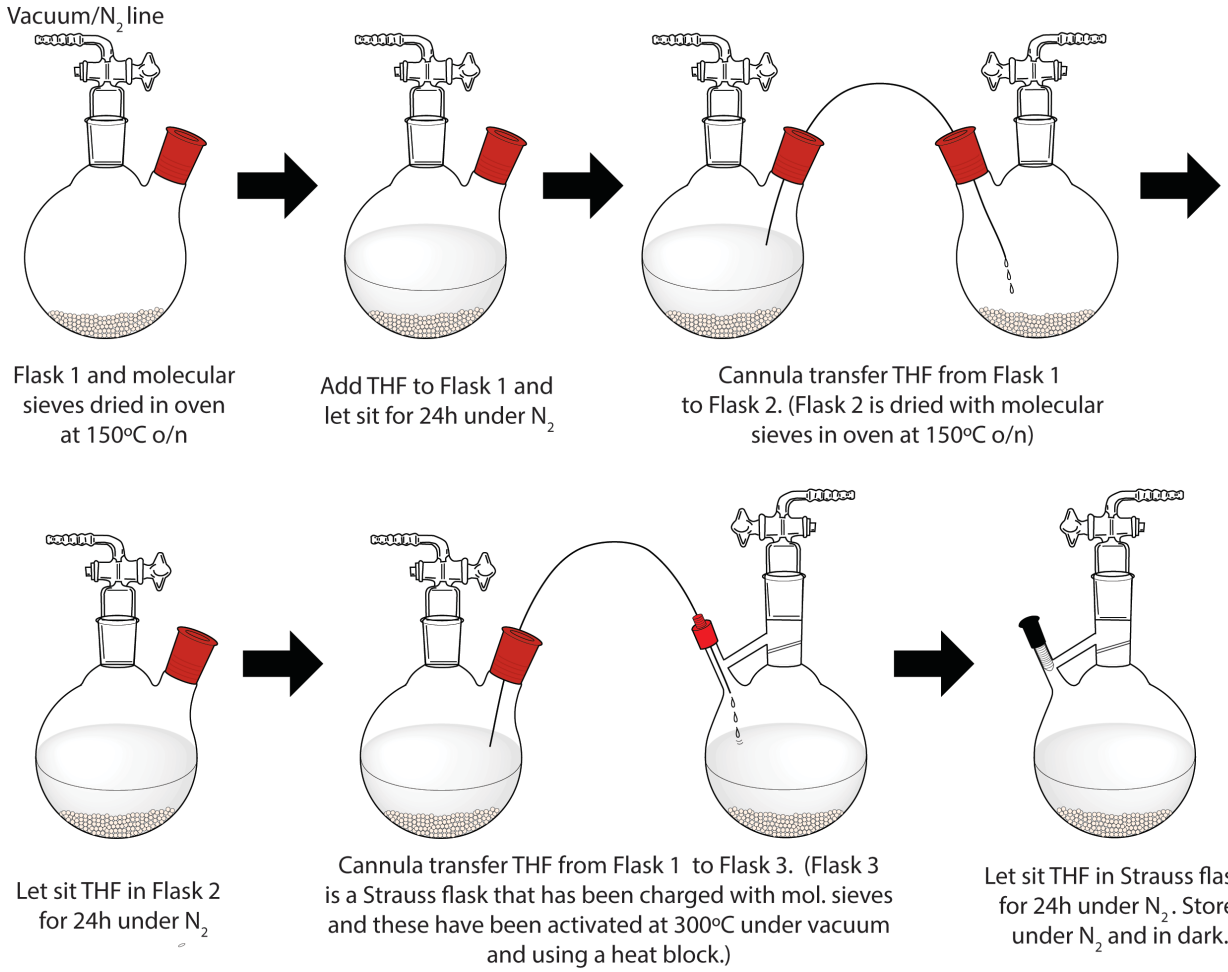

Figure A7-1. Representative schematic of the THF drying process.

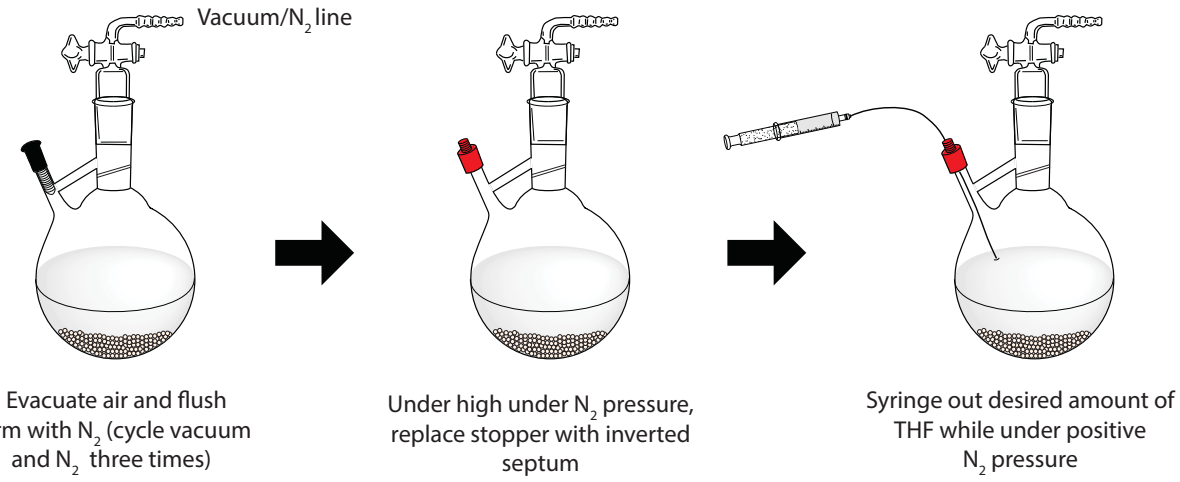

Figure A7-2. Collecting THF from Strauss flask.

Appendix 8:
Protocol for Measuring Log D Values of Fluorescent Probes

Synopsis

This appendix describes an experimental protocol for the determination of logD values for fluorescent probes. This protocol should apply to any fluorescent dye for the detection of metals and small molecules.

Protocol

Creating a standard curve:

Use a 1 mM stock solution of probe in DMSO to create a standard curve in 1-octanol (250 uL per point/sample). For this curve, a minimum of 4-5 points is required. It is recommended to use more points than needed in case there are some outliers due to pipetting errors. An example for the construction of a typical curve is presented in Tables A8-1 and A8-2.

Procedure:

2. Add amount of 1-octanol needed for standard sample directly to clear bottom 96-well plate.
3. Add amount of 1 mM probe stock solution to corresponding standard sample directly in 96-well plate.
4. Mix the probe solution and 1-octanol directly in well. To do this it is important to use the same pipetting motion for all samples to account for any loss of octanol in pipette. (i.e. Mix *x* number of times per well, dispense octanol, wait *x* number of seconds and dispense again.)

Sample preparation:

The logD value determination is run in triplicate; therefore 3 samples are prepared following the procedure below. The concentration of the samples is chosen arbitrarily as long as the response recorded (UV-VIS absorbance or fluorescence) from it lies in between the values used in the standard curve.

Procedure:

1. In an Eppendorf tube (1.6 mL) add 500 µL of 1-octanol and 500 µL of PBS buffer (pH 7.4). To this, add 3 µL of 1 mM stock probe.
2. Vortex the sample for 2-3 min to allow mixing.
3. Centrifuge the sample for 3 min to allow separation of phases.
4. Without disturbing the aqueous layer, carefully transfer 250 µL of the octanol layer to well in 96-well plate.

Data collection and analysis:

Data can be collected as UV-VIS absorbance or fluorescence spectra. For xanthene-based dyes (i.e. fluorescein, rhodols, rhodamines), collecting absorbance spectra should give reliable results. However, for BODIPY-based probes (and other very lipophilic scaffolds), fluorescence spectra should be collected as absorbance is not sensitive enough to detect small changes in the concentration of probe between octanol and aqueous layers.

Procedure:

1. Using plate reader, set collection mode to Spectral Scanning.
2. Collect spectra with at least +/- 10 nm from maxima.
3. Export data as a text file and run data analysis in Excel. An example of the analysis is shown in Table A8-3.

Figures and Tables

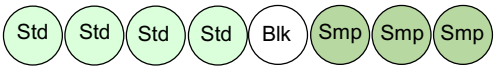

Figure A8-1. Layout of standards and samples in 96-well plate.

Final Concentration (μM)	Amount of 1 mM probe stock (μL)	Amount of 1-octanol (μL)
4	1	249
8	2	248
12	3	247
16	4	246

Table A8-1. Typical concentration values for the construction of a calibration curve.

Calibration Curve Ctrl-CF3						
Standard concentration (μM)	2	4	8	--	16	20
Integrated Absorbance	2.280	3.019	5.071	--	9.218	11.097

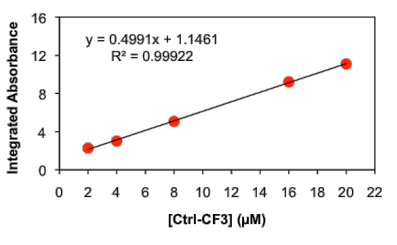

Table A8-2. Data analysis example for the construction of a calibration curve.

Samples					
	1	**2**	**3**	**Average**	**Formulas**
Integrated Absorbance	3.885	3.855	4.072	3.937333333	*sum of absorbance values*
[probe]$_{octanol}$	5.48767782	5.4275696	5.86235223	5.592533226	*substitute absorbance in calibration curve equation*
[probe]$_{PBS}$	5.12E-01	5.72E-01	1.38E-01	4.07E-01	*[total] - [octanol]*
logD	1.02984545	0.9768827	1.62930274	**1.137516373**	*LOG(PBS/octanol)*
				0.037450295	*Standard Deviation*

Table A8-3. Example of data analysis for the determination of log D values.